AUTOMATION AND VERIFICATION OF ANKARA WIND TUNNEL

A THESIS SUBMITTED TO
THE GRADUATE SCHOOL OF NATURAL AND APPLIED SCIENCES
OF
MIDDLE EAST TECHNICAL UNIVERSITY

BY

ARGÜN KATIRCI

IN PARTIAL FULFILLMENT OF THE REQUIREMENTS
FOR
THE DEGREE OF MASTER OF SCIENCE
IN
AEROSPACE ENGINEERING

SEPTEMBER 2006

Approval of the Graduate School of Natural and Applied Sciences

_____

Prof. Dr. Canan ÖZGEN

Director

I certify that this thesis satisfies all the requirements as a thesis for the degree of Master of Science.

_____

Prof. Dr. Nafiz ALEMDAROĞLU
Head of Department

This is to certify that we have read this thesis and that in our opinion it is fully adequate, in scope and quality, as a thesis for the degree of Master of Science.

_____

Prof. Dr. Nafiz ALEMDAROĞLU

Supervisor

Examining Committee Members

Prof. Dr. Nafiz ALEMDAROĞLU	(METU, AE)	_____
Prof. Dr. Yusuf ÖZYÖRÜK	(METU, AE)	_____
Prof. Dr. Kahraman ALBAYRAK	(METU, ME)	_____
Assoc. Prof. Dr. Serkan ÖZGEN	(METU-AE)	_____
Dr. Gökmen MAHMUTYAZICIOĞLU	(TÜBİTAK-SAGE)	_____

I hereby declare that all information in this document has been obtained and presented in accordance with academic rules and ethical conduct. I also declare that, as required by these rules and conduct, I have fully cited and referenced all material and results that are not original to this work.

Name, Last name: Argün KATIRCI

Signature :

ABSTRACT

AUTOMATION AND VERIFICATION OF ANKARA WIND TUNNEL

Katırcı, Argün
M.Sc., Department of Aerospace Engineering
Supervisor: Prof. Dr. Nafiz ALEMDAROĞLU

September 2006, 185 pages

All the operational and measurement systems of Ankara Wind Tunnel was modified to operate automatically under the control of a central computer system programmed using the Lab View programming language.

A cruciform air-to-air missile with triangular canard control and a trapezoidal wing model was tested by a 35mm diameter internal balance at Mach 0.2 and data was compared with the test data of the same model's test that was performed at NASA Langley Research Center.

Keywords: Data Acquisition System, Internal Balance, Wind Tunnel, Sidewinder

ÖZ

ANKARA RÜZGAR TÜNELİNİN OTOMASYONU VE DOĞRULAMA TESTLERİ

Katırcı, Argün
Yüksek Lisans, Havacılık ve Uzay Mühendisliği Bölümü
Tez Yöneticisi: Prof. Dr. Nafiz ALEMDAROĞLU

Eylül 2006, 185 sayfa

Ses altı hızlarda çalışan Ankara Rüzgar Tünelinin tüm sistemleri Lab View programı kullanılarak tam otomatik olarak merkezi bir bilgisayar kontrolünde yönetilmiş, deneyler sırasında tüm sistemelerin çalışması ve ölçümler otomatik olarak gerçekleştirilmiştir.

0.2 Mach sayısında havadan havaya bir füze modeli ile 35 mm'lik iç balans kullanılarak testler yapılmış ve bu modelin NASA Langley Research Center'da yapılan test sonuçları ile elde edilen sonuçlar karşılaştırılmıştır.

Anahtar kelimeler: Veri Toplama Sistemi, İç Balans, Rüzgar Tüneli, Sidewinder

To My Family

ACKNOWLEDGEMENT

I would like to express my special thanks to my supervisor Prof. Dr. Nafiz ALEMDAROĞLU for his guidance, tolerance and understanding.

I would like to thank TÜBİTAK-SAGE for all their support throughout this study. I would like state my gratitude to my colleagues Emel MAHMUTYAZICIOĞLU for her support, guidance and discussions on the subject, Alper ÜNVER for his great help at "electrical and electronic stuff", Birşen ERDEM for her support at model and model support system manufacturing process, Süleyman KURUN for his ideas, Levent YALÇİN for his discussions on the subject, Koray DAYANÇ for his patience, Aysun ÇELEBİ and İlke AYDINCAK for their help and finally Salih KAYABAŞI of his great support at "everything" at Ankara Wind Tunel.

I would like to thank my family who supported me throughout my life for their trust, understanding and patience.

TABLE OF CONTENTS

LIST OF TABLES

LIST OF FIGURES

LIST OF SYMBOLS

a	Speed of Sound
b	Span
c	Chord length
C_A	Axial Force Coefficient
C_m	Pitching Moment Coefficient
C_N	Normal Force Coefficient
C_l	Roll Moment Coefficient
C_n	Yaw Moment Coefficient
C_Y	Side Force Coefficient
Mach	Mach Number
P_{atm}	Atmospheric pressure
$P_{pito\text{-}tube}$	Test section dynamic pressure
P_{wall}	Wall static pressure difference
Re	Reynolds Number
T	Freestream temperature
V	Velocity
α	Angle of Attack
ρ	Density
μ	Viscosity
ϕ	Roll Angle

Superscripts

T Transpose

Acronyms

AWT Ankara Wind Tunnel
AMS Automated Measurement System
DAS Data Acquisition System
DAC Data Acquisition Card
MSS Model Support System

CHAPTER 1

INTRODUCTION

Wind tunnels are essential tools for experimental aerodynamic studies where real flow effects are observed under the controlled environments. For having productive tests in these experimental facilities, various measurement and control systems must be integrated to the wind tunnels. The raw data obtained from these measurement systems must be acquired, analyzed and stored automatically with the minimum human intervention. In addition, to reduce the number of "the men in the loop" it is desired to have a central computerized data acquisition system that can do the measurement and the control of these systems automatically.

The main subject of this thesis is to establish such a data acquisition system to Ankara Wind Tunnel (AWT) and to write a program that can perform experiments by using this system automatically under the control of a central computer.

AWT is a low subsonic closed circuit wind tunnel whose test section dimensions are 3.05 m in width, 2.44 m in height and 6.10 m in length. The maximum flow velocity is 90 m/s, with approximately a Mach number of 0.3. The drive motor of AWT is a 1000 HP motor (750 kW power). The general layout of AWT is shown in Figure 1, and its technical and geometrical properties are listed below:

1. Test room: 3.05 m x 2.44 m x 6.10 m
2. Diffuser and Safety Screen with 5 degree expansion angle
3. First Turning Vanes Group
4. Propeller and Stator

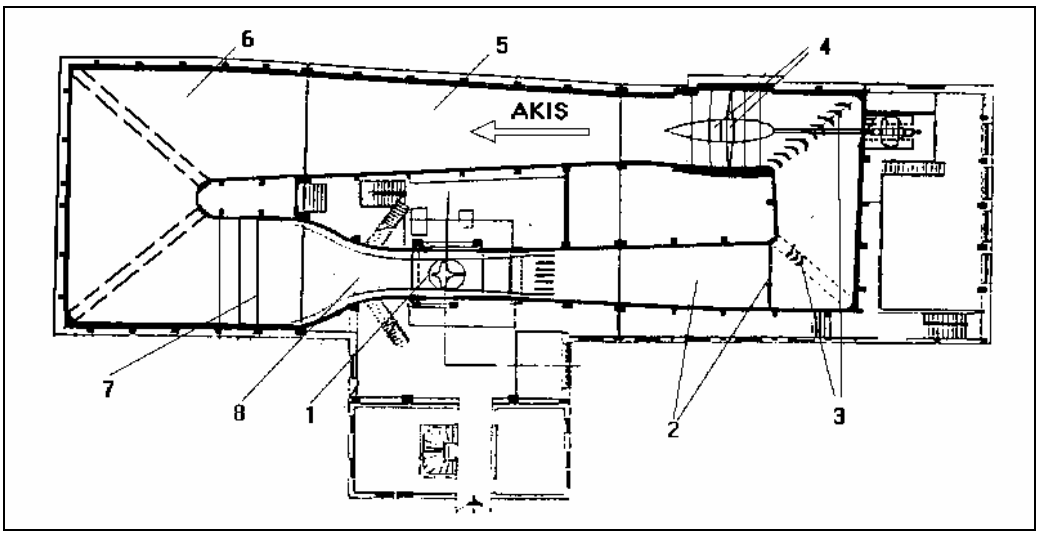

Figure 1 Sketch of AWT

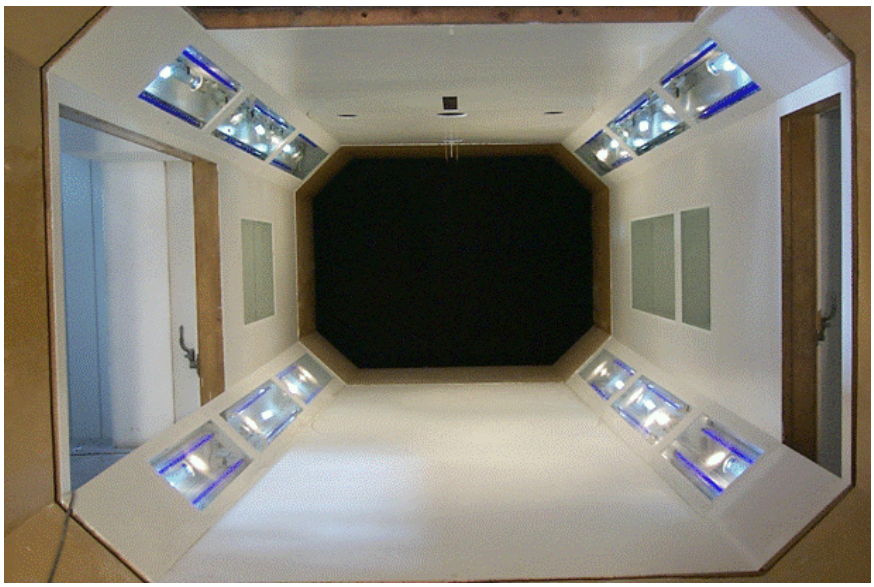

Figure 2 Test Room

5. Pressure Room
6. Second Turning Vanes Group

7. Turbulent Screens
8. Contraction cone with 7.5 contraction ratio (in terms of area)

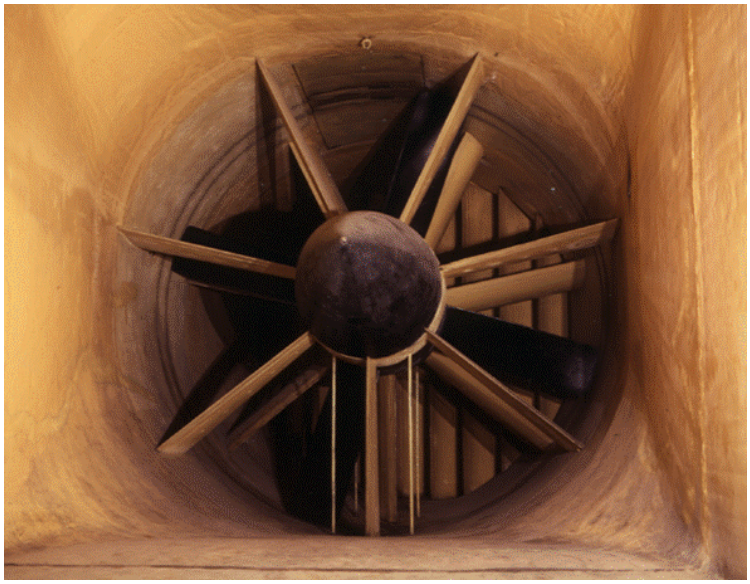

Figure 3 Propeller and Stators

AWT was built between 1946 and 1950 in order to support the Turkish aircraft industry and to have an educational, research and development facility. Unfortunately after construction of AWT, it has never been used untill 1993 when a series of modernization projects were started at TÜBİTAK-SAGE. After completion of its modernization, modification and calibration of the balance system of AWT in 1999 [1], the calibration and instrumentation was performed in 2000. [2]. AWT is operated under TUBITAK-SAGE administration since 2000.

The aim of this thesis is to install a data acquisition system that can perform the experiments automatically under the control of a central computer with a program that is written in LabVIEW programming language. Under the scope of this thesis, following actions are taken:

After the installations of new Data Acquisition Cards, which are the product of National Instruments, the measurement and control systems (Figure 4) integration with this new Data Acquisition System (DAS) was performed and are detailed in Chapter 2

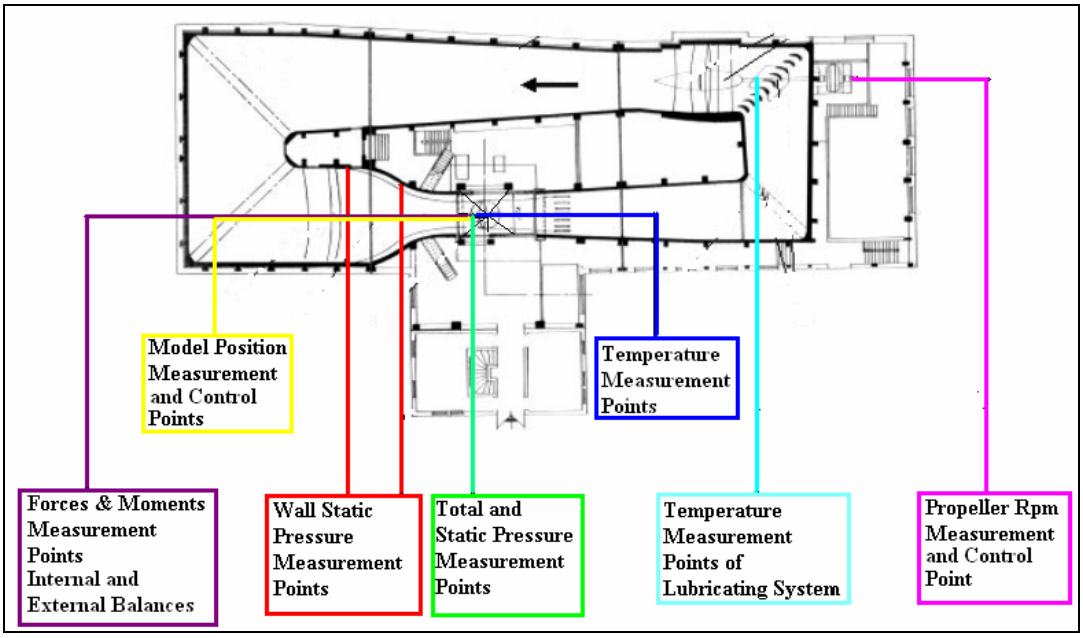

Figure 4 Measurement and Control Points of AWT

In Chapter 3, implementation of the data acquisition unit to the measurement systems is given. After integrating all of old systems of AWT (such as pressure measurement systems and external balance system) to the new DAS and rewritting the data acquisition code which was previously written in "Test Point" programming language [2] with the new LabVIEW programming language, the new systems (such as internal balance system, servo/step motor controller, thermocouple, multi channel pressure measurement system) are integrated to the DAS and the necessary subroutines are all written in LabVIEW programming language. Finally the automatic control of fan driver system is performed and the

final version of Ankara Wind Tunnel – Automated Measurement System program is written.

Chapter 4 is devoted to the test case results. The result of AWT-AMS is compared with measurements performed in NASA Langley Research Center. The base pressure correction, which is a must for the applications with sting type balances, is given and the results of AWT-AMS are represented and compared with the measurements performed in NASA Langley Research Center.

In Chapter 5, the global evaluation of the total study is done, concluding remarks are made and recommendations on the future work are presented.

CHAPTER 2

MEASUREMENT SYSTEMS and MODEL SUPPORT SYSTEM (MSS) of AWT

The pressure and temperature has to be measured in a wind tunnel in order to get the flow parameters like velocity, viscosity, Re number, Mach number, etc. To estimate the aerodynamic loads and moments of the wind tunnel model there must be a measurement system, balance system, that can measure loads and moments by using load cells or strain gages. In addition, there must be a control and a positioning mechanism to give the required angle of attack to the model under the test.

In order to measure these parameters and to give the angle of attack to the model, AWT has:

- 3 Pressure Transducers (1 Absolute, 2 Differential)
- 1 64-Channel Pressure Scanner System
- 4 K-type Thermocouples
- 7 Dynamometer External Balance
- 2 Internal Balance Systems (one with 22 mm and the other with 35 mm internal diameter)
- 3 Servomotors
- 1 Step motor

as the measurement and control devices.

Unfortunately these devices are not enough for having a productive system. The analog outputs of these devices have to be converted into digital data in order to be processed and stored in data files. These can be done with various Analog to Digital (A/D) Converter cards, or the Data Acquisition Cards (DAC).

The DACs of AWT and their usage can be seen in Table 1:

Table 1 DACs and their usage

Main DAC	DAC	Terminal Block	Total Channel #	Used Channel #	Aplication / Measurements
6052E	1140	1301	8	3	Pressure Transducer
	1121	1321	4	2	DC Engine RPM measurements
	1121	1321	4	-	-
	1520	1314	8	7	External Balance
	1520	1314	8	6 1	Internal Balance Pressure Scanner Output
	1163R	1326	32	2 6	DC Engine RPM command Pressure Scanner Command
	1162HV	1326	32	-	-
	1112		8	4	Thermocouple
6024E		SCB68	32	-	-
7344		UMI-7764	4	4	Servo/Step motor

In this chapter short descriptions and technical specifications of these devices and DACs will be presented as the subsystems of AWT.

2.1 PRESSURE MEASUREMENT

Pressure values are the most essential input to get the flow parameters with temperature values. For this reason the atmospheric and dynamic pressure must be measured. In addition there is a multiple pressure measurement system in order to get the surface pressure distribution of the models.

2.1.1 ABSOLUTE PRESSURE MEASUREMENT

To measure the atmospheric pressure in AWT a 0-20 psi SETRA® absolute pressure transducer (Appendix-A) is installed in the control room.

Figure 5 Pressure Transducer and Manometer

2.1.2 DIFFENTIAL PRESSURE MEASUREMENT

The dynamic pressure is estimated by processing both the test section's dynamic pressure and the wall static pressure difference values (Figure 6). To measure these two pressures two SETRA® pressure transducers with a range of ±0.5 psi (Appendix-A) are installed in the control room.

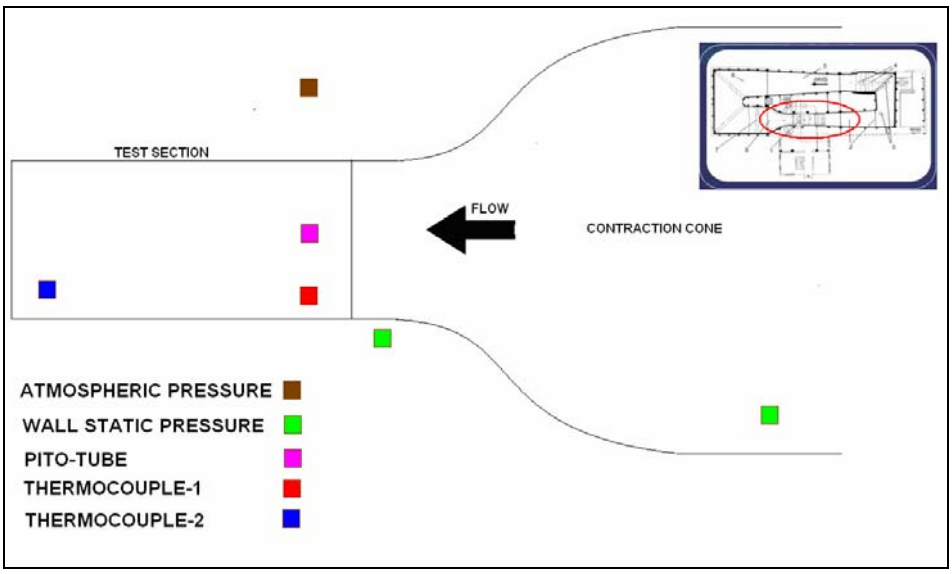

Figure 6 Pressure and Temperature Measurement Locations in AWT

2.1.3 MULTI-CHANNEL PRESSURE MEASUREMENT SYSTEM (PRESSURE SCANNER)

During wind tunnel testing, it is generally desired to measure the pressure distribution along the surface of the aerodynamic model to be tested. When this is the case, a large number of pressures are measured at the same time (or successively). For this purpose there is a 64-Channel Electronic Pressure Transducer [3] at AWT. (Figure 7)

Figure 7 64-Channel Pressure Transducer

2.1.4 DATA ACQUISITION CARD for PRESSURE MEASUREMENTS

Before mentioning about DAC a short description of the Data Acquisition System (DAS) of AWT is given to understand the DAS as a whole. AWT DAS has 3 main PCI cards: PCI-6052E, PCI-7344, and PCI-6024E; 8 Data Acquisition Cards: SCXI-1140, SCXI-1121, SCXI-1520, SCXI-1163R, SCXI-1162HV, SCXI-1112 and 9 Screw Terminals: SCXI-1301, SCXI-1321, SCXI-1314, SCXI-1326, UMI-7764 and SCB-68 which are all the product of National Instruments©.

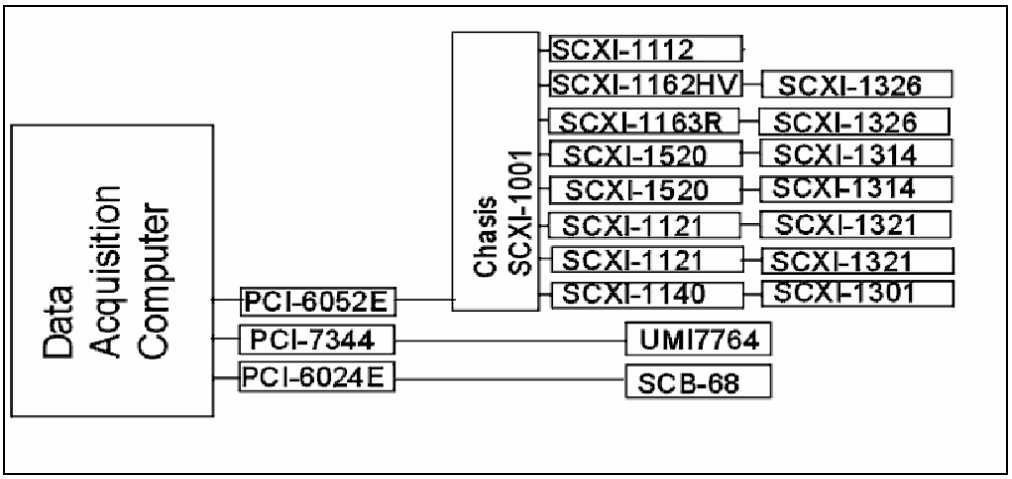

Figure 8 Data Acquisition System

PCI-6052E which is the heart of DAS is a 333 kS/s, 16-Bit, 16-Analog-Input Multifunction DAQ. A 12-slot chassis SCXI-1001 is connected to this PCI card which means that 12 DAC can be installed into this chassis in order to collect data. As seen from Figure 8, 8 DAC with their own terminal blocks are installed to the SCXI-1001 which means that all the data acquisition process is done with PCI-6052E. [4]

PCI-7344 is 4-Axis Stepper/Servo Motor Controller for PCI connection and is used to control the Servo and Step motors in AWT which are used for giving angle of attack to the model or displacement to the transverse mechanisms. [5]

PCI-6024E is a low cost DAQ which is a 200 kS/s, 12-Bit, 16-Analog-Input Multifunction DAQ. 6024E is a backup for 6052E in case of any malfunction of the PCI-6052E. [6]

With some exception there is mostly one DAC with its terminal block for connecting the output cables of measurement devices or command cables of control devices to the DAC. For example, the pressure transducer measurements are performed by using SCXI-1140 with connection terminal block SCXI-1301 and for measurements of pressure scanner SCXI-1520 is used with its terminal block SCXI-1314 as seen from Table 1. (The detailed connection diagram can be seen at Appendix B)

2.1.4.1 SCXI-1140

The SCXI-1140 is a 8-Channel Simultaneous-Sampling Differential Amplifier Module whose technical specifications are given as follows: [7]

- 8 simultaneously sampled input channels
- NI-DAQmx Measurement Services software to simplify configuration and measurements
- ±30 V maximum overvoltage protection, powered on
- Connections for external sample-and-hold timing signal

2.1.4.2 SCXI-1301

The SCXI-1301 is the terminal block for SCXI-1140 whose technical specifications are as follows: [8]

- 20 screw terminals for signal connections
- Shielded for quick, convenient signal connections
- Mounts to front of SCXI module
- Recommended for use with the SCXI-1140/1181/1181K

2.1.4.3 SCXI-1163R

The SCXI-1163R is a 32-Channel Solid State Relay (SSR) module whose technical specifications are as follows:

- 32-Channel Optically Isolated Solid-State Relays
- Eight banks of 4x1(1-wire) multiplexers
- Operating speed of 750 cycles/s
- Fully software programmable
- Switching capacity of 200 mA at 240 VDC/Vrms

2.1.4.4 SCXI-1326

The SCXI-1326 is a High Voltage Screw Terminal Block whose technical specifications are as follows:

- 48-screw terminals for signal connections
- For high-voltage digital input or digital output applications
- Shielded for quick, convenient signal connections
- Mounts to front of SCXI module
- For use with the SCXI-1162/1162HV/1163/1163R

2.2 TEMPERATURE MEASUREMENT

For temperature measurements, 2 K-type thermocouples are installed at the test section of AWT (Figure 6) one at the beginning of the test section and the other at the end of the test section. These two temperature measurements are averaged to get the mean temperature value of the test section.

2.2.1 K-TYPE THERMOCOUPLE

Thermocouples are commonly used temperature sensors because of their low cost, versatility and ruggedness. Thermocouples consist of two different metals joined together, making a continuous circuit. When one junction has a different temperature from the other an electromotive force (voltage) occurs. There are several types of thermocouples, constructed from different metals and with differing temperature ranges and accuracies. K-type thermocouple is a Chromel-Alumel thermocouple with a temperature range of -200 to 1200 ^{o}C.

Figure 9 K-Type Thermocouple and PT-100

2.2.2 Resistor Thermometers

Before using thermocouples in AWT a resistance thermometer system, called PT-100 sensors, are used for measuring the temperature. But after performing some

measurements both with thermocouples and the resistor thermometer (PT-100) some oscillations were observed in the resistor thermometer measurements. (Figure 10)

If one examines these measurement results, it will be observed that the standard deviation of the measurements done with PT-100s is larger than that of the thermocouple measurements. In addition the difference of maximum and minimum values of each PT-100 is about 0.4 °C while this difference is only 0.03 °C for thermocouple measurements. Also forward and backward temperature measurements realized in the AWT test section with PT-100 do not correspond to each other, while the temperatures measured with the thermocouples are in close agreement. (Table 2)

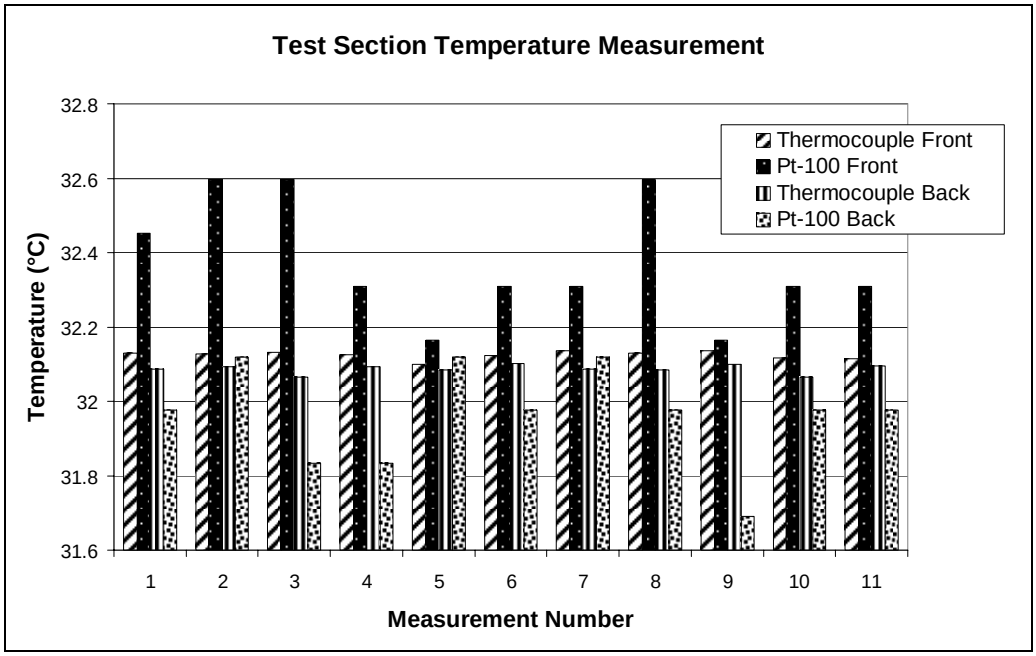

Figure 10 PT-100 Measurements vs. Thermocouple Measurements

Therefore thermocouple measurements are considered to be more reliable and are installed in the test section to measure the temperature of the free stream flow.

Table 2 PT-100 Measurements vs. Thermocouple Measurements

	Thermocouple		Pt-100	
Measurement #	**Front**	**Back**	**Front**	**Back**
1	32.13	32.087	32.452595	31.976373
2	32.128	32.093	32.596705	32.11861
3	32.132	32.065	32.596705	31.834136
4	32.125	32.093	32.308513	31.834136
5	32.1	32.085	32.16443	32.11861
6	32.124	32.101	32.308513	31.976373
7	32.137	32.087	32.308513	32.11861
8	32.129	32.085	32.596705	31.976373
9	32.137	32.1	32.16443	31.691872
10	32.116	32.065	32.308513	31.976373
11	32.115	32.096	32.308513	31.976373
Standard Deviation	0.010925367	0.012222929	0.162558183	0.134260093
Mean	32.12481818	32.087	32.37401227	31.96343991
Max	32.137	32.101	32.596705	32.11861
Min	32.1	32.065	32.16443	31.691872
Difference	0.037	0.036	0.432275	0.426738

2.2.3 DATA ACQUISITION CARD for TEMPERATURE MEASUREMENTS

2.2.3.1 SCXI-1112

SCXI-1112 is an 8-Channel Thermocouple Input Module with technical specifications are as follows: [11]

- Cold-junction compensation per channel
- Onboard calibration reference
- Instrumentation amplifier per channel
- Open thermocouple detection LEDs

2.3 FORCE MEASUREMENT SYSTEMS of AWT

There are two force and moment measurement systems at AWT. These are the external balance (which the balance system is outside of the model) and internal balance (which has two sting type internal balance) systems.

2.3.1 EXTERNAL BALANCE SYSTEM

Designed originally as a purely mechanical system, this system is modified and converted to be an electro-mechanical system with 7 dynamometers installed to the original design. After the completion of the modernization, modification and calibration of the balance system of AWT by Cap. Z. Tolga Yıldız [1], AWT has an operational external balance with 7 dynamometers (Figure 11) each with a load limit of 600 kg. The external balance is located above the test section (at the roof of the test section) (Figure 12) and the model is mounted to the external balance upside down (belly facing upwards) with two struts. [2]

Figure 11 AWT External Balance and Dynamometer # 2

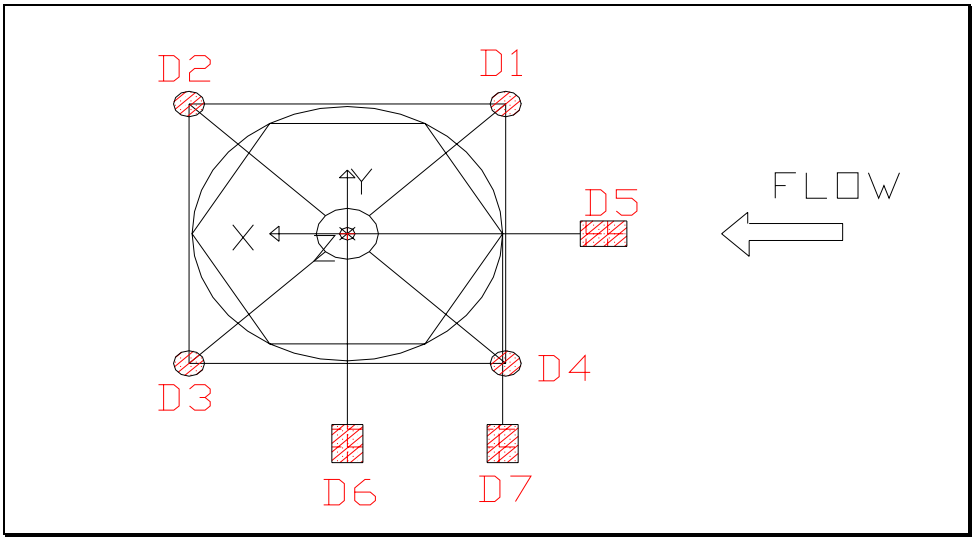

Figure 12 Dynamometers Locations of AWT Balance System

2.3.2 INTERNAL BALANCE SYSTEM

AWT is now equipped with two new internal balances which are 35 mm (Figure 13) and 22 mm in diameter and whose load limits are given in the Table 3.

Figure 13 35 mm Internal Balance

Table 3 Internal Balance Load Limits

Component	35 mm	22 mm
Drag	375 N	80 N
Side Force	1000 N	225 N
Lift	1000 N	225 N
Roll Moment	150 Nm	10 Nm
Pitch Moment	150 Nm	15 Nm
Yaw Moment	100 Nm	15 Nm

2.3.3 DATA ACQUISITION CARD for FORCE MEASUREMENTS

2.3.3.1 SCXI-1520

SCXI-1520 is a pressure, force, load, and torque sensor measurement module with technical specifications as follows: [12]

- 8-channel simultaneous sampling (SSH)
- 0-10 V programmable voltage excitation per channel
- Programmable lowpass filters per channel
- Programmable offset nulling and shunt calibration per channel
- Remote sense feature that ensures accurate voltage excitation to sensor

2.3.3.2 SCXI-1314

The SCXI-1314 is the terminal block for SCXI-1520 whose technical specifications are as follows: [13]

- For use with SCXI-1520 Universal Strain Gauge module
- Socketed resistors (120, 350 Ohm) for quarter-bridge completion
- Socketed shunt calibration resistors (100 kOhm)
- Shielded for quick, convenient signal connections
- Mounts to front of SCXI module

2.4 MODEL SUPPORT SYSTEM

Model Support System (MSS) has two purposes. (Figure 14) One is to mount the model inside the test room and the other is to give the model an angle of attack.

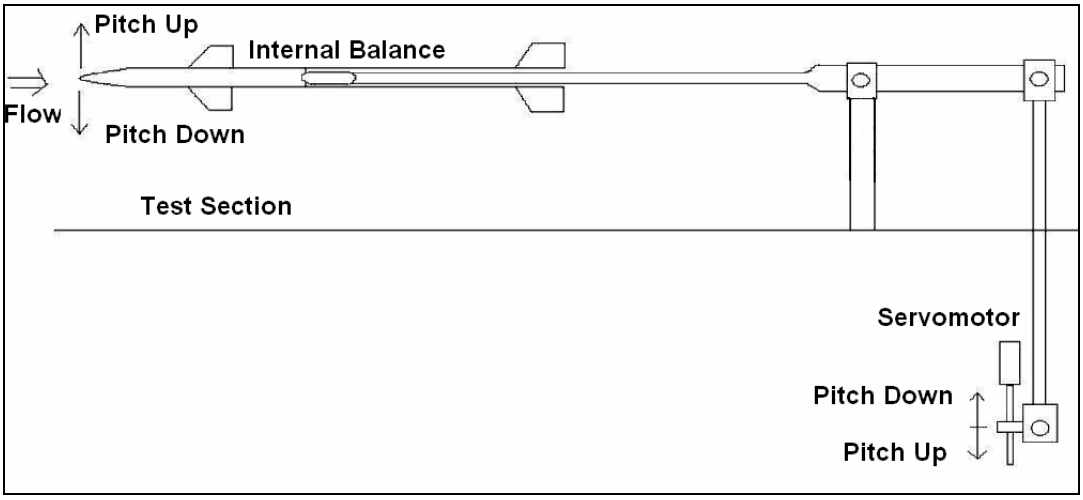

Figure 14 Sketch of MSS

The model is installed inside the test section by means of model arm. The internal balance system is mounted to the front of this model arm whose end is connected to the motion arm which is connected to a screw mechanism which is driven by a servo motor for angle of attack positioning. The main pedestal is connected to the nearly half of the model arm which caries most of the loads. As the servomotor (Figure 15) drives the screw, the motion arm is moving upwards or downwards and the model pitches up or down respectively.

Figure 15 Servomotor and Driver

Figure 16 MSS (Side and Isometric View Respectively)

2.4.1 DATA ACQUISITION CARD at MSS

2.4.1.1 PCI-7344

PCI-7344 is 4-Axis Stepper/Servo Motor Controller for PCI connection card, whose technical specifications are given as follows: [14]

- Blended motion profiles
- Electronic gearing and 2D/3D interpolation
- 4-axis controller, each axis configurable for stepper or DC motor control
- 62 µs PID loop update rate
- Quadrature encoder or analog feedback
- Includes NI-Motion software for Windows 2000/NT/XP/Me/9x

2.4.1.2 UMI-7764

UMI-7764 is the terminal block for PCI-7344 whose technical specifications are given as follows: [15]

- Connects NI 7334/7344 controllers to third-party power drives
- 1 or 20 MHz quadrature encoder rates
- Built-in inhibit logic
- Host bus +5 VDC monitor with built-in driver inhibit control
- Per-axis motion signal breakout

CHAPTER 3

AUTOMATION of MEASUREMENT and CONTROL SYSTEMS

Separate measurement systems are not functional unless having a program that converts all the raw output signals into physically meaningful quantities like pressure, force or temperature. In addition, some functions of AWT like giving angle of attack to the model, rpm command to the fan drive, has to be done automatically under the control of a program to reduce the test time and the man hours in the control room.

For this reason a program, Ankara Wind Tunnel - Automated Measurement System (AWT-AMS), was written in LabVIEW© programming language and all the systems were modified to operate automatically under the control of a central computer system.

3.1 AUTOMATED FLOW PARAMETERS' MEASUREMENTS

The atmospheric pressure, dynamic pressures and temperature are measured automatically by AWT-AMS to get the flow parameters (velocity, Re number, Mach number, viscosity, density, etc,).

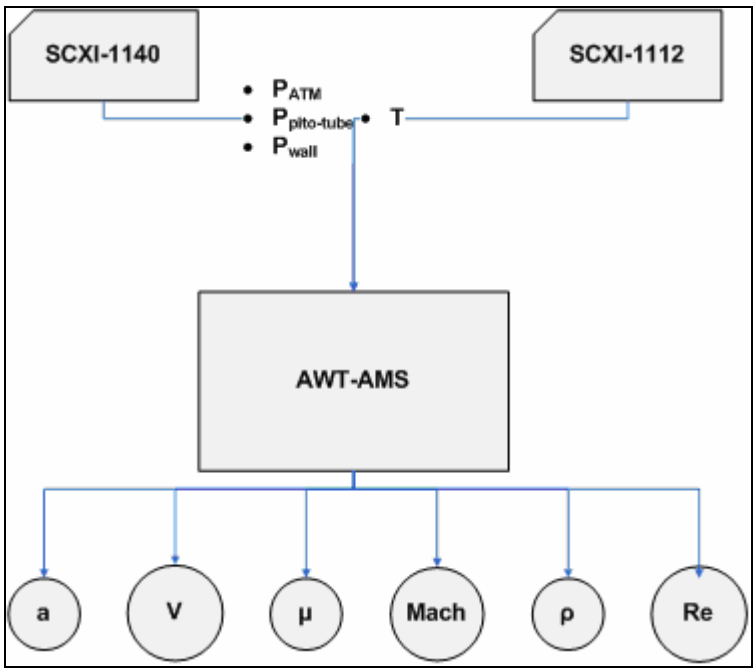

Figure 17 Input and Outputs of Flow Parameters Tool of AWT-AMS

After getting temperature and pressure measurements, various parameters about flow can be calculated automatically as seen in Figure 18. [2]

Where:

T: Freestream temperature

P_{atm}: Atmospheric pressure

$P_{pitot-tube}$: Test section dynamic pressure

P_{wall}: Wall static pressure

a: Speed of sound

Mach: Mach Number

V: Velocity

Re: Reynolds Number

μ: Viscosity

ρ: Density

c: Reference length

d, e, f: Constant

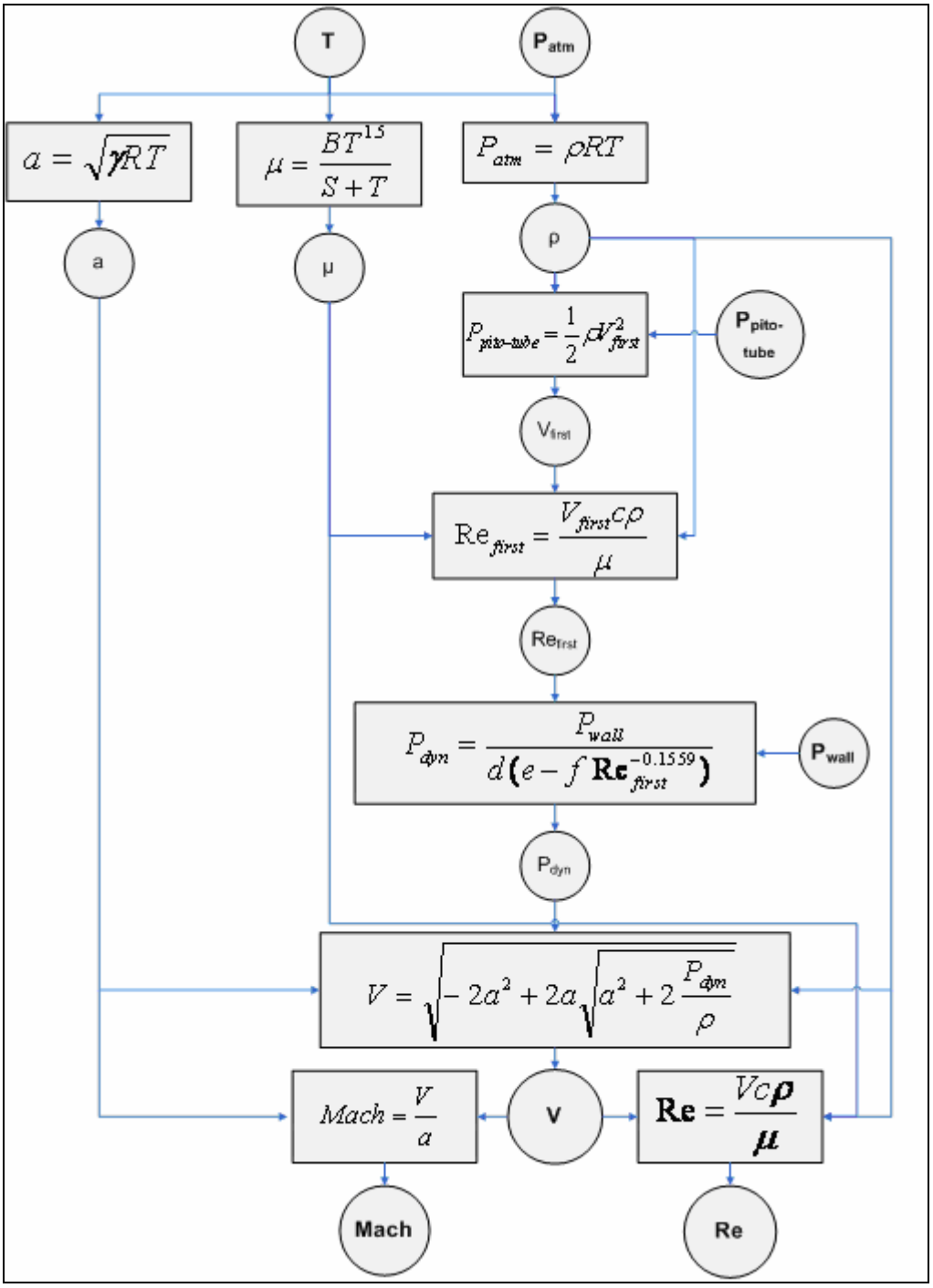

Figure 18 Flow Parameter's Flow Chart

3.2 AUTOMATED FORCE MEASUREMENTS

As mentioned before, to estimate the aerodynamic loads on a model AWT has two balance systems; one is the External Balance System and the other is the Internal Balance System. The output signals of each of these balances are converted to aerodynamic coefficients by using the respective calibration matrices automatically at AWT-AMS. (Figure 19)

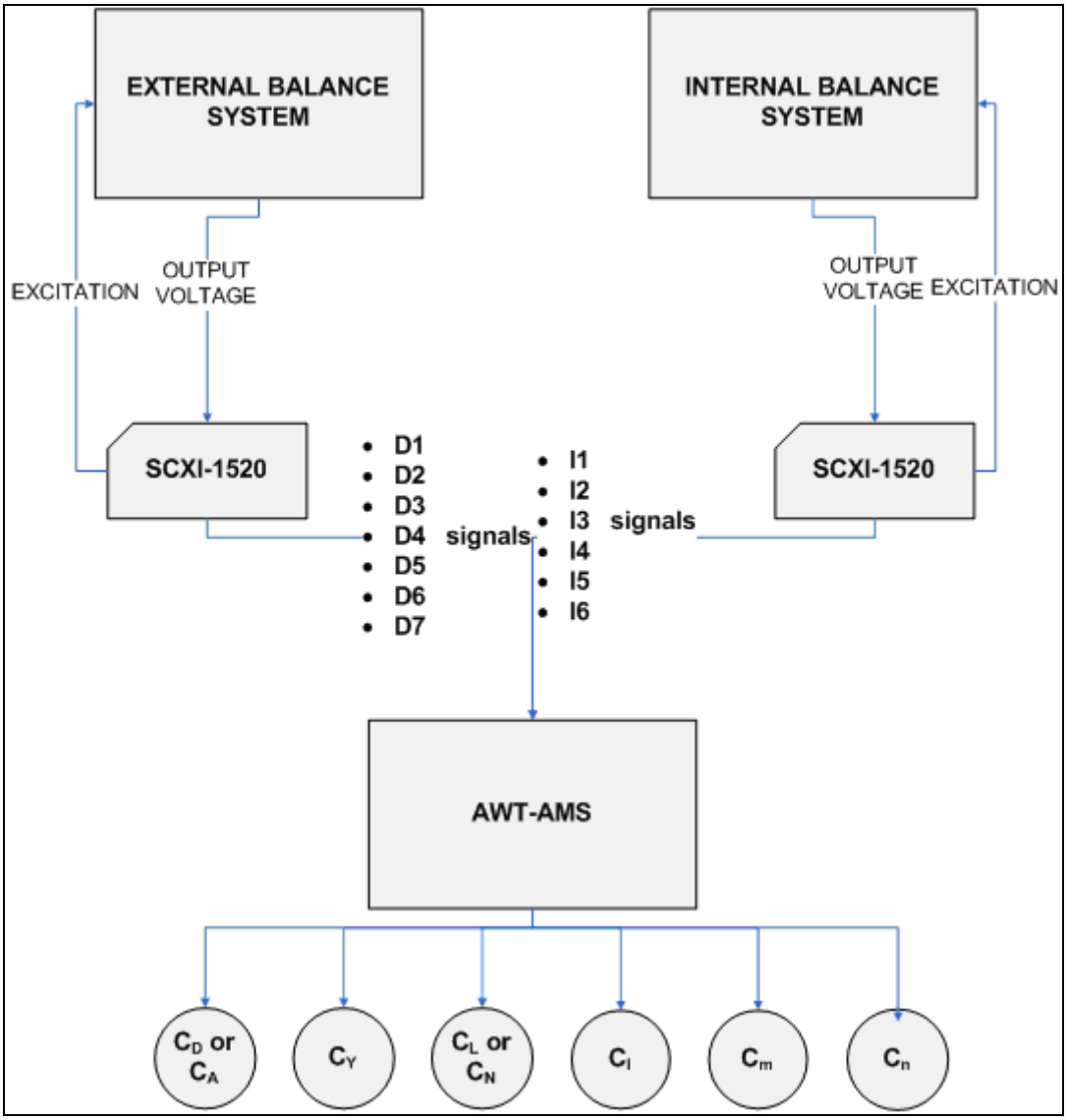

Figure 19 Input and Outputs of Forces and Moments Tool of AWT-AMS

With some differences both External and Internal Balance data acquisition and calculation algorithm are the same. The mean of raw data is taken from balances and after creating a signal matrix, the forces and moments are calculated by multiplying the signal matrix with the calibration matrix. Then the results are displayed and stored as output of the test results.

3.2.1 AUTOMATED EXTERNAL BALANCE MEASUREMENTS

The External Balance [1], [2] has 7 dynamometers whose output signals' (D1, D2, D3, D4, D5, D6, and D7) and their combinations give the 3 forces' and the 3 moments' signal as follows:

R_1=-D5
R_2=-D6
R_3=-(D1 + D2 + D3 + D4)
R_4=-D1 - D2 + D3 + D4)
R_5=-D1 + D2 + D3 - D4)
R_6=-D6 + D7

R_n is the output signal for the relevant component.

where n = 1 to 6:

1= Drag Force
2= Side Force
3= Lift Force
4= Rolling Moment
5= Pitching Moment
6= Yawing Moment

3.2.1.1 CALIBRATION of EXTERNAL BALANCE

In order to get physical meaning of output signals of External Balance; the output signals must be linked with real loads. For this reason, the known loadings are applied to the calibration model (Figure 20 and Figure 21) and the output signals are measured and stored automatically by AWT-AMS. The loadings and their physical meanings are as follows: [2]

$F_X = C - (X1+X2)$	Drag Force
$F_Y = Y1 - Y2$	Side Force
$F_Z = Z1 + Z2 + Z3 + Z4$	Lift Force
$M_X = (Z3 - Z4)\ \Delta y$	Roll Moment
$M_Y = (Z1 - Z2)\ \Delta x$	Pitch Moment
$M_Z = (X1 - X4)\ \Delta y$	Yaw Moment

Where as seen from Figure 20:

Z: the loading basket at Z direction
Y: the loading basket at Y direction
X: the loading basket at X direction
CENTER: the loading basket at the center line
Δy: moment arm at y direction
Δx: moment arm at x direction

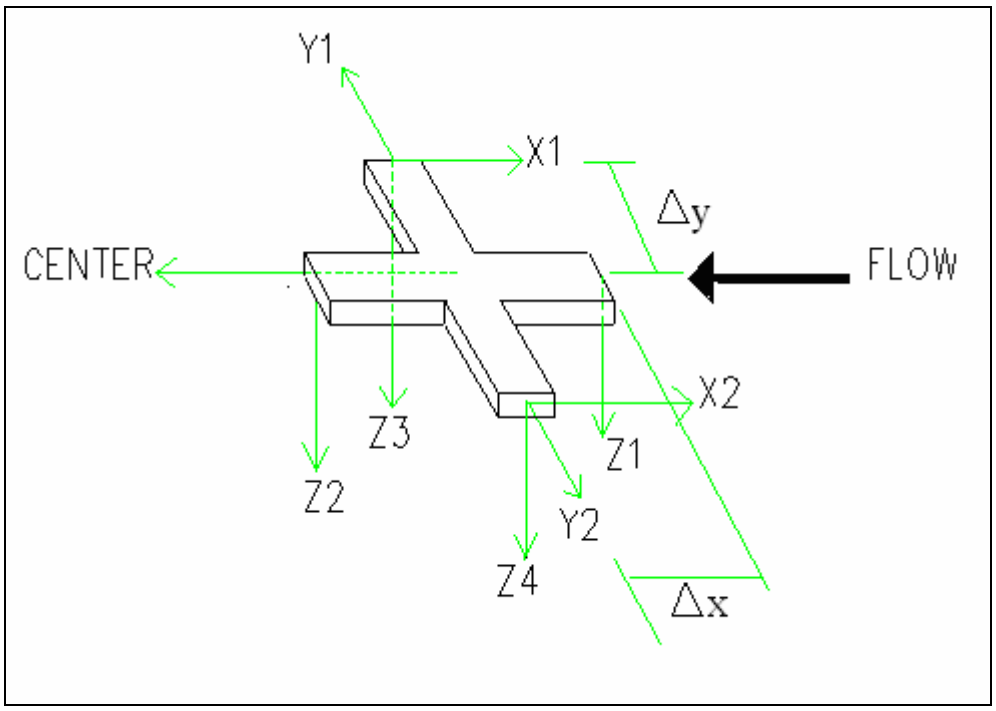

Figure 20 Locations of Loading Baskets at Calibration Model

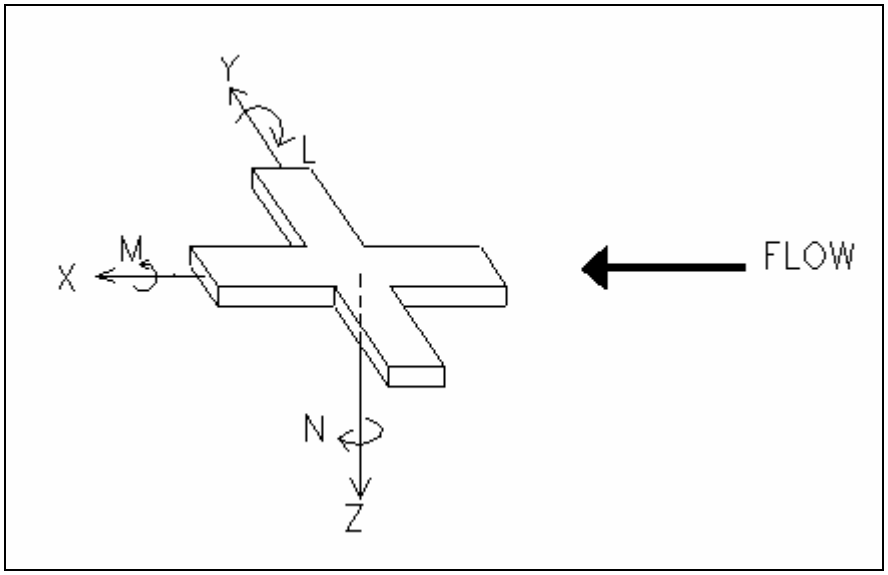

Figure 21 Axis of Calibration Model

Table 4 External Balance Calibration Combination

Pure Lift	Pitch / Yaw
Pure Pitch	Lift / Yaw
Pure Roll	Lift / Drag
Pure Drag	Roll / Drag
Pure Yaw	Pitch / Drag
Pure Side	Side / Yaw
Lift / Roll	Side / Drag
Lift / Pitch	Side / Lift
Pitch / Roll	Side / Lift
Drag / Yaw	Side / Roll
Roll / Yaw	

3.2.1.2 MATHEMATICAL INTERPRETATION of CALIBRATION COEFFICIENTS

After loading the known loadings with different combinations given in Table 4 and storing the corresponding output signals, the relation between the loadings and signals namely "Calibration Matrix" is obtained by using CalibMat program which is written in Matlab© programming language. [16]

Finally after getting the output signals from the dynamometers of the external balance, the aerodynamic loads on the model can be calculated by using the following relations automatically by AWT-AMS. (Appendix C)

$$[L]_{l\times 6} = [R]_{l\times N} \cdot [X]_{N\times 6}$$

Where N is the coefficient number:

- N=6 First order with 6 coefficients
- N=27 Second order with 27 coefficients
- N=33 Third order with 33 coefficients
- N=84 Second order with 84 coefficients
- N=96 Third order with 96 coefficients

L is the Loading hence 3 Forces and 3 Moments.

$$[L]_{1\times 6} = [F_X \quad F_Y \quad F_Z \quad M_X \quad M_Y \quad M_Z]^T$$

R is the Output Signal Matrix.

X is the Calibration Matrix.

Note that:

1. N gives the calibration matrix coefficient number. The bigger N means that the order of the calibration matrix is bigger.
2. When there is an interaction between the system components, the order of the calibration matrix is getting bigger to compensate for these interactions.

3.2.1.3 VERIFICATION RESULTS

To verify the calibration matrix (which is a 3rd order with 96 coefficients) a few loading are applied and the measured forces and moments are compared with the applied loadings. The verification loadings are applied as pure loads and 3-combinations loads or 6-component loads.

Pure loading results are given in Figure 22 to Figure 27. When the results are investigated (Table 5-Table 13) it is seen that Lift Force is the most accurate one (Error is about %1) while the yaw moment results are the worst (%20 error) but note that the applied loads are very low when compare with the limits (600 kg) of

each dynamometer. In addition to the Lift Force the Roll Moments values are as accurate as Lift Forces (Error is about %1). The Drag Force and Pitch Moment errors are in the range of % 5 while the Error of the Side Force is about % 10.

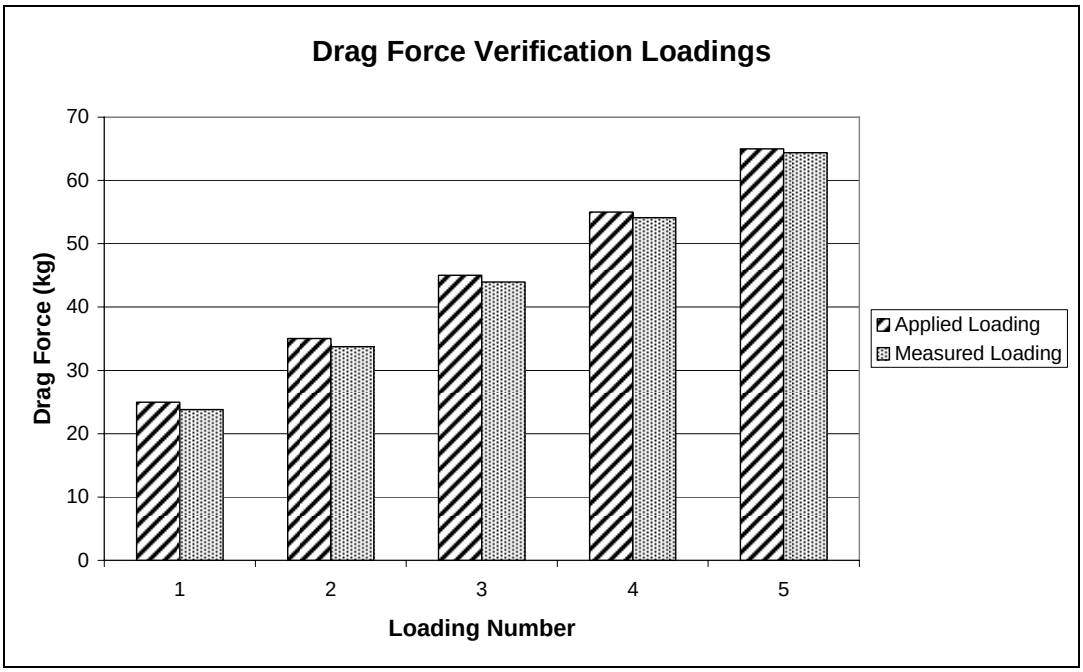

Figure 22 Drag Force Verification Results (Pure Loading)

Table 5 Drag Force Verification Results with Errors

Loading Number	1	2	3	4	5
Applied	25	35	45	55	65
Measured	23.79	33.75	43.98	54.11	64.41
Error %	4.85	3.56	2.27	1.63	0.91

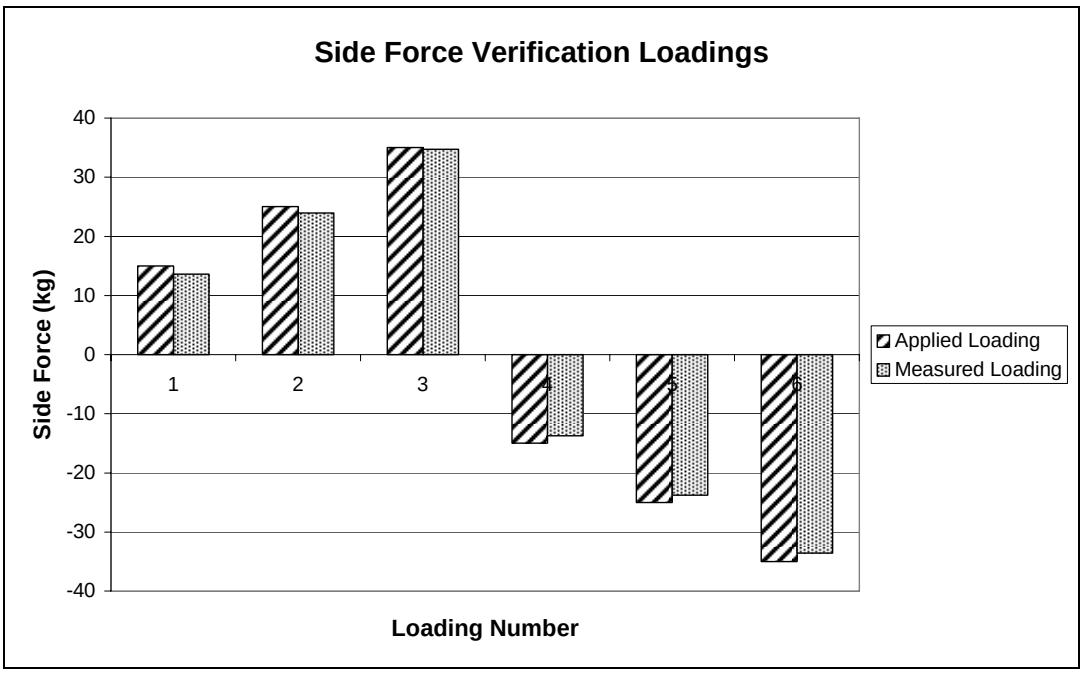

Figure 23 Side Force Verification Results (Pure Loading)

Table 6 Side Force Verification Results with Errors

Loading Number	1	2	3	4	5	6
Applied	15	25	35	-15	-25	-35
Measured	13.60	23.94	34.69	-13.71	-23.76	-33.56
Error %	9.34	4.25	0.89	-8.61	-4.96	-4.12

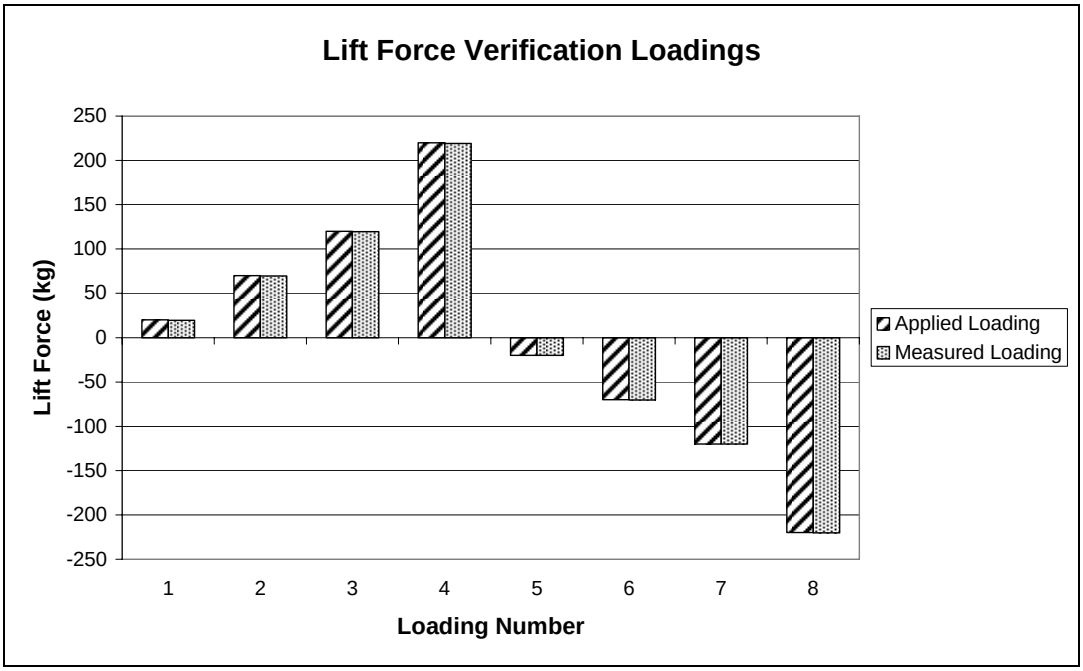

Figure 24 Lift Force Verification Results (Pure Loading)

Table 7 Lift Force Verification Results with Errors

Loading Number	1	2	3	4
Applied	20	70	120	220
Measured	19.62	69.61	119.36	219.13
Error %	1.90	0.55	0.53	0.39
Loading Number	5	6	7	8
Applied	-20	-70	-120	-220
Measured	-20.06	-70.21	-120.12	-220.41
Error %	-0.31	-0.30	-0.10	-0.18

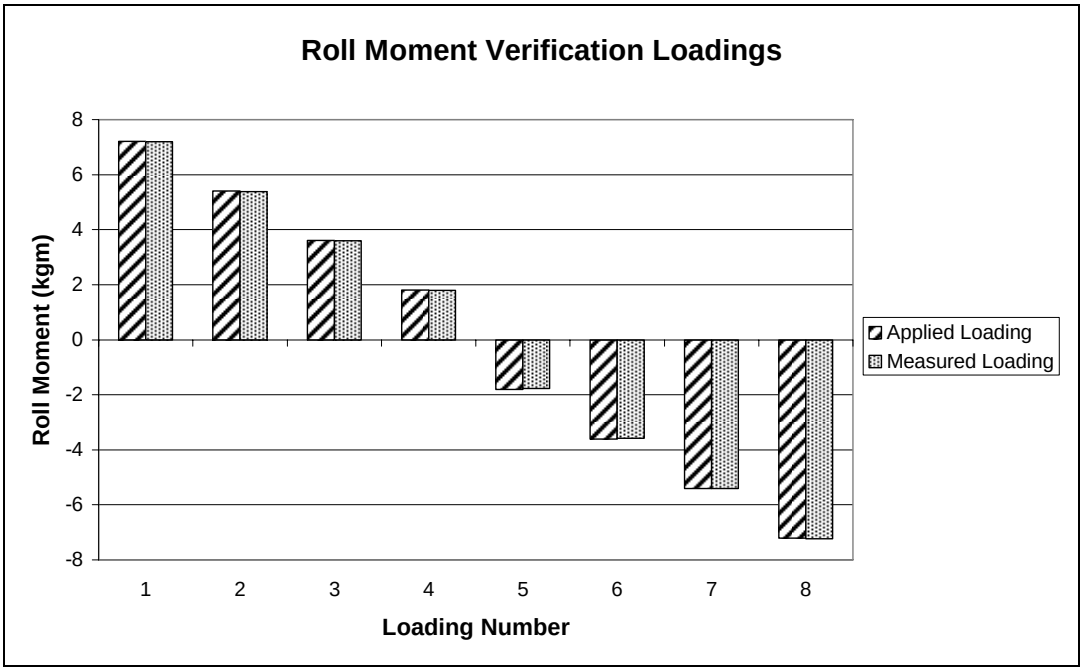

Figure 25 Roll Moment Verification Results (Pure Loading)

Table 8 Roll Moment Verification Results with Errors

Loading Number	1	2	3	4
Applied	7.208	5.406	3.604	1.802
Measured	7.201	5.381	3.590	1.799
Error %	0.091	0.460	0.392	0.154
Loading Number	5	6	7	8
Applied	-1.802	-3.604	-5.406	-7.208
Measured	-1.774	-3.584	-5.414	-7.228
Error %	-1.577	-0.544	-0.141	-0.274

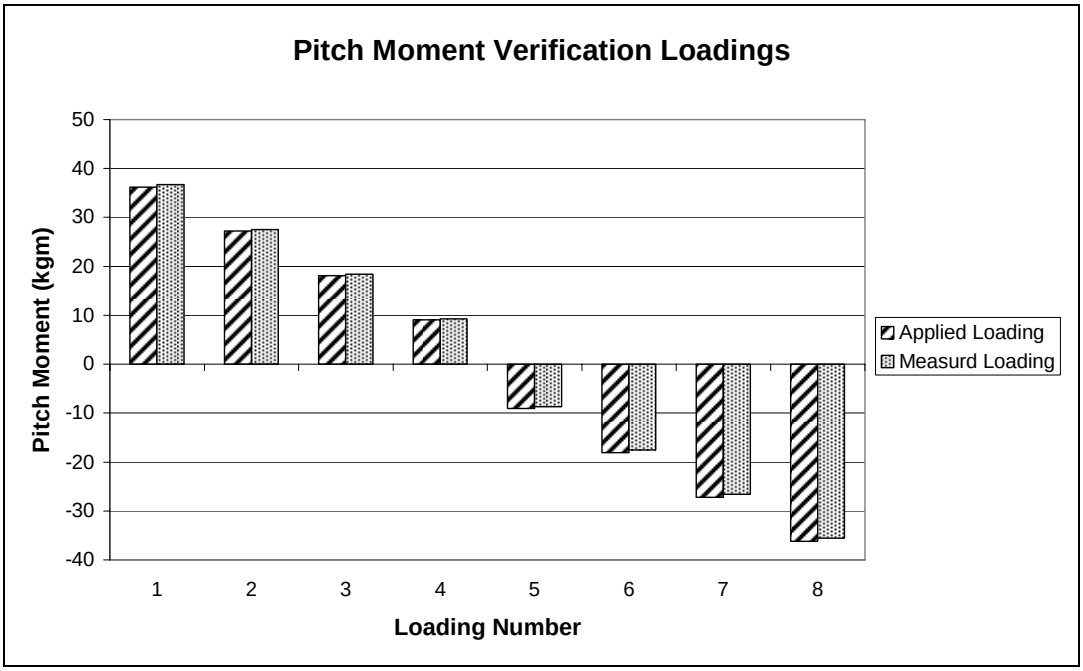

Figure 26 Pitch Moment Verification Results (Pure Loading)

Table 9 Pitch Moment Verification Results with Errors

Loading Number	1	2	3	4
Applied	36.2	27.2	18.1	9.06
Measured	36.704	27.509	18.431	9.293
Error %	1.393	1.135	1.831	2.570
Loading Number	5	6	7	8
Applied	-9.06	-18.1	-27.2	-36.2
Measured	-8.682	-17.548	-26.578	-35.546
Error %	-4.175	-3.050	-2.287	-1.805

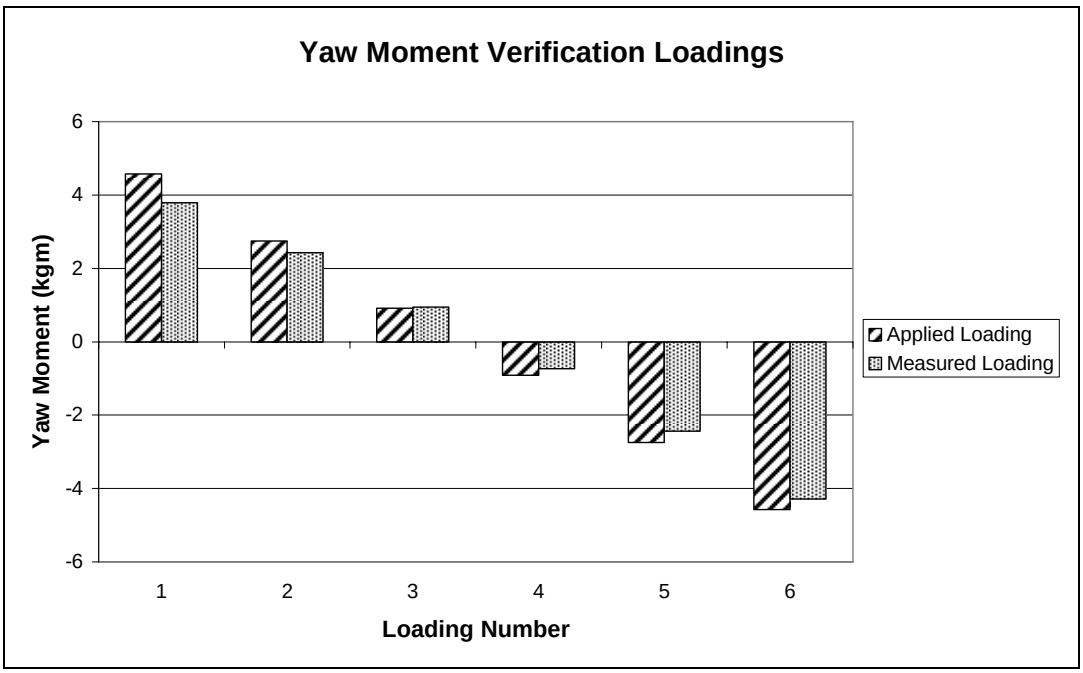

Figure 27 Yaw Moment Verification Results (Pure Loading)

Table 10 Yaw Moment Verification Results with Errors

Loading Number	1	2	3	4	5	6
Applied	4.57	2.74	0.91	-0.91	-2.74	-4.57
Measured	3.788	2.432	0.945	-0.734	-2.441	-4.287
Error %	17.105	11.242	3.826	-19.307	-10.923	-6.186

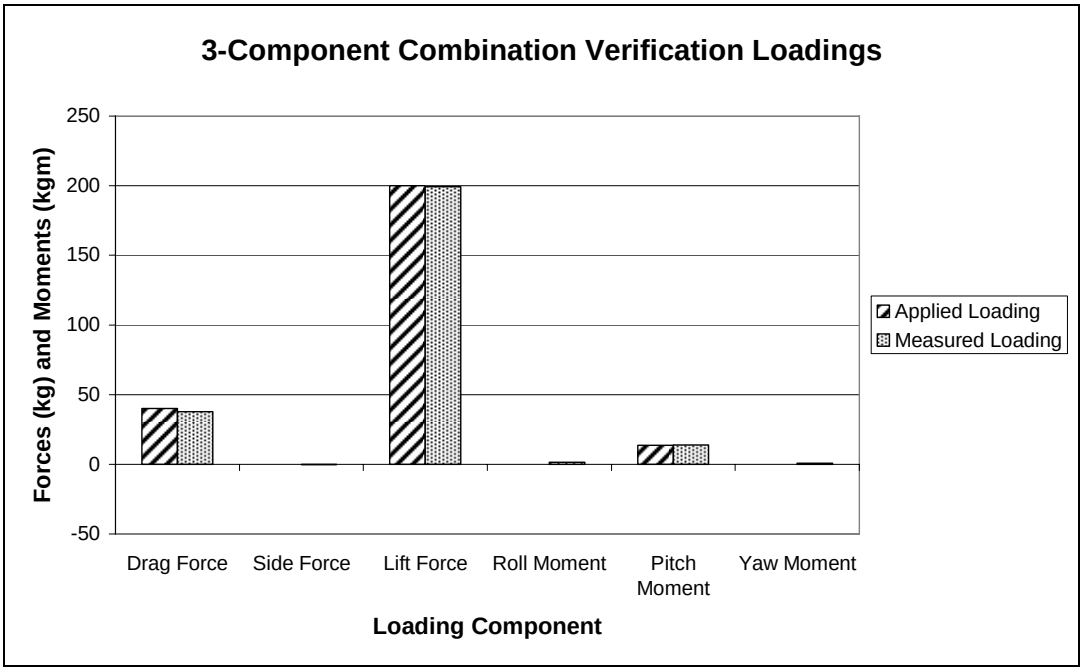

Figure 28 3-Component Loadings Verification Result

Table 11 3-Component Verification Results with Errors

Comp.	Drag Force	Side Force	Lift Force	Roll Moment	Pitch Moment	Yaw Moment
Applied	40	0	200	0	13.5825	0
Measured	37.822	-0.255	199.409	1.457	13.725	0.800
Error %	5.445	-	0.296	-	1.051	-

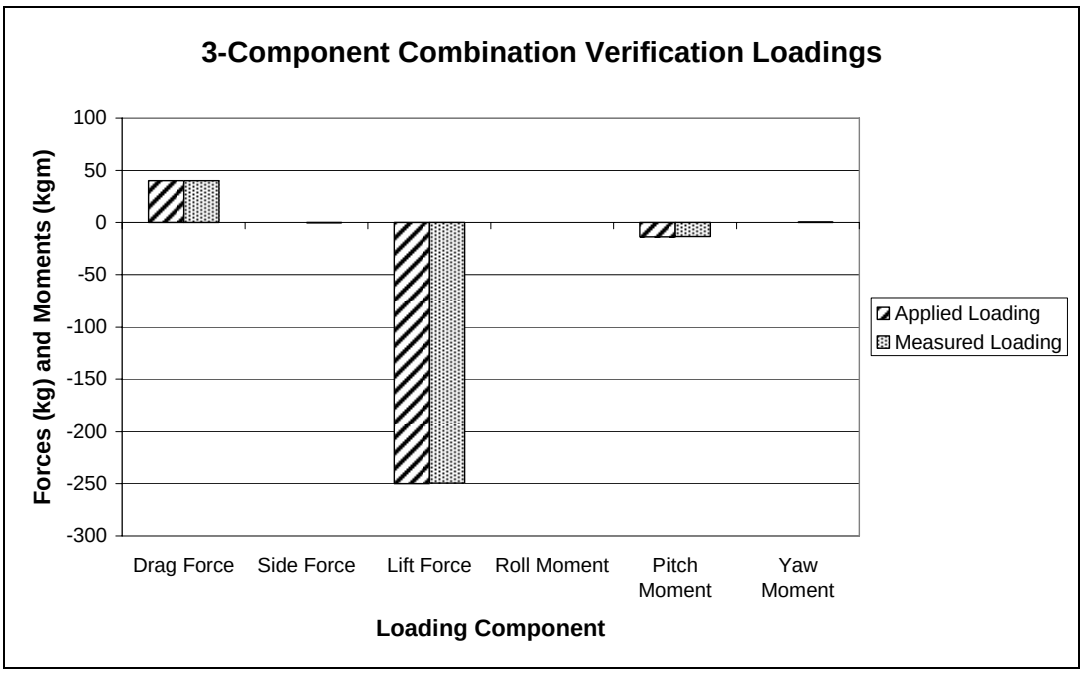

Figure 29 3-Component Loadings Verification Result

Table 12 3-Component Verification Results with Errors

Comp.	Drag Force	Side Force	Lift Force	Roll Moment	Pitch Moment	Yaw Moment
Applied	40	0	-250	0	-13.5825	0
Measured	40.174	-0.327	-249.450	0.027	-13.371	0.433
Error %	0.435	-	-0.220	-	-1.558	-

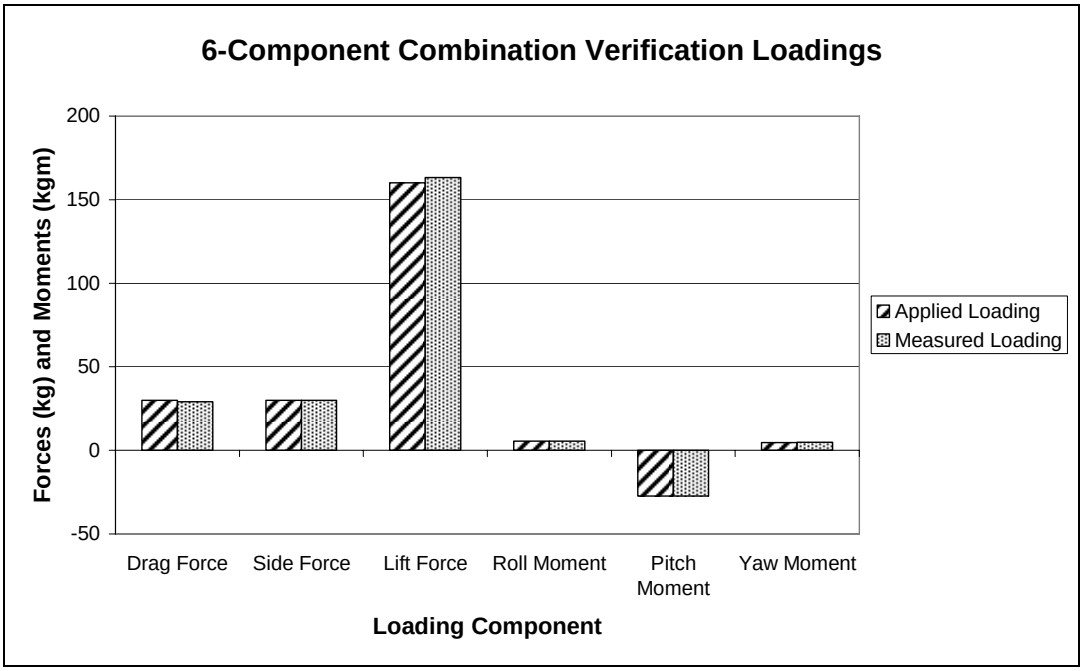

Figure 30 6-Component Loadings Verification Result

Table 13 6-Component Verification Results with Errors

Comp.	Drag Force	Side Force	Lift Force	Roll Moment	Pitch Moment	Yaw Moment
Applied	30	30	160	5.406	-27.2	4.57
Measured	29.114	29.916	163.231	5.519	-27.195	4.907
Error %	2.955	0.281	2.019	2.096	-0.018	7.385

3.2.2 AUTOMATED INTERNAL BALANCE MEASUREMENTS

Both 22 mm (Figure 95) and 35 mm (Figure 96) internal balances have 6 Wheatstone Strain-gage pairs whose output signals' (I1, I2, I3, I4, I5, and I6) give the 3 forces' and the 3 moments' signals as follows:

$R_1 = I1$

$R_2 = I2$

$R_3 = I3$

$R_4 = I4$

$R_5 = I5$

$R_6 = I6$

R_n is the output signal for the relevant component.

where n = 1 to 6:

1	=	Axial Force
2	=	Side Force
3	=	Normal Force
4	=	Rolling Moment
5	=	Pitching Moment
6	=	Yawing Moment

Note that while the External Balance system gives Drag Force and Lift Force, the Internal Balance system gives Axial and Normal Force as shown in Figure 92. This is one of the main differences between the two balance systems.

3.2.2.1 MATHEMATICAL INTERPRETATION of CALIBRATION COEFFICIENTS

The calibration matrix for internal balance system is a second order with 27 coefficients matrix while the external balance system uses third order with 96 coefficients. Because the interaction for internal balance is lower than that of the external balance system, a lower order with fewer coefficients is enough for calculating the forces and the moments on the internal balance system.

$$
\begin{aligned}
L(n) = {} & R_1 X_{n1} + R_2 X_{n2} + R_3 X_{n3} + R_4 X_{n4} + R_5 X_{n5} + R_6 X_{n6} + \\
& R_{11} X_{n11} + R_{22} X_{n22} + R_{33} X_{n33} + R_{44} X_{n44} + R_{55} X_{n55} + R_{66} X_{n66} + \\
& R_{12} X_{n12} + R_{13} X_{n13} + R_{14} X_{n14} + R_{15} X_{n15} + R_{16} X_{n16} \\
& R_{23} X_{n23} + R_{24} X_{n24} + R_{25} X_{n25} + R_{26} X_{n26} \\
& R_{34} X_{n34} + R_{35} X_{n35} + R_{36} X_{n36} \\
& R_{45} X_{n45} + R_{46} X_{n46} \\
& R_{56} X_{n56}
\end{aligned}
\qquad \textbf{(3.1)}
$$

where n = 1 to 6:

1= Axial Force

2= Side Force

3= Normal Force

4= Rolling Moment

5= Pitching Moment

6= Yawing Moment

L(n): is the calculated aerodynamic load, kg or kgm.

R_n: is the output signal for the relevant component.

X_{nm}: is a calibration coefficient within the overall equation.

M: specifies the axis or axes from which the coefficient was derived.

The full calibration matrix for a 6 component balance consists of 6 columns and 27 rows and is shown on Equation 3.2. The 27 coefficients in each column are those which are required for the full determination of one aerodynamic load.

Table 14 shows an example calibration matrix for a 6 component balance. This matrix consists of 6 columns and 27 rows, but some of these terms in the overall matrix may be determined as zero or insignificant. The first column beginning with 308.47, -1.9464, etc, contains all the coefficients to determine the Drag in kg. Similarly, the second column contains all the coefficients for Side Force, the third

column for Lift, the fourth for Roll Moment, fifth for Pitch Moment and sixth for Yaw Moment.

To the left hand side of the table is a column of one or two digit number. These refer to signal output channel. The signal channels are numbered 1 to 6. (1 = Drag, 2 = Side, 3 = Lift, 4 = Roll, 5 = Pitch, 6 = Yaw)

$$\begin{vmatrix} R_1 \\ R_2 \\ R_3 \\ R_4 \\ R_5 \\ R_6 \\ R_{11} \\ R_{22} \\ R_{33} \\ R_{44} \\ R_{55} \\ R_{66} \\ R_{12} \\ R_{13} \\ R_{14} \\ R_{15} \\ R_{16} \\ R_{23} \\ R_{24} \\ R_{25} \\ R_{26} \\ R_{34} \\ R_{35} \\ R_{36} \\ R_{45} \\ R_{46} \\ R_{56} \end{vmatrix}^T \times \begin{vmatrix} X_{11} & X_{21} & X_{31} & X_{41} & X_{51} & X_{61} \\ X_{12} & X_{22} & X_{32} & X_{42} & X_{52} & X_{62} \\ X_{13} & X_{23} & X_{33} & X_{43} & X_{53} & X_{63} \\ X_{14} & X_{24} & X_{34} & X_{44} & X_{54} & X_{64} \\ X_{15} & X_{25} & X_{35} & X_{45} & X_{55} & X_{65} \\ X_{16} & X_{26} & X_{36} & X_{46} & X_{56} & X_{66} \\ X_{111} & X_{211} & X_{311} & X_{411} & X_{511} & X_{611} \\ X_{122} & X_{222} & X_{322} & X_{422} & X_{522} & X_{622} \\ X_{133} & X_{233} & X_{333} & X_{433} & X_{533} & X_{633} \\ X_{144} & X_{244} & X_{344} & X_{444} & X_{544} & X_{644} \\ X_{155} & X_{255} & X_{355} & X_{455} & X_{555} & X_{655} \\ X_{166} & X_{266} & X_{366} & X_{466} & X_{566} & X_{666} \\ X_{112} & X_{212} & X_{312} & X_{412} & X_{512} & X_{612} \\ X_{113} & X_{213} & X_{313} & X_{413} & X_{513} & X_{613} \\ X_{114} & X_{214} & X_{314} & X_{414} & X_{514} & X_{614} \\ X_{115} & X_{215} & X_{315} & X_{415} & X_{515} & X_{615} \\ X_{116} & X_{216} & X_{316} & X_{416} & X_{516} & X_{616} \\ X_{123} & X_{223} & X_{323} & X_{423} & X_{523} & X_{623} \\ X_{124} & X_{224} & X_{324} & X_{424} & X_{524} & X_{624} \\ X_{125} & X_{225} & X_{325} & X_{425} & X_{525} & X_{625} \\ X_{126} & X_{226} & X_{326} & X_{426} & X_{526} & X_{626} \\ X_{134} & X_{234} & X_{334} & X_{434} & X_{534} & X_{634} \\ X_{135} & X_{235} & X_{335} & X_{435} & X_{535} & X_{635} \\ X_{136} & X_{236} & X_{336} & X_{436} & X_{536} & X_{636} \\ X_{145} & X_{245} & X_{345} & X_{445} & X_{545} & X_{645} \\ X_{146} & X_{246} & X_{346} & X_{446} & X_{546} & X_{646} \\ X_{156} & X_{256} & X_{356} & X_{456} & X_{556} & X_{656} \end{vmatrix} = \begin{vmatrix} L_1 \\ L_2 \\ L_3 \\ L_4 \\ L_5 \\ L_6 \end{vmatrix}^T \quad \textbf{(3.2)}$$

Table 14 Calibration Matrix Example

	1	2	3	4	5	6	
1	308.47	0.1314	1.1547	-0.5738	-0.0182	-0.2350	SECTION 1 PRIMARY TERMS
2	-1.9464	25.1754	-1.7114	0.0484	-0.0755	-0.1770	
3	0.5399	-0.003	104.597	-0.0317	0.0342	0.0058	
4	-3.2453	0.0187	0.1605	147.76	-0.164	0.0617	
5	-0.1077	-0.2918	-1.1421	0.6351	13.465	-0.0230	
6	1.9420	-0.3228	-0.6459	-1.5732	0.0195	10.7415	
11	0.0500	-0.0006	0.0433	0.0147	-0.0011	-0.0038	SECTION 2 SQUARED TERMS
22	0.0456	0	-0.0228	0.0031	-0.0020	-0.0059	
33	0.0050	-0.0011	-0.0008	-0.0189	-0.0002	-0.0008	
44	-0.0074	-0.0004	0.0134	-0.0155	0.0007	-0.0023	
55	0.0076	-0.0013	0.0034	-0.0270	0.0015	-0.0039	
66	0.0319	-0.0007	-0.0331	-0.0229	-0.0002	0.0013	
12	-0.0193	-0.0046	-0.0876	0.0180	-0.0014	-0.0030	SECTION 3 CROSS-PRODUCT TERMS
13	-0.0076	-0.0010	0.0592	-0.0002	0.0002	-0.0001	
14	-0.0004	-0.0002	-0.0003	0.0038	-0.0009	-0.0086	
15	0.0330	0.0004	0.0030	-0.0064	0	-0.0097	
16	0.0124	0.0002	0.0025	-0.0982	-0.0026	-0.0019	
23	0.0192	0.0006	0.0002	0	0	-0.0003	
24	0.0349	0.0015	0.0004	-0.0279	0.0005	-0.0121	
25	0.0618	0.0023	-0.0002	-0.0209	-0.0006	-0.0087	
26	-0.0009	-0.0010	0.0019	-0.0528	-0.0046	-0.0050	
34	-0.0036	-0.0001	-0.0015	-0.0045	-0.0009	0	
35	-0.0031	-0.0004	-0.0011	0.0234	0.0007	0	
36	0.0001	0.0001	0.0001	0.0034	0.0001	-0.0004	
45	-0.0155	-0.0003	-0.0368	-0.0417	-0.0003	-0.0056	
46	0.0393	0.0014	-0.64	-0.0046	0.0001	-0.0007	
56	0.032	0.0006	-0.0510	-.0071	-0.0002	0.0003	

Note that:

1. The primary calibration coefficients for each component are shown as the largest value coefficient in each column in section 1 (i.e. the "leading diagonal")
2. Section 1 interactions are significantly smaller than the primary coefficients.
3. Squared and Cross Product terms look very small, however they are multiplied by larger output signal values (i.e. $Lift^2$, Lift * Pitch or Side Force * Drag outputs, etc)

3.2.2.2 ELECTRICAL INTERFACE

Internal balances require a nominal 10V excitation supply voltage to each bridge which can be monitored permanently using the installed sense wires. This allows normalized outputs to be used prior to application of the calibration matrix. The resistance of each bridge is nominally 1000Ω.

The sting balances are fitted with standard leadwire cables that have 36 cores, each being 7/0.1mm, and include overall screen and protective sleeve. Nominal external diameter is 7.2mm.

The balances are identically wired and the cable identification and functions are shown in Table 15.

Table 15 Cable Identification and Functions

Component	Cable Function	Color Coding
Fx Drag	+ Signal	Red

Component	Cable Function	Color Coding
Fx Drag	- Signal	Blue
Fx Drag	+ Excitation	Red / Black
Fx Drag	- Excitation	White / Brown
Fx Drag	+ Sense	Red / Brown
Fx Drag	- Sense	Brown / Black
Fy Side Force	+ Signal	Orange
Fy Side Force	- Signal	Brown
Fy Side Force	+ Excitation	Yellow / Blue
Fy Side Force	- Excitation	Grey / Green
Fy Side Force	+ Sense	White / Blue
Fy Side Force	- Sense	Yellow / Brown
Fz Lift	+ Signal	Green
Fz Lift	- Signal	Yellow
Fz Lift	+ Excitation	Red / Blue
Fz Lift	- Excitation	Violet / Black
Fz Lift	+ Sense	Green / Red
Fz Lift	- Sense	White / Violet
Mx Roll Moment	+ Signal	Pink
Mx Roll Moment	- Signal	Turquoise
Mx Roll Moment	+ Excitation	Yellow / Green
Mx Roll Moment	- Excitation	Orange / Green
Mx Roll Moment	+ Sense	White / Green
Mx Roll Moment	- Sense	Green / Blue
My Pitch Moment	+ Signal	White
My Pitch Moment	- Signal	Black
My Pitch Moment	+ Excitation	Yellow / Red
My Pitch Moment	- Excitation	Grey / Brown
My Pitch Moment	+ Sense	White / Red
My Pitch Moment	- Sense	Yellow / Violet

Component	Cable Function	Color Coding
Mz Yaw Moment	+ Signal	Violet
Mz Yaw Moment	- Signal	Grey
Mz Yaw Moment	+ Excitation	Blue / Black
Mz Yaw Moment	- Excitation	Grey / Blue
Mz Yaw Moment	+ Sense	Orange / Blue
Mz Yaw Moment	- Sense	Green / Black
Not Connected	Screen	Braid

3.2.2.3 CALIBRATION SLEEVE and RIG

The Sting Balances are calibrated using the Aerotech Calibration Rig and standard in-house practice for load application. Figure 94 shows the sketch of calibration rig that is used for the calibration of the two Sting Balances.

The assembled Calibration Body has precision-machined flats along its length at each quadrant. The sleeve has three toleranced loading holes on each flat, one positioned in line with the Balance centre line for applying Lift and Side Forces loads and two outboard holes for loading of Pitch and Yaw Moments.

The Roll Loading Arm fits around the Calibration Body and is positioned onto the Lift / Side Force loading points. Two outboard toleranced loading holes exist for applying the Roll Moment.

Figure 31 Calibration Sleeve and Rig with Calibration Apparatus

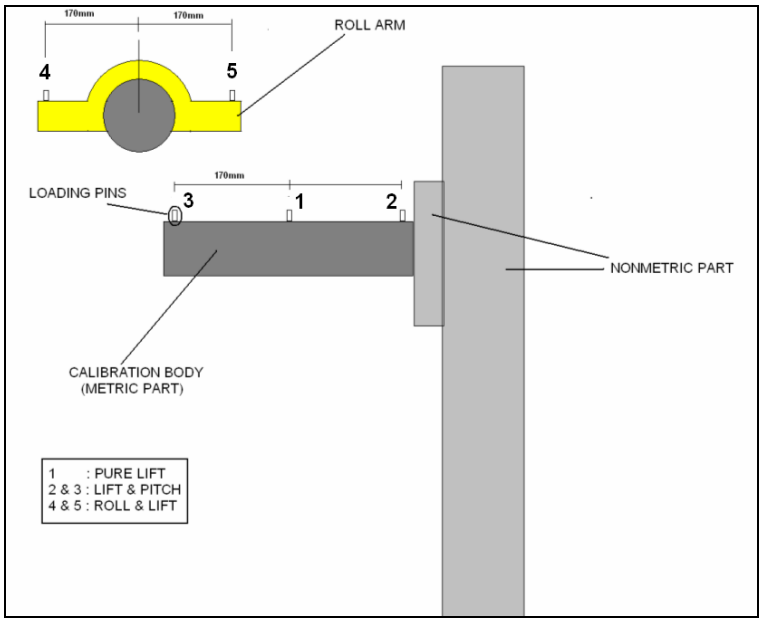

Figure 32 Calibration Rig with Some Loading Configuration

3.2.2.4 RESOLUTION RESULTS

To estimate the resolution of the DAC for internal balance application, the applied loads are measured with two different resolutions. One is a low resolution ±500 mV/V for both forces and moments, the other is a high resolution with ±1 mV/V for forces and ±2 mV/V for moments. The measurements were performed at zero loads thus the internal balance readings must be close to zero for all forces and moments.

When the results were analyzed (Figure 33 - Figure 38) it is seen that the high resolution values are very close to zero and to each other at repeated readings than the low resolution values as expected.

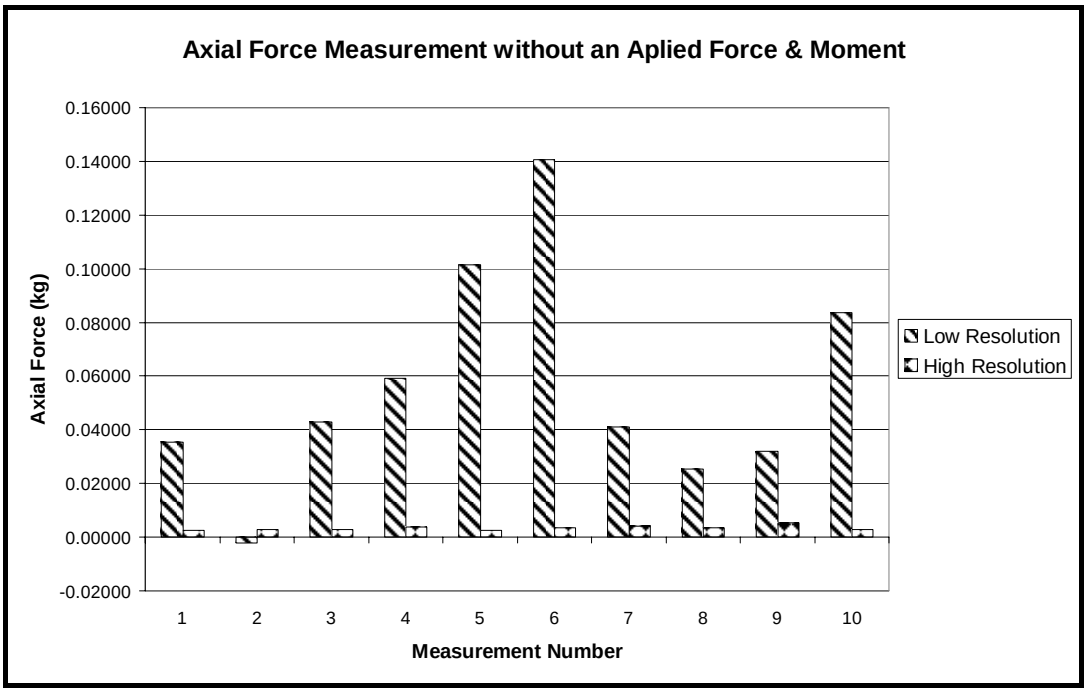

Figure 33 Axial Force Measurements at No Loading Condition

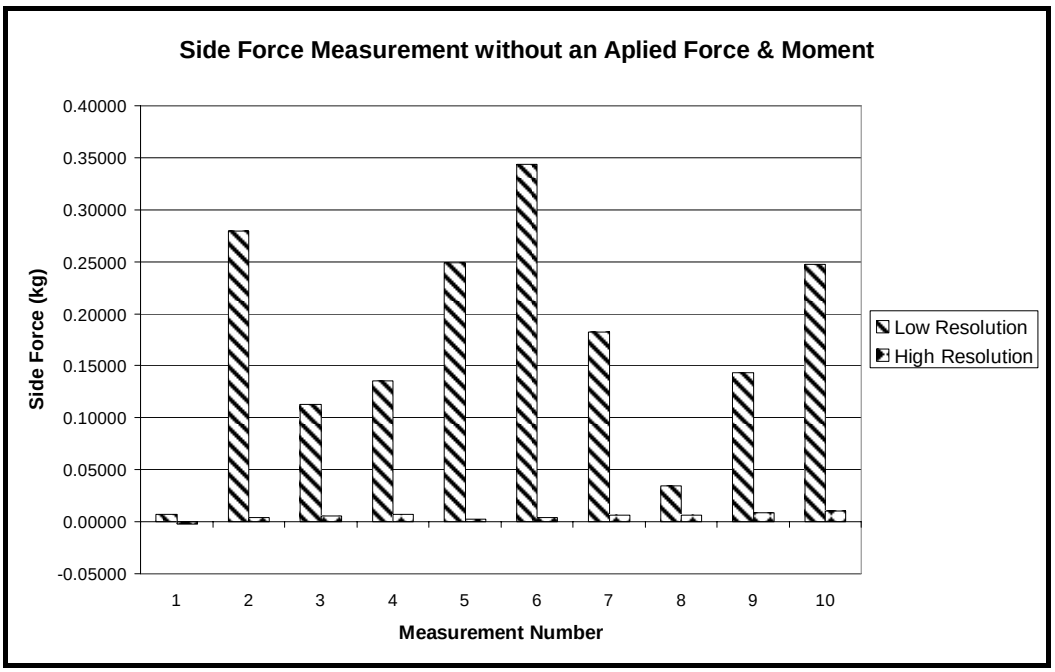

Figure 34 Side Force Measurements at No Loading Condition

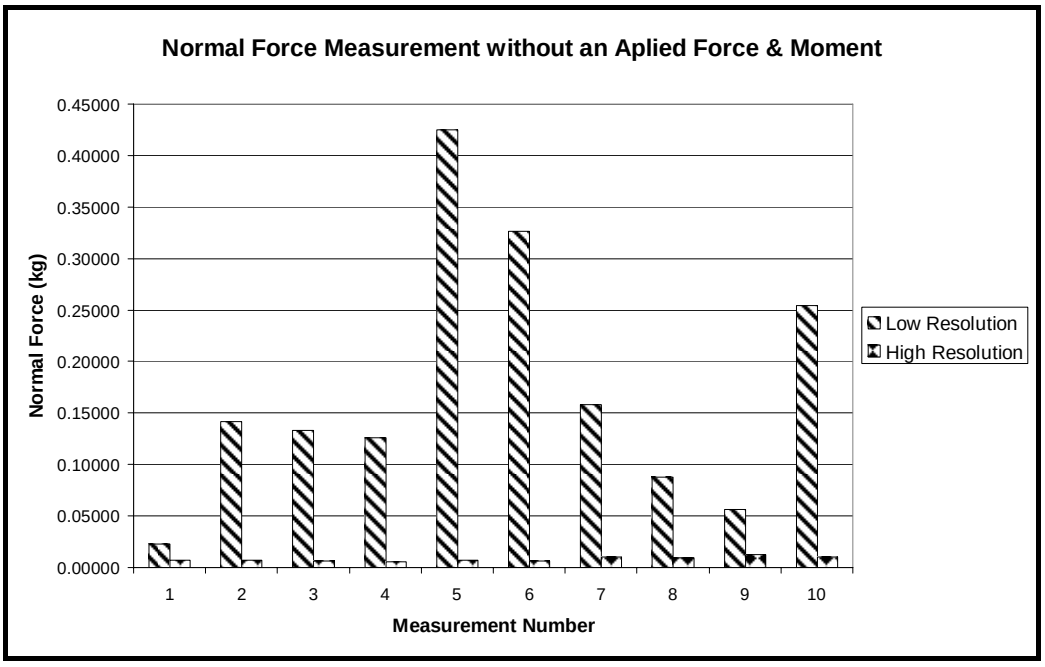

Figure 35 Normal Force Measurements at No Loading Condition

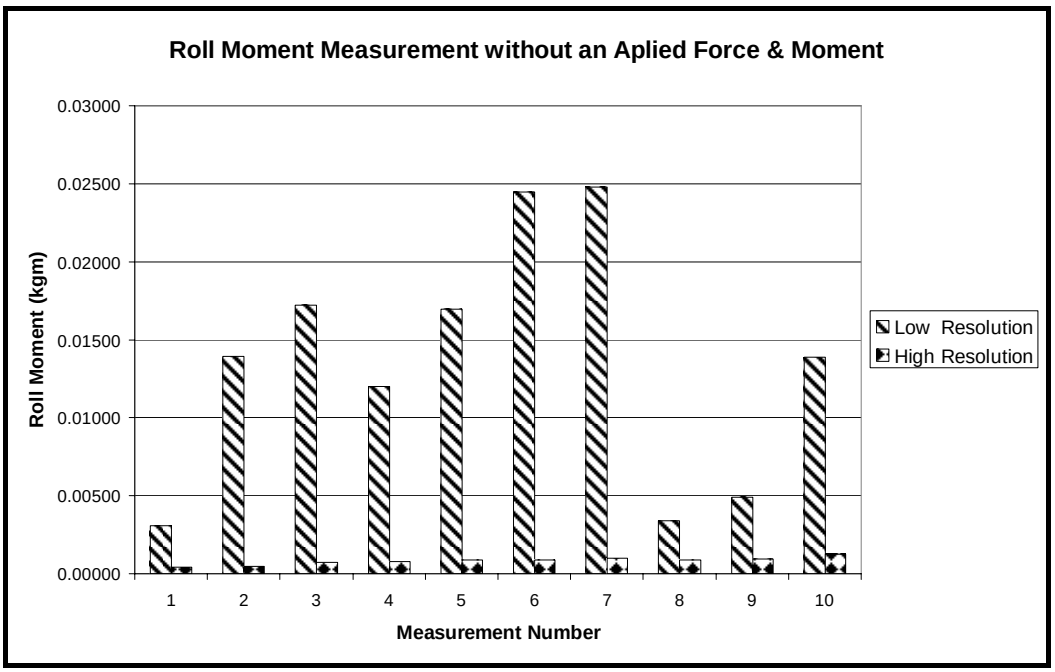

Figure 36 Roll Moment Measurements at No Loading Condition

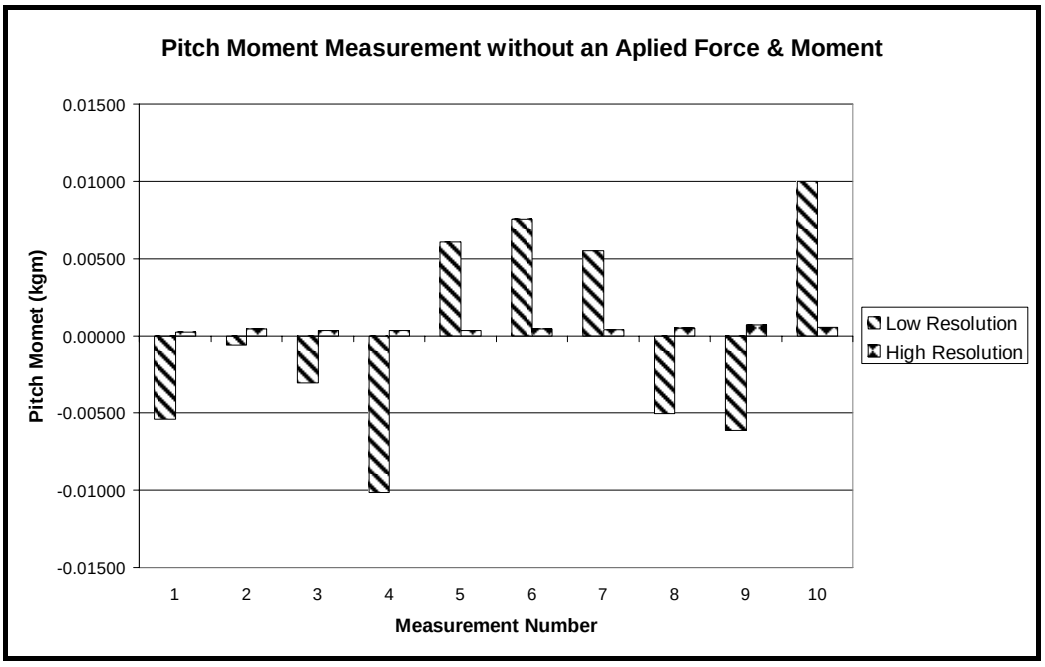

Figure 37 Pitch Moment Measurements at No Loading Condition

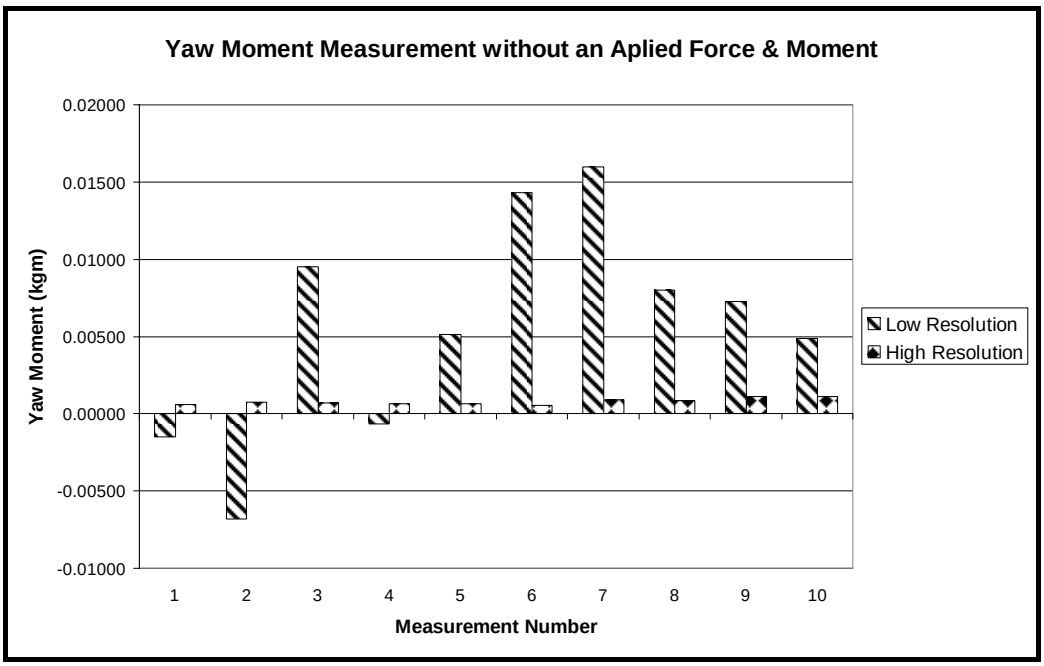

Figure 38 Yaw Moment Measurements at No Loading Condition

Table 16 Nominal Sensitivities for Internal Balances

Component	35 mm Balance	22 mm Balance
Fx	0.5 mV/V	0.7 mV/V
Fy	0.6 mV/V	0.9 mV/V
Fz	0.6 mV/V	0.9 mV/V
Mx	1.1 mV/V	0.5 mV/V
My	1.6 mV/V	1.2 mV/V
Mz	1.0 mV/V	1.2 mV/V

As seen from Table 17 and Table 18 the standard deviation, the difference between maximum and minimum values of high resolution readings are smaller than low resolution results and the mean of high resolution readings are much closer to the

theoretical value “zero” than low resolution readings. In addition the maximum outputs of the internal balances are ±0.9 mV/V for forces and ± 1.6 mV/V for moments as seen from Table 16. For these reasons the resolution of DAC for internal balances are arranged ±1 mV/V for forces and ±2 mV/V for moments.

Table 17 Low Resolution Results

± 500 mV						
Loading Number	**Axial Force (kg)**	**Side Force (kg)**	**Normal Force (kg)**	**Roll Moment (kgm)**	**Pitch Moment (kgm)**	**Yaw Moment (kgm)**
1	0.03548	0.00679	0.02257	0.00310	-0.00540	-0.00152
2	-0.00228	0.27913	0.14126	0.01393	-0.00058	-0.00680
3	0.04299	0.11244	0.13279	0.01719	-0.00305	0.00952
4	0.05924	0.13564	0.12616	0.01198	-0.01017	-0.00065
5	0.10133	0.24896	0.42461	0.01698	0.00608	0.00513
6	0.14067	0.34395	0.32603	0.02448	0.00754	0.01429
7	0.04105	0.18250	0.15796	0.02480	0.00550	0.01598
8	0.02550	0.03454	0.08752	0.00341	-0.00503	0.00798
9	0.03207	0.14301	0.05621	0.00491	-0.00614	0.00725
10	0.08348	0.24747	0.25457	0.01386	0.00997	0.00487
Mean	0.05595	0.17344	0.17297	0.01346	-0.00013	0.00561
Standard D.	0.04177	0.10783	0.12561	0.00789	0.00690	0.00708
Maximum	0.14067	0.34395	0.42461	0.02480	0.00997	0.01598
Minimum	-0.00228	0.00679	0.02257	0.00310	-0.01017	-0.00680
Difference	0.14294	0.33716	0.40205	0.02169	0.02014	0.02278

Table 18 High Resolution Results

± 1 or 2 mV						
Loading Number	**Axial Force (kg)**	**Side Force (kg)**	**Normal Force (kg)**	**Roll Moment (kgm)**	**Pitch Moment (kgm)**	**Yaw Moment (kgm)**
1	0.00241	-0.00222	0.00682	0.00043	0.00021	0.00060
2	0.00301	0.00368	0.00719	0.00049	0.00046	0.00076
3	0.00291	0.00590	0.00597	0.00073	0.00032	0.00069
4	0.00374	0.00686	0.00532	0.00078	0.00034	0.00065
5	0.00245	0.00244	0.00695	0.00087	0.00031	0.00064
6	0.00342	0.00394	0.00601	0.00087	0.00044	0.00054
7	0.00399	0.00670	0.01014	0.00101	0.00038	0.00093
8	0.00353	0.00654	0.00948	0.00087	0.00052	0.00087
9	0.00521	0.00879	0.01219	0.00094	0.00070	0.00111
10	0.00277	0.01017	0.00992	0.00123	0.00056	0.00110
Mean	0.00334	0.00528	0.00800	0.00082	0.00042	0.00079
Standard D.	0.00084	0.00352	0.00227	0.00024	0.00014	0.00020
Maximum	0.00521	0.01017	0.01219	0.00123	0.00070	0.00111
Minimum	0.00241	-0.00222	0.00532	0.00043	0.00021	0.00054
Difference	0.00280	0.01238	0.00686	0.00081	0.00049	0.00057

3.2.2.5 WIND-OFF LOADING RESULTS

Because the internal balance system is a new system, verification loadings, or wind-off loadings, are performed to understand the behavior and the usage of

internal balance and to verify the calibration matrix. The verification loadings are applied as pure loads, 2-combinations loads and 3-combination loads.

To apply the loads to internal balance in the direction of Normal Force, Side Force, Pitch Moment and Yaw Moment the calibration rig and the body are used as shown in Figure 39. For example if the top of the calibration rig is upwards one can load positive normal force by loading Pin 1 or Pin 2 and 3 with equal loads or Pin 1 with Pin 2 and Pin 3 with equal loads. While the top of the calibration rig is looking upwards one can load positive pitch moment if the loads at pin 2 are higher than Pin 3 or visa versa for negative pitching moment. By turning the top of calibration rig 90° with respect to symmetry axes one can have combination for positive side force and yaw moment combinations. And if it is turned 90° again negative normal force and pitch moment and 90° again negative side force and yaw moment can be applied to internal balance.

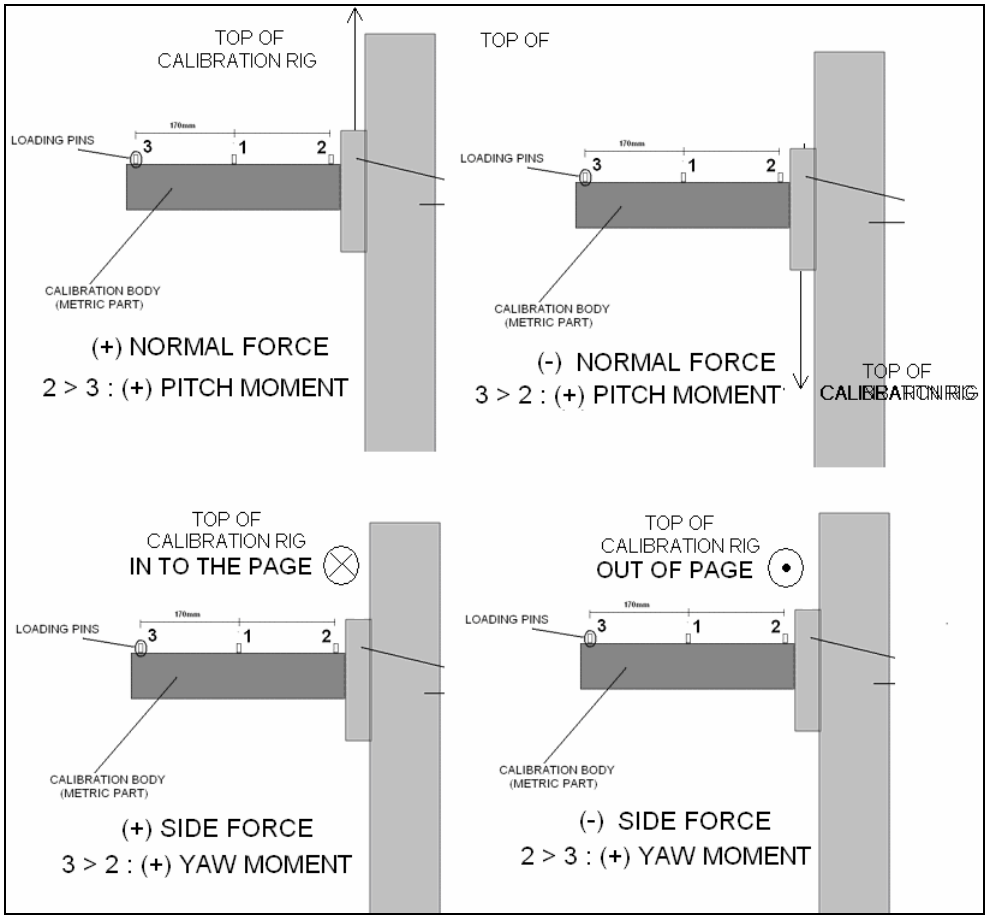

Figure 39 Normal / Side Force, Pitch / Yaw Moment Loading Configuration

Roll moment loadings are applied by using roll moment arm as shown Figure 40. The roll moment moment arm has 170 mm length (like yaw and pitch moment moment arm) for 35 mm internal balance which means that if there is a 1 kg of loading difference between Pins 1 and 2 loads, the applied roll moment is 0.17 kg.m with positive sign.

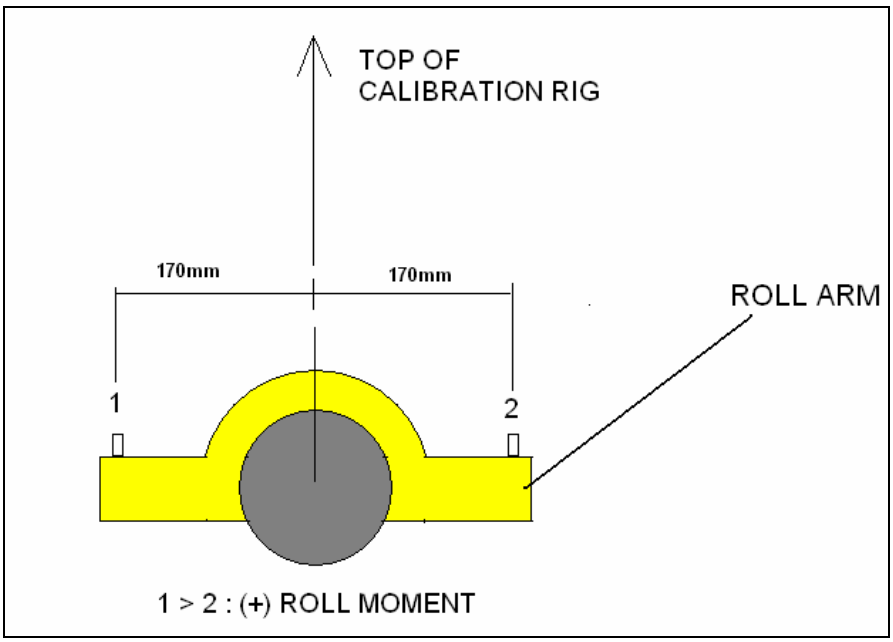

Figure 40 Roll Moment Loading Configuration

Loads in axial directions are applied with a frame and a pulley system as shown in Figure 41. Unfortunately this application has losses because of the strain in the cables and the friction generated at the pulleys. But in order to apply 2-combination or 3-combination loads a pulley system must be built. Only pure loading at axial forces direction can be applied by turning the calibration rig 90° w.r.t perpendicular to symmetry axes. The calibration rig does not have any degree of freedom in any direction.

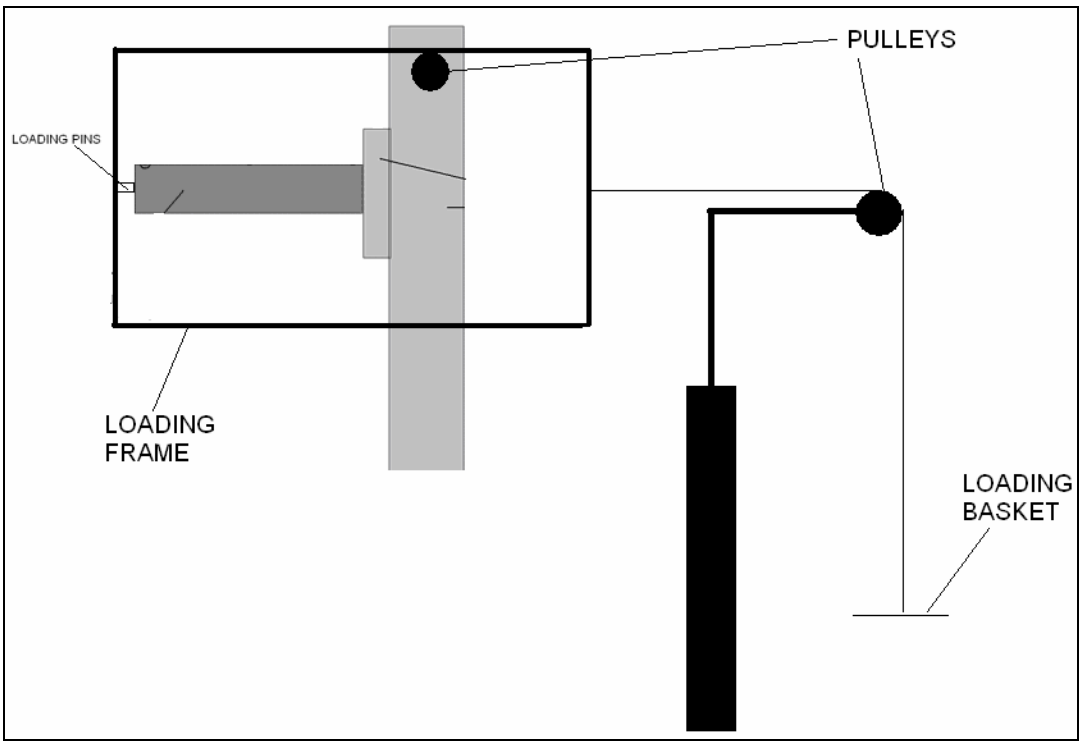

Figure 41 Axial Force Loading Configuration

After installing the calibration rig to calibration apparatus, the internal balance is installed to the calibration rig. Then the calibration body is mounted to internal balance as seen at Figure 43. To apply loads to internal balance at a point exactly a male and female conical pins are manufactured with their frames which can be named as loading basket. (Figure 42) These pins and the loading basket are installed at the location on the calibration rig finally. (Figure 31) Then the loading can be applied for wind-off loadings.

Figure 42 Loading Pins and Loading Basket

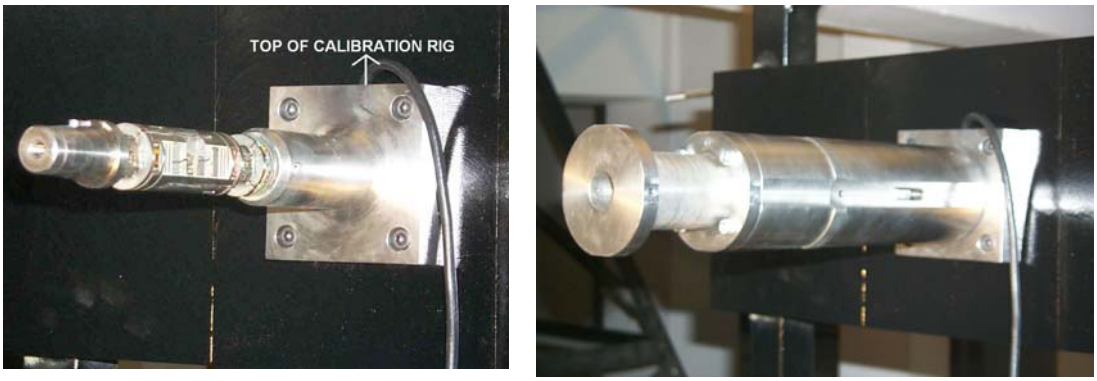

Figure 43 Installation Calibration Rig to Calibration Apparatus

For wind-off loadings the following loading combinations are applied and the results are given at APPENDIX F and the summary of the errors are given in Table 19.

- Pure Axial Force

- Pure Side Force
- Pure Normal Force
- Pure Roll Moment (compulsory with Normal Force)
- Pure Pitch Moment (compulsory with Normal Force)
- Pure Yaw Moment (compulsory with Side Force)
- 2-D combination Normal Force with Axial Force
- 2-D combination Side Force with Axial Force
- 3-D combination Pitch Moment - Normal Force - Axial Force
- 3-D combination Roll Moment - Normal Force - Axial Force
- 3-D combination Roll Moment - Side Force - Axial Force
- 3-D combination Yaw Moment - Side Force - Axial Force

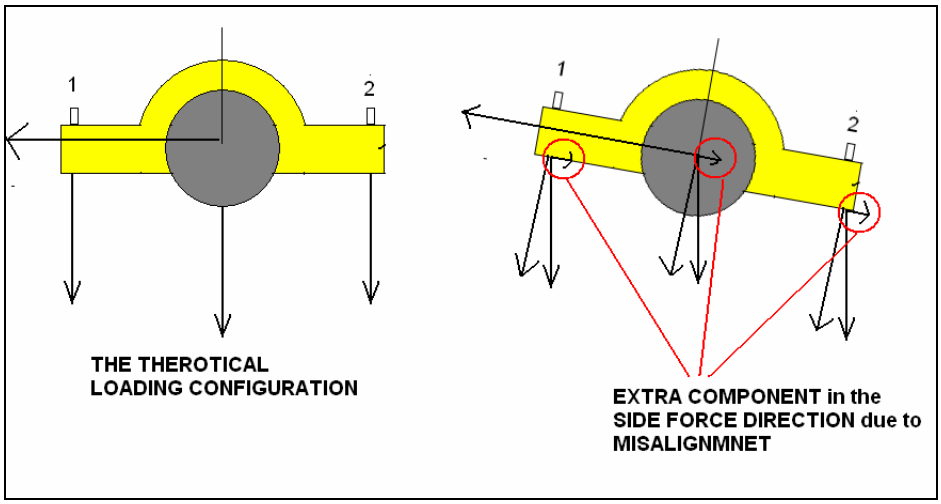

Figure 44 Misalignment at Roll Moment Loadings

Table 19 Wind-Off Loading Errors

COMBINATION	COMPONENT	ERROR %
PURE	Axial	~2
	Side	<1
	Normal	<1
	Roll	<2
	Pitch	<1
	Yaw	<1
2D (Normal and Axial)	Normal	<1
	Axial	<2
2D (Side and Axial)	Side	<1
	Axial	<2
3D (Pitch-Normal-Axial)	Pitch	~2
	Normal	~1
	Axial	~2
3D (Roll-Normal-Axial)	Roll	~2.5
	Normal	~1
	Axial	~6
3D (Roll-Side-Axial)	Roll	~1.5
	Side	~1.5
	Axial	~6
3D (Yaw-Side-Axial)	Yaw	~2
	Side	~1
	Axial	~2

As seen from the table the pure loadings results are more accurate when compared to combination loads. The accuracy of two component loadings for, Axial Force and Roll Moment, is of the order of %2 while the others are of the order of %1. The

axial force loadings are applied with the help of pulley and cables as mentioned before, for this reason the %2 error is considered to be reasonable for axial force. To apply roll moment to the internal balance the roll arm is used and the loading is applied to this arm. When roll moment is applied to the system unfortunately there was a misalignment of the internal balance with respect to the normal direction and swathe errors are increased due to this defect, as indicated in Figure 44. The error in the roll moment loading can be up to 1 kg of side force while it should be 0 kg. (Figure 45)

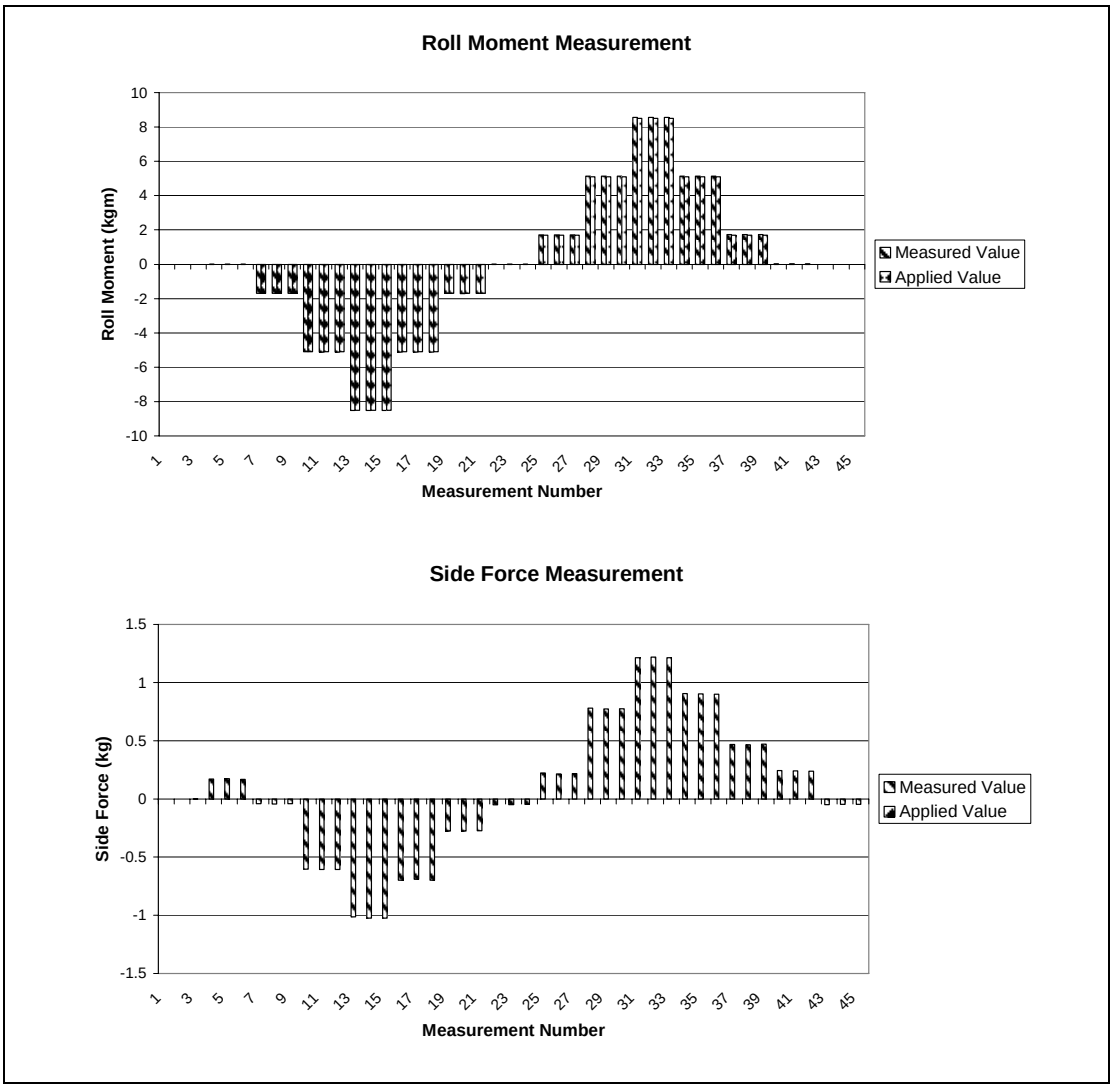

Figure 45 Measured Side Force due to Roll Moment Application

These errors are getting larger for 3-D combinations as can be seen from the table. But the worst case scenario is created during the combined application of the roll moment and axial force due to the misalignment problem and the friction losses at pulley and cables.

3.2.2.6 MISALINGMENT PROBLEM

As mentioned in the previous section when roll moment loading is applied due to the misalignment of the calibration rig and the body there occurs an additional side force and the errors are increased when compared to other loading cases. Unfortunately the calibration rig has no degrees of freedom which mean that the calibration rig can not be moved or can not be given any angles in any directions.

To understand this misalignment problem a pitching moment loading was applied with a mechanism which has single degree of freedom whose angle of attack could be changed. And the axial force component is measured both with alpha correction and without alpha correction. As seen from the results the measured axial force is smaller at the loadings with alpha correction than without alpha correction loadings.

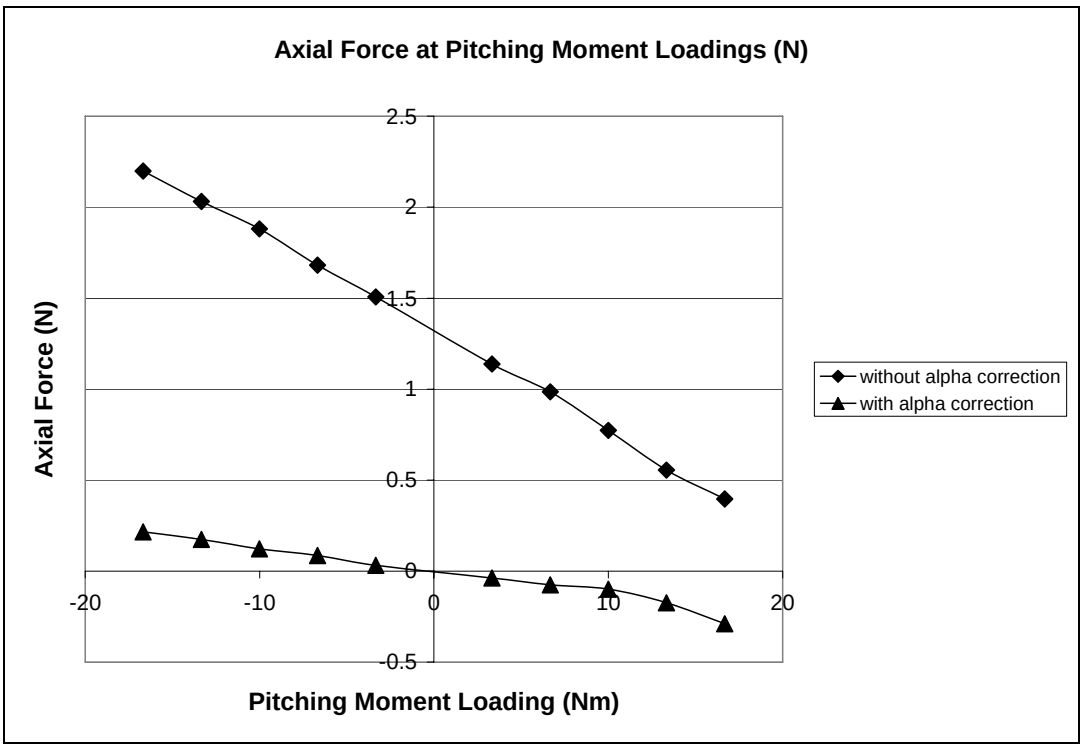

Figure 46 Measured Axial Force for Pitching Moment Loading

For this reason loadings has to be carried out using a leveled calibration process to simulate a model support system that will be used in conjunction with balances. At each loading point the Balance attitude was adjusted such that the Calibration Loading Sleeve was level, to correct for the Balance deflection that occurred. The calibration rig must have at least 2-degrees of freedom one at angle of attack for pitch and yaw moments loadings and one at x-direction for roll moment loadings for future applications at AWT like re-calibration or verification of internal balances.

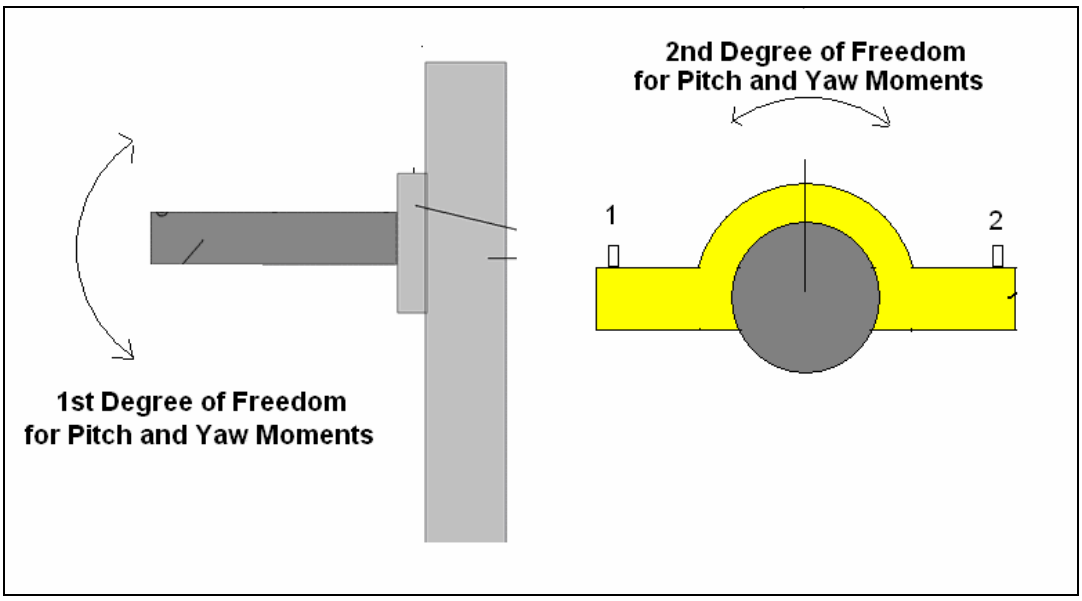

Figure 47 Future Application for Calibration Rig

3.3 AUTOMATED ANGLE OF ATTACK CONTROL

To give the desired angle of attack to the test model, a servo motor or a stepper motor is in conjunction with the Internal and External Balance Systems. Both the servo and the stepper motors are controlled automatically by AWT-AMS as shown in Figure 48. There is a closed loop between the AWT-AMS with Servo or Step Motor Driver which commands and encoders value are connected with PCI-7344.

The command to the stepper or servo motor driver is step or count value respectively instead of giving the command as an angle directly. This is because of the nonlinearity of the system which means that the same step or count value is not equal to the same angle of attack value at every angle of attack range. The angle of attack value is taken directly from an inclinometer which is located inside the model or on the model arm.

AWT-AMS gives the commands and takes the encoder value to / from servo or step motor drivers not to / from servo or step motor directly. The drivers of the motors communicate with the motors again in a closed loop control system. Hence there are 2 closed loops in the system one with AWT-AMS and the driver and the other is with the driver and the motor.

As shown in Figure 49 servo motor driver is connected with X3 and X5 connections to AWT-AMS with UMI-7764 and with X2 and X9 connection to servo motor. As shown in Table 20 the X3 connection is the connection for commands to driver from UMI-7764 and X5 is used for the encoder connection to UMI-7764. X9 is the connection to servo motor and X2 is the encoder connection to servomotor. As mentioned before there are 2 closed loops at the system. This is why there are 2 encoder connections and 2 command connections for servomotor driver. (APENDIX-B)

Step motor connection is the same as the servomotor connections with the difference such that there is no encoder connection between the step motor driver and the AWT-AMS.

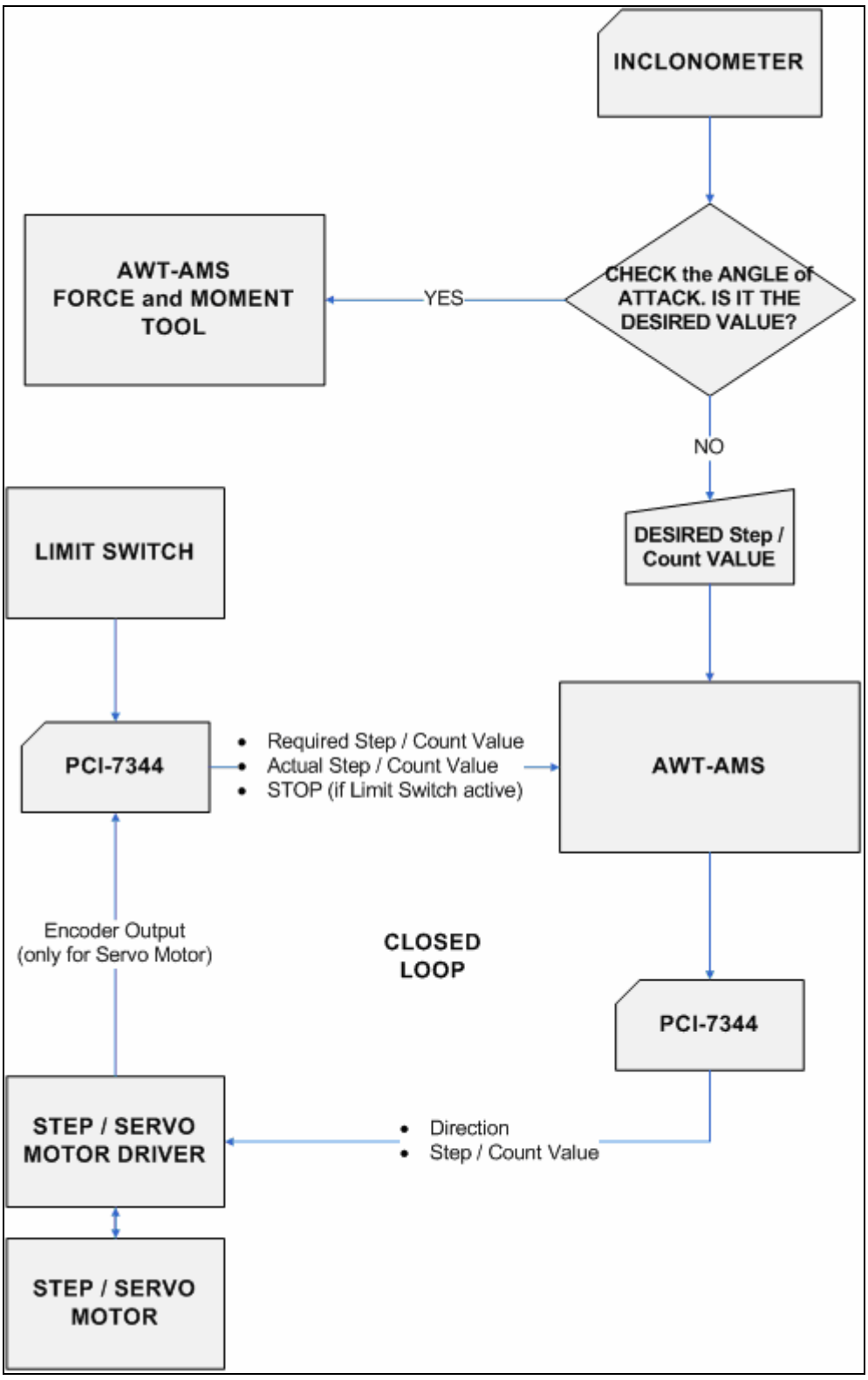

Figure 48 Inputs and Output of Angle of Attack Control Tool of AWT-AMS

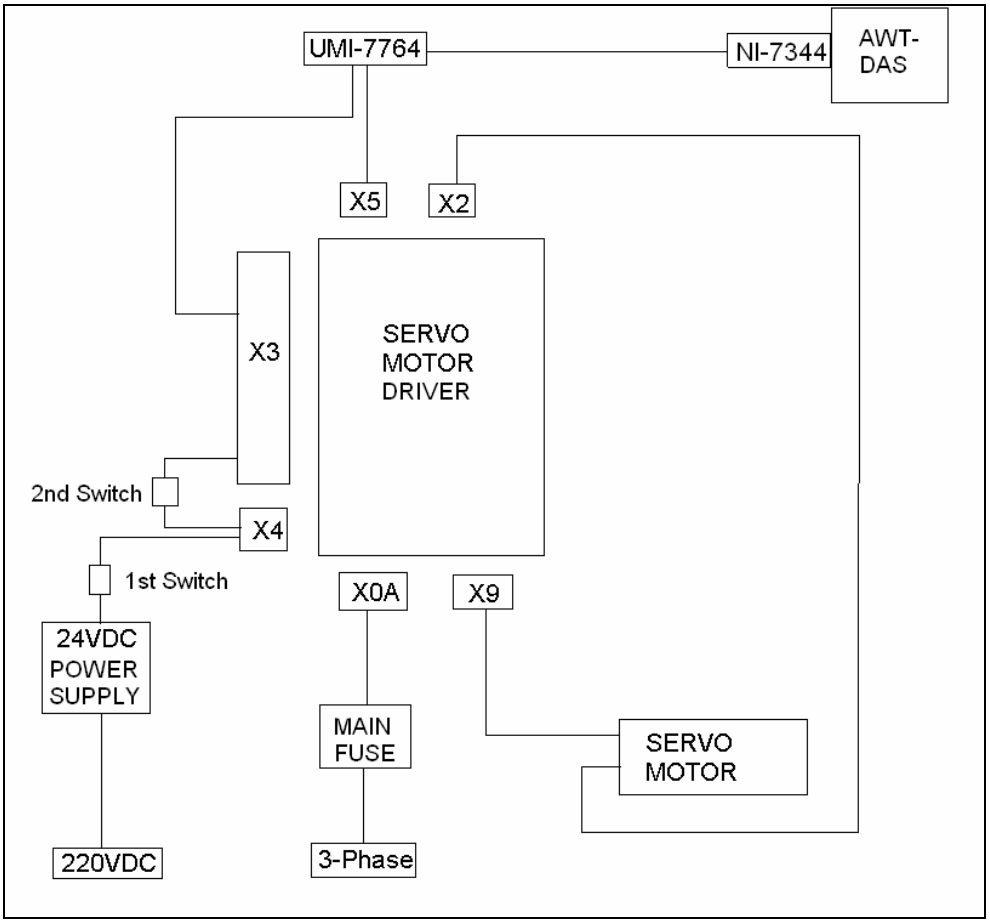

Figure 49 Servomotor Connections

Table 20 Servomotor Connector Name and Their Application

Connection	Connection Name
XOA	Main Power Supply (3-Phase)
X9	Motor Connection
X2	Resolver Connection
X4	24VDC Auxiliary Supply
X3	Control and Monitoring Connection
X5	Encoder Simulation

3.4 AUTOMATED FAN DRIVER CONTROL

The flow velocity inside the wind tunnel is controlled by adjusting the rpm of the fan motor. In the old system this control was done by hand with a technician or with an engineer and this increased the operation and the adjusting time. This old system is integrated to the new DAS and the desired program is implemented to AWT-AMS as RPM Controller Panel. (Figure 51)

In the new system RPM control is done with manually or automatically with AWT-AMS RPM Controller Panel. For the manual control the operator can increase or decrease the RPM value manually. The only difference of this technique with the old one is that the rpm command is given with DAS to the drive motor.

The second technique is the automatic adjustment of the rpm with AWT-AMS. The operator enters only the desired RPM value to AWT-AMS and the rpm commands are given to the system automatically with a 100 rpm/minute increase and decrease rate. In other words, the motor reaches 400 rpm in approximately 4 minutes and stops from 400 rpm in approximately 4 minutes.

Figure 50 Old Fan Driver RPM Controller

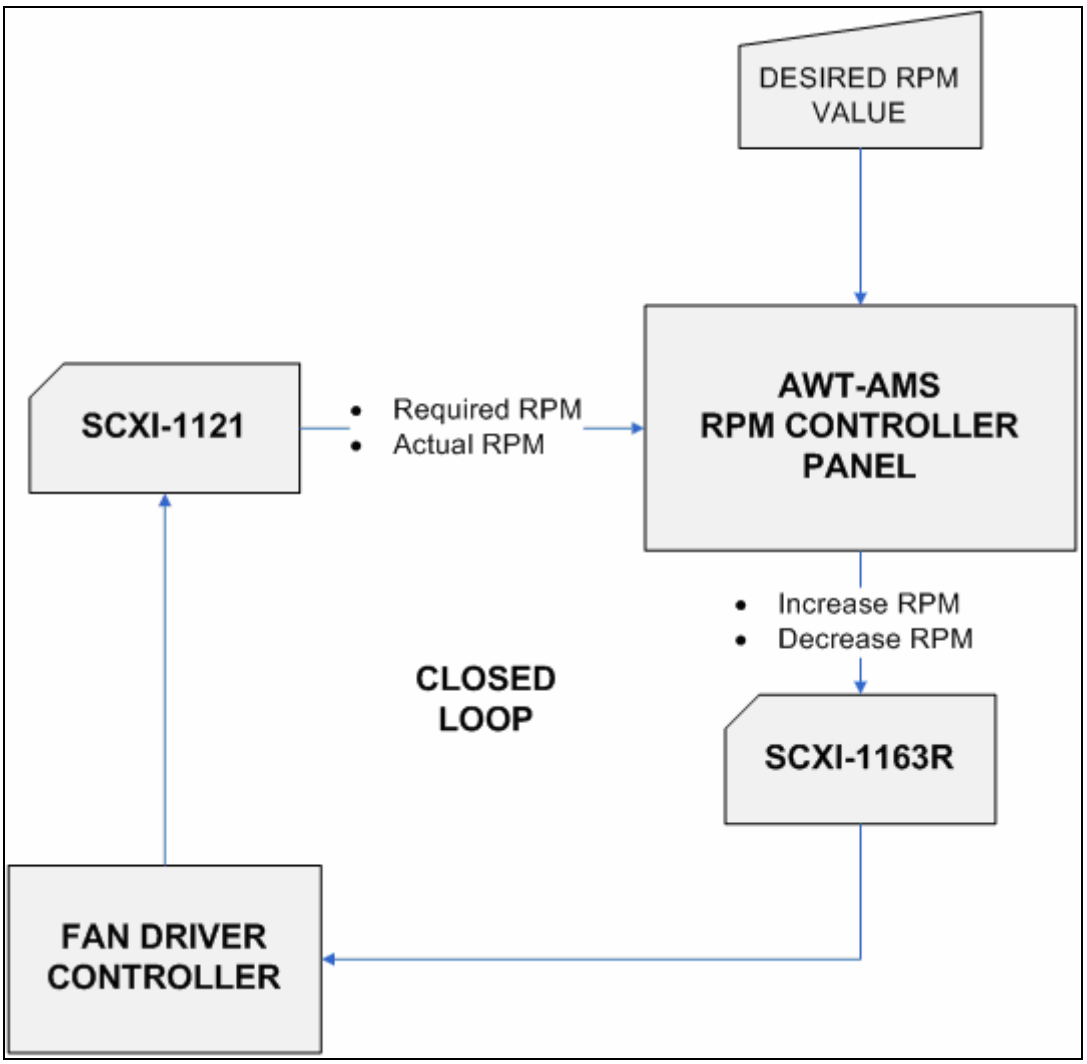

Figure 51 AWT-AMS RPM Controller Panel Closed Loop

3.5 AUTOMATED MULTI-CHANNEL PRESSURE SYSTEM MEASUREMENT

AWT-AMS can control the Multi-Channel Pressure Measurement System automatically. The operator only enters the value of the total number of pressure points that will be measured at the test. The control loop of the AWT-AMS Multi-Channel Pressure Measurement System Tool is repeated as many times as the number input to the program. (Figure 52)

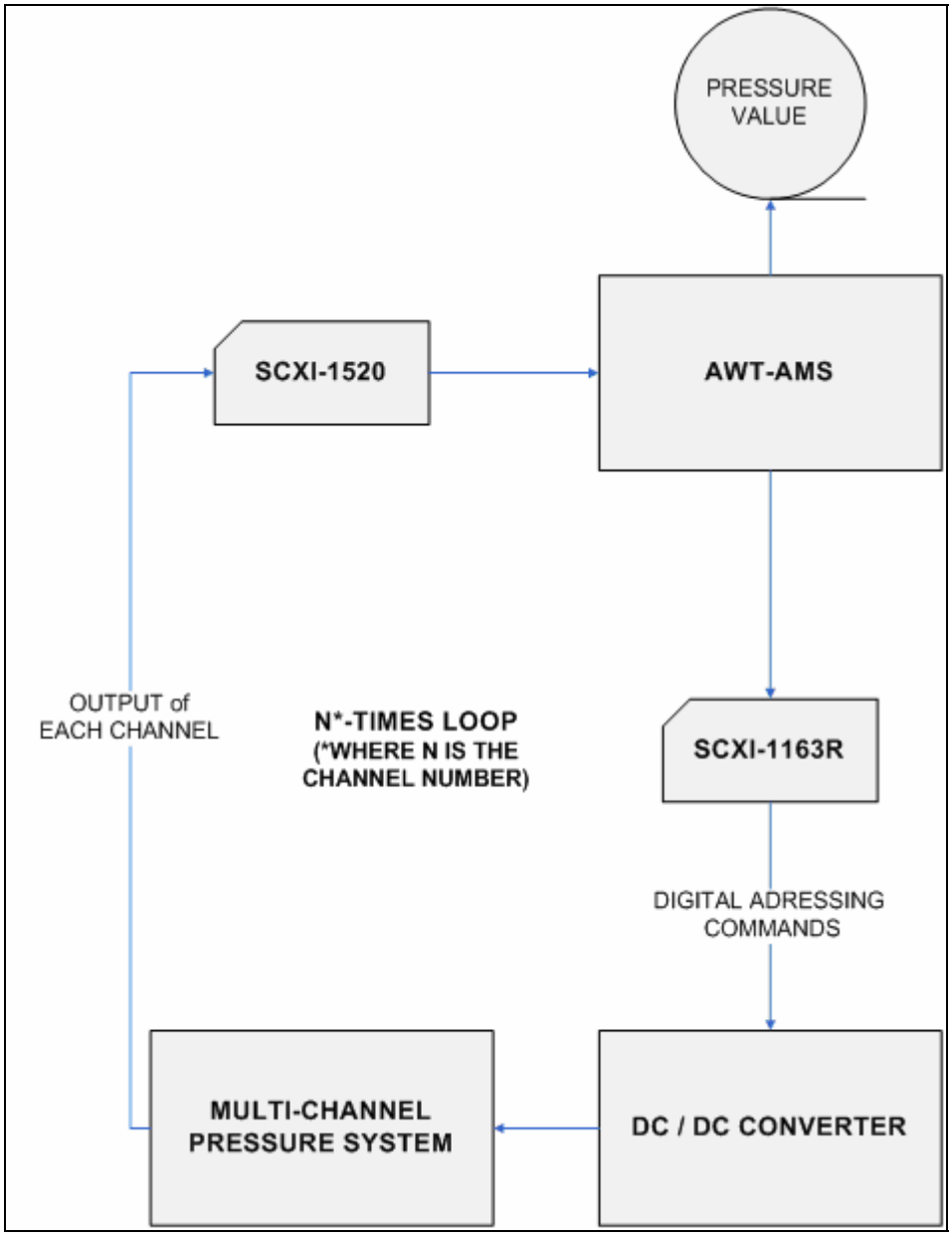

Figure 52 AWT-AMS Multi-Channel Pressure System Control Loop

3.6 AWT-AMS

AWT-AMS is written in LabVIEW programming language which is a high level iconic programming tool for creating custom test, measurement, and data

acquisition applications. LabVIEW is a user-friendly program and, is used by means of pushbuttons. The user interface part of the measurement code is written in Turkish, since it is used practically in AWT. The operator can see the data from both figures and from indicators so a meaningless jump of the data can be easily observed and the measurement can be repeated again. The screen shots for the AWT-AMS programme can be seen in Appendix F.

3.6.1 AWT-AMS CODE ALGORİTM

The algorithm of AWT-AMS is given in this section as follows:

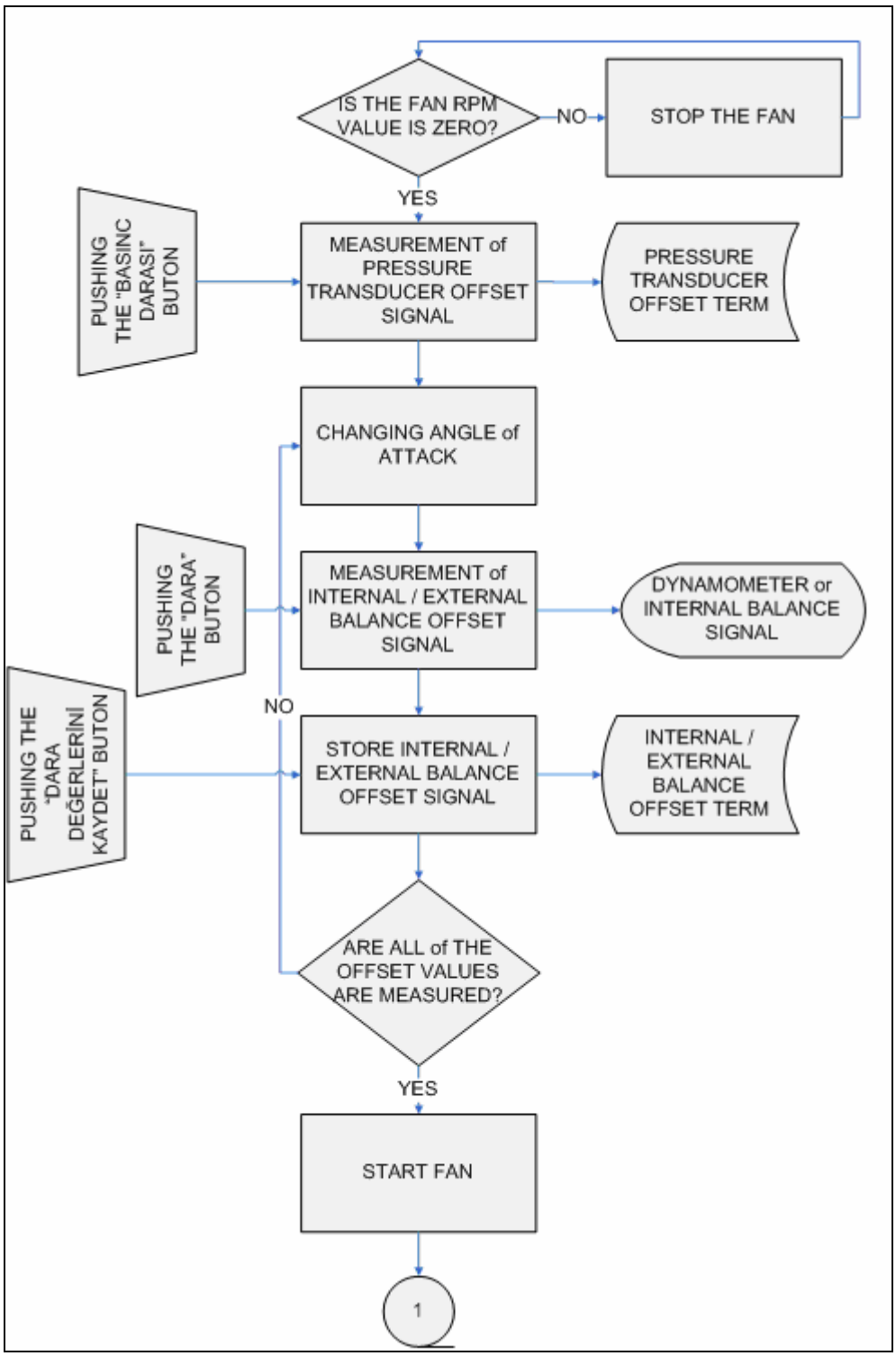

Figure 53 AWT-AMS Flowchart (Measurement and Storing of Offset Parameters)

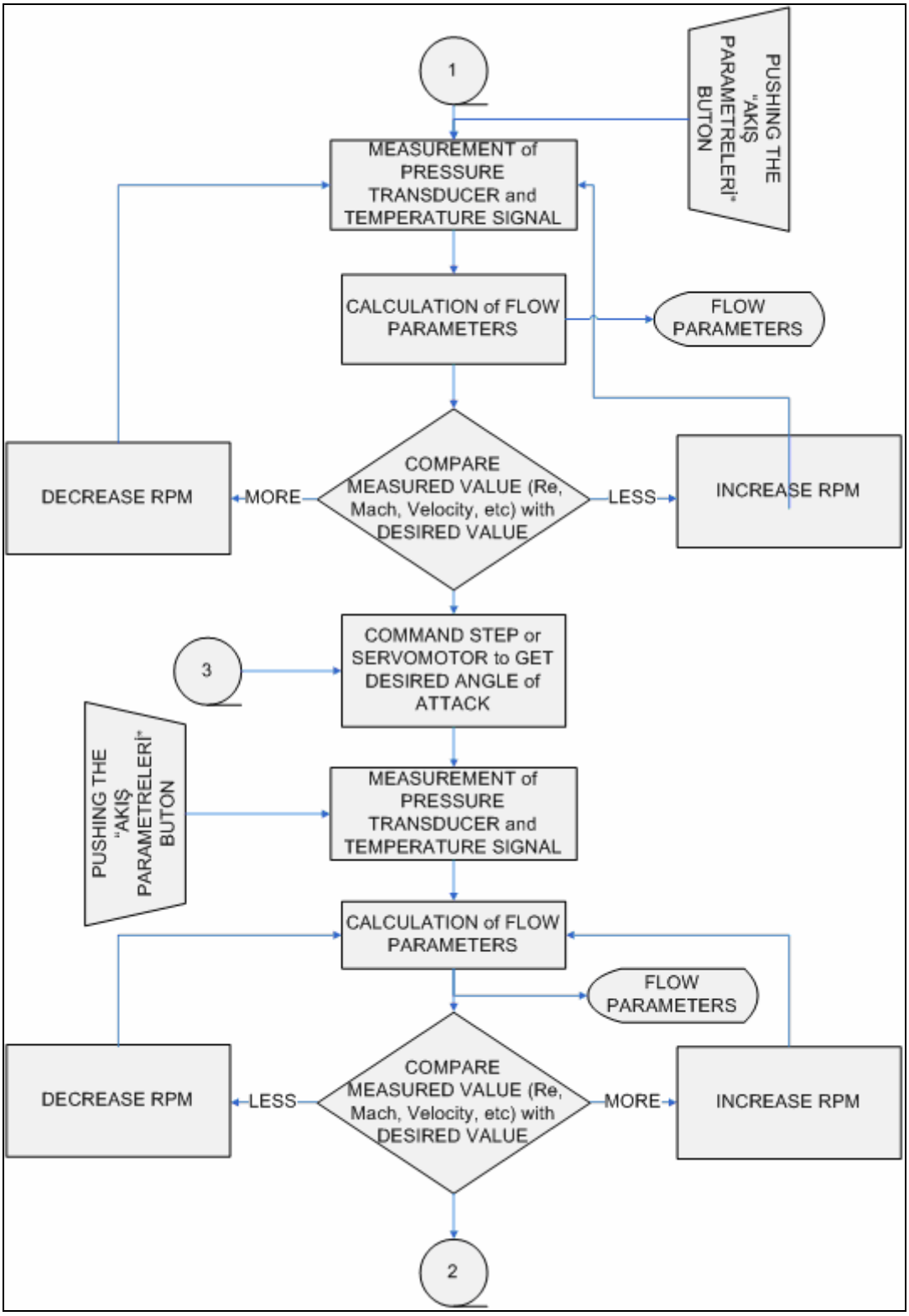

Figure 54 AWT-AMS Flowchart (Getting Test Conditions)

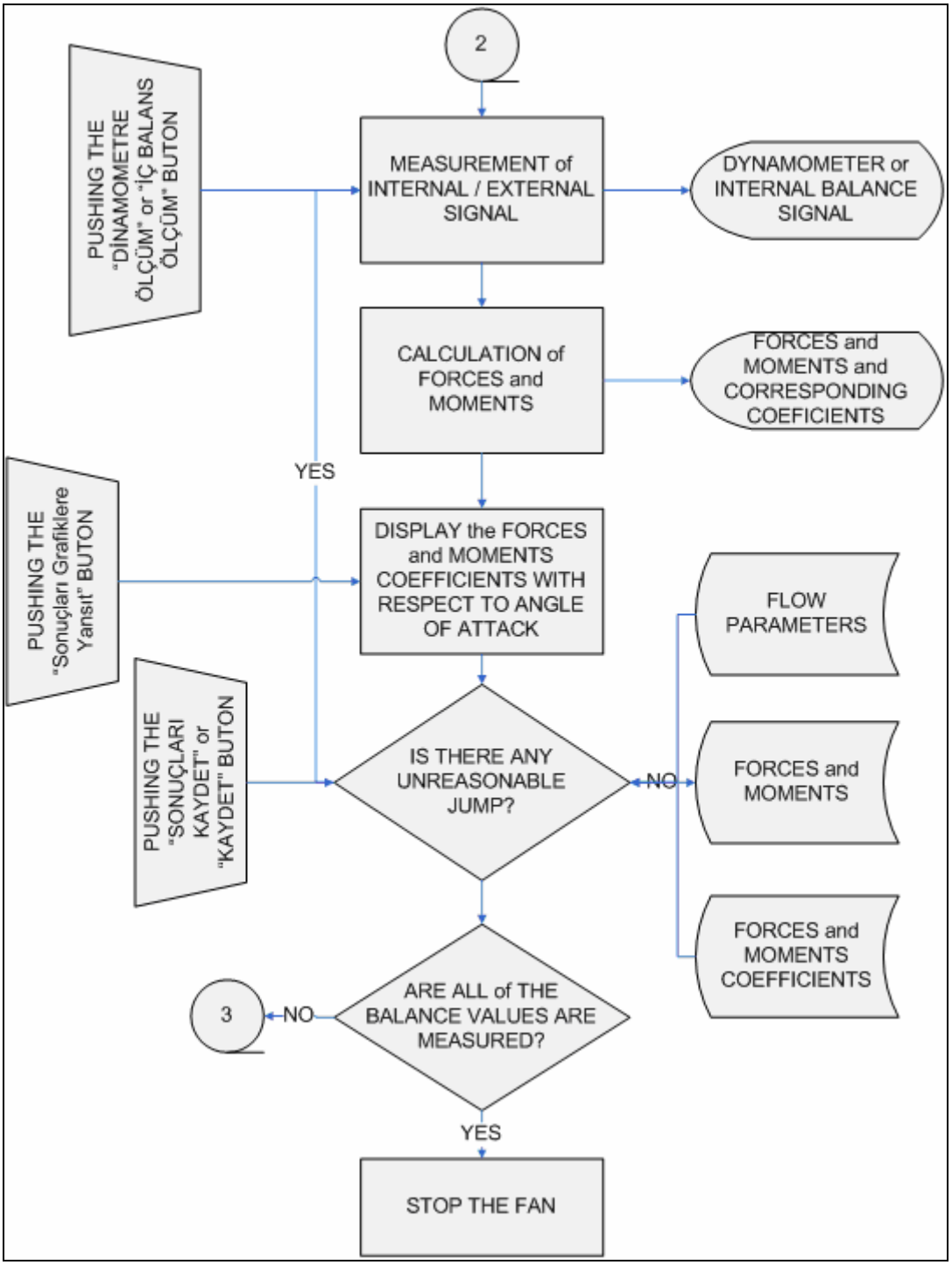

Figure 55 AWT-AMS Flowchart (Measurement and Displaying of Model Forces and Moments)

.

CHAPTER 4

VALIDATION and VERIFICATION of AUTOMATED MEASUREMENT SYSTEM (AMS)

For validation and verification of AWT-AMS a model of an air-to-air missile (Sidewinder) with cruciform fins and triangular canard controls having trapezoidal wings is chosen since experimental data are available for this model. This model was previously tested in NASA Langley Research Center Wind Tunnel in 1974. [21] The model was tested for various Mach numbers ranging from 0.2 to 4.63 with two canard and wings in + configuration (as seen from forward $\phi = 0°$) and as well as in X configuration of the wing (as seen from forward $\phi = 45°$). The results of + and X wing configurations for 0.2 Mach number is taken from the graphs and the results of AWT-AMS is compared with this available data.

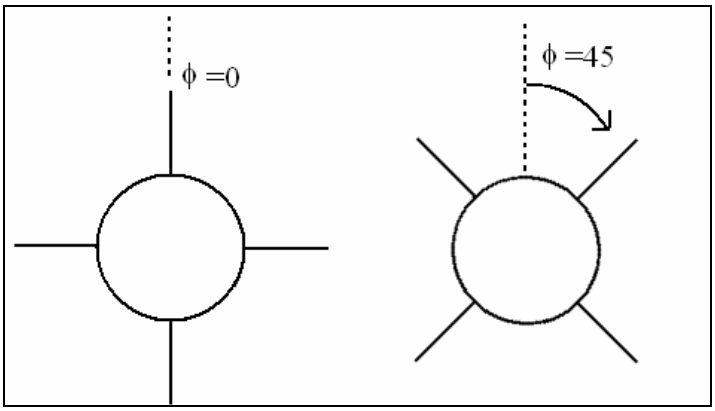

Figure 56 Wing and Canard Position with respect to Body (+ Wing and X Wing Respectively)

4.1 SIDEWINDER

The drawing and the picture of the model are given in Figure 57-Figure 60. The model fuselage has a fineness ratio (l/d) about 22 and incorporates a hemispherical nose. The model has a canard and tail fins which detailed dimensions are given in Figure 59. Two mounting hangers (launch straps) are located on the body between the canards and tail fins. Unfortunately the details of these hangers are not given in the NASA report but fortunately for comparison the basic and launch straps off models was tested and the results are represented for both cases. [21]

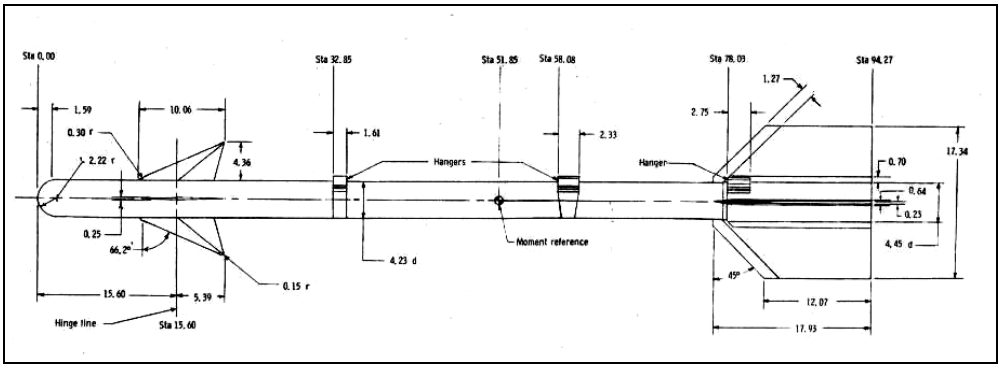

Figure 57 Model Drawing

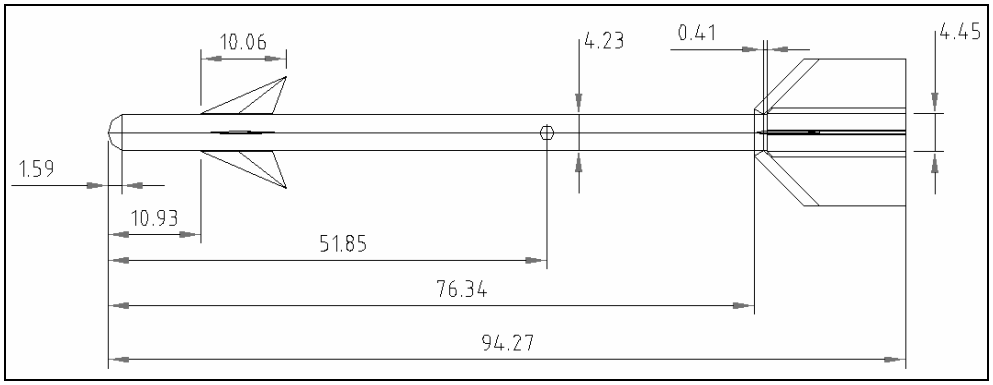

Figure 58 Model Drawing (all dimensions are in centimeters)

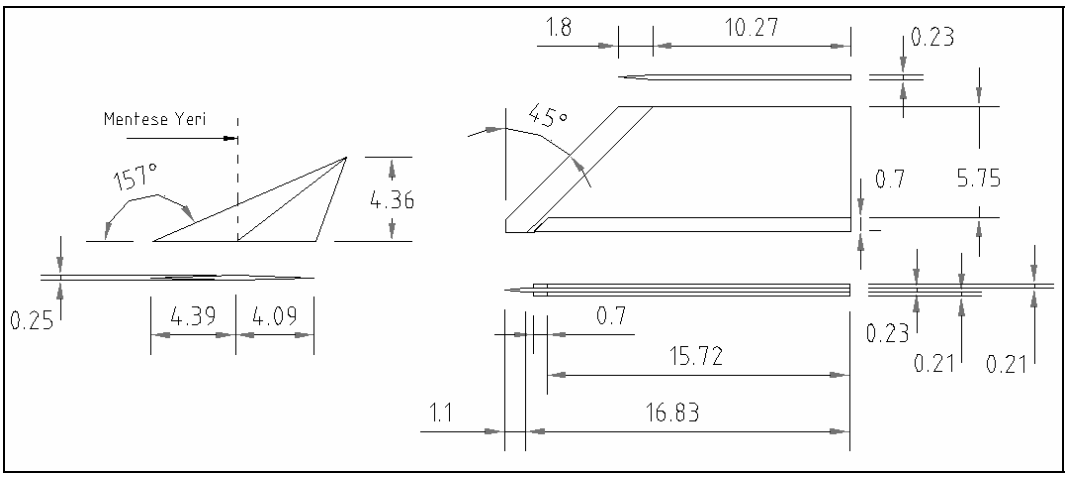

Figure 59 Details of the Fin and Canard Geometries (all dimensions are in centimeters)

Figure 60 Presented Model of Sidewinder Missile Manufactured in SAGE

4.2 NASA RESULTS

NASA tests are performed in 8-Foot Wind Tunnel of Langley Research Center at a Reynolds number of 6.56 10^6 per meter and a Mach number of 0.2. During the

tests, boundary-layer transition strips were placed 3.05 cm aft the model nose and 1.02 cm aft, streamwise, on all lifting surfaces. Sand, sparsely sprinkled, in 0.16-cm-wide strips was used where the sand particles were individually placed three diameters apart. [21]

Aerodynamic forces and moments were measured by means of a six-component electrical strain-gage balance located within the model and, in turn, rigidly fastened to a sting-support system. Pressures in the model balance camber were measured by means of a single static orifice.

The basic and launch straps off model results is given in figures between Figure 61 to Figure 66. The launch straps have an effect on axial force measurement as is expected. The effects of the launch straps on the other longitudinal characteristics, namely pitch moment and normal force are quite small. The launch straps off model results are taken to compare the AWT results.

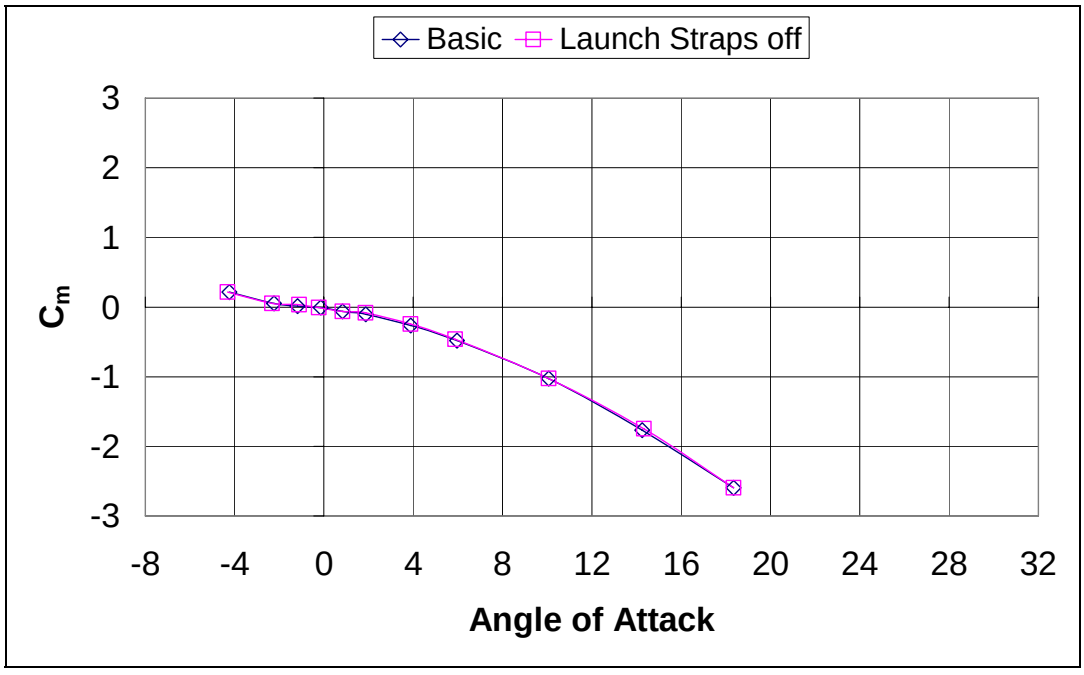

Figure 61 NASA Results, Pitch Moment (M=0.2, $\phi = 0°$)

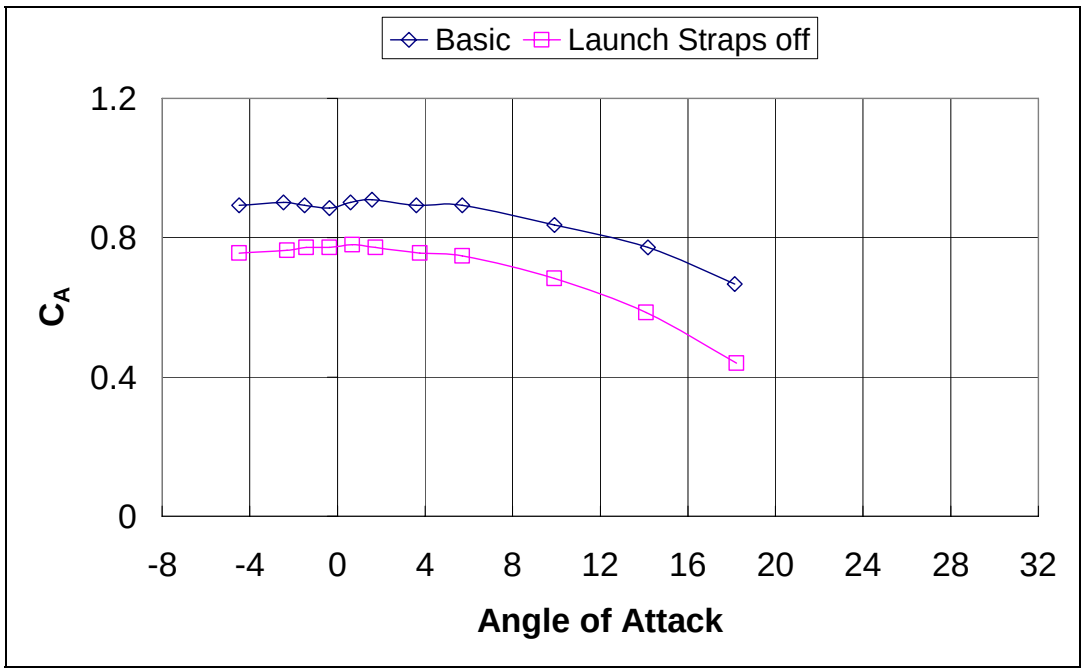

Figure 62 NASA Results, Axial Force (M=0.2, $\phi = 0°$)

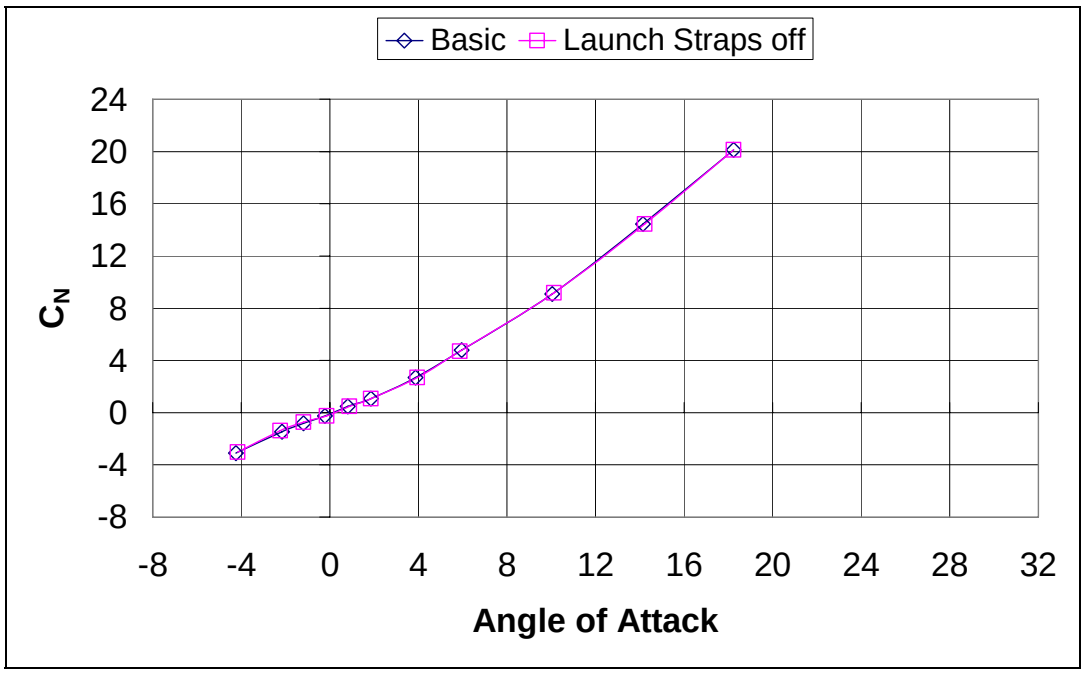

Figure 63 NASA Results, Normal Force (M=0.2, $\phi = 0°$)

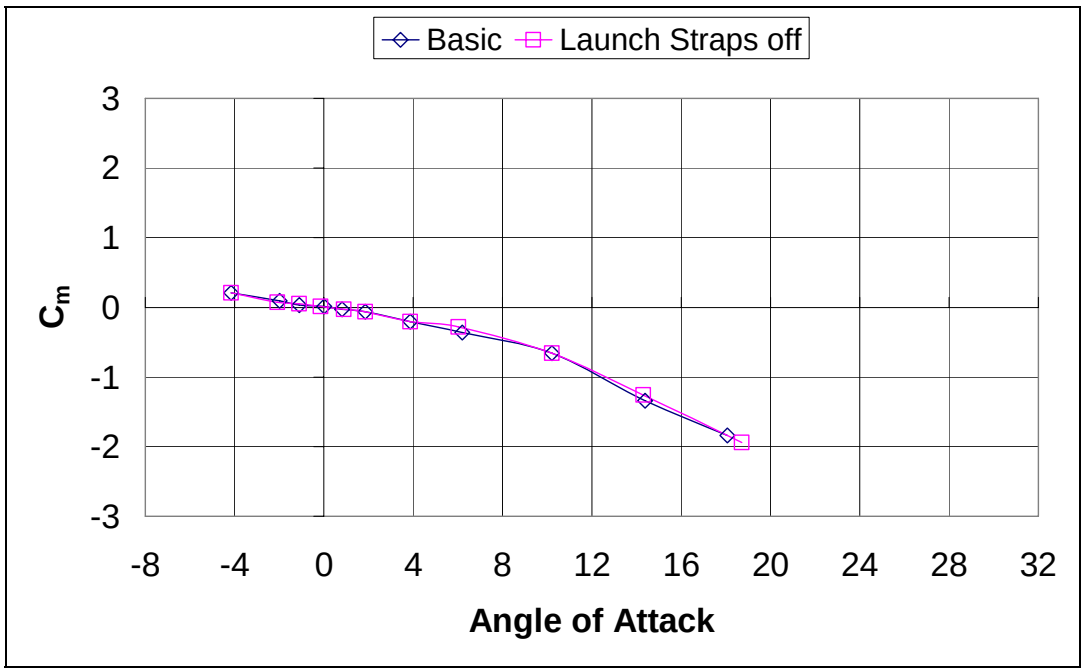

Figure 64 NASA Results, Pitch Moment (M=0.2, $\phi = 45°$)

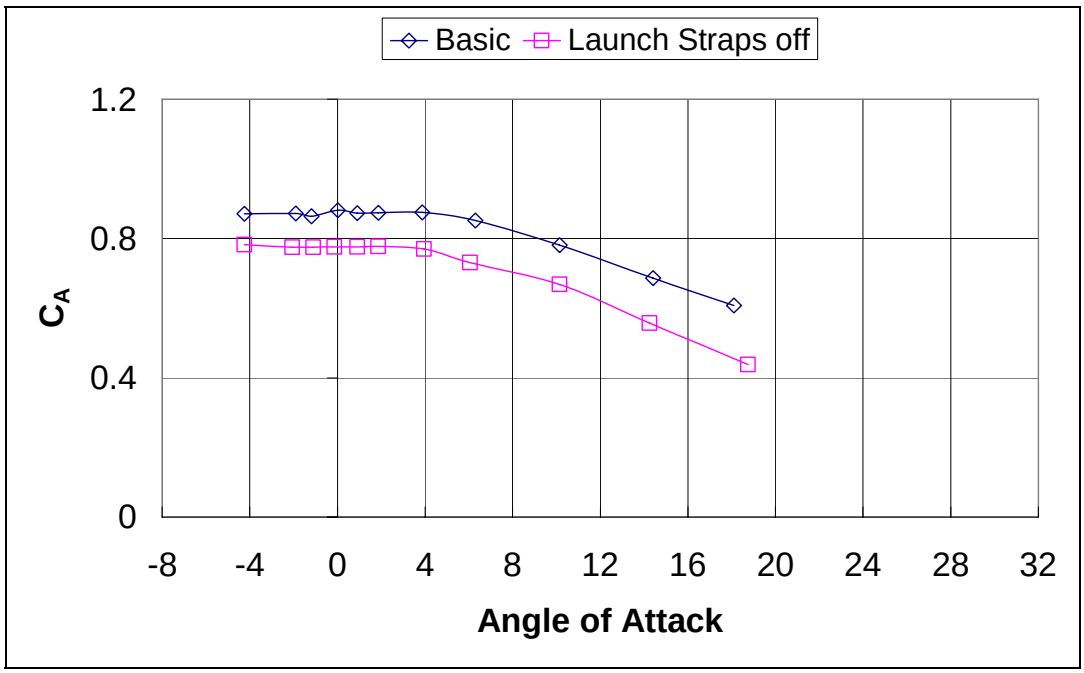

Figure 65 NASA Results, Axial Force (M=0.2, $\phi = 45°$)

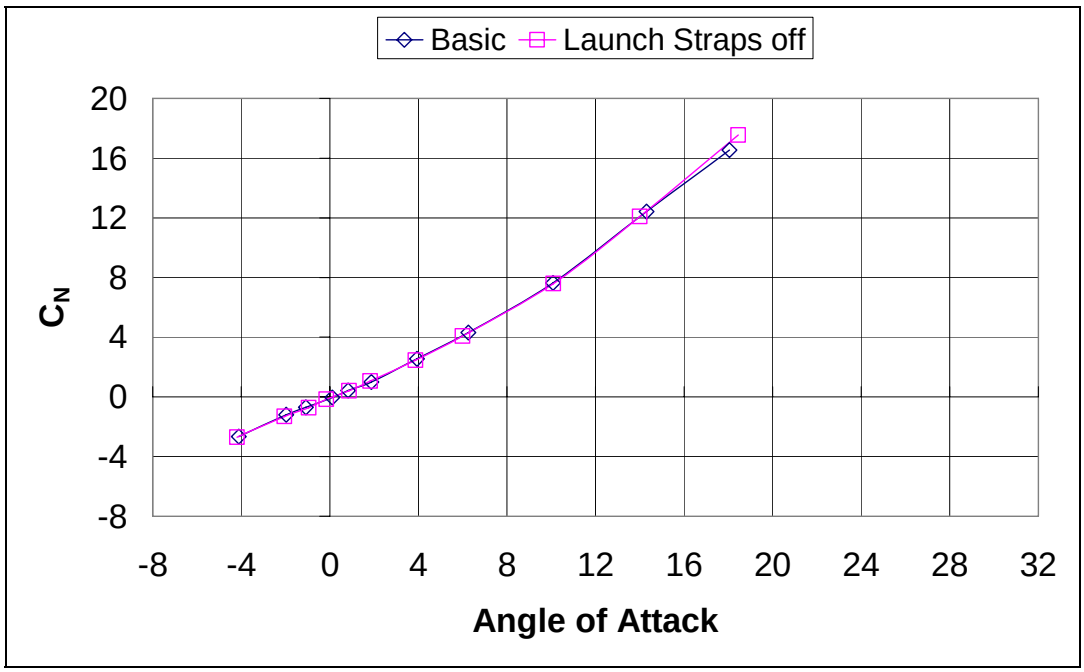

Figure 66 NASA Results, Normal Force (M=0.2, $\phi = 45°$)

4.3 AWT RESULTS

Because AWT is an atmospheric wind tunnel it is not possible to make the tests at the same Reynolds number that was attained in the Langley Research Center Wind Tunnel. For this reason, only the Mach number similarity is considered to be satisfied and the present tests were performed at the same Mach number of 0.2 (with the tolerances -0 , +0.001) and approximately at 1.97 10^6 Reynolds Number per meter.

During these tests to satisfy the similarity of the velocity field and the growth of the boundary layer, the boundary layer is tripped using strips of sand papers of grid sizes 90 at the nose and on all of the lifting surfaces (canards and wings). For body the strips are located at 3.05 cm aft of the nose, which is the same value as for the NASA tests, and at the leading edges of all lifting surfaces, which is 1.05 cm for NASA tests. (Figure 67 and Figure 68)

Figure 67 Nose and Canard Strips Respectively

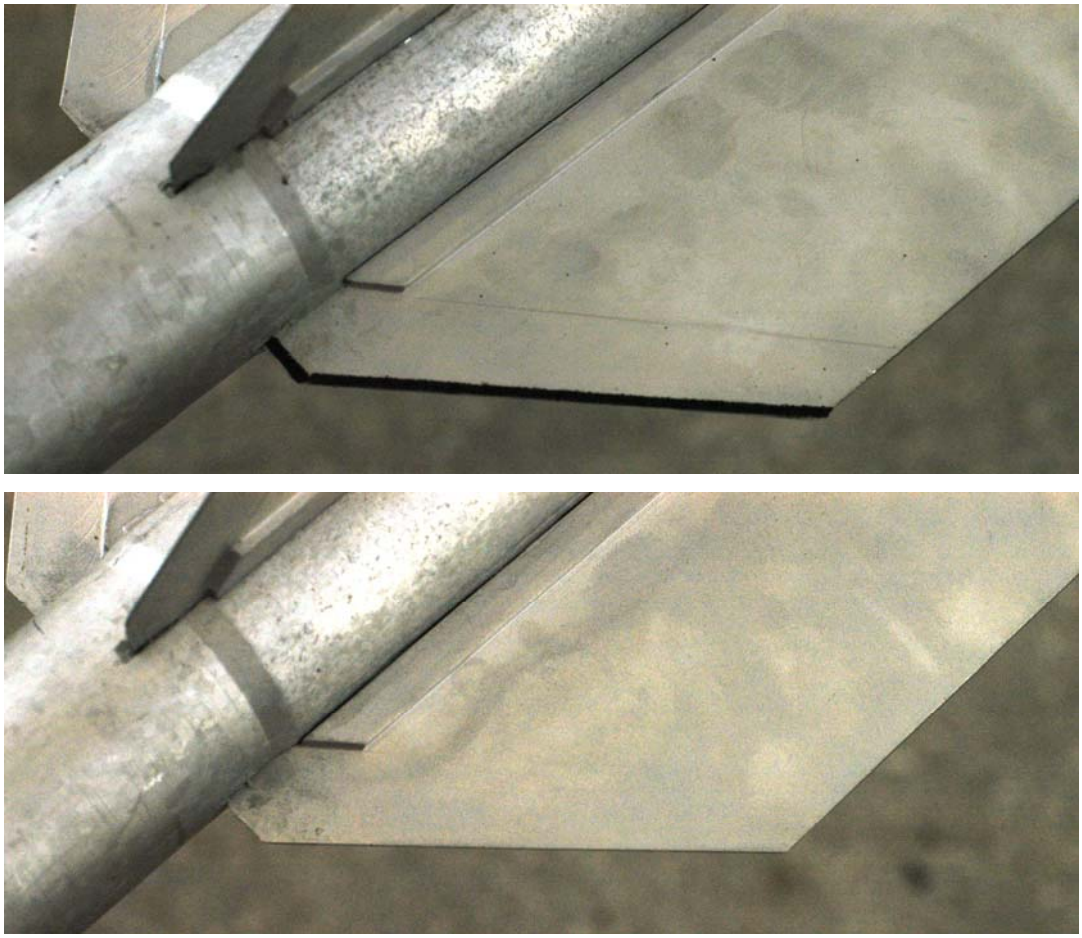

Figure 68 Wing with and without Strips Respectively

After the completion of the model preparation and its installation to the MSS in the test section of AWT (Figure 69 and Figure 70), the tests are performed and the results are given in Figure 71-Figure 77 for $\phi = 0°$ configuration and in Figure 78-Figure 80 for $\phi = 45°$ configuration. For checking the repeatability of AWT-AMS results for both of the cases two sets of tests are performed for each configuration and the results are given as AWT Run 1 and AWT Run 2.

Figure 69 Model at the Test Section (Side View)

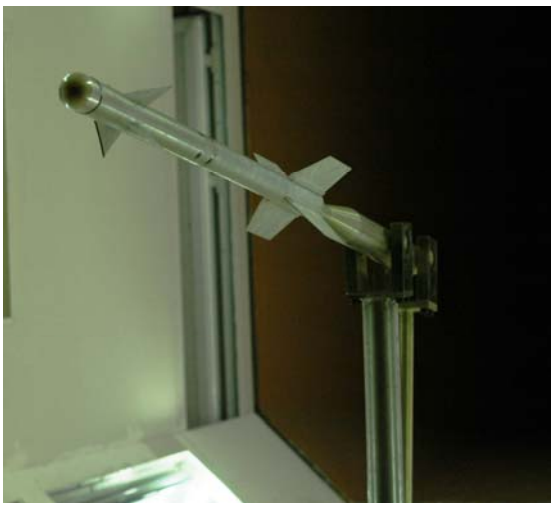

Figure 70 Model at the Test Section, X-Wing Configuration, Isometric View

The pitching moment coefficients, which are found by NASA and AWT-AMS, for $\phi = 0°$ is given in Figure 71. As seen from the graph AWT results are in good agreement with NASA results at low angles of attack. For high angles of attack they are still in good agreement but with a small difference.

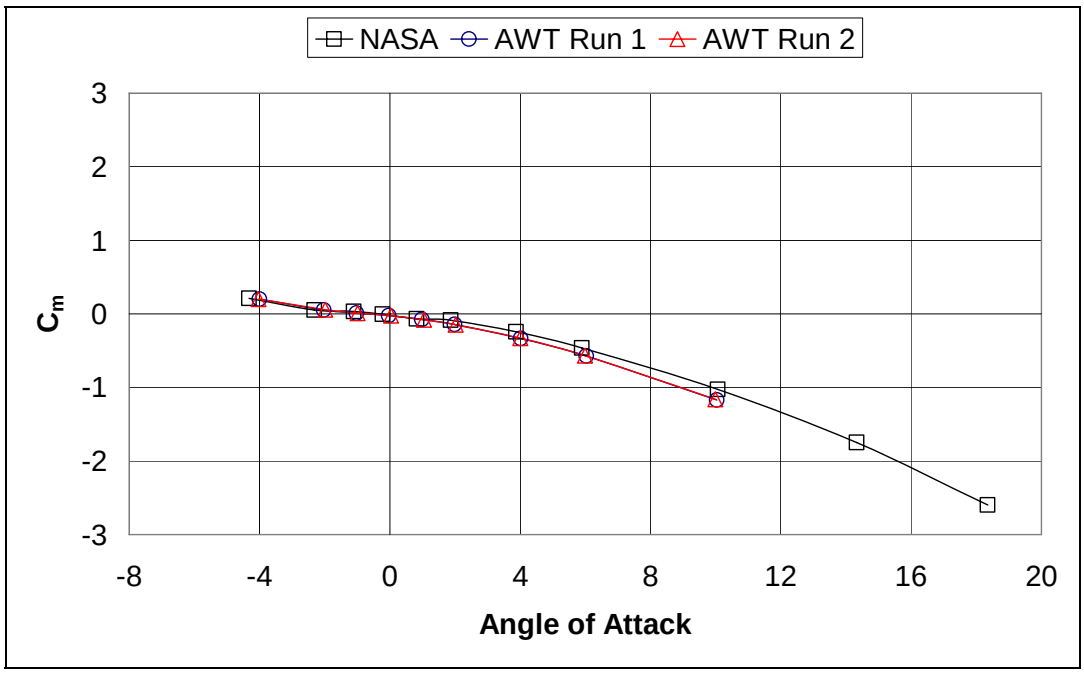

Figure 71 Comparison of AWT / NASA Results, Pitch Moment ($\phi = 0°$)

After investigation of the Axial Force results (Figure 72) it is seen that the results are to much bigger than the NASA results. After a literature survey it is seen that a correction, base pressure correction, is applied at the test which sting type balance is used.

A large part of wind-tunnel testing involves the use of rear sting-supported models. Experimental data for sting-support effects on model characteristics are needed in order to estimate more exactly free-flight conditions. [18] One of the major reasons

for this is that base pressure is influenced to a large extent by the existence of the sting extending from the model base which supports the model in the tunnel. [19]

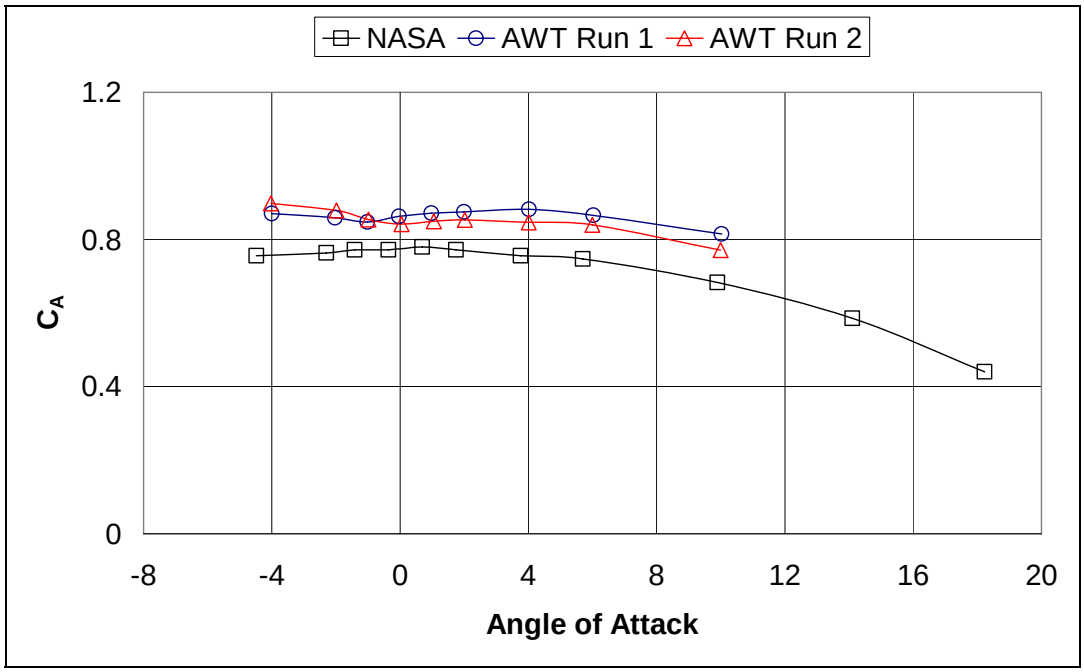

Figure 72 Comparison of AWT / NASA Results, Axial Force ($\phi = 0°$)

As seen from Figure 73, because of the sting support at the base, the pressure distribution in free-flight conditions does not occur and the axial force is measured bigger than the free-flight condition. In addition, in the test case report, [21], it is stated that the test results are corrected for base pressure effects, which means therefore, that the present results must also be corrected if we want to compare the two results. For correction the base pressure must be measured at the base of the model. In these experiments the base pressure was measured from 4 points as seen from Figure 74 by means of Multi Channel Pressure System whose output gives the pressure difference with respect to a reference pressure which is the atmospheric pressure. Fortunately this value is what will be used for base pressure correction as well.

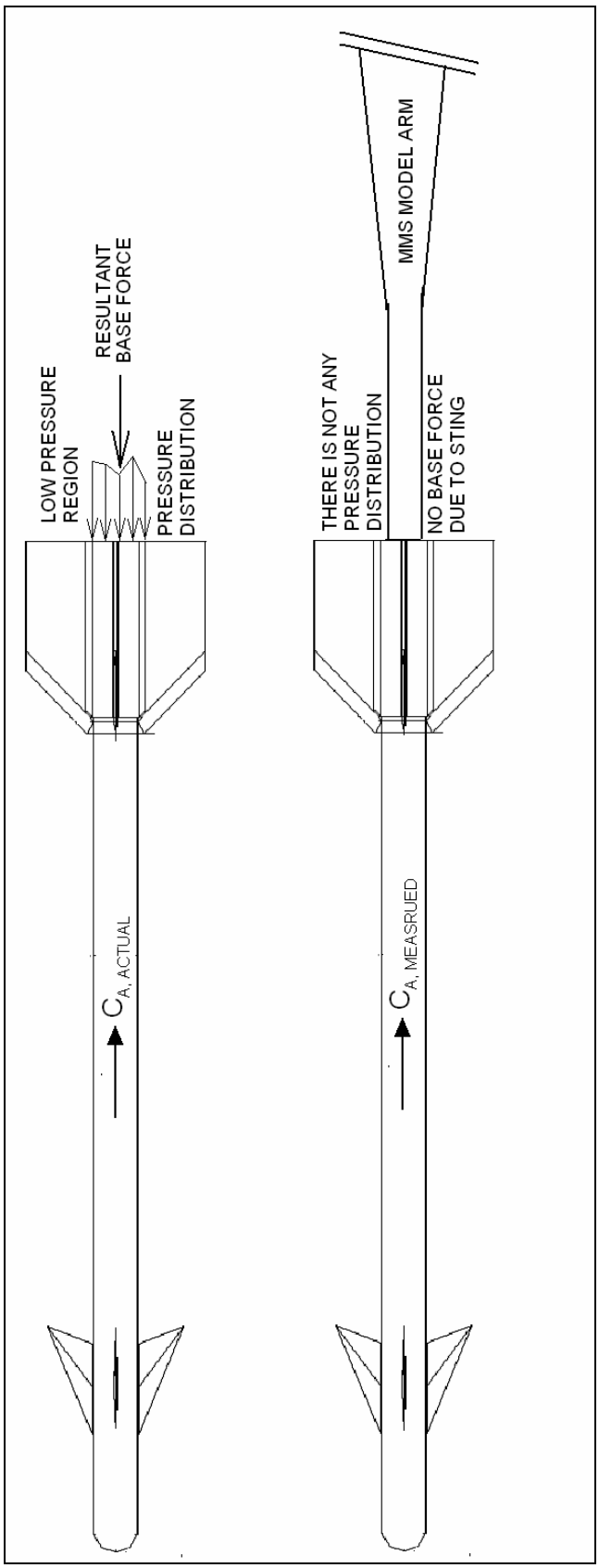

Figure 73 Base Pressure with and without MSS Sting

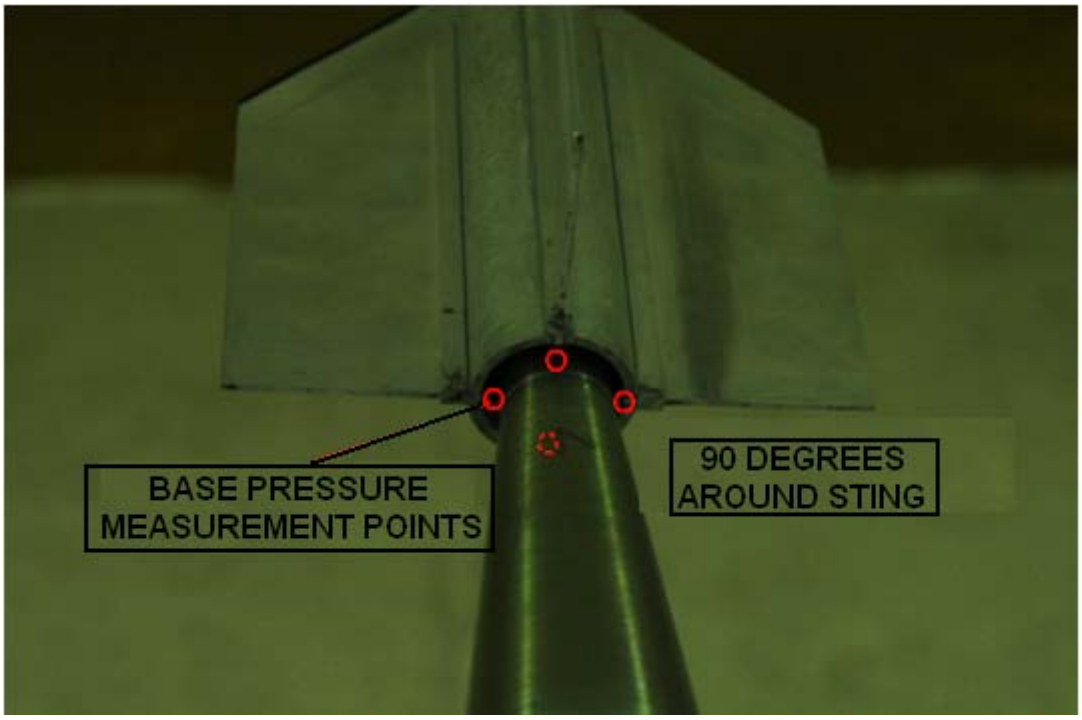

Figure 74 Base Pressure Measurement Points

$$F_{AC} = F_{AM} - S_b(p - p_b) \tag{4.1}$$

where F_{AC} = Corrected (actual) axial force

F_{AM} = Measured axial force with sting

S_b = Base Area

p = Reference Pressure (Atmospheric Pressure)

p_b = Base Pressure which is measured at the base of the model

$$\frac{F_{AC}}{\frac{1}{2}\rho V^2 S} = \frac{F_{AM}}{\frac{1}{2}\rho V^2 S} - \frac{S_b(p - p_b)}{\frac{1}{2}\rho V^2 S} \tag{4.2}$$

in this case $S = S_b$ so:

$$C_{AC} = C_{AM} - \frac{(p - p_b)}{\frac{1}{2}\rho V^2} \tag{4.3}$$

where C_{AC} = Corrected (actual) axial force

C_{AM} = Measured axial force with sting

C_{AB} = Axial Base Coefficient $\frac{(p - p_b)}{\frac{1}{2}\rho V^2}$

So the final equation becomes:

$$C_{AC} = C_{AM} - C_{AB} \tag{4.4}$$

As seen from Figure 75, NASA results and the AWT results are in good agreement for low angles of attack (<6°) the difference between two results gets bigger at high angle of attack. The error, which the definition is given in equation 4.5,.of AWT results are at the order of %15 for high angle of attack. (Table 21)

$$\%error = 100 \times \left| \frac{C_{AB\,AWT} - C_{AB\,NASA}}{C_{AB\,NASA}} \right| \tag{4.5}$$

Table 21 Base Axial Force Results with Error

NASA		AWT		Error %
α	C_{AB}	α	C_{AB}	
-4.258	0.104	-4.258	0.107	2.261
-2.186	0.105	-2.186	0.101	3.130
-1.208	0.104	-1.208	0.102	1.391
-0.200	0.104	-0.200	0.103	0.136
0.778	0.103	0.778	0.105	1.537
1.814	0.104	1.814	0.107	2.919
3.829	0.106	3.829	0.111	4.587
5.874	0.112	5.874	0.115	2.666
10.021	0.125	10.021	0.138	11.100
14.138	0.130	14.138	0.152	16.987

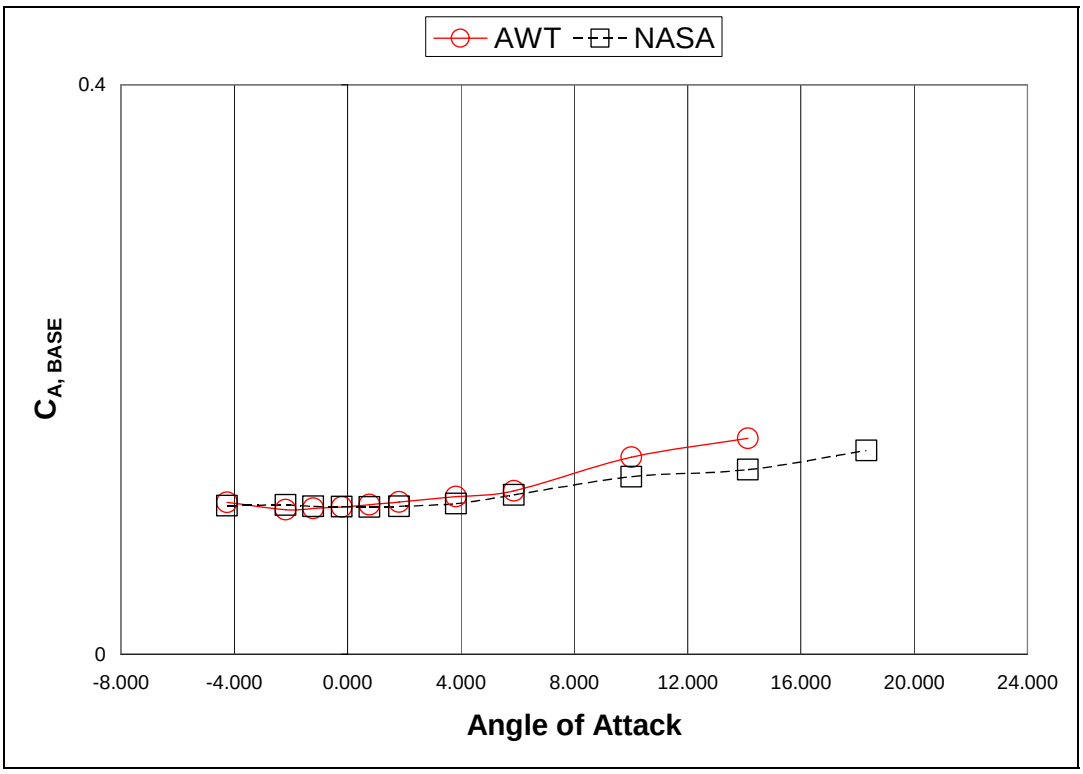

Figure 75 Base Axial Force with respect to Angle of Attack

After the correction it is seen that the Axial Force coefficient which is found by AWT-AMS comes closer to the coefficient that is found by NASA. For this reason the base pressure correction is applied to the all results.

The axial force coefficient are given in Figure 76. AWT V1 results are more or less the same with the NASA results but AWT V2 results are not as “perfect” as AWT V1 results. It can easily be said that they are in good agreement with NASA results. For the Normal Force coefficient (Figure 77) both results of AWT, V1 and V2, coincide with each other and with NASA results as well with a small shift at low angles of attack. This shift gets smaller for high angles of attack.

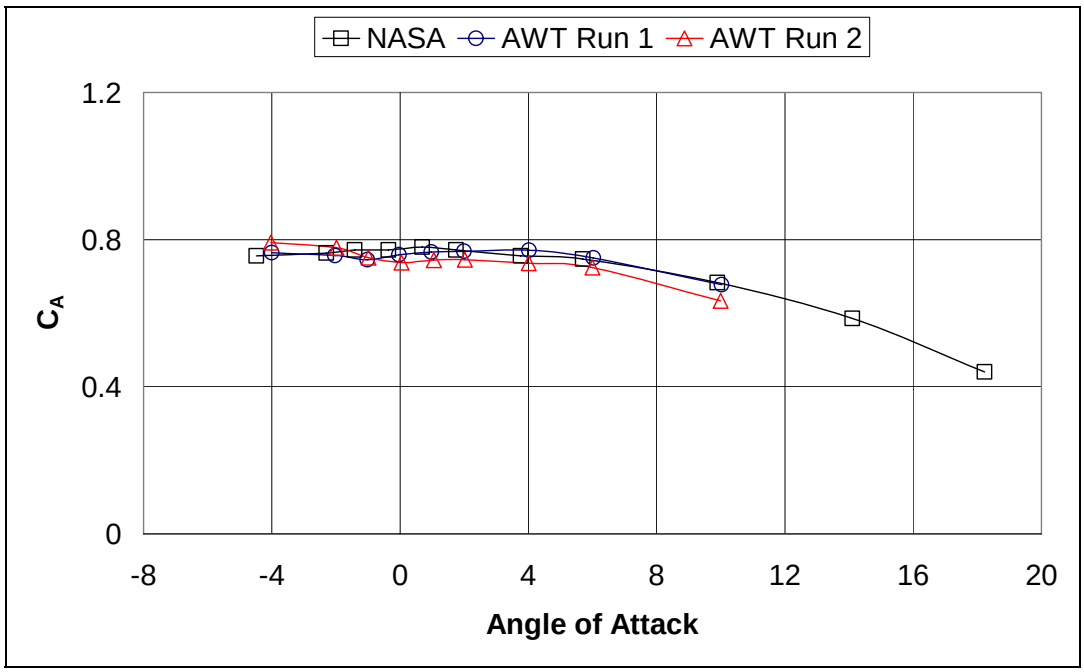

Figure 76 Comparison of AWT / NASA Results, Axial Force ($\phi = 0°$)

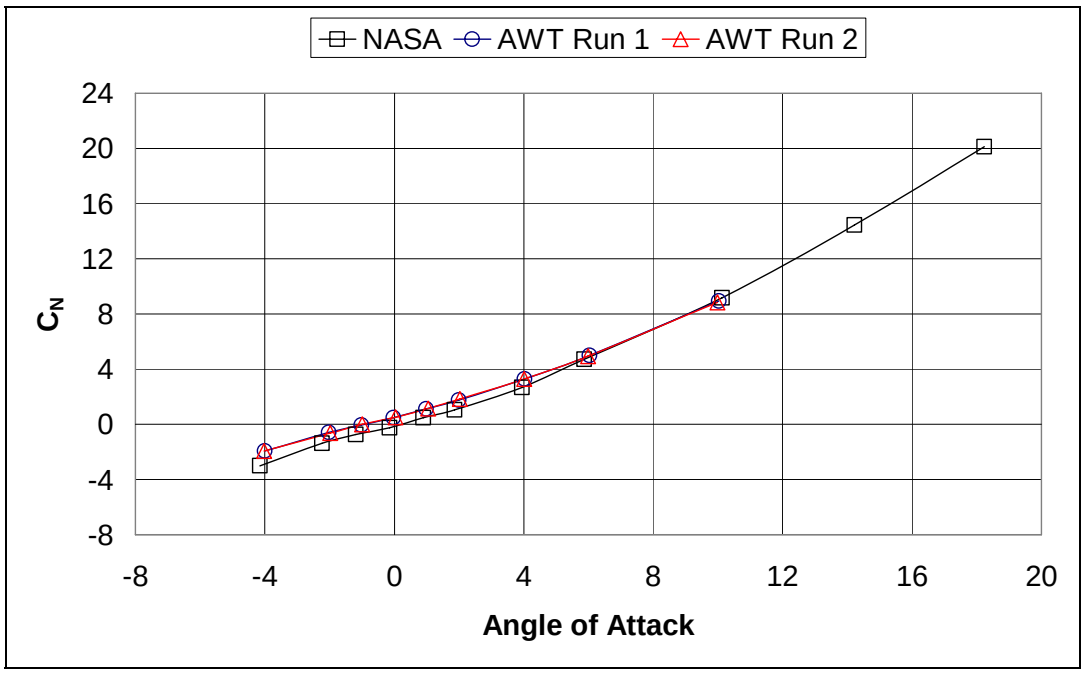

Figure 77 Comparison of AWT / NASA Results, Normal Force ($\phi = 0°$)

Beside these small shifts in normal force and pitch moment and the shift in axial force coefficients between AWT V1 and AWT V2, the results of AWT-AMS are in quite good agreement with the NASA results for $\phi = 0°$ configuration.

When comparing the results of pitching moment of $\phi = 45°$ case, it can be seen that AWT-AMS results are in good agreement with NASA results with a small shift. (Figure 78) For axial force component the results of AWT-AMS are very close to NASA results for low angles of attack. But unfortunately for high angles of attack the results are not close to of NASA results. (Figure 79)

The normal force results of AWT-AMS (Figure 80) are in good agreement, but not identical with the NASA results. In addition the slope of the normal force coefficient with respect to the angle of attack for the AWT-AMS result is different from that of the NASA results'.

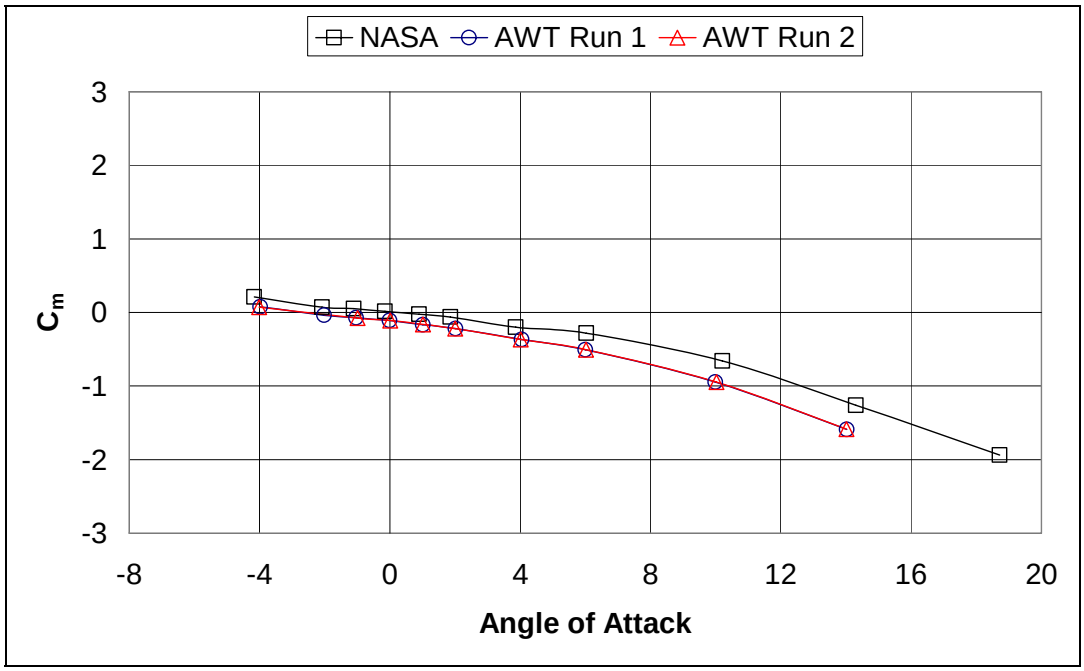

Figure 78 Comparison of AWT / NASA Results, Pitch Moment ($\phi = 45°$)

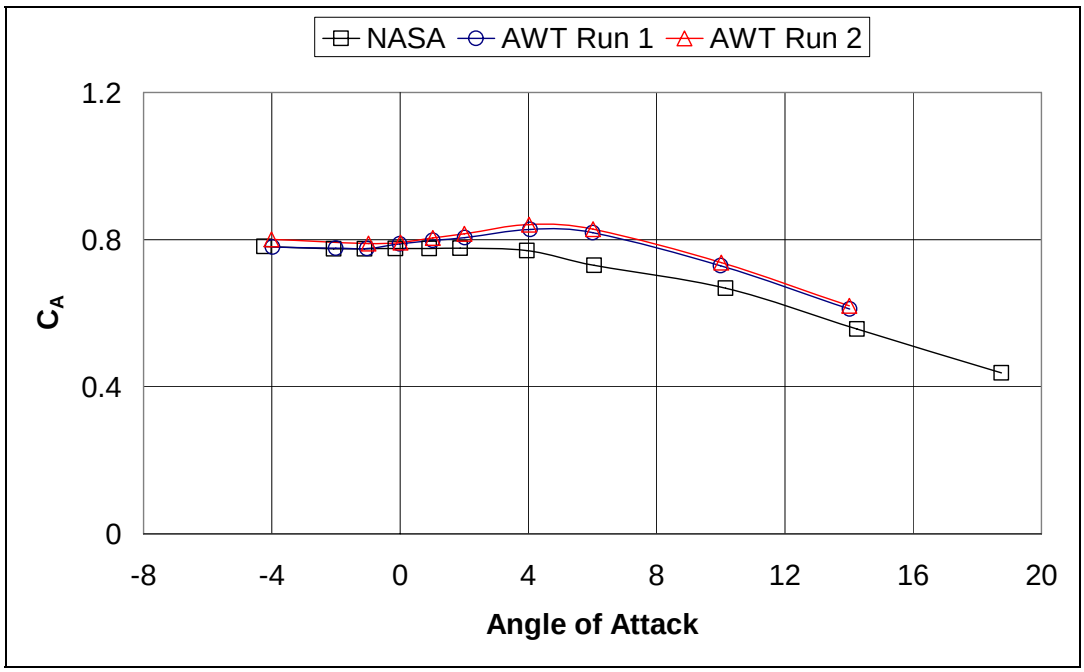

Figure 79 Comparison of AWT / NASA Results, Axial Force ($\phi = 45°$)

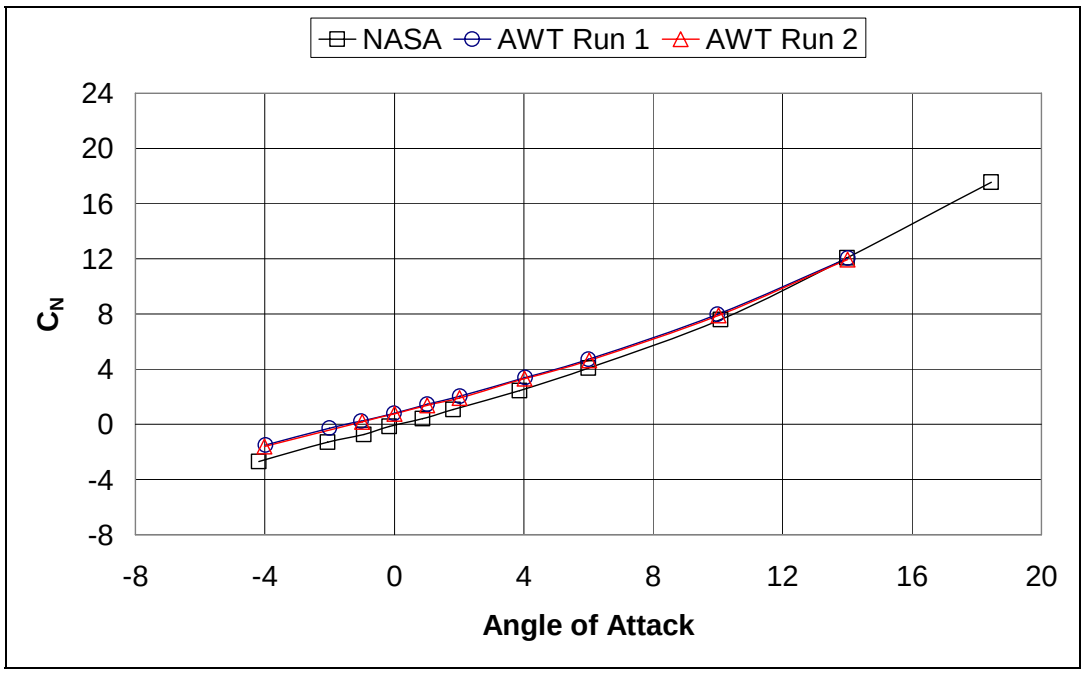

Figure 80 Comparison of AWT / NASA Results, Normal Force ($\phi = 45°$)

AWT-AMS results for $\phi = 45°$ configuration are in good agreement with NASA results except the shift in axial force coefficients. In addition the repeatability of the test results is very good for this case. But the results of $\phi = 0°$ case are even closer to the NASA results than $\phi = 45°$ case.

4.4 VERIFICATION and VALIDATION

When comparing the results of AWT-AMS with NASA results, it must be kept in mind that the two models are not identical. It must be considered that the model is the most important factor for wind tunnel testing. Any small misalignment of the model affects all of the aerodynamic measurements. The manufacturing tolerances, some possible misalignment of parts at the installation of model can significantly affect the results.

Another parameter, that affects the results, is the Reynolds number. The two Reynolds numbers are significantly different from each other. The Reynolds number for Langley Research Center was 6.56 10^6 per meter, whereas the one for AWT was 1.97 10^6 per meter for AWT. The Reynolds number difference leads different transition locations hence different aerodynamic behaviors, especially for Axial Force coefficients, on the model. The location of the transition point can be controlled by strips but the strips used for two wind tunnels were also different.

As a result even though, there are lots of discrepancies in terms of experimental facilities, one can still say that the results obtained in AWT-AMS are in good agreement with NASA results. There are some slight shifts in some coefficients but the behavior of the coefficients are very similar. The model, Reynolds number and transition strips effects can cause these shifts in the coefficients.

CHAPTER 5

CONCLUSION

In this study, a data acquisition system is designed, built and implemented to the Ankara Wind Tunnel to perform the tests automatically with minimum human intervention under the command of a central computer and a program, Ankara Wind Tunnel – Automated Measurement System, which is written in LabVIEW programming language. With in the scope of this thesis, following actions were performed:

The old data acquisition system is replaced with the new data acquisition cards, which are the products of National Instruments, and the integration of the existing measurement system (Pressure Transducer, Resistance Thermometers, and External Balance System) with this new DAS was performed. After the installation of the new cards to this measurement system, the software which is written in Test Point programming language is re-written in LabVIEW programming language. In the new system the temperature measurements are performed with Thermocouples instead of resistance thermometers used in the old system.

After getting the temperature and pressure values, the flow parameters are calculated with the new program. The external balance calibration was performed with the new program AWT-AMS.

New measurement systems such as Internal Balance System, Multi-Channel Pressure Measurement System, Servo and Step motor controller systems are also integrated to the AWT's new data acquisition system. A new Model Support

System (MSS) is designed ,manufactured and installed in the test section of AWT for use with Internal Balance System.

Before using the Internal Balance System for the tests, to understand the working principles of the internal balance and to find out the accuracy of the system a calibration rig is designed and manufactured to perform some wind-off loading. For wind-off loadings, the known loads are applied to the system and the results are compared with the applied values.

To give the MSS the desired angle of attack during the tests automatically, a servomotor drive system is installed to the DAS and the tests are conducted with this new mechanism. In addition, a stepper motor is installed to the DAS to automate the angle of attack mechanism of the existing external balance system.

The RPM control mechanism of the AWT Driver is installed to the new DAS and the RPM control is done by AWT-AMS automatically.

To test the accuracy and the reliability of the new system, a test case is experimented in the AWT. This is the test for Sidewinder missile model. The model was previously tested in the NASA Langley Research Center and some aerodynamic data are available in the literature. A similar model of Sidewinder is manufactured with the given drawings in the model report and the test with this model are conducted at Mach 0.2 at AWT. The results are then compared with those obtained in NASA and the capacity of DAS and AWT-AMS are evaluated.

Base pressure correction which is a must for sting type internal balance applications are performed for the AWT results by measuring the pressure at the base of the model with multi-channel pressure system.

This thesis forms a major step to have internal balance test at AWT. Through the work presented in this thesis, it has become possible to have automated controlled tests with minimum human interference under the command of a central computer.

Although the system can work properly, some improvements are still needed for AWT. These improvements can be summarized as follows:

At the verification test, it is observed that the MSS load limits are not as high as internal balances. In addition the designed MSS have only one degree of freedom-angle of attack-; MSS must be turned manually to have a side slip test. For these reasons a new MSS must be designed for having larger load limits and it must have 2 degrees of freedom that the angle of attack and the side slip angles can be given with servo motors automatically.

Although wind-off loadings can be applied with the recent calibration rig, misalignment problem results in extra loadings. A new calibration rig that has two degrees of freedom must be designed and at each loading point the balances must be leveled accurately.

AWT-AMS can be improved with installation of new DAC to DAS and a fully automatic program can be written in LabVIEW. The program can work with an input file, batch file, and the corresponding measurement, model attitude control can be done fully automatically with this program.

REFERENCES

[1] YILDIZ T. Z., "**Modernisation, Modification and Calibration of The Mechanical Balance System of Ankara Wind Tunnel**", Ankara, 1999.

[2] OZDEMIR E., "**Calibration and Instrumentatıon of Ankara Wind Tunnel**", 2000

[3] "**ESP-Miniature Pressure Scanners User's Manual**", Pressure Systems Inc, (1999)

[4] "**6052E User Manual**", National Instruments Corporation, (1999)

[5] "**7344 Hardware User Manual**", National Instruments Corporation, (1999)

[6] "**6024E User Manual**", National Instruments Corporation, (1994)

[7] "**SCXI-1140 User Manual**", National Instruments Corporation, (1994)

[8] "**SCXI-1300/1301 Terminal Block Installation Guide**", National Instruments Corporation, (2000)

[9] "**SCXI-1163R User Manual**", National Instruments Corporation, (1994)

[10] "**SCXI-1326 High Voltage Terminal Block Instalation Guide**", National Instruments Corporation, (1999)

[11] "**SCXI-1112 User Manual"**, National Instruments Corporation, (1999)

[12] "**SCXI-1520 User Manual"**, National Instruments Corporation, (2001)

[13] "**SCXI-1314 Universal Strain Terminal Block Installation Guide**", National Instruments Corporation, (2000)

[14] "**7344 Hardware User Manual"**, National Instruments Corporation, (1999)

[15] "**Universal Motion Interface (UMI) Accessory User Guide**", National Instruments Corporation, (1999)

[16] "**Calculation and Analysis of Strain Gauge Balance Calibration Matrix Mathematical Models**", TUBITAK-SAGE., (2000)

[17] "**35mm and 22mm Sting Balances Calibration Report for TÜBİTAK-SAGE~ANKARA WIND TUNNEL**", Aerotech ATE Ltd., (2003)

[18] Maurices S. Chan, "**An Experimental Investigation of Sting-Supoort Effects on Drag and a Comparision with Jet Effects at Transonic Speeds**", NACA Report 1353 1958

[19] Alan Pope, Kenneth L. Goin "**High-Speed Wind Tunnel Testing**", 1978

[20] Colin P. Britcher, "**Subsonic Sting Interference on the Aerodynamic Characteristics of a Family of Slanted-Base Ogive-Sylinders**" NASA Report 4299 1990

[21] Ernald b. Graves and Roger H. Fournier, "**Stability and Control Characteristics at :Mach Numbers from 0.2 to 4.63 of a Cruciform Air-To-Air Missile with Triangular Canard Controls and a Trapezoidal Wing**" NASA Technical Momerandum X-3070 1974

APPENDIX A

PRESSURE TRANSDUCER and MANOMETER

A.1 PRESSURE TRANSDUCER

Applications

Fuel Cells

Energy Management Systems

Pump Speed Control

Filter Condition Monitoring

Process Control

Refrigeration Equipment

HVAC

Model 230 Specifications	
Electrical Output Voltage	0 to 5 VDC 0 to 10 VDC
Electrical Output Current	4 to 20 mA
Accuracy (RSS Method)	±0.25% Full Scale
Type of Pressure	Differential (can be wet both sides)

Pressure Ranges	Unidirectional: 0 to 1, 2, 5, 10, 25, 50, 100 psid Bi-directional: 0 to ±0.5, ±1, ±2.5, ±5, ±10, ±25, ±50 psid
Thermal Effects	Thermal Compensation °F (°C): 30 to 150 (-1 to 65) %FS/100°F(100°C)max.zero: ±2.0 (±3.6) %FS/100°F(100°C)max.span: ±2.0 (±3.6)
Media	Gases or liquids compatible with 300 series and 17-4PH stainless steel, and Viton® "O" ring. (Hydrogen not recommended for use with 17-4 PH stainless steel.) *Viton® is a registered trademark of DuPont Dow Elastomers

A.2 PRESSURE MANOMETER

Features

Dual Channel

User Adjustable Hi/Lo Alarms

Easy Front Panel Setup

Pressure Displayed in Desired Engineering Units

Tabletop or Panel Mount

12 VDC & 24 VDC Power Supply (UL Approved)

1/8 DIN Package (Meter)

1/4 DIN Package (Manometer)

Internal Reference Voltage for Easy Calibration

Datum 2000™ Specifications	
Display	Type: Light emitting diode Color: Red Height of Digits: 0.56 inch Maximum Readout: -9999 to +31999 Reading Rate: 2 to 3 times per second depending on input voltage Overload Signal (over range reading): OVEr Underload Signal (under range reading): UndEr Polarity Signal: Negative only Brightness: Constant
Accuracy (Readout Only)	At 73°F (23°C): ±0.01%R ±1 digit At 60°F to 95°F (16°C to 35°C): ±0.04%R ±1 digit
Environmental	Operating Temperature: +32°F to +130°F (0°C to 55°C) Storage Temperature: -40°F to +185°F (-40°C to +85°C)
Electrical Data	Power: Domestic: 24 VDC (115 VAC 60 Hz, 12 watt adapter provided w/ -1 models)

	European: 24 VDC (220 VAC 50 Hz, 14 watt adapter provided w/-2 models) Adapter has European 2 prong plug with turret Power Cord Length: 6 feet (approx.)
Physical	Width: 3.61 inches (92mm) Height: Meter: 1.74 inches (44mm) Manometer: 3.50 inches (89mm) Depth (including connector): 7 inches: (178 mm) (Allow at least 1/2" more for wires attached to terminal strip)
Cutout Dimensions	Cutout Dimensions: Meter: 1/8 DIN: 3.67 in. x 1.80 in. (46 mm x 93 mm) Manometer: 1/4 DIN: 3.67 in. x 3.56 in. (90 mm x 93 mm) Front Panel: Meter: 3.82 in x 1.97 in. (98 mm x 50 mm) Manometer: 3.82 in x 3.74 in. (98 mm x 95 mm)
Analog Output	Transducer: Same as transducer output voltage Transmitters: No analog output. The DATUM 2000™ terminates the current loop.
Adjustment Capabilities (accessible through the user set-up menus)	Voltage Inputs: +11 to -11 volts Current Inputs: 0 to 20 mA Maximum Reading: +31999 Minimum Reading:

	-9999
Input Specifications	Transmitter Inputs Signal: 4-20 mA Transmitter Inputs Impedance: 150 ohm Transmitter Inputs Voltage Drop: 3 VDC (max.) Transducer Inputs Signal: +11 VDC to -11 VDC Transducer Inputs Impedance: 45k ohm

APPENDIX B

CONNECTION DIAGRAMS

B.1 PRESSURE TRANSDUCER CONNECTION

The pressure transducers are connected to SCXI-1301 hence SCXI-1140 to read the output voltages to get the three pressure values:

$P_{ATMOSPHERIC}$: The output of 0-20 psi absolute pressure transducer which gives the atmospheric pressure value. It is connected to Channel 5 of SCXI-1140 with screw terminal SCXI-1301 differentially.
P_{WALL}: The output of ±0.5 psi differential pressure transducer which gives the wall static pressure difference. It is connected to Channel 4 of SCXI-1140 with screw terminal SCXI-1301 differentially.
$P_{PITO-TUBE}$: The output of ±0.5 psi differential pressure transducer which gives the dynamic pressure at the test section. It is connected to Channel 0 of SCXI-1140 with screw terminal SCXI-1301 differentially.

The connection diagram of pressure transducer with SCXI-1301 hence SCXI-1140 is shown at the figure.

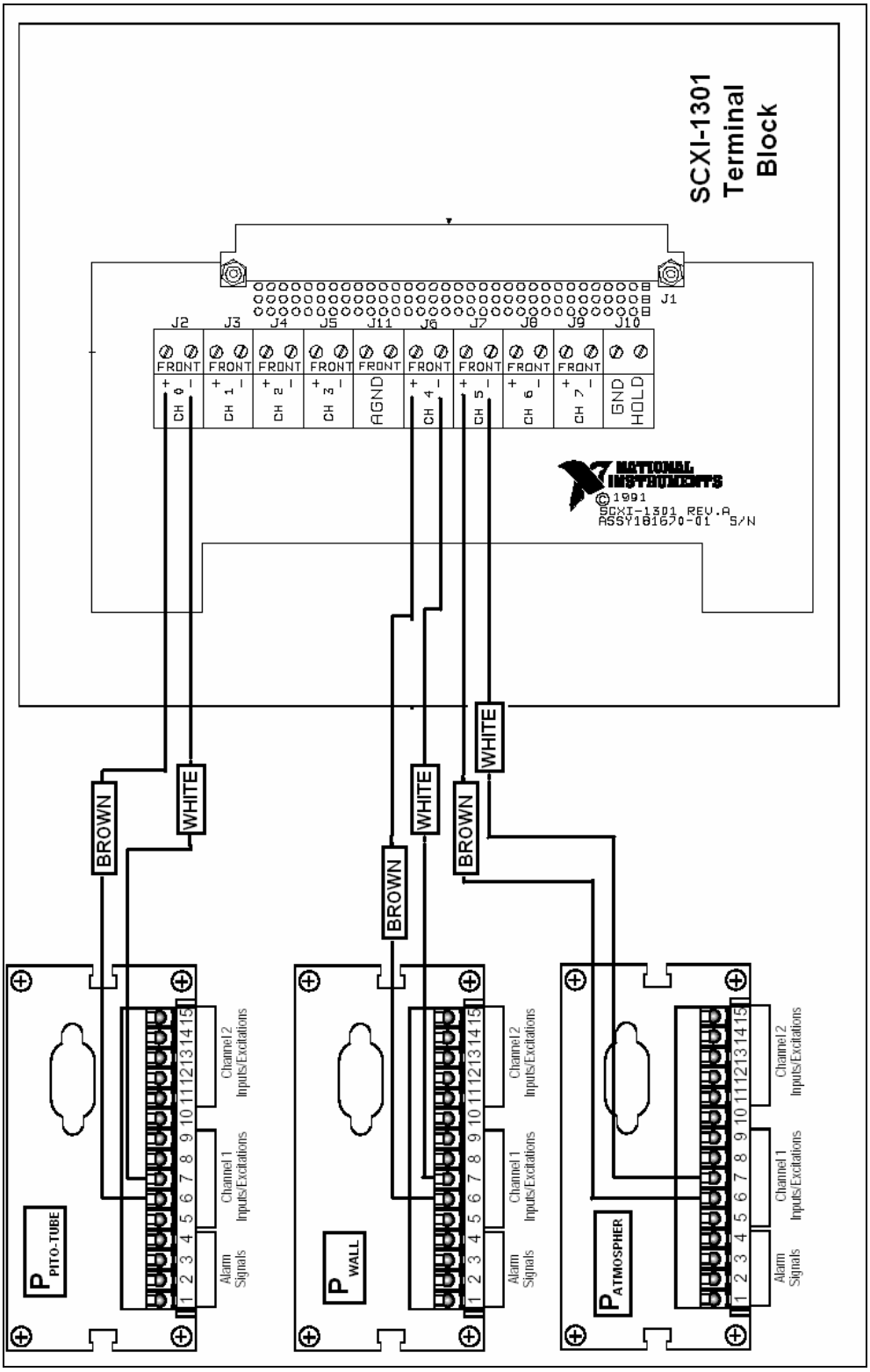

Figure 81 Pressure Transducer Connection Diagram

B.2 THERMOCOUPLE CONNECTION

The thermocouples are connected directly to SCXI-1121 without any screw terminal. There are 4 measurements points at wind tunnel:

T1: Climatic Room Temperature 1

T2: Climatic Room Temperature 2

T3: Test Room Temperature 1

T4: Test Room Temperature 2

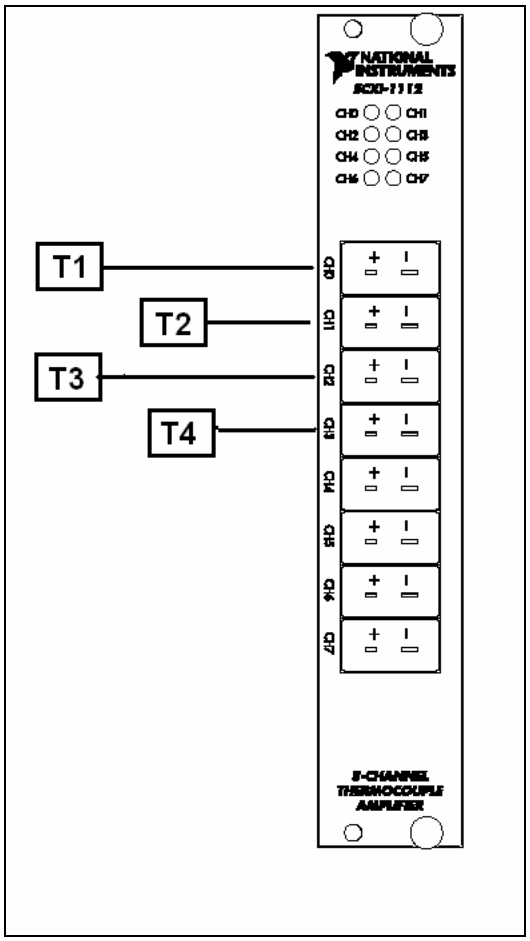

Figure 82 Thermocouple Connection Diagram

For getting reed of the temperature effects of External Balance System, it was built a Climatic Room around of the External Balance System. And to measure this room temperature two thermocouples are installed and the temperature is measured with these two thermocouples. These two values are averaged to get the final value.

Two thermocouples are installed to the test room (forward and backwards of the test room) to get the temperature value. The averaged value of these two device is taken into account for the calculations.

B.3 EXTERNAL BALANCE CONNECTION

The dynamometers on the External Balance System and the Strain Gauges of Internal Balance System are connected to SCXI-1314 screw terminal block and hence to SCXI-1520. As mentioned before SCXI-1520 is a special DAC for this type of applications.

The SCXI-1520 provides DC voltage for exciting a Wheatstone bridge. For half-bridge and full-bridge applications, the excitation voltage is available at terminal block connections P+ and P–. For quarter-bridge applications, connection is made to terminals P+ and QTR; the latter terminal allows connection to the quarter-bridge completion resistor.

Excitation voltage originates from two output buffers dedicated to each channel. Because each channel is controlled independently, a short circuit across the excitation terminals of one channel has no effect on the excitation of another channel. The output buffers have negative feedback connections at the terminal block remote-sense terminals, RS+ and RS–. You can run separate wires from the bridge to these terminals so that the amplifiers obtain feedback directly from the bridge, thereby forcing bridge voltage to equal the desired setting.

The analog input signal from the strain-gauge bridge is connected to S+ and S– of the terminal block. The connections can be seen from Table 22 and Figure 83.

Table 22 SCXI-1314 Signal Names

Signal Name	Condition
SCB (2 terminals)	Shunt calibration B signal
SCA (2 terminals)	Shunt calibration A signal
P -	Negative excitation signal
P +	Positive excitation signal
QTR	Quarter-Bridge completion resistor connection
S +	Positive input signal
S -	Positive input signal
RS +	Positive remote sense signal
RS -	Positive remote sense signal

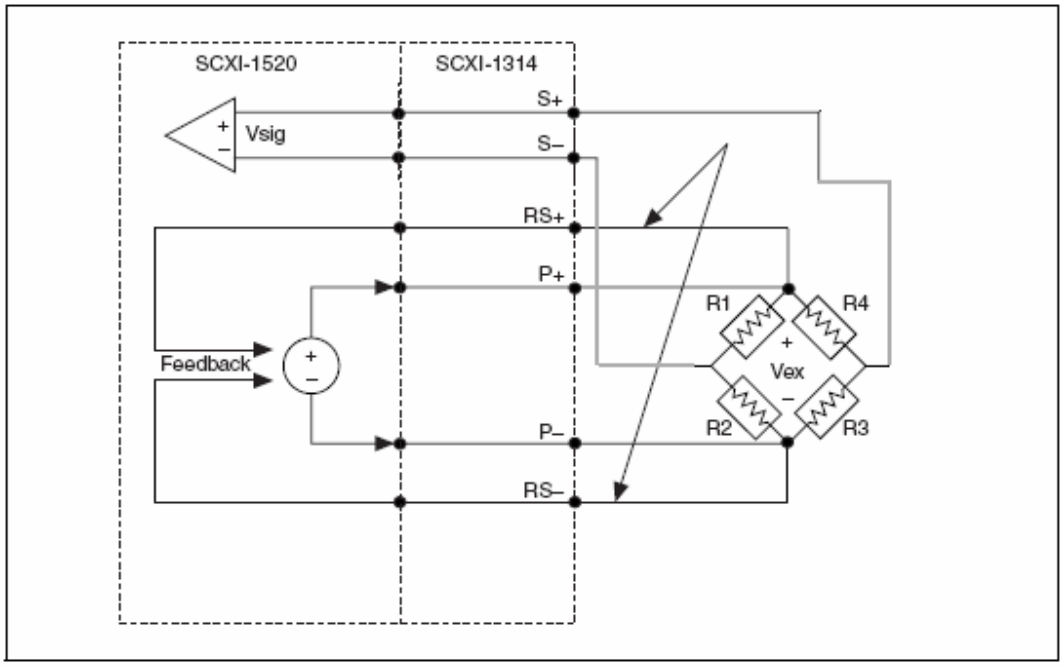

Figure 83 SCXI-1314 and SCXI-1520 Connections

The seven dynamometers connections are the same with each other and given at Table 23. the 1st dynamometer is connected to the 1sr channel while the 2nd dynamometer to 2nd channel and so on for all seven dynamometer.

Table 23 External Balance Connections

Channel Number	Channel n
SCB (2 terminals)	
SCA (2 terminals)	
P -	Yellow
P +	Green
QTR	
S +	Red
S -	Blue
RS +	Black
RS -	White
Related Component	Dynamometer n
Where n is 1 to 7	

B.4 INTERNAL BALANCE CONNECTION

The Internal Balance System connections are done with SCXI-1314 and SCXI-1520 like the External Balance System which the idea is exactly the same. 10 VDC excitation value is given with P- and P+ with remote sense connections RS- and RS+. The output of the internal balance is taken with S- and S+ connections. The connections are given at Table 24 for internal balance.

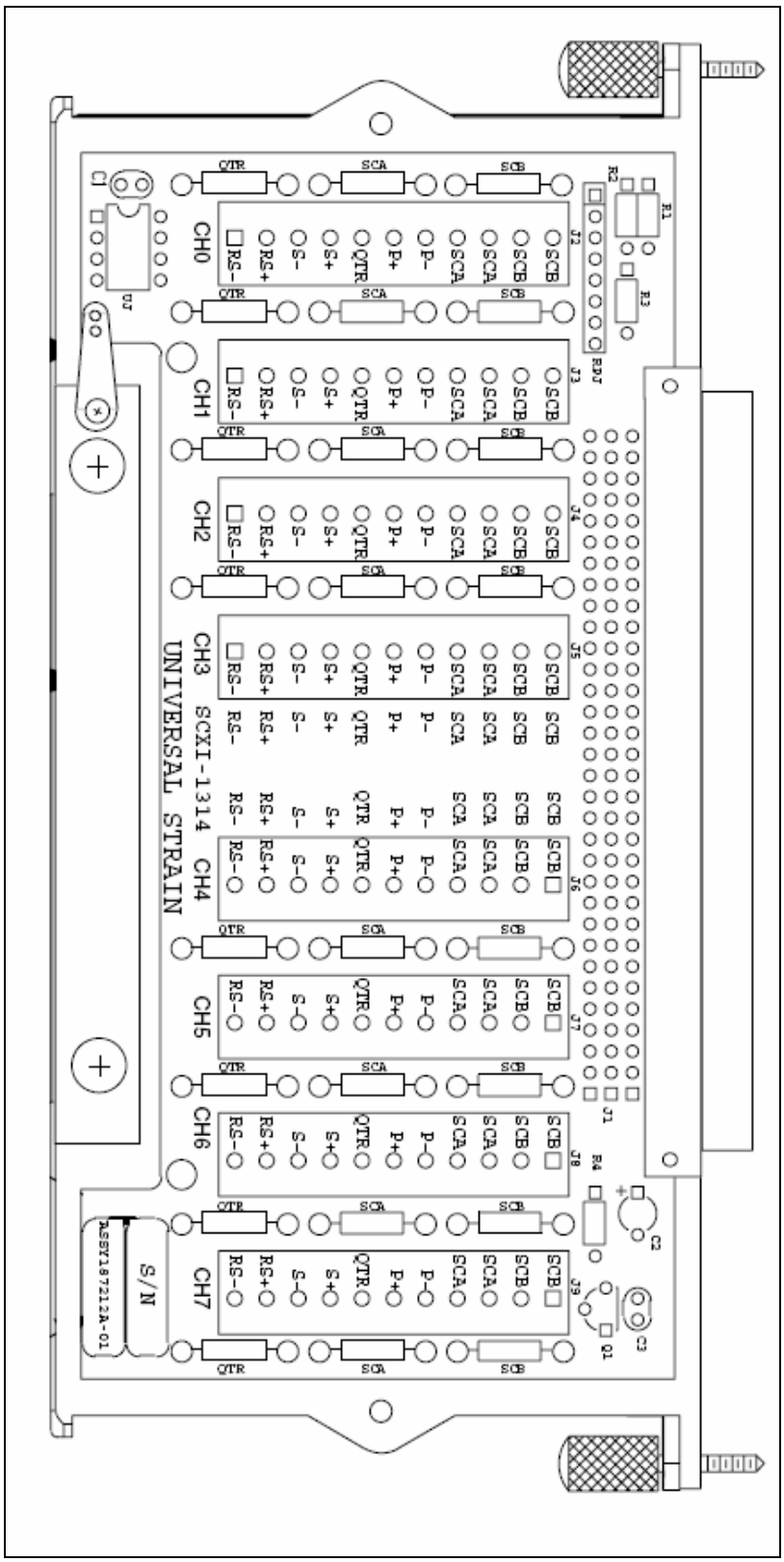

Figure 84 SCXI-1314 Screw Terminal Signal Connections

Table 24 Internal Balance Connections

Channel Number	Channel 1	Channel 2	Channel 3
SCB (2 terminals)			
SCA (2 terminals)			
P -	White / Brown	Grey / Green	Violet / Black
P +	Red / Black	Yellow / Blue	Red / Blue
QTR			
S +	Red	Orange	Green
S -	Blue	Brown	Yellow
RS +	Red / Brown	White / Blue	Green / Red
RS -	Brown / Black	Yellow / Brown	White / Violet
Related Component	Axial Force	Side Force	Normal Force
Channel Number	Channel 4	Channel 5	Channel 6
SCB (2 terminals)			
SCA (2 terminals)			
P -	Orange / Green	Grey / Brown	Grey / Blue
P +	Yellow / Green	Yellow / Red	Blue / Black
QTR			
S +	Pink	White	Violet
S -	Turquoise	Black	Grey
RS +	White / Green	White / Red	Orange / Blue
RS -	Green / Blue	Yellow / Violet	Green / Black
Related Component	Roll Moment	Pitch Moment	Yaw Moment

B.5 SERVO MOTOR CONNECTION

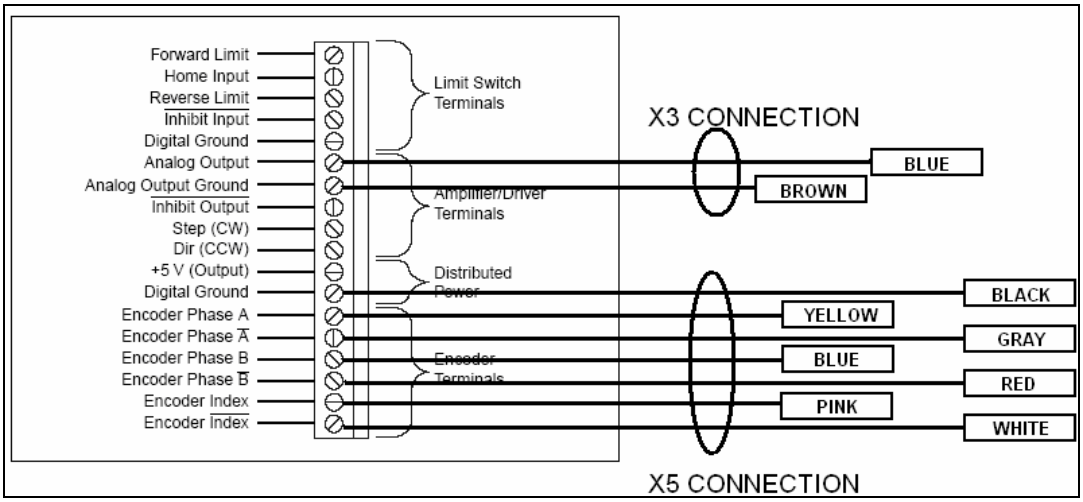

Figure 85 Servomotor UMI-7764 connection diagram

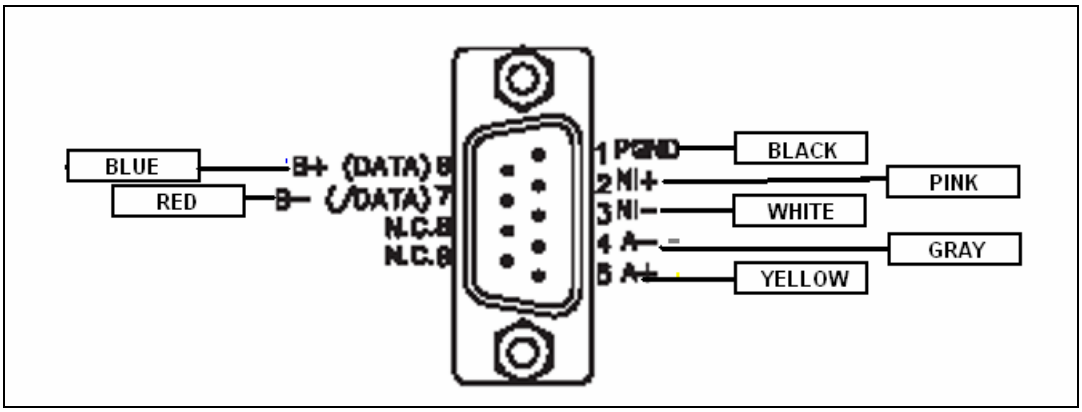

Figure 86 Servomotor X5 connection

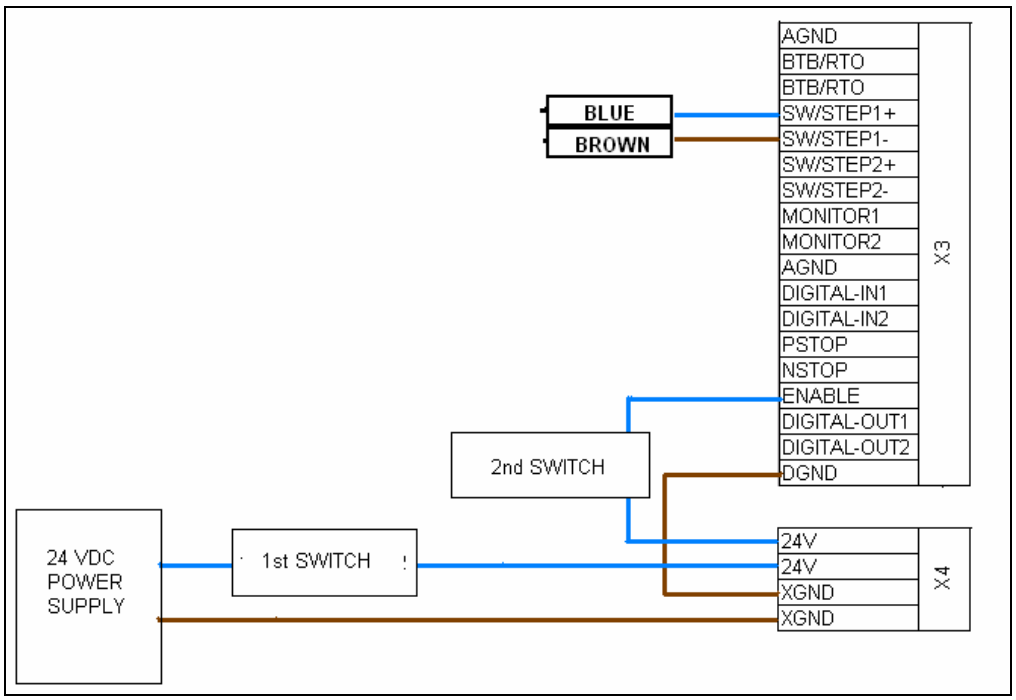

Figure 87 Servomotor Driver X3 and X4 connection diagram

B.6 STEPMOTOR CONNECTION

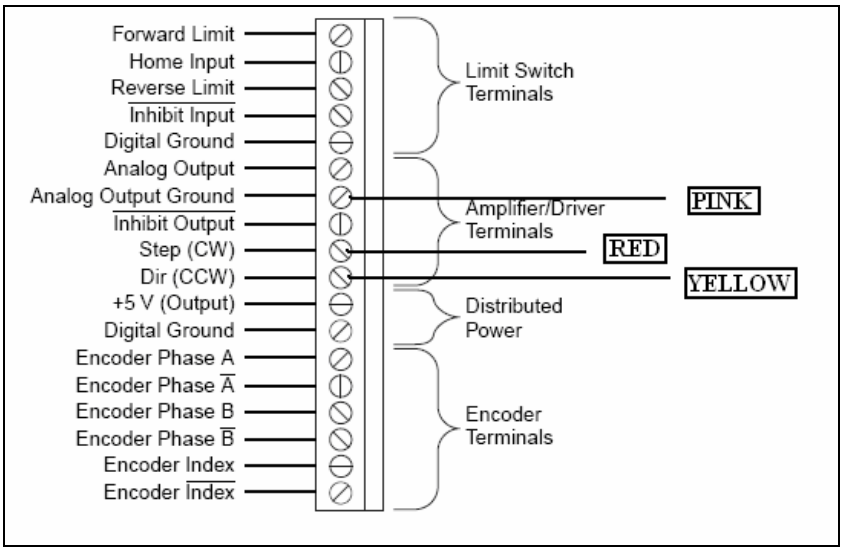

Figure 88 Step motor UMI-7764 Connection

B.7 MULTI-CHANNEL PRESSURE SYSTEM CONNECTION

Multi-Channel Pressure System is controlled with SCXI-1163R DAC and the output of the system is collected with SCXI-1520 as seen from Figure 89. The connections can be grouped into three:

1. Power Supply Connections: Connection for DC / DC converter supply 30 V DC.
2. Digital Address / Command Connections: Commands are given from this connection. (SCXI-1163R)
3. Output Connections: The output of the system is taken from this connection. (SCXI-1520)

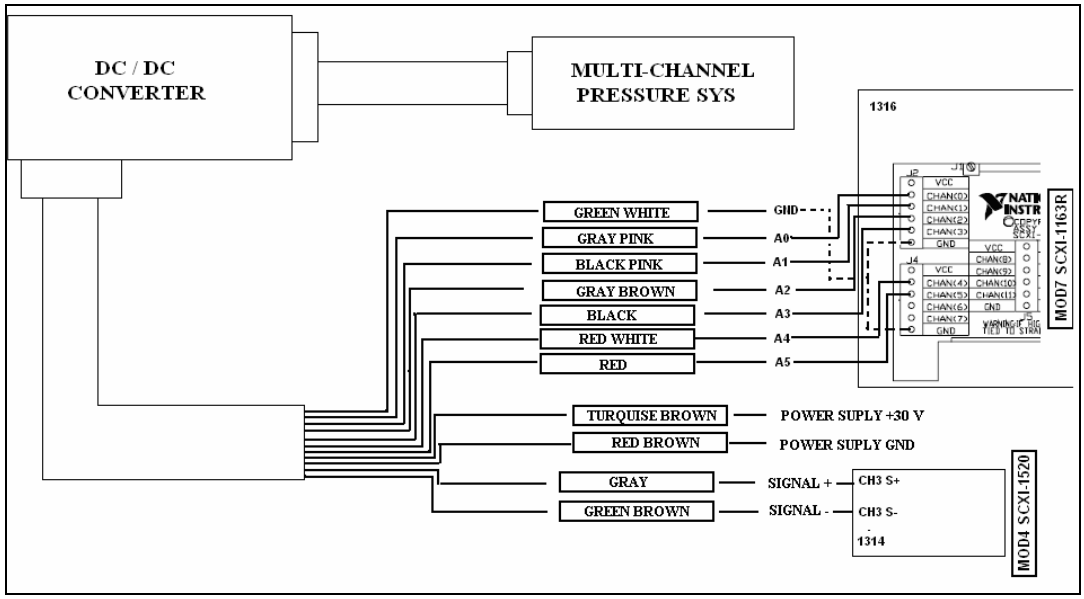

Figure 89 Multi-Channel Pressure System Connection

The commands are given to the Pressure System through 6 connections: A0, A1, A2, A3, A4 and A5. But how can it command up to 64 channels? The digital address is key word at this application.

When there is a 12 V difference between these 6 connections with GND these connections are addressed or in other words became active. And with a simple calculation in the base 2 the desired channel can be addressed or activated and the outputs of the system gives that channel's output. A sample addressing is like this:

Table 25 Addressing Sample

	A5	A4	A3	A2	A1	A0
Voltage difference	12	0	12	0	0	12
Multiplier	2^5	2^4	2^3	2^2	2^1	2^0
	32	0	8	0	0	1

TOTAL: 32 + 0 + 8 + 0 + 0 + 1 = 41 → Digital Address Channel Number

42 → Real Channel Number

And hence channel 41 is activated. Note that in the digital media all the channel numbers start with 0. But in reality the channel 41 is channel 42. It must be kept in mind. This addressing is continued till all the channels are scanned and the outputs are converted to the pressures and stored to the files.

B.8 RPM CONTROL CONNECTIONS

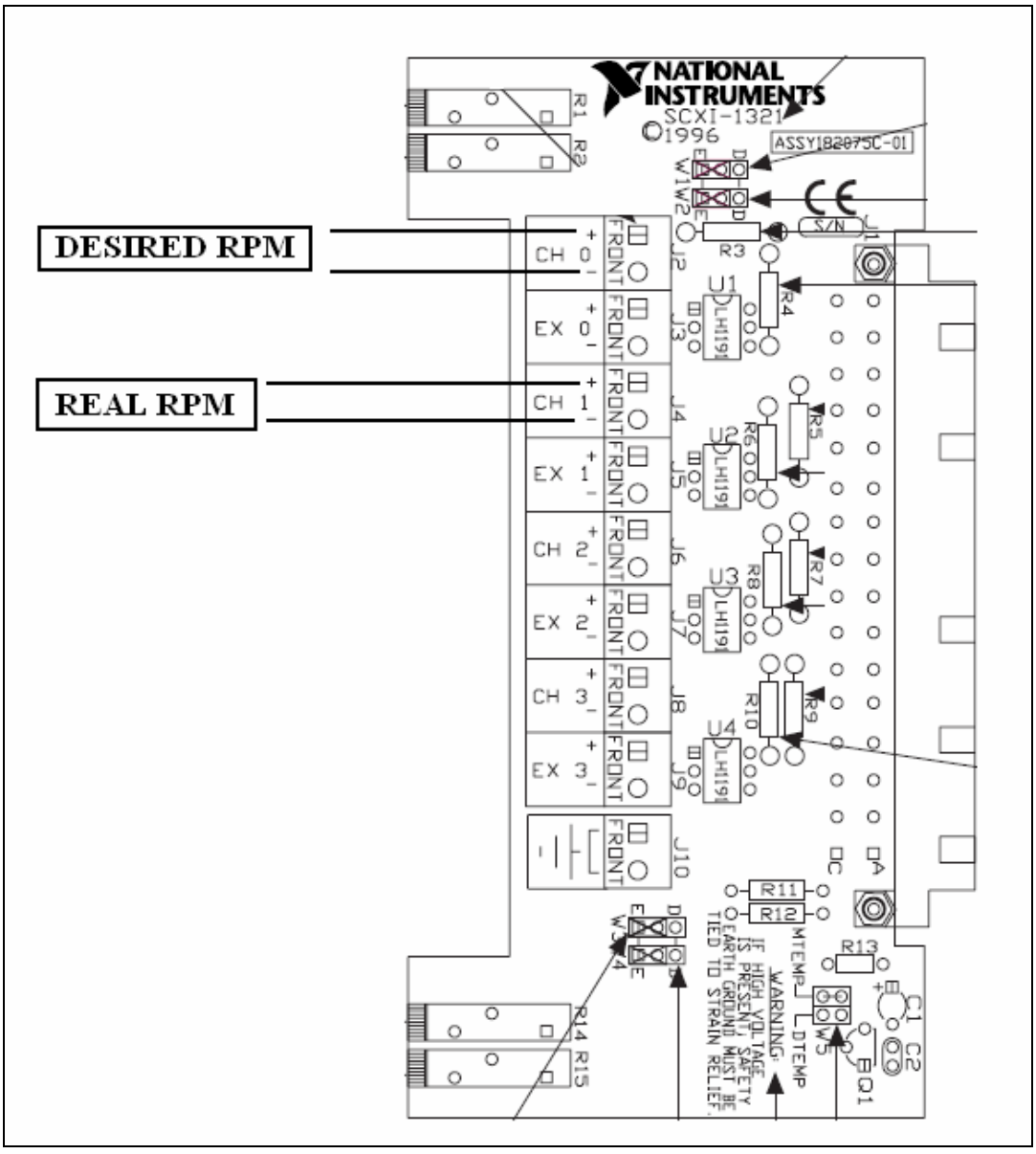

Figure 90 Motor Rpm / SCXI-1121 Connections

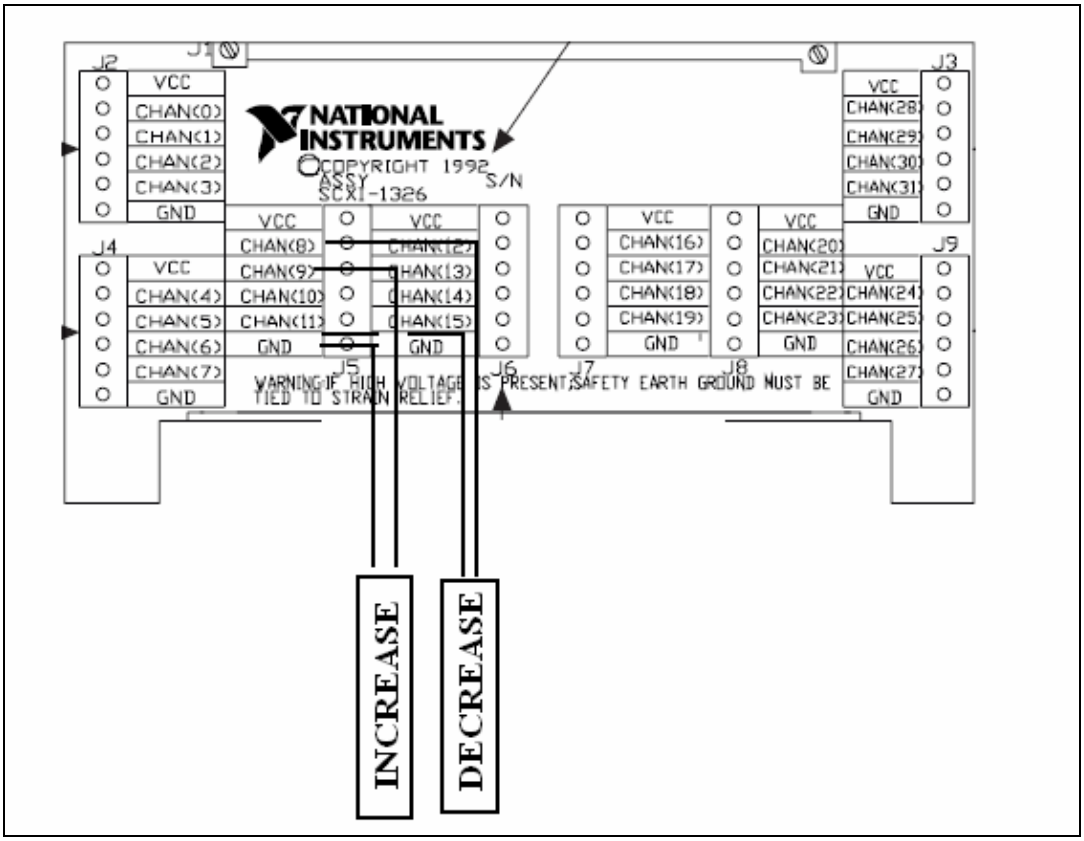

Figure 91 Motor RPM Command / SCXI-1163R Connections

APPENDIX C

EXTERNAL BALANCE CALIBRATION MATRIX

C.1 FIRST ORDER WITH 6 COEFFICIENTS

$$L(n) = R_1 X_{n1} + R_2 X_{n2} + R_3 X_{n3} + R_4 X_{n4} + R_5 X_{n5} + R_6 X_{n6}$$

C.2 SECOND ORDER WITH 27 COEFFICIENTS

$$\begin{aligned} L(n) = {} & R_1 X_{n1} + R_2 X_{n2} + R_3 X_{n3} + R_4 X_{n4} + R_5 X_{n5} + R_6 X_{n6} + \\ & R_{11} X_{n11} + R_{22} X_{n22} + R_{33} X_{n33} + R_{44} X_{n44} + R_{55} X_{n55} + R_{66} X_{n66} + \\ & R_{12} X_{n12} + R_{13} X_{n13} + R_{14} X_{n14} + R_{15} X_{n15} + R_{16} X_{n16} \\ & R_{23} X_{n23} + R_{24} X_{n24} + R_{25} X_{n25} + R_{26} X_{n26} \\ & R_{34} X_{n34} + R_{35} X_{n35} + R_{36} X_{n36} \\ & R_{45} X_{n45} + R_{46} X_{n46} \\ & R_{56} X_{n56} \end{aligned}$$

C.3 THIRD ORDER WITH 33 COEFFICIENTS

$$
\begin{aligned}
L(n) = {} & R_1 X_{n1} + R_2 X_{n2} + R_3 X_{n3} + R_4 X_{n4} + R_5 X_{n5} + R_6 X_{n6} + \\
& R_{11} X_{n11} + R_{22} X_{n22} + R_{33} X_{n33} + R_{44} X_{n44} + R_{55} X_{n55} + R_{66} X_{n66} + \\
& R_{12} X_{n12} + R_{13} X_{n13} + R_{14} X_{n14} + R_{15} X_{n15} + R_{16} X_{n16} \\
& R_{23} X_{n23} + R_{24} X_{n24} + R_{25} X_{n25} + R_{26} X_{n26} \\
& R_{34} X_{n34} + R_{35} X_{n35} + R_{36} X_{n36} \\
& R_{45} X_{n45} + R_{46} X_{n46} \\
& R_{56} X_{n56} \\
& R_{111} X_{n111} + R_{222} X_{n222} + R_{333} X_{n333} + R_{444} X_{n444} + R_{555} X_{n555} + R_{666} X_{n666}
\end{aligned}
$$

Where

$$R_{|1|} = |R_1|$$

$$R_{2|3|} = R_2 \times |R_3|$$

$$R_{|16|} = |R_1| \times |R_6|$$

$$R_{111} = R_1 \times R_1 \times R_1$$

C.4 SECOND ORDER WITH 84 COEFFICIENTS

$$
\begin{aligned}
L(n) = {} & R_1 X_{n1} + R_2 X_{n2} + R_3 X_{n3} + R_4 X_{n4} + R_5 X_{n5} + R_6 X_{n6} + \\
& R_{|1|} X_{n|1|} + R_{|2|} X_{n|2|} + R_{|3|} X_{n|3|} + R_{|4|} X_{n|4|} + R_{|5|} X_{n|5|} + R_{|6|} X_{n|6|} + \\
& R_{11} X_{n11} + R_{22} X_{n22} + R_{33} X_{n33} + R_{44} X_{n44} + R_{55} X_{n55} + R_{66} X_{n66} + \\
& R_{|1|1|} X_{n1|1|} + R_{2|2|} X_{n2|2|} + R_{3|3|} X_{n3|3|} + R_{4|4|} X_{n4|4|} + R_{5|5|} X_{n5|5|} + R_{6|6|} X_{n6|6|} + \\
& R_{12} X_{n12} + R_{13} X_{n13} + R_{14} X_{n14} + R_{15} X_{n15} + R_{16} X_{n16} \\
& R_{23} X_{n23} + R_{24} X_{n24} + R_{25} X_{n25} + R_{26} X_{n26} \\
& R_{34} X_{n34} + R_{35} X_{n35} + R_{36} X_{n36} \\
& R_{45} X_{n45} + R_{46} X_{n46} \\
& R_{56} X_{n56} \\
& R_{|12|} X_{n|12|} + R_{|13|} X_{n|13|} + R_{|14|} X_{n|14|} + R_{|15|} X_{n|15|} + R_{|16|} X_{n|16|} \\
& R_{|23|} X_{n|23|} + R_{|24|} X_{n|24|} + R_{|25|} X_{n|25|} + R_{|26|} X_{n|26|} \\
& R_{|34|} X_{n|34|} + R_{|35|} X_{n|35|} + R_{|36|} X_{n|36|} \\
& R_{|45|} X_{n|45|} + R_{|46|} X_{n|46|} \\
& R_{|56|} X_{n|56|} \\
& R_{1|2|} X_{n1|2|} + R_{1|3|} X_{n1|3|} + R_{1|4|} X_{n1|4|} + R_{1|5|} X_{n1|5|} + R_{1|6|} X_{n1|6|} \\
& R_{2|3|} X_{n2|3|} + R_{2|4|} X_{n2|4|} + R_{2|5|} X_{n2|5|} + R_{2|6|} X_{n2|6|} \\
& R_{3|4|} X_{n3|4|} + R_{3|5|} X_{n3|5|} + R_{3|6|} X_{n3|6|} \\
& R_{4|5|} X_{n4|5|} + R_{4|6|} X_{n4|6|} \\
& R_{5|6|} X_{n5|6|} \\
& R_{|1|2} X_{n|1|2} + R_{|1|3} X_{n|1|3} + R_{|1|4} X_{n|1|4} + R_{|1|5} X_{n|1|5} + R_{|1|6} X_{n|1|6} \\
& R_{|2|3} X_{n|2|3} + R_{|2|4} X_{n|2|4} + R_{|2|5} X_{n|2|5} + R_{|2|6} X_{n|2|6} \\
& R_{|3|4} X_{n|3|4} + R_{|3|5} X_{n|3|5} + R_{|3|6} X_{n|3|6} \\
& R_{|4|5} X_{n|4|5} + R_{|4|6} X_{n|4|6} \\
& R_{|5|6} X_{n|5|6}
\end{aligned}
$$

C.5 THIRD ORDER WITH 96 COEFFICIENTS

$$
\begin{aligned}
L(n) = {} & R_1 X_{n1} + R_2 X_{n2} + R_3 X_{n3} + R_4 X_{n4} + R_5 X_{n5} + R_6 X_{n6} + \\
& R_{|1|} X_{n|1|} + R_{|2|} X_{n|2|} + R_{|3|} X_{n|3|} + R_{|4|} X_{n|4|} + R_{|5|} X_{n|5|} + R_{|6|} X_{n|6|} + \\
& R_{11} X_{n11} + R_{22} X_{n22} + R_{33} X_{n33} + R_{44} X_{n44} + R_{55} X_{n55} + R_{66} X_{n66} + \\
& R_{1|1|} X_{n1|1|} + R_{2|2|} X_{n2|2|} + R_{3|3|} X_{n3|3|} + R_{4|4|} X_{n4|4|} + R_{5|5|} X_{n5|5|} + R_{6|6|} X_{n6|6|} + \\
& R_{12} X_{n12} + R_{13} X_{n13} + R_{14} X_{n14} + R_{15} X_{n15} + R_{16} X_{n16} \\
& R_{23} X_{n23} + R_{24} X_{n24} + R_{25} X_{n25} + R_{26} X_{n26} \\
& R_{34} X_{n34} + R_{35} X_{n35} + R_{36} X_{n36} \\
& R_{45} X_{n45} + R_{46} X_{n46} \\
& R_{56} X_{n56} \\
& R_{|12|} X_{n|12|} + R_{|13|} X_{n|13|} + R_{|14|} X_{n|14|} + R_{|15|} X_{n|15|} + R_{|16|} X_{n|16|} \\
& R_{|23|} X_{n|23|} + R_{|24|} X_{n|24|} + R_{|25|} X_{n|25|} + R_{|26|} X_{n|26|} \\
& R_{|34|} X_{n|34|} + R_{|35|} X_{n|35|} + R_{|36|} X_{n|36|} \\
& R_{|45|} X_{n|45|} + R_{|46|} X_{n|46|} \\
& R_{|56|} X_{n|56|} \\
& R_{1|2|} X_{n1|2|} + R_{1|3|} X_{n1|3|} + R_{1|4|} X_{n1|4|} + R_{1|5|} X_{n1|5|} + R_{1|6|} X_{n1|6|} \\
& R_{2|3|} X_{n2|3|} + R_{2|4|} X_{n2|4|} + R_{2|5|} X_{n2|5|} + R_{2|6|} X_{n2|6|} \\
& R_{3|4|} X_{n3|4|} + R_{3|5|} X_{n3|5|} + R_{3|6|} X_{n3|6|} \\
& R_{4|5|} X_{n4|5|} + R_{4|6|} X_{n4|6|} \\
& R_{5|6|} X_{n5|6|} \\
& R_{|1|2} X_{n|1|2} + R_{|1|3} X_{n|1|3} + R_{|1|4} X_{n|1|4} + R_{|1|5} X_{n|1|5} + R_{|1|6} X_{n|1|6} \\
& R_{|2|3} X_{n|2|3} + R_{|2|4} X_{n|2|4} + R_{|2|5} X_{n|2|5} + R_{|2|6} X_{n|2|6} \\
& R_{|3|4} X_{n|3|4} + R_{|3|5} X_{n|3|5} + R_{|3|6} X_{n|3|6} \\
& R_{|4|5} X_{n|4|5} + R_{|4|6} X_{n|4|6} \\
& R_{|5|6} X_{n|5|6} \\
& R_{111} X_{n111} + R_{222} X_{n222} + R_{333} X_{n333} + R_{444} X_{n444} + R_{555} X_{n555} + R_{666} X_{n666} \\
& R_{|111|} X_{n|111|} + R_{|222|} X_{n|222|} + R_{|333|} X_{n|333|} + R_{|444|} X_{n|444|} + R_{|555|} X_{n|555|} + R_{|666|} X_{n|666|}
\end{aligned}
$$

APPENDIX D

INTERNAL BALANCE SKETCHES

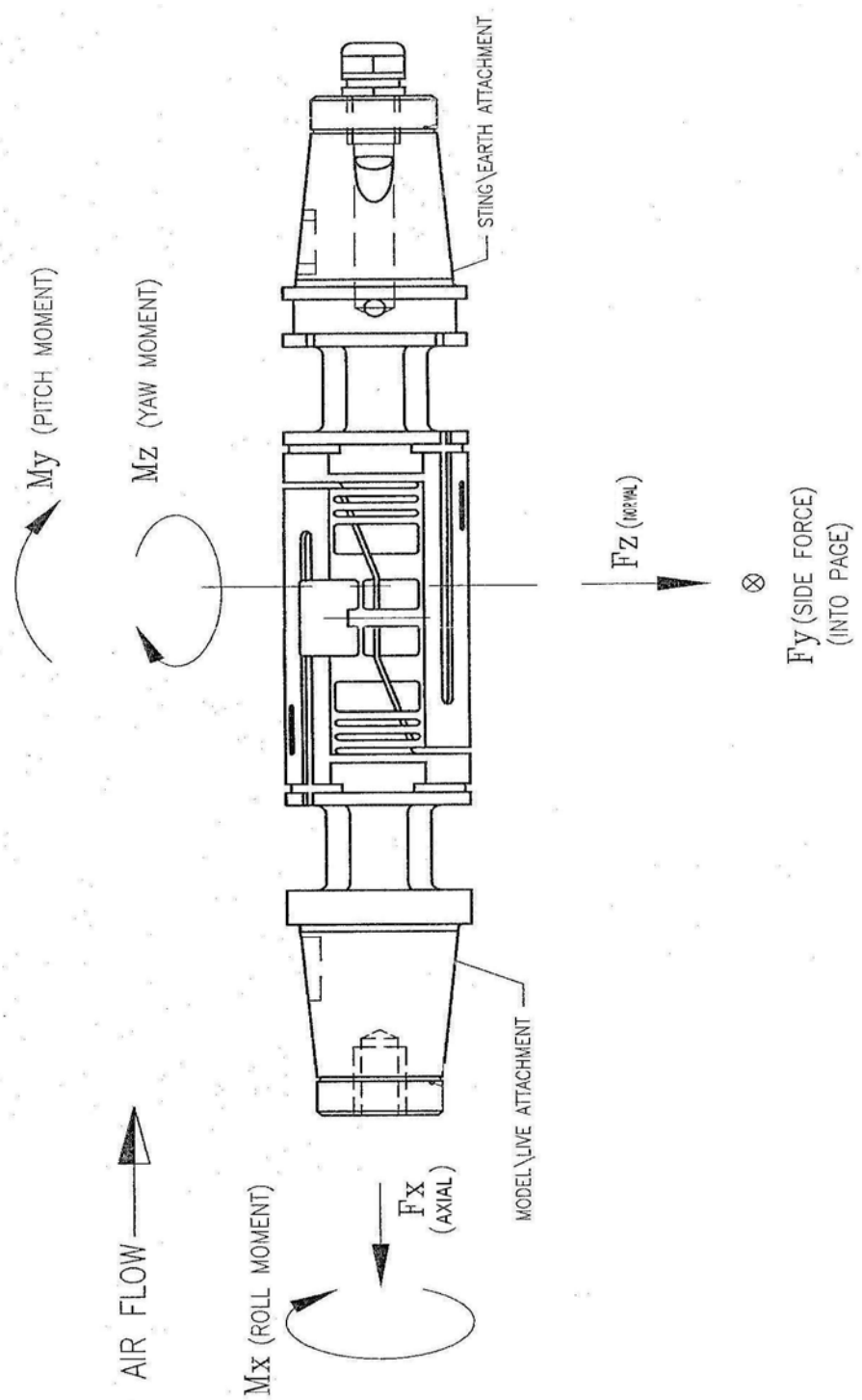

Figure 92 Sign Convention

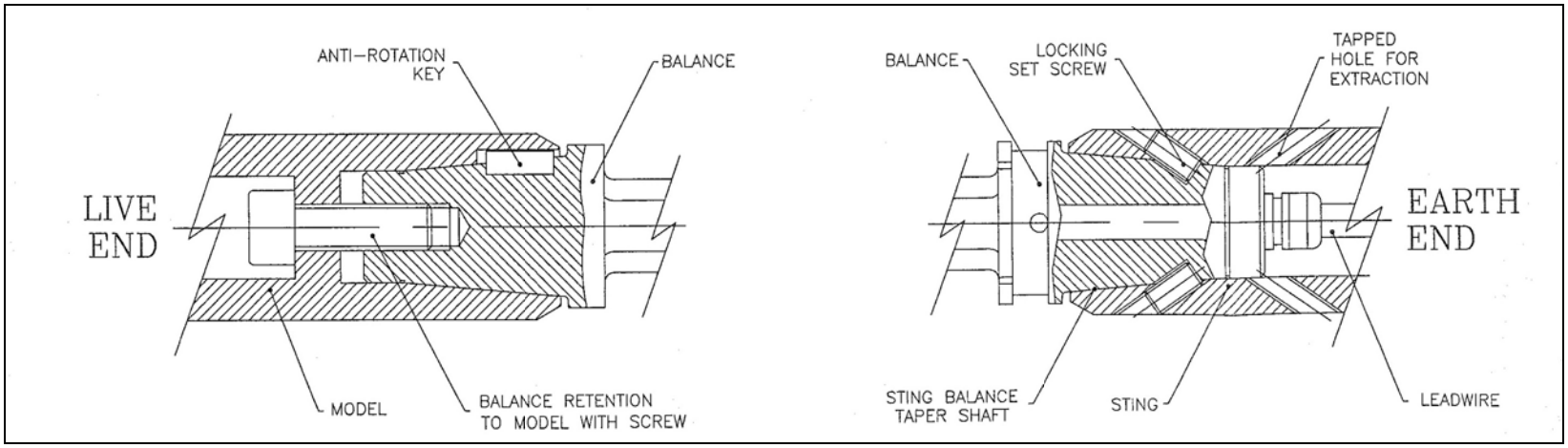

Figure 93 Sting Balance Mounting

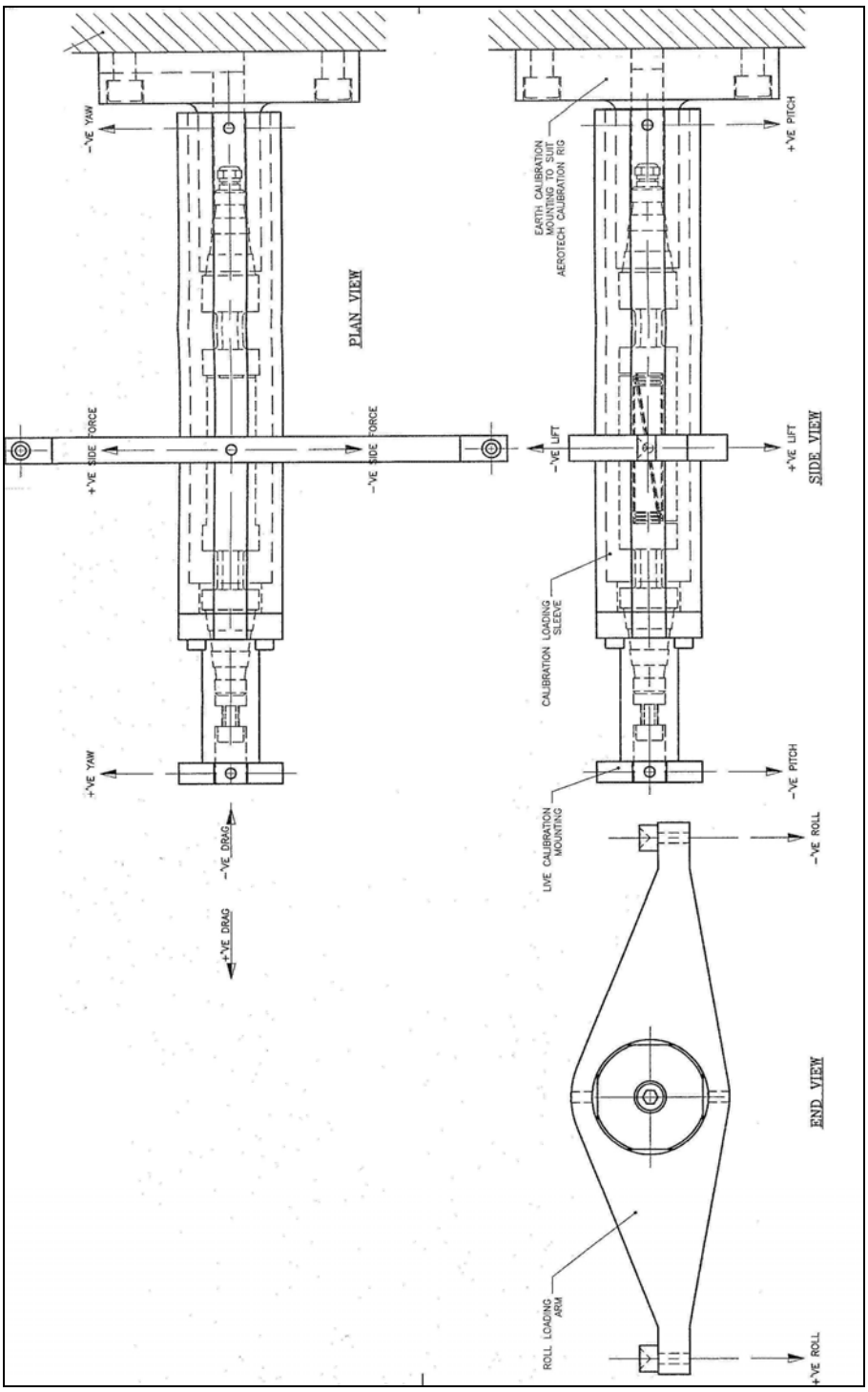

Figure 94 Calibration Configuration

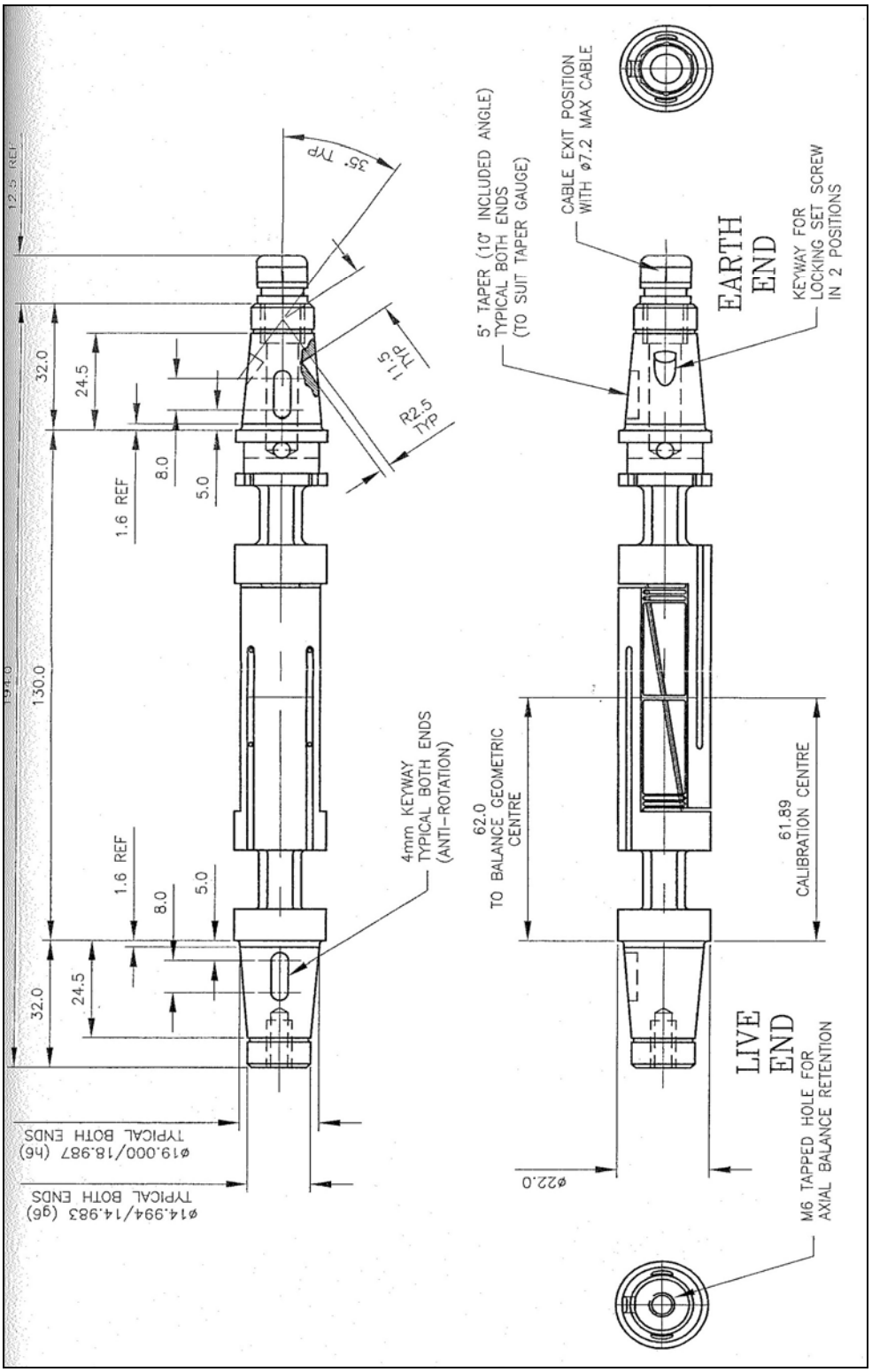

Figure 95 22mm Balance Configuration

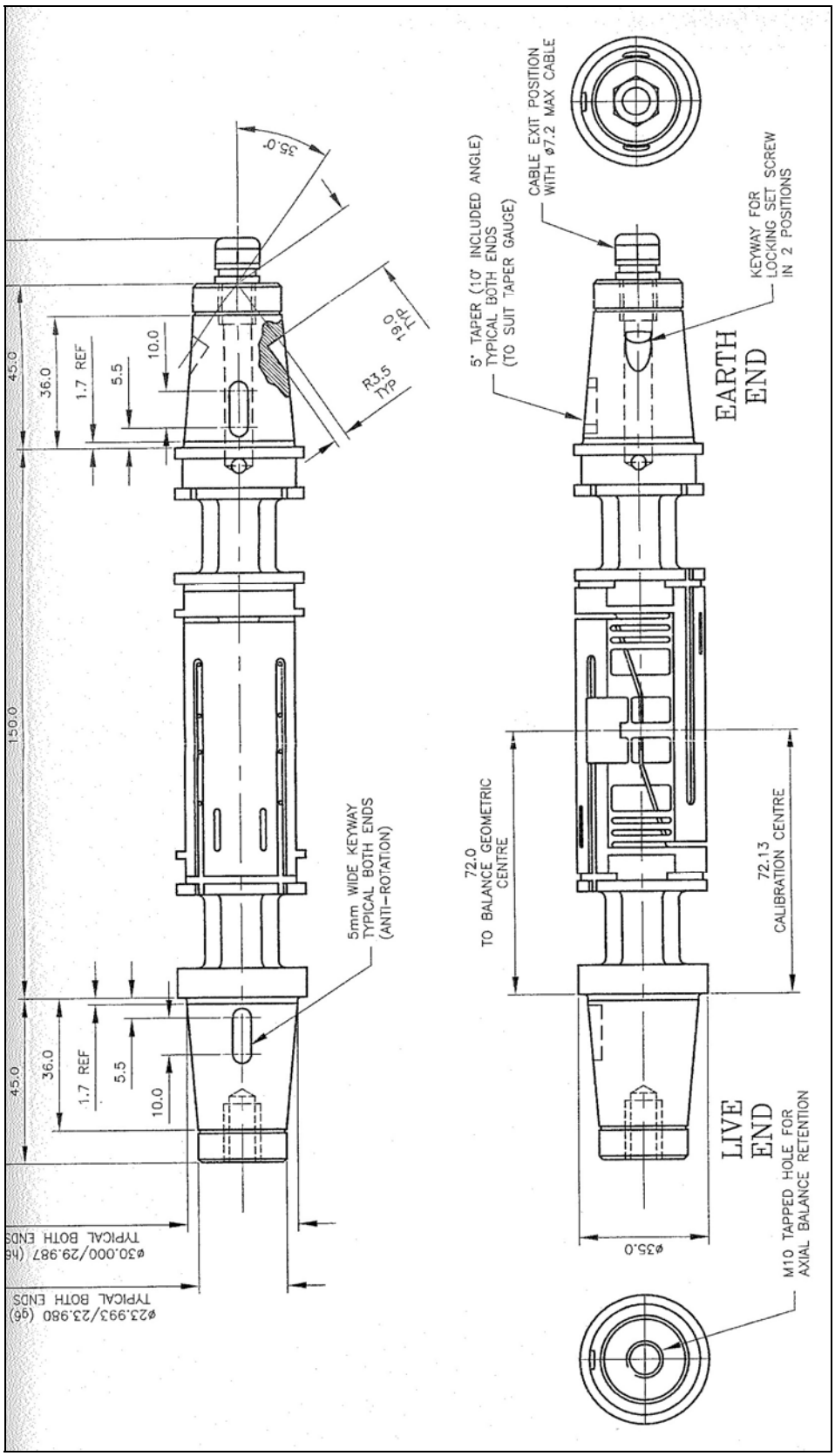

Figure 96 35mm Balance Configuration

APPENDIX E

AWT-AMS

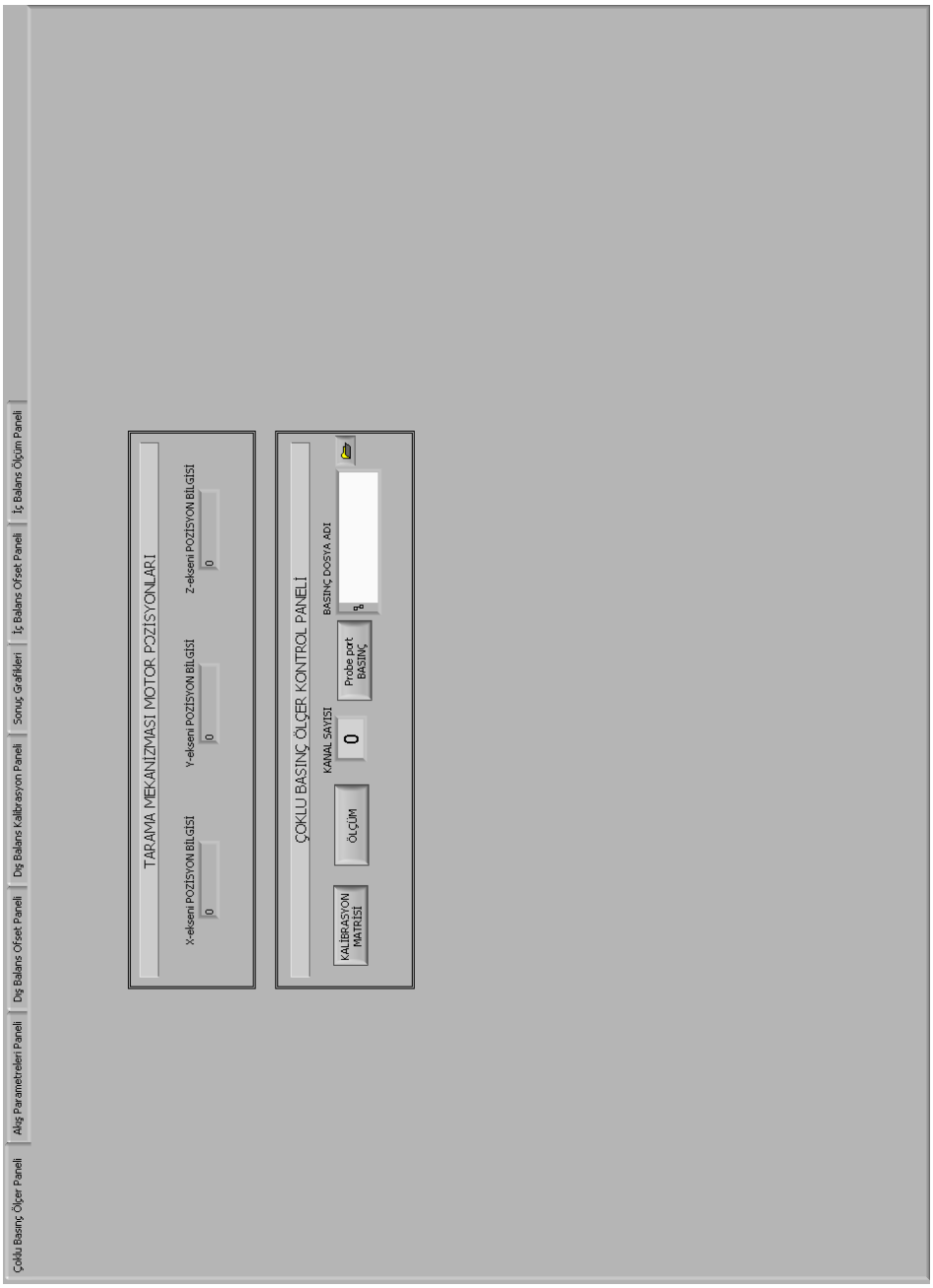

Figure 97 Multi-Channel Pressure System Panel

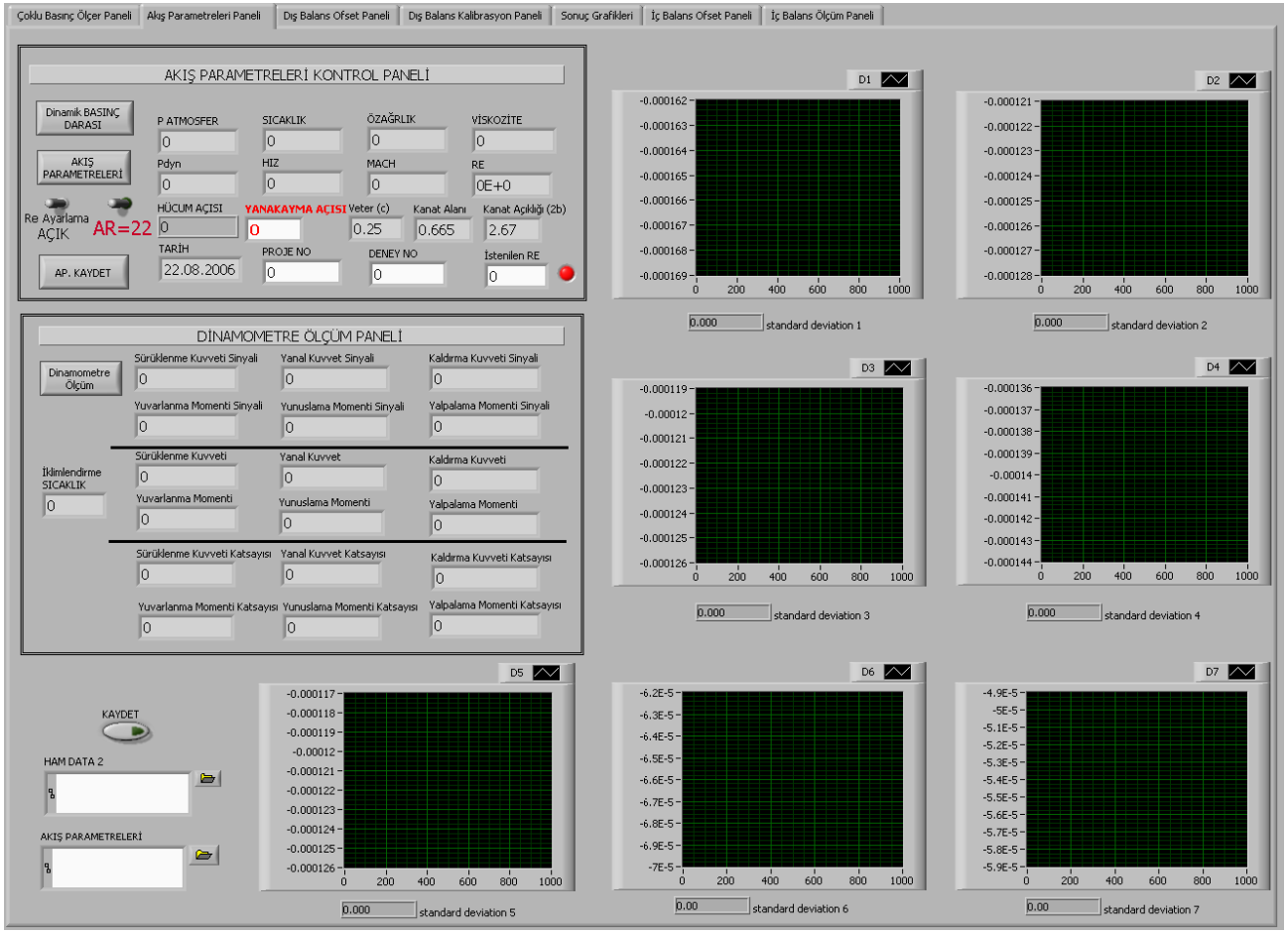

Figure 98 External Balance Panel

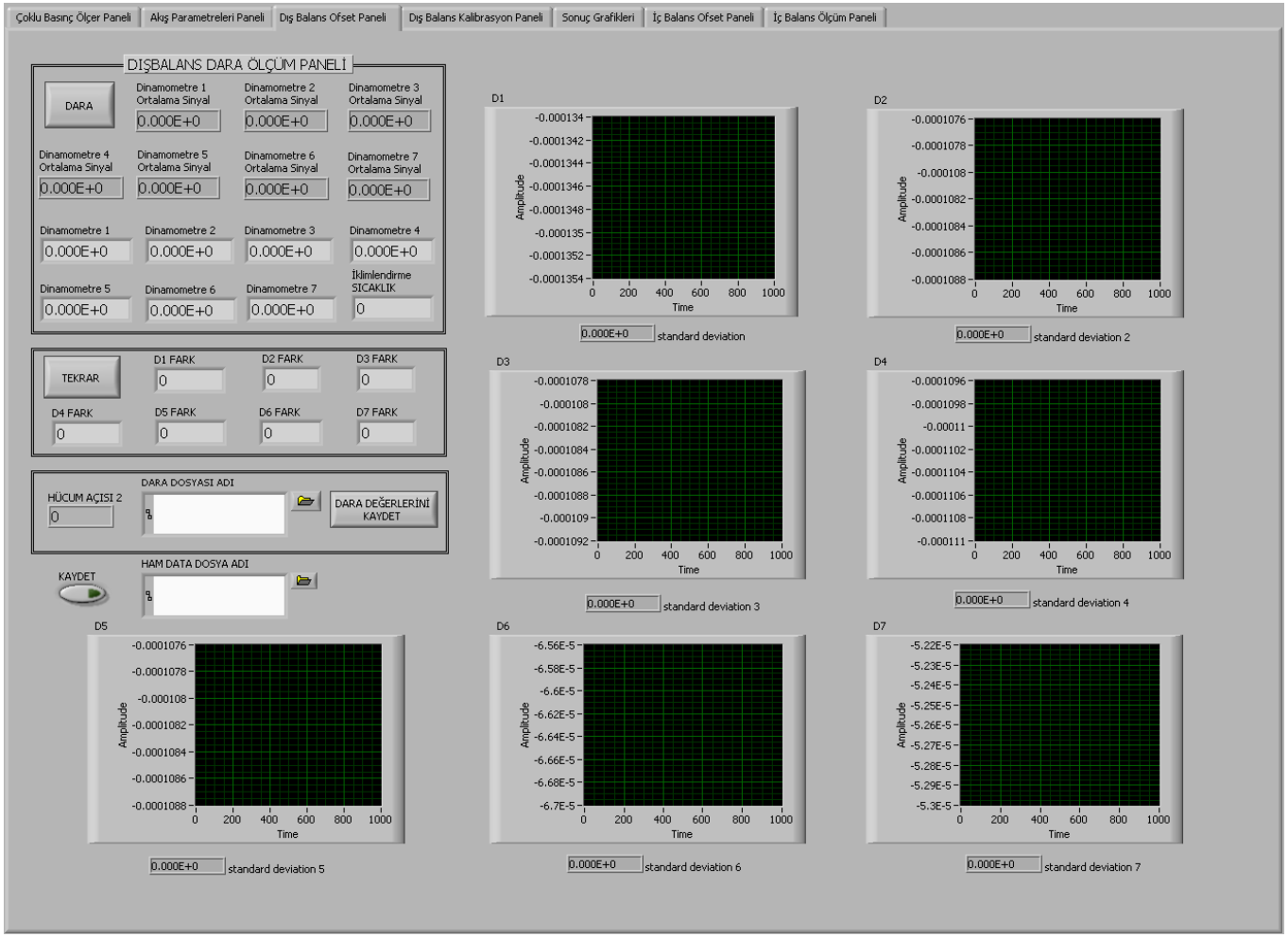

Figure 99 External Balance Offset Panel

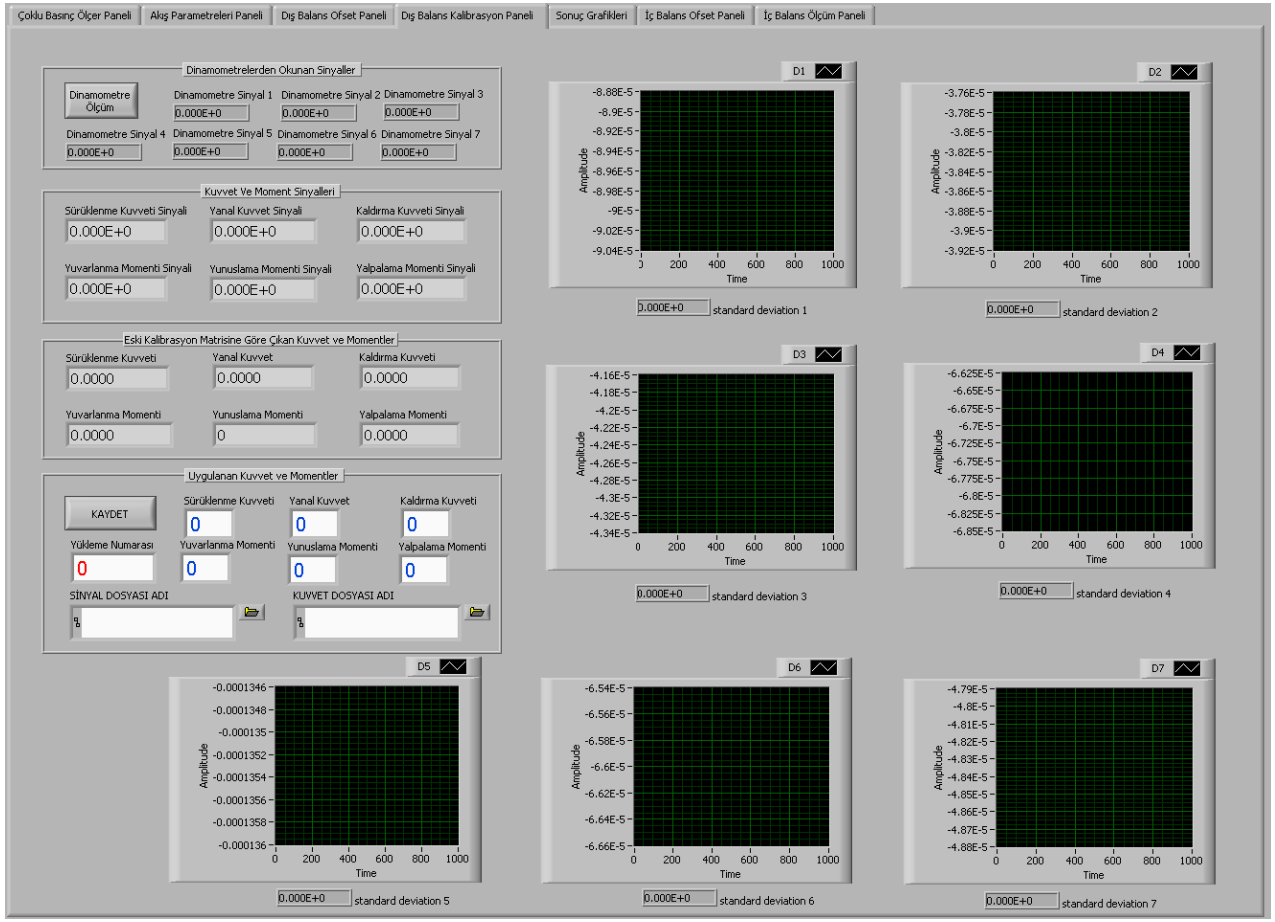

Figure 100 External Balance Calibration Panel

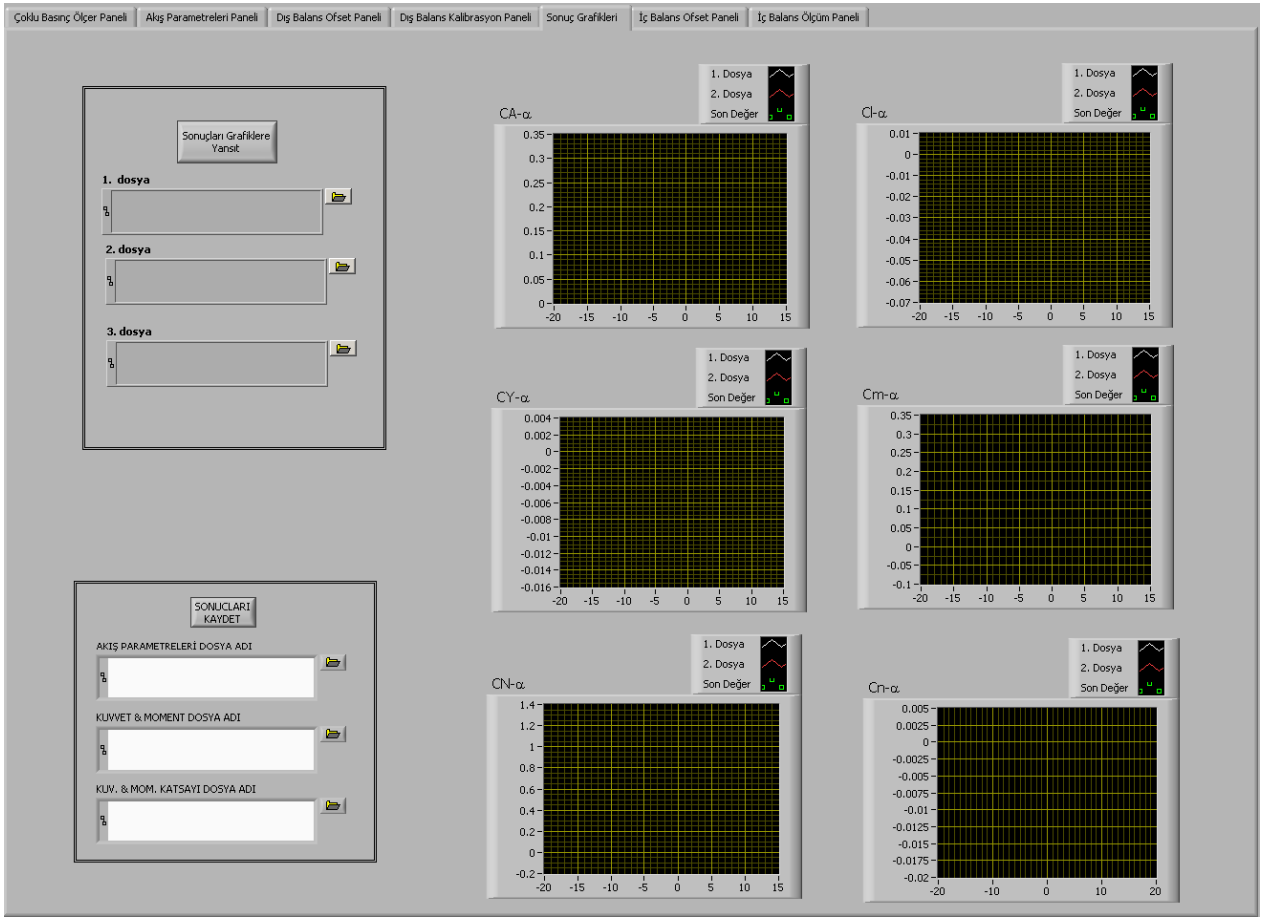

Figure 101 Results Panel

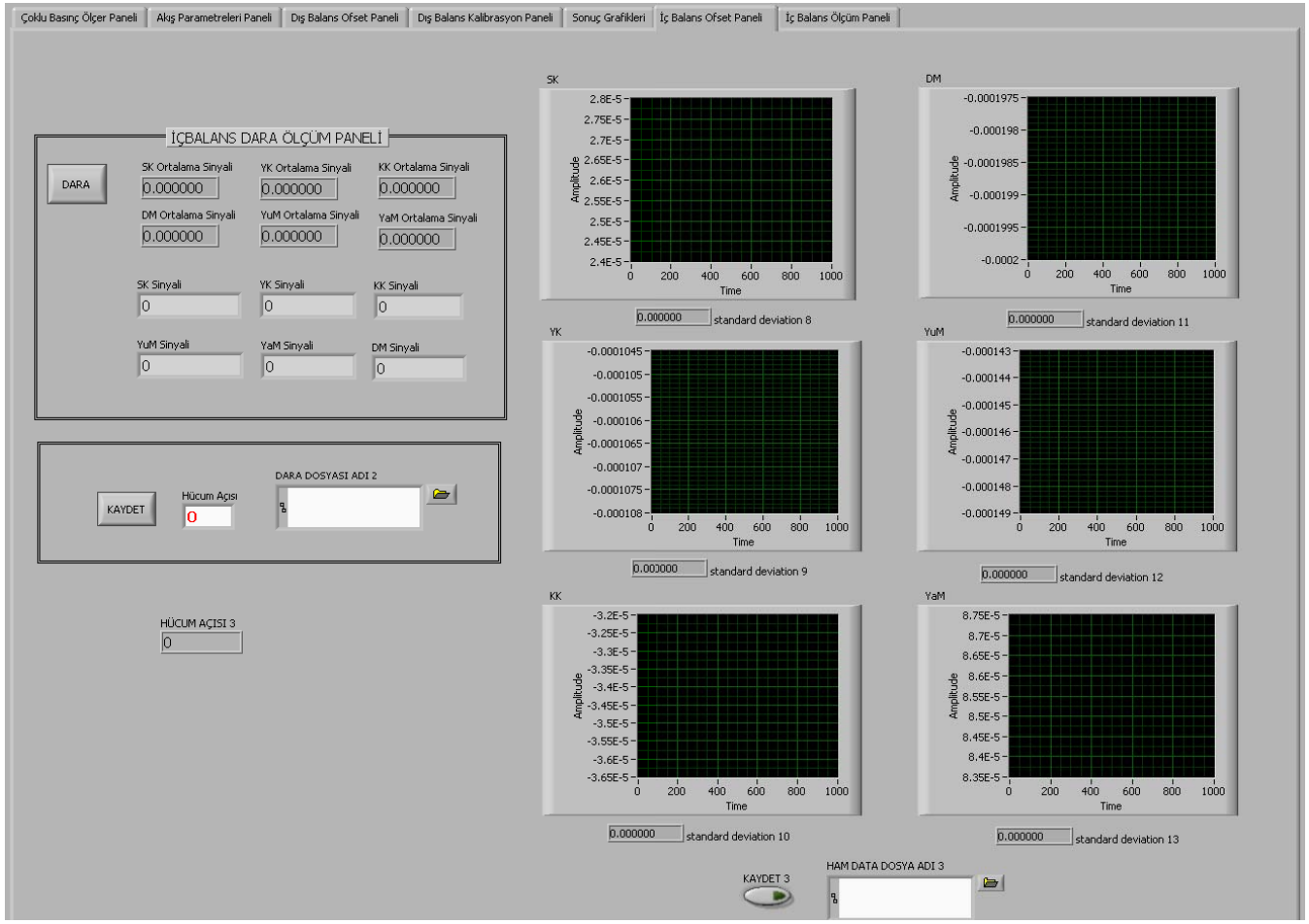

Figure 102 Internal Balance Offset Panel

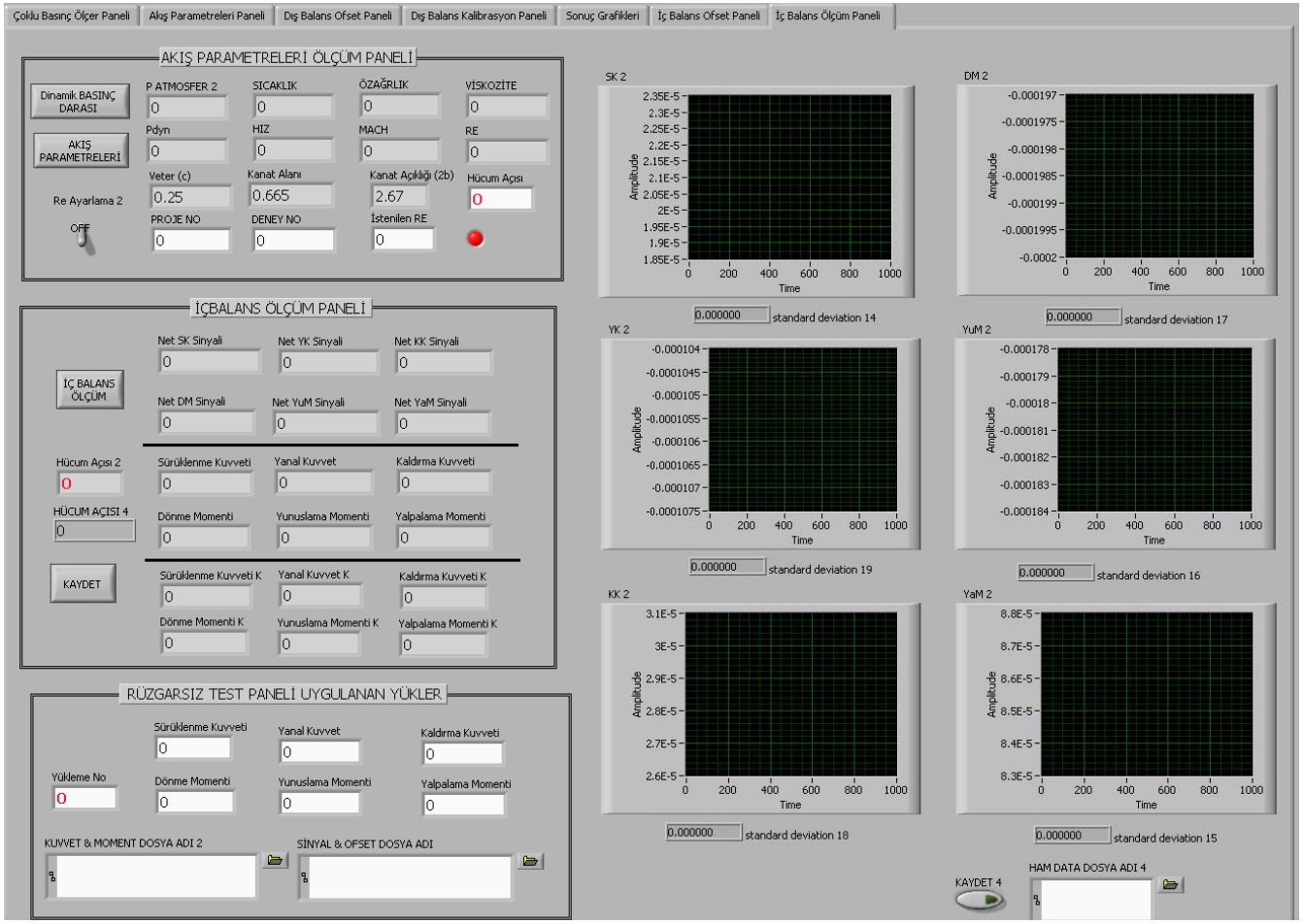

Figure 103 Internal Balance Panel

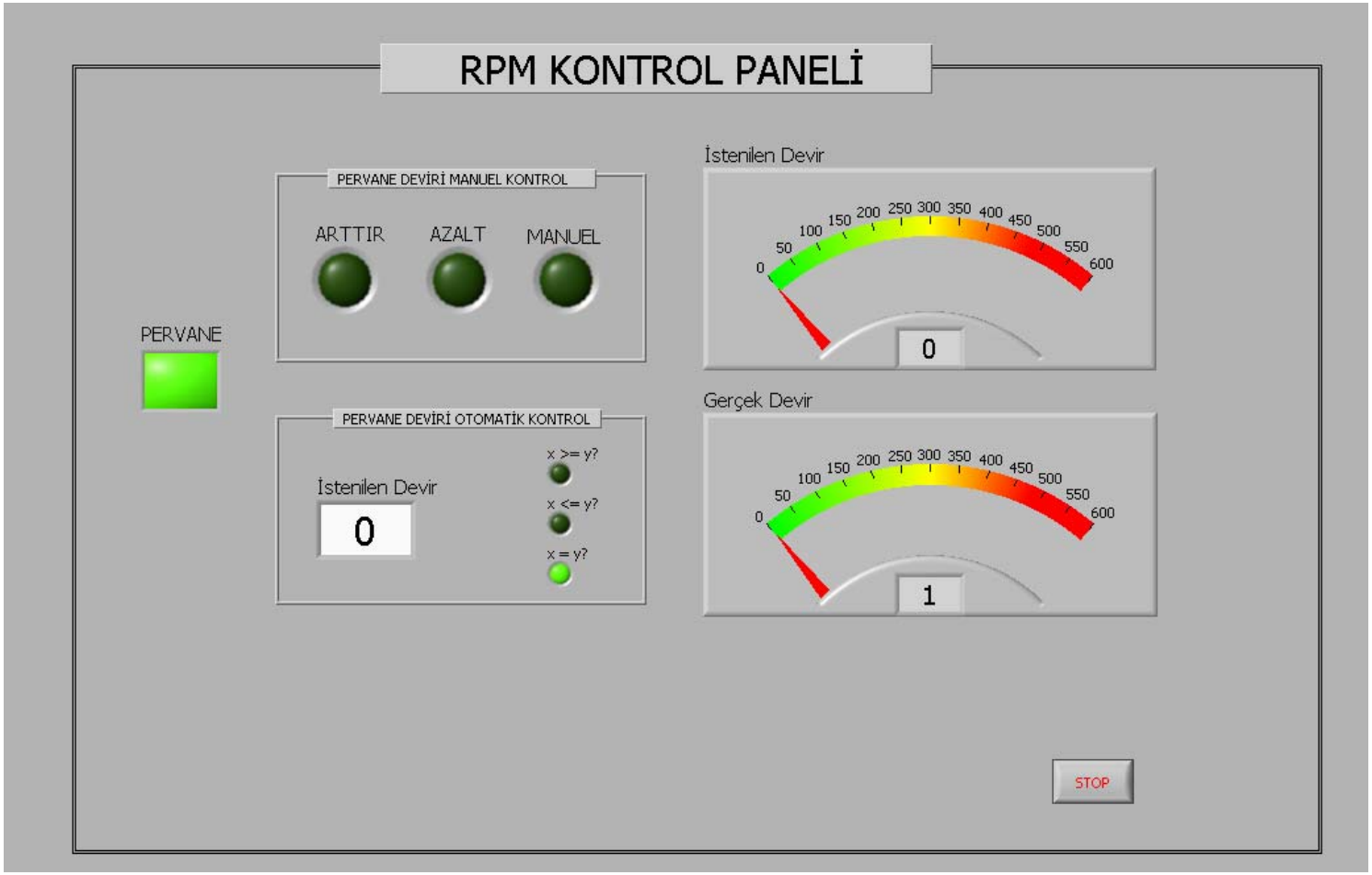

Figure 104 RPM Control Panel

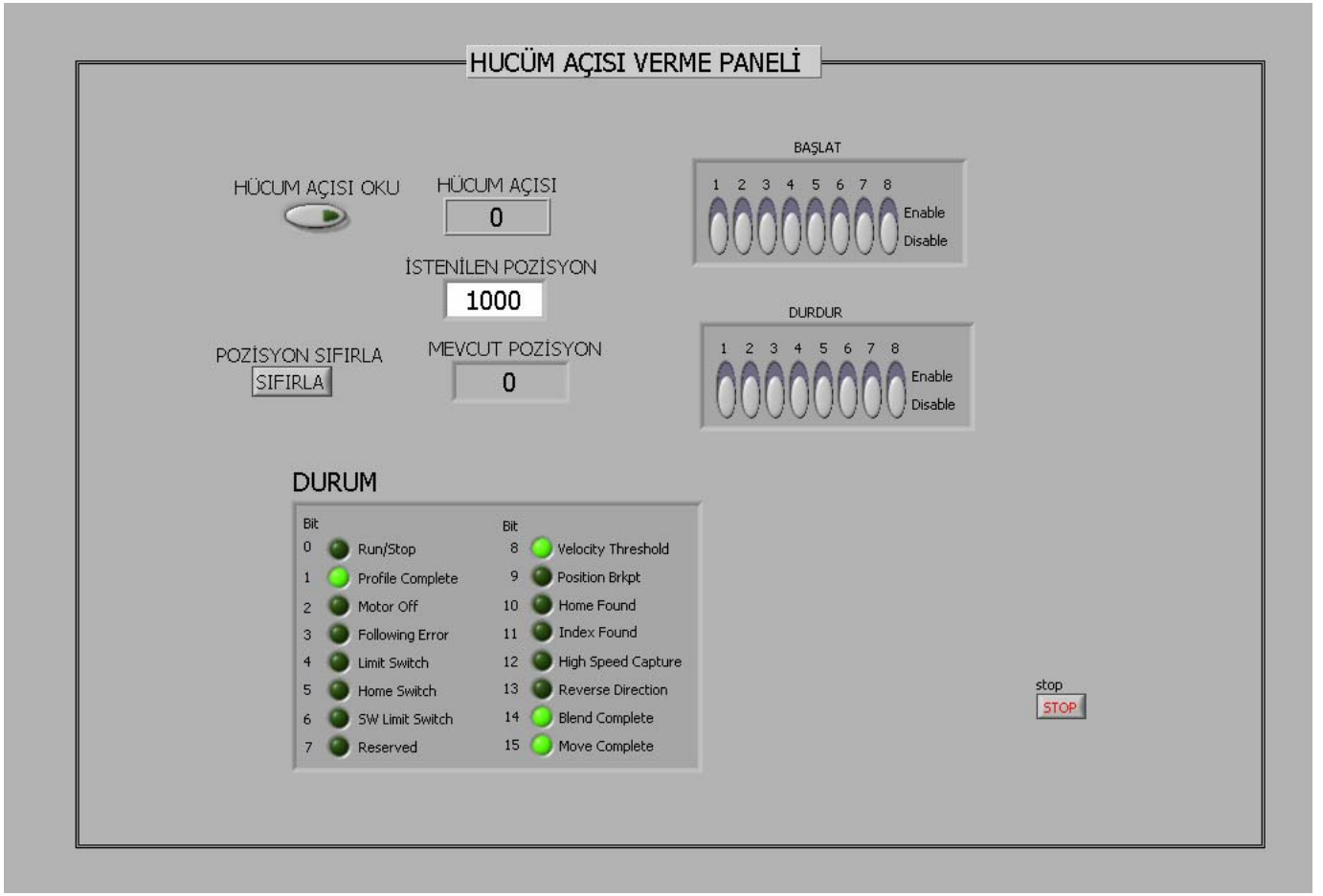

Figure 105 Angle of Attack Control Panel

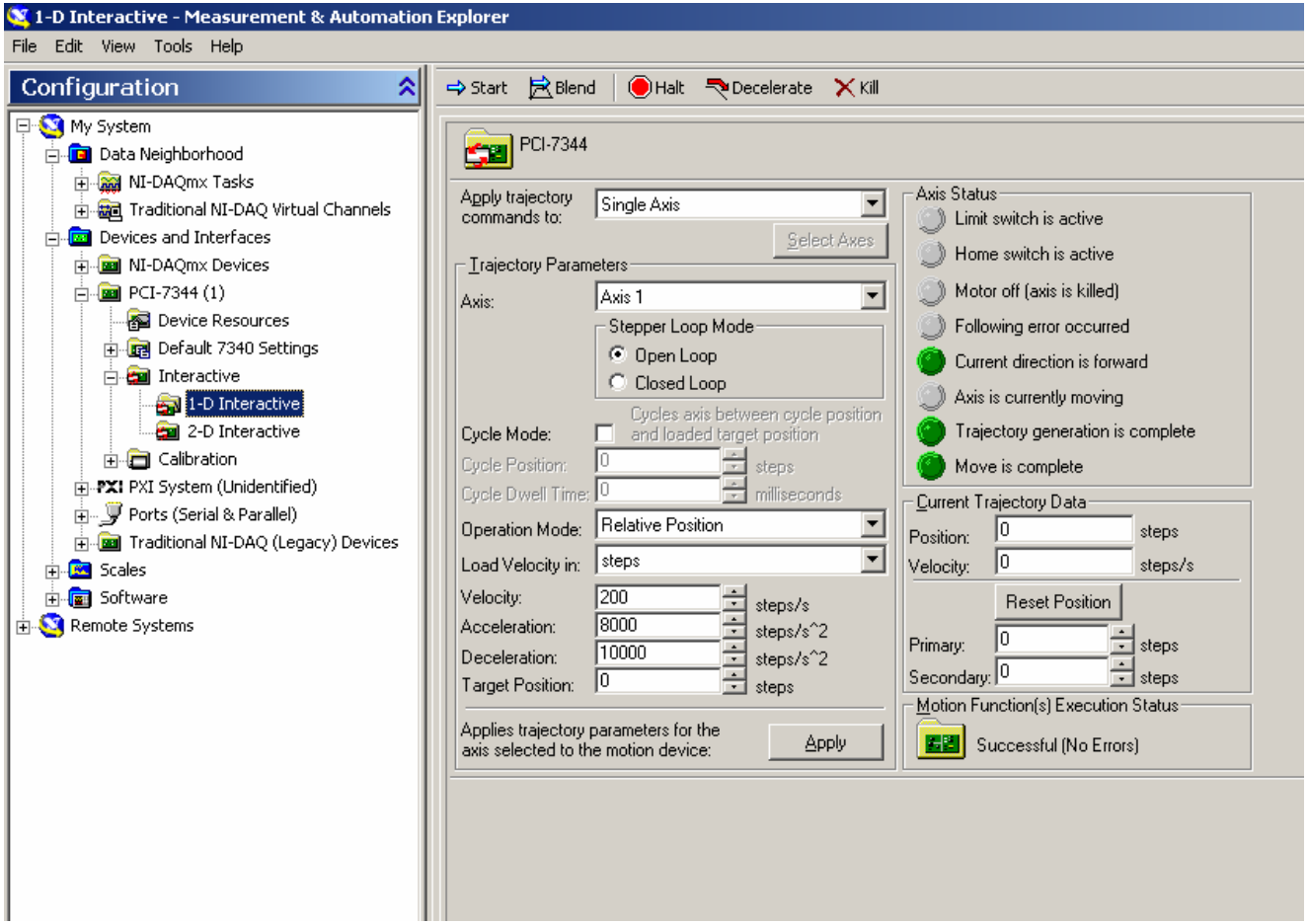

Figure 106 Measurement and Automation Explorer Angle of Attack Control Panel

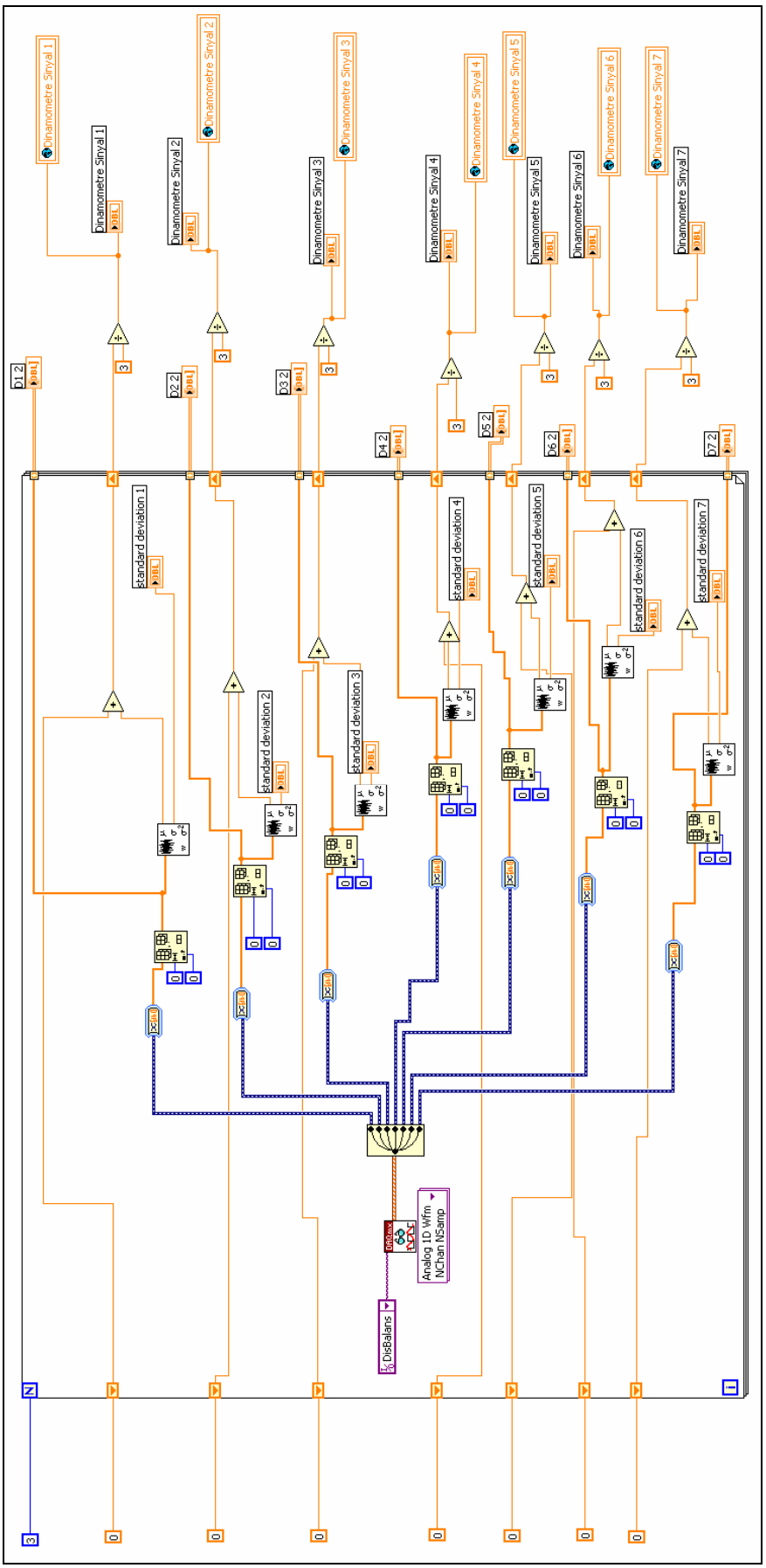

Figure 107 Sample Block Diagram

APPENDIX G

WIND-OFF LOADING RESULTS

F.1. PURE NORMAL FORCE LOADING RESULTS

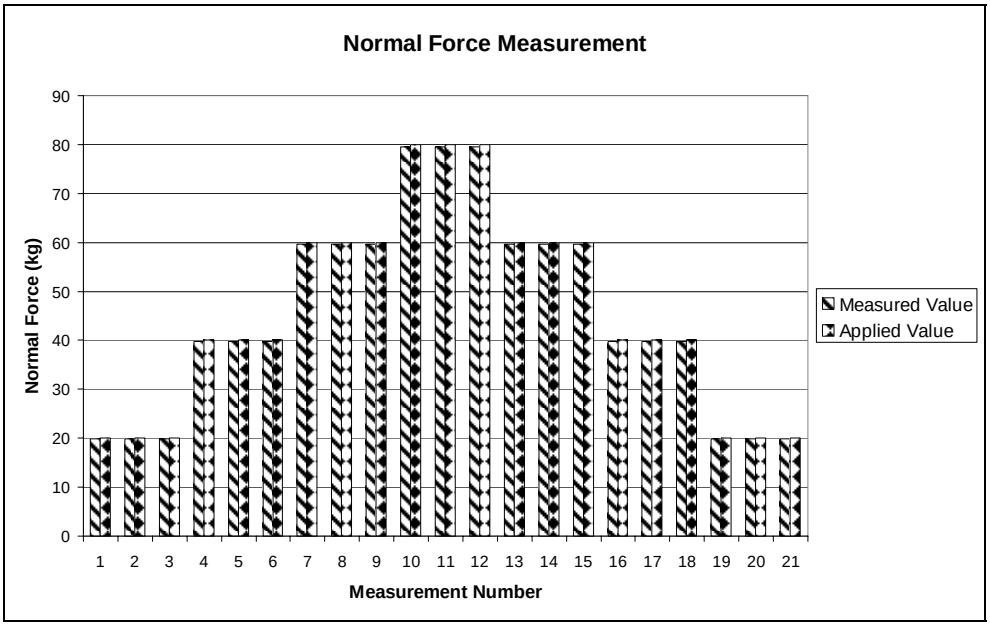

Figure 108 Positive Normal Force Loadings and Readings

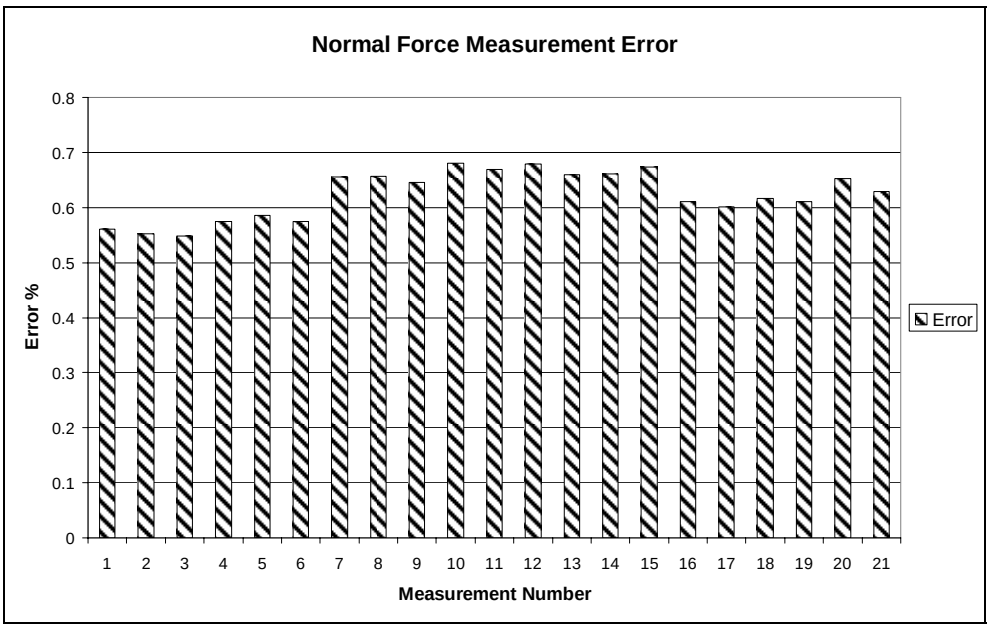

Figure 109 Positive Normal Force Readings Error

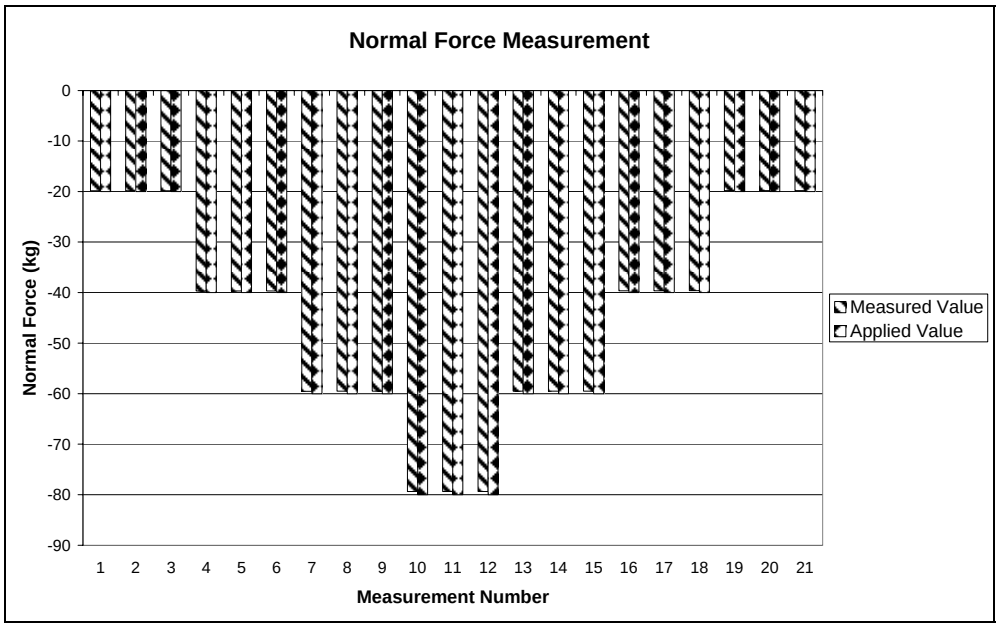

Figure 110 Negative Normal Force Loadings and Readings

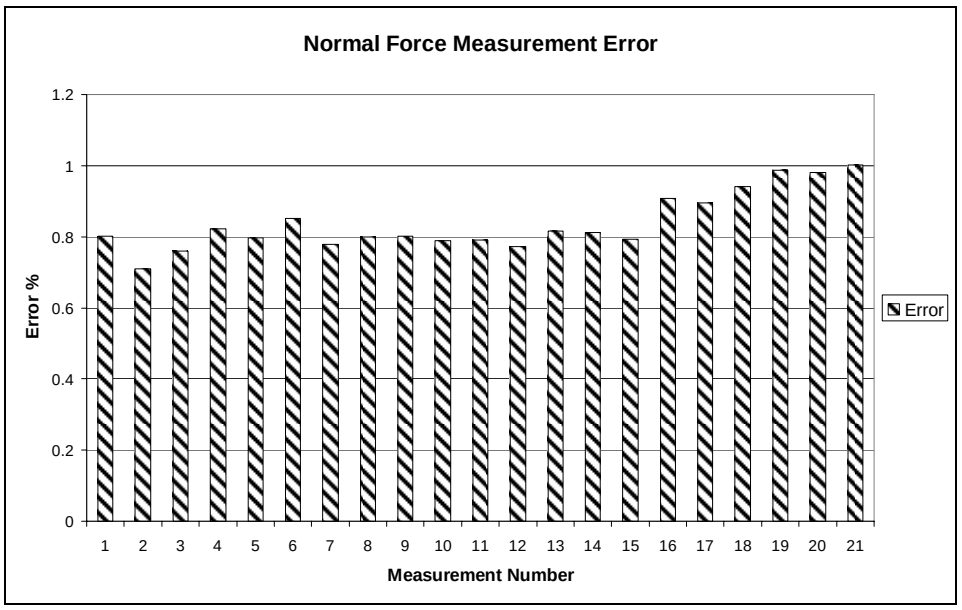

Figure 111 Negative Normal Force Readings Error

F.2. PURE SIDE FORCE LOADING RESULTS

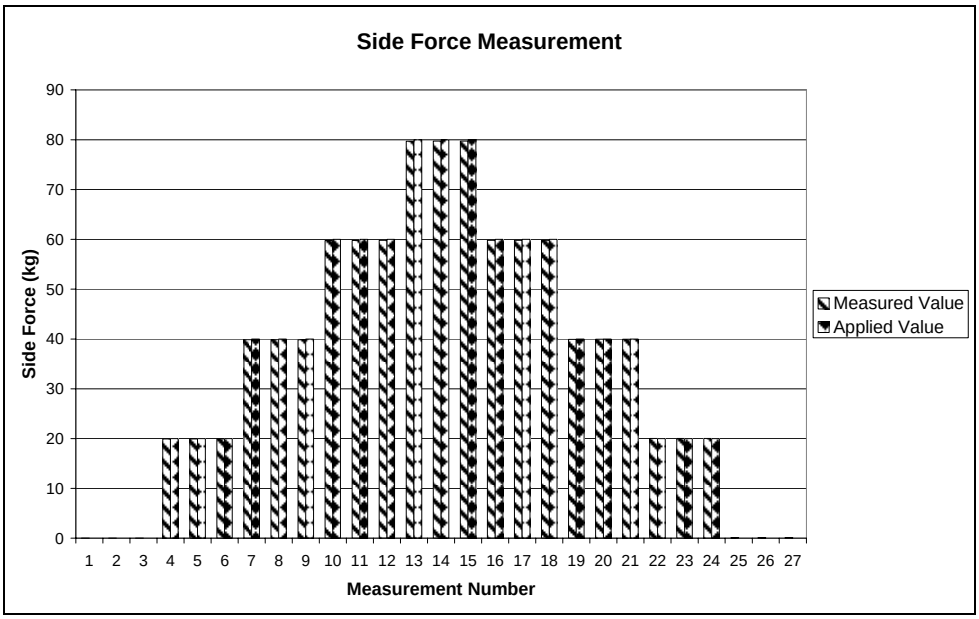

Figure 112 Positive Side Force Loadings and Readings

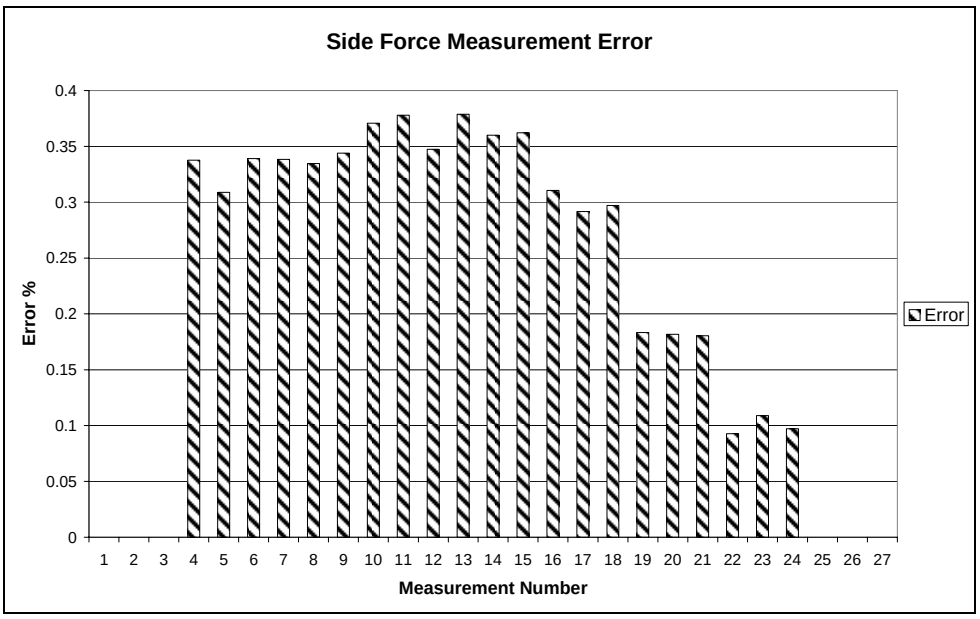

Figure 113 Positive Side Force Readings Error

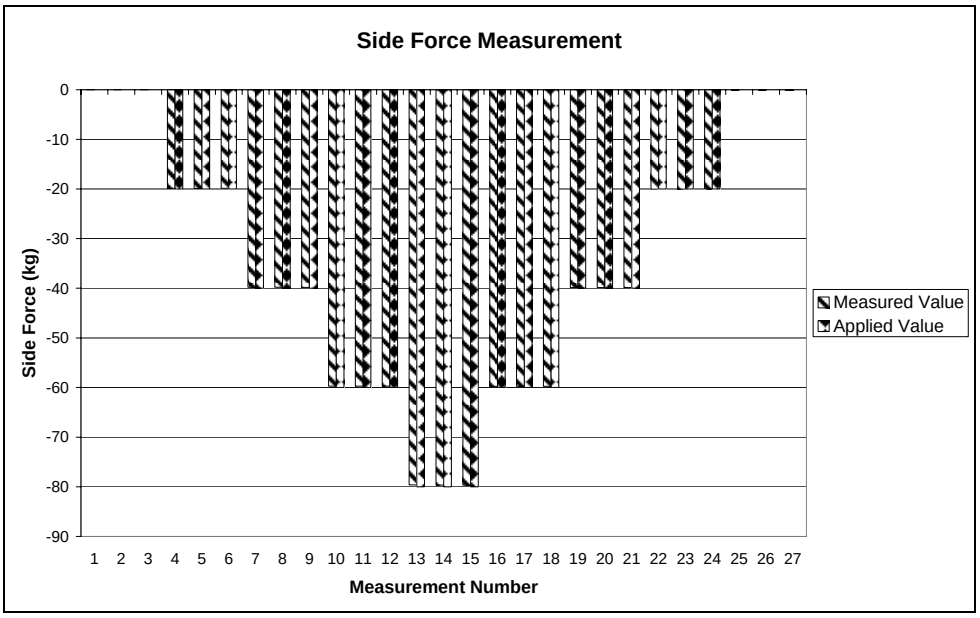

Figure 114 Negative Side Force Loadings and Readings

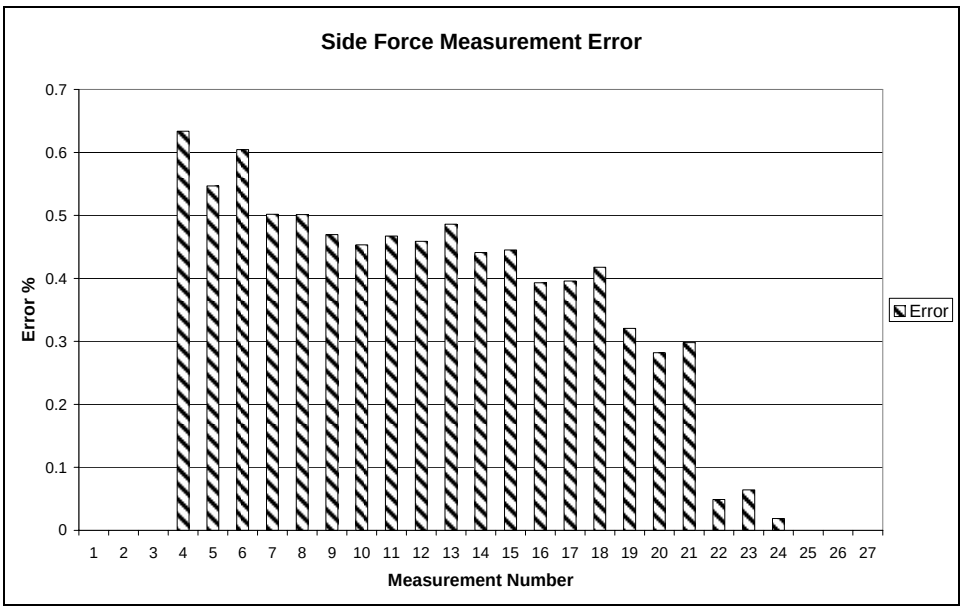

Figure 115 Negative Side Force Readings Error

F.3. PURE AXIAL FORCE LOADING RESULTS

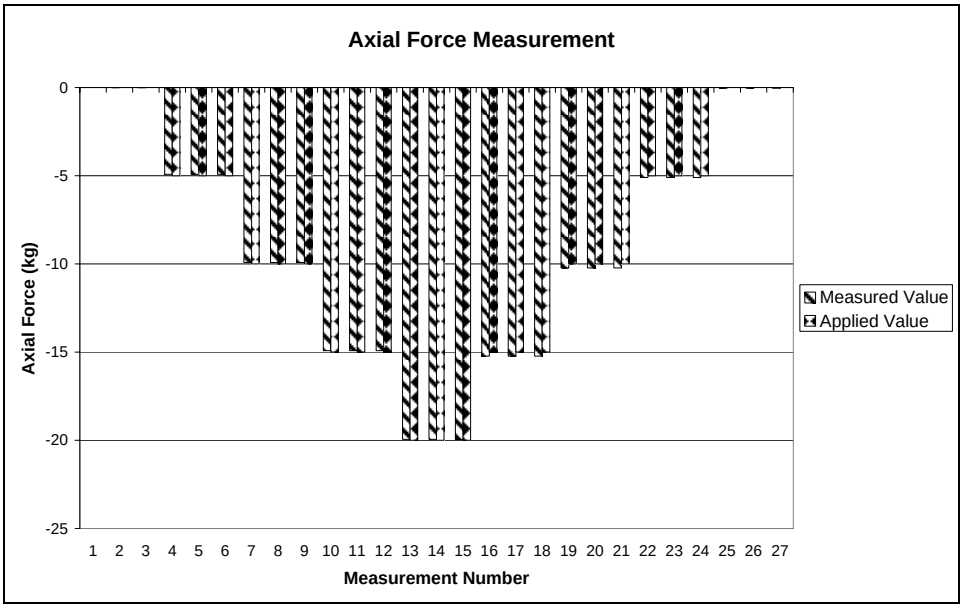

Figure 116 Axial Force Loadings and Readings

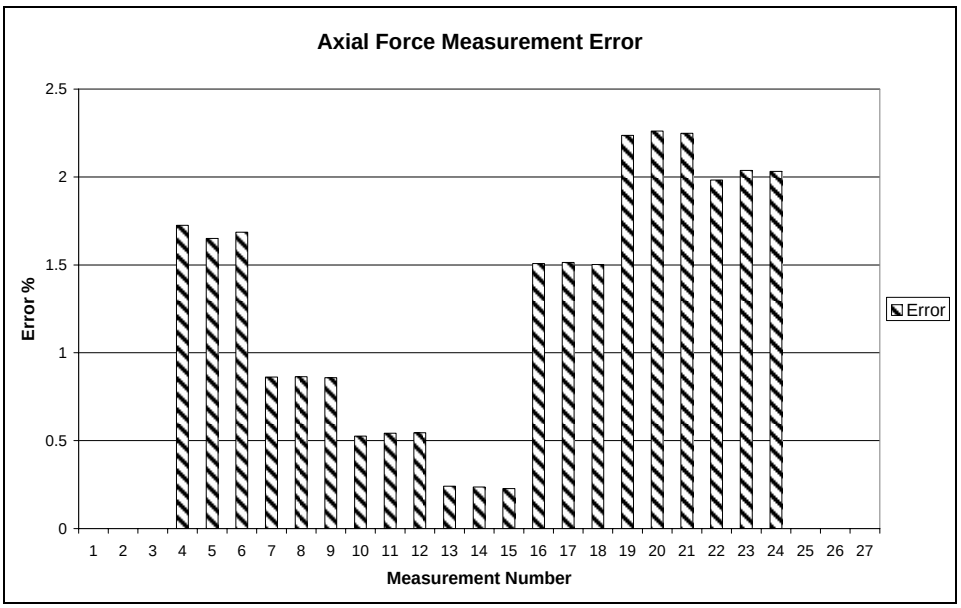

Figure 117 Axial Force Readings Error

F.4. RESULTS of ROLL M. LOADING with NORMAL F.

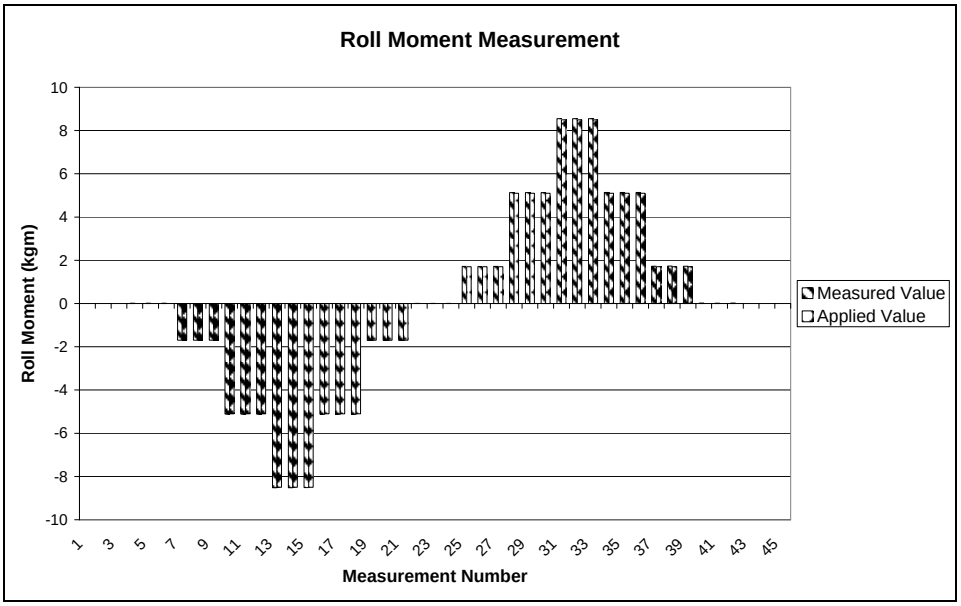

Figure 118 Roll Moment Loadings and Readings

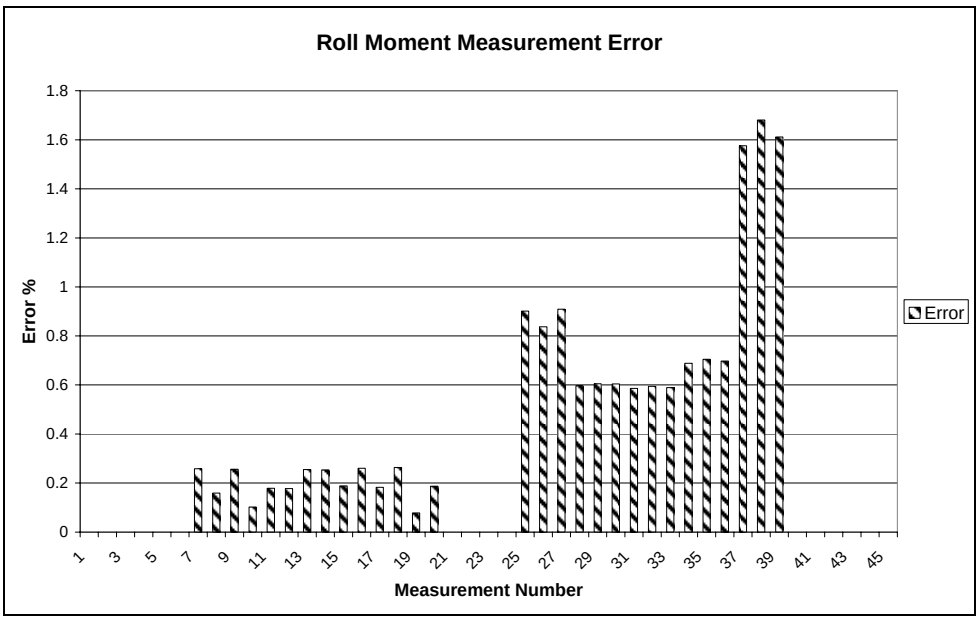

Figure 119 Roll Moment Readings Error

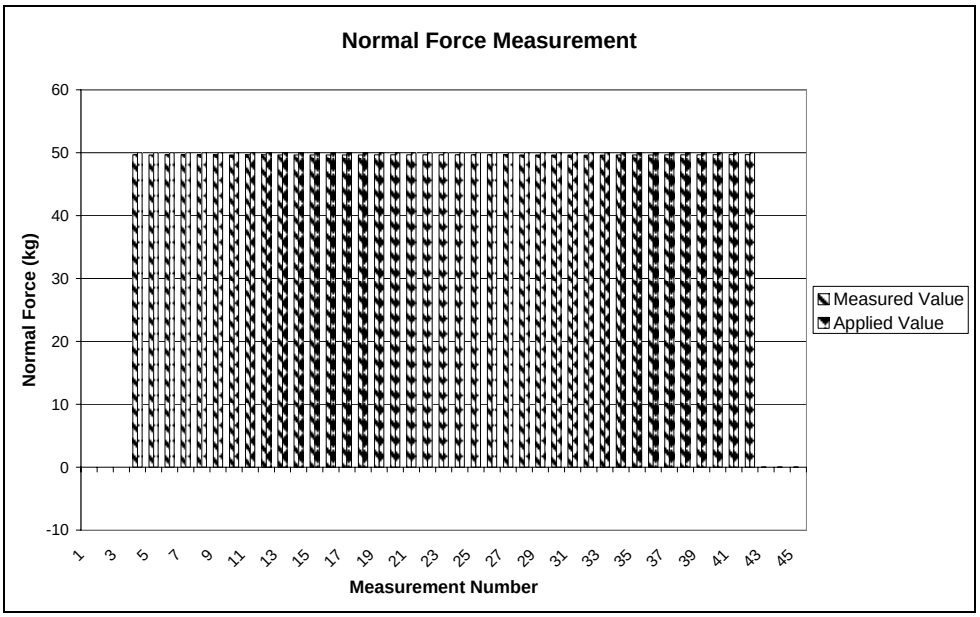

Figure 120 Normal Force Loadings and Readings

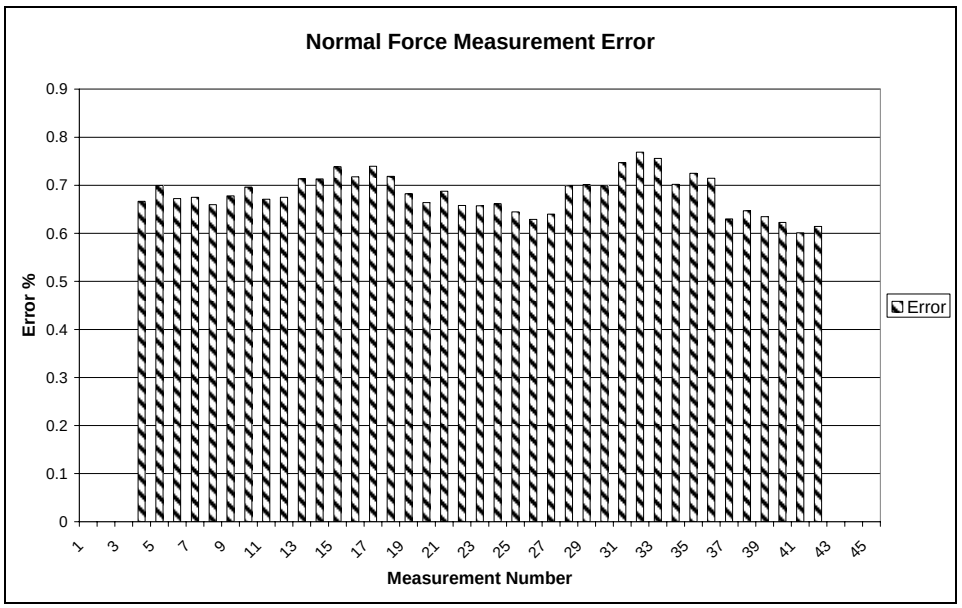

Figure 121 Normal Force Readings Error

F.5. RESULTS of YAW MOMENT LOADING with SIDE FORCE

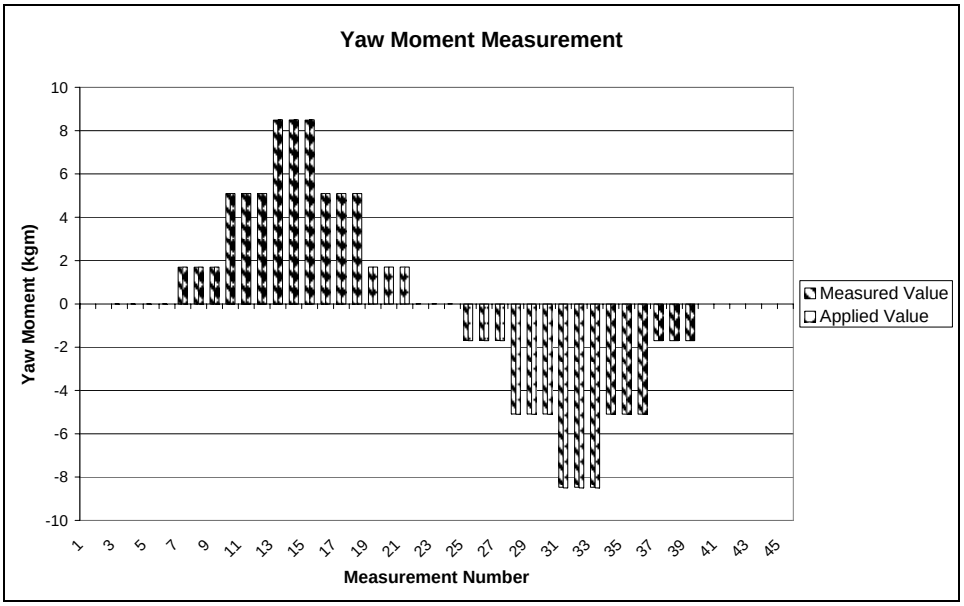

Figure 122 Yaw Moment Loadings and Readings

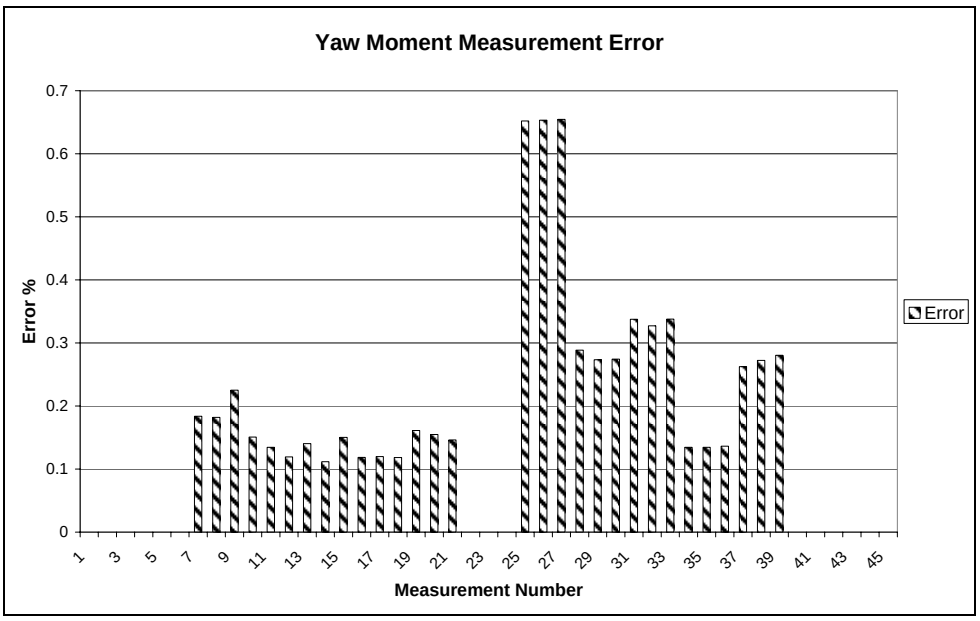

Figure 123 Yaw Moment Readings Error

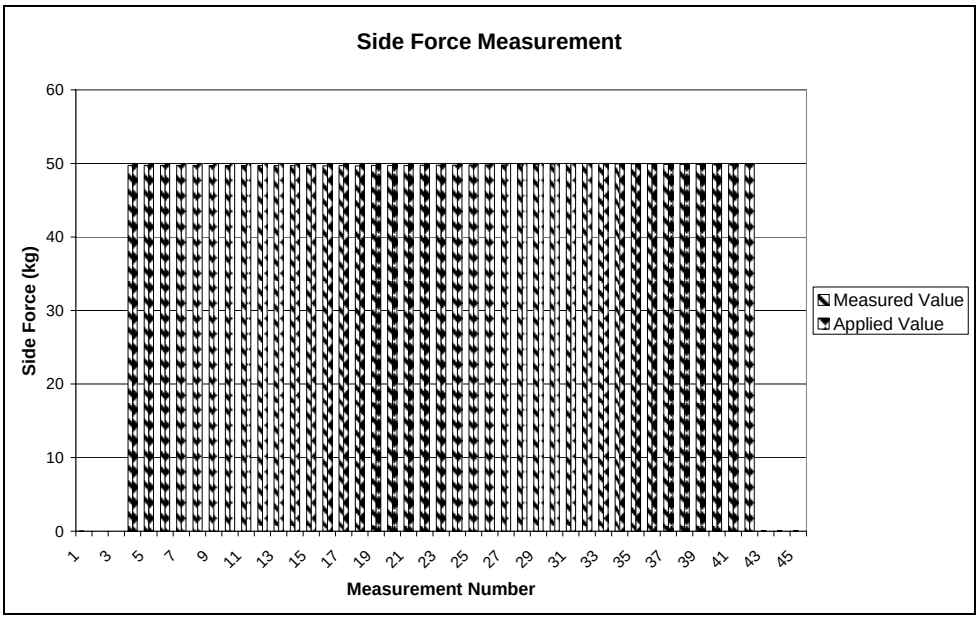

Figure 124 Side Force Loadings and Readings

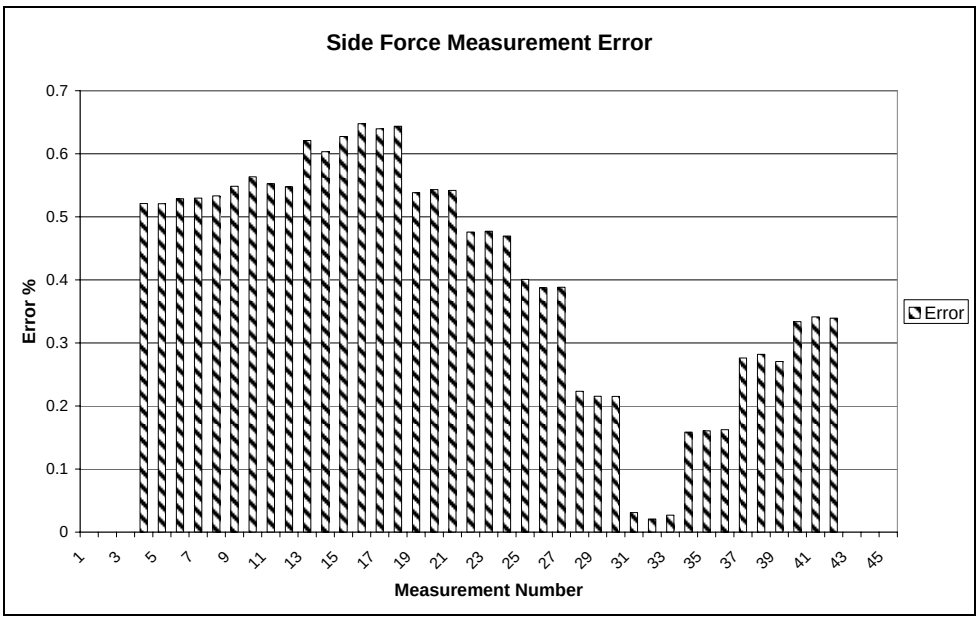

Figure 125 Side Force Readings Error

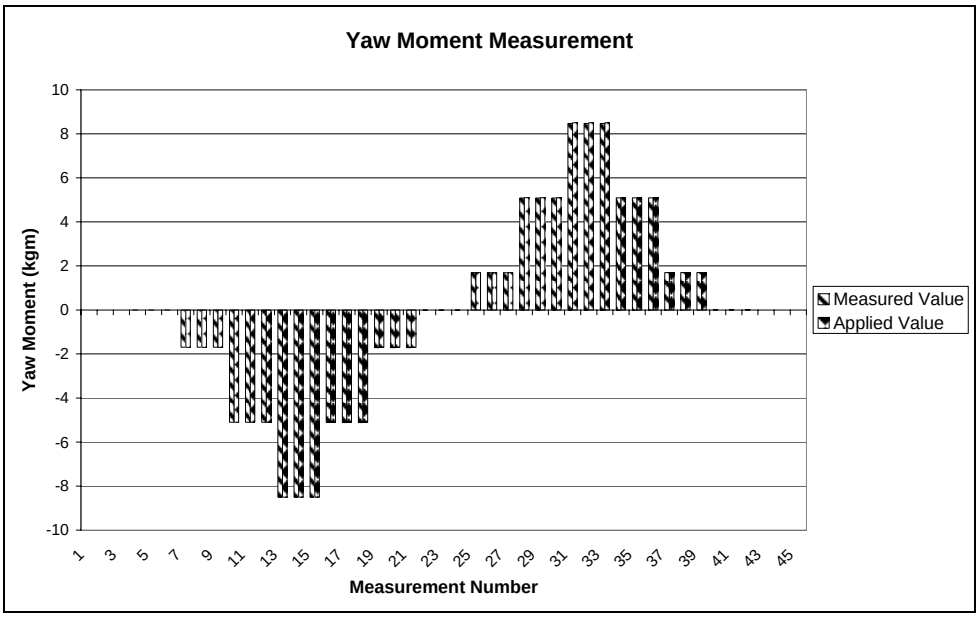

Figure 126 Yaw Moment Loadings and Readings

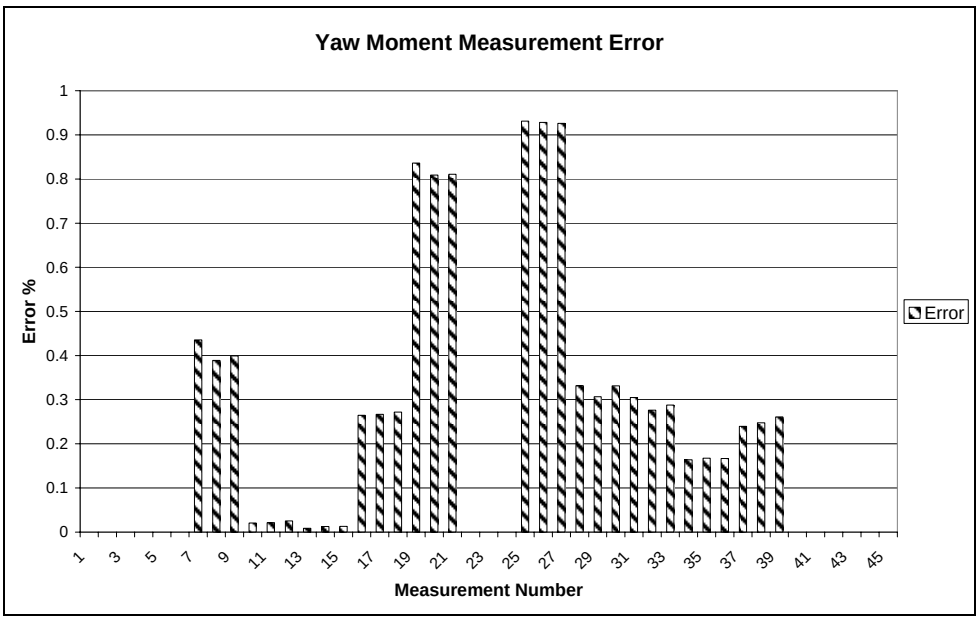

Figure 127 Roll Moment Readings Error

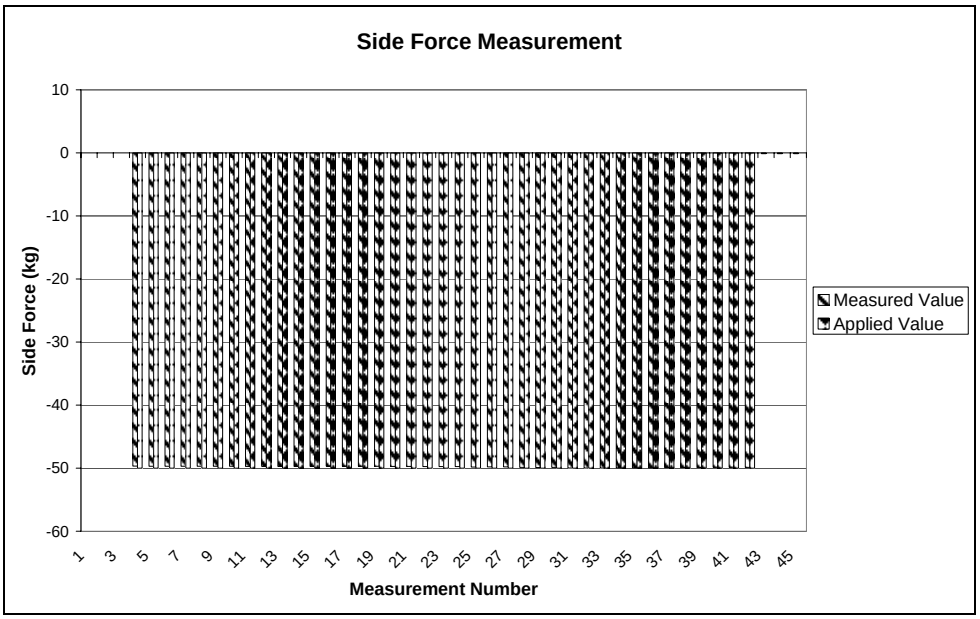

Figure 128 Side Force Loadings and Readings

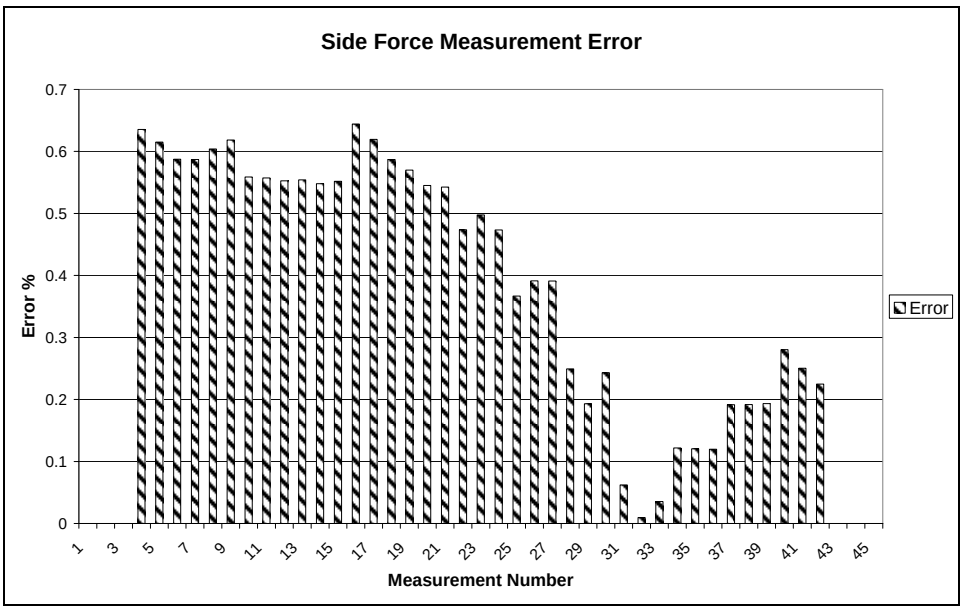

Figure 129 Side Force Readings Error

F.6. RESULTS of PITCH M. LOADING with NORMAL F.

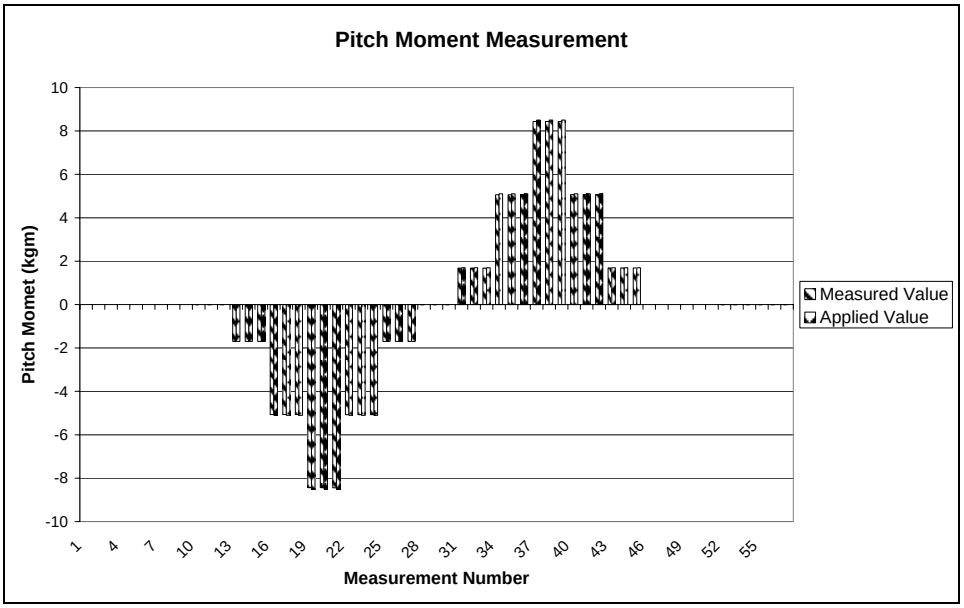

Figure 130 Pitch Moment Loadings and Readings

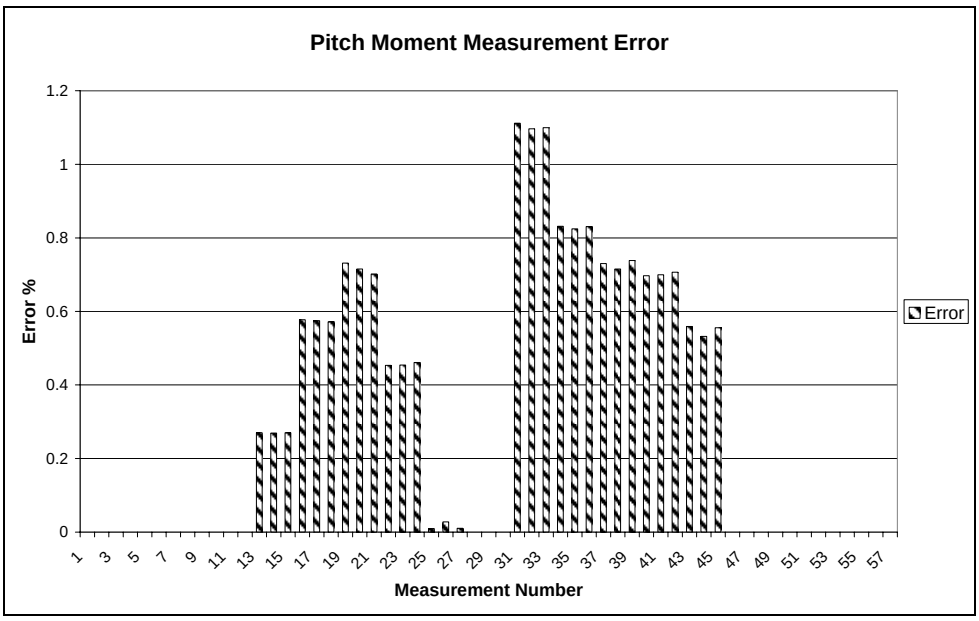

Figure 131 Pitch Moment Readings Error

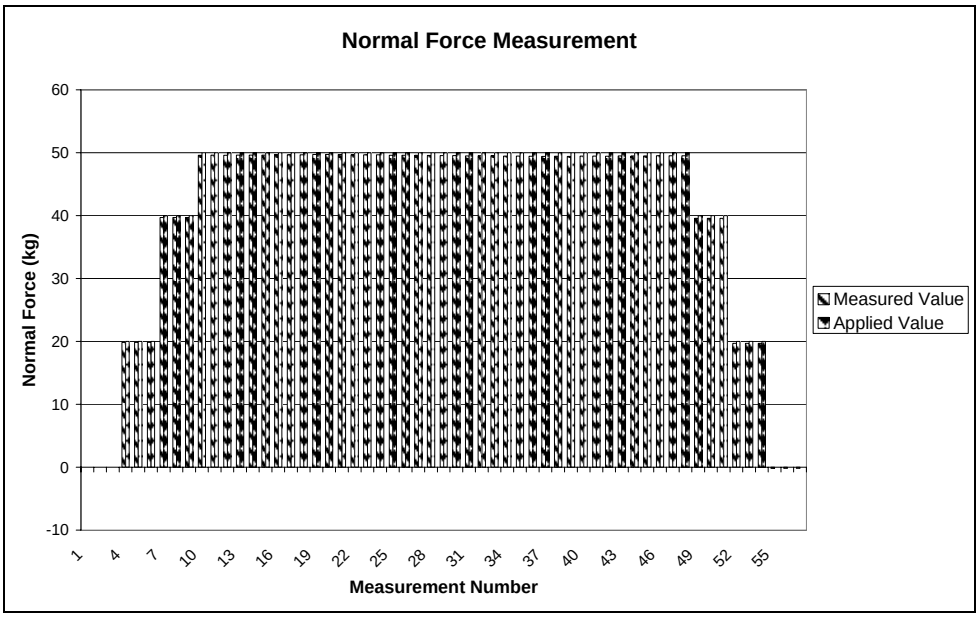

Figure 132 Normal Force Loadings and Readings

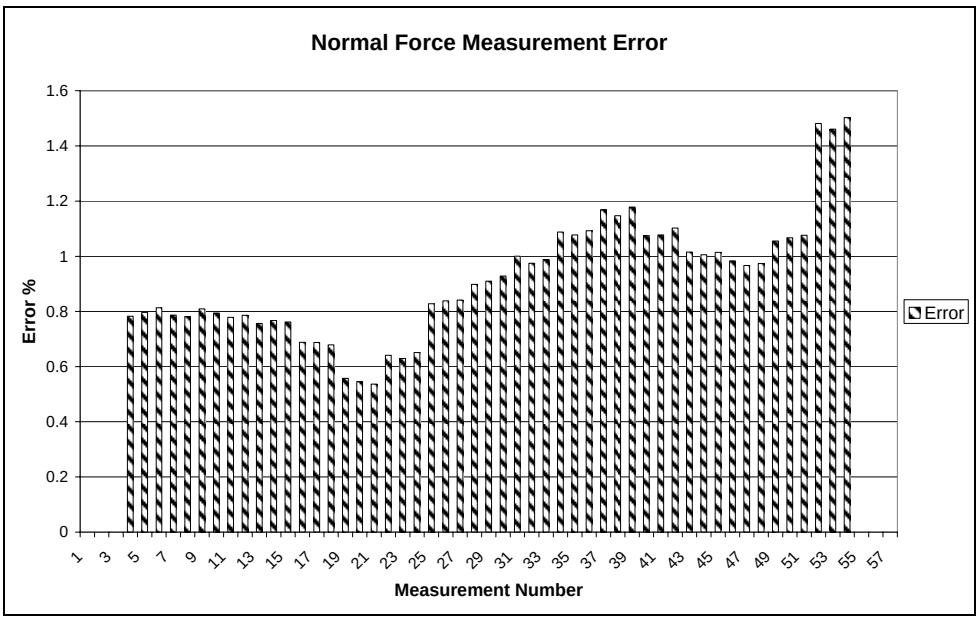

Figure 133 Normal Force Readings Error

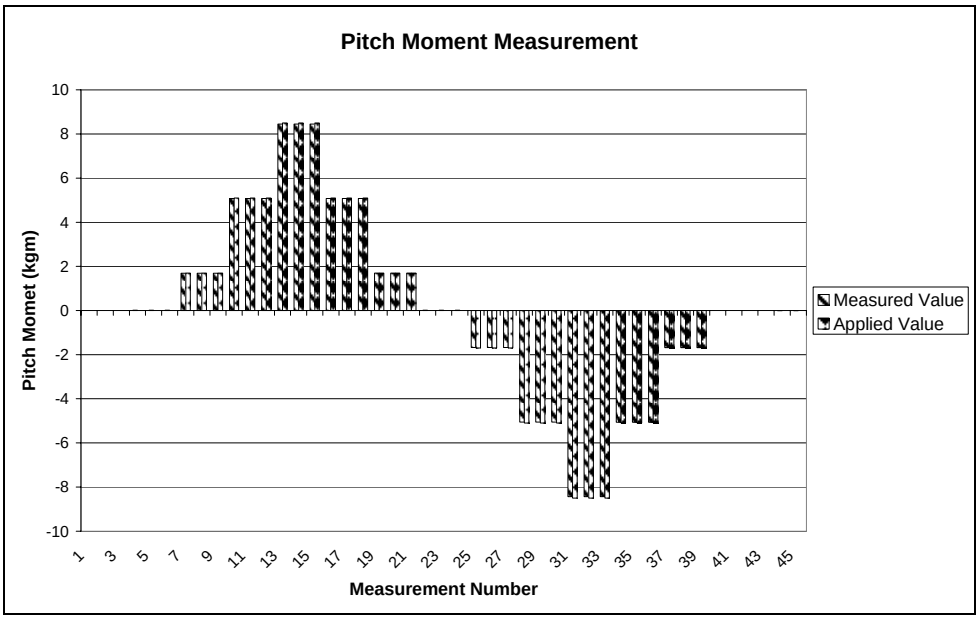

Figure 134 Pitch Moment Loadings and Readings

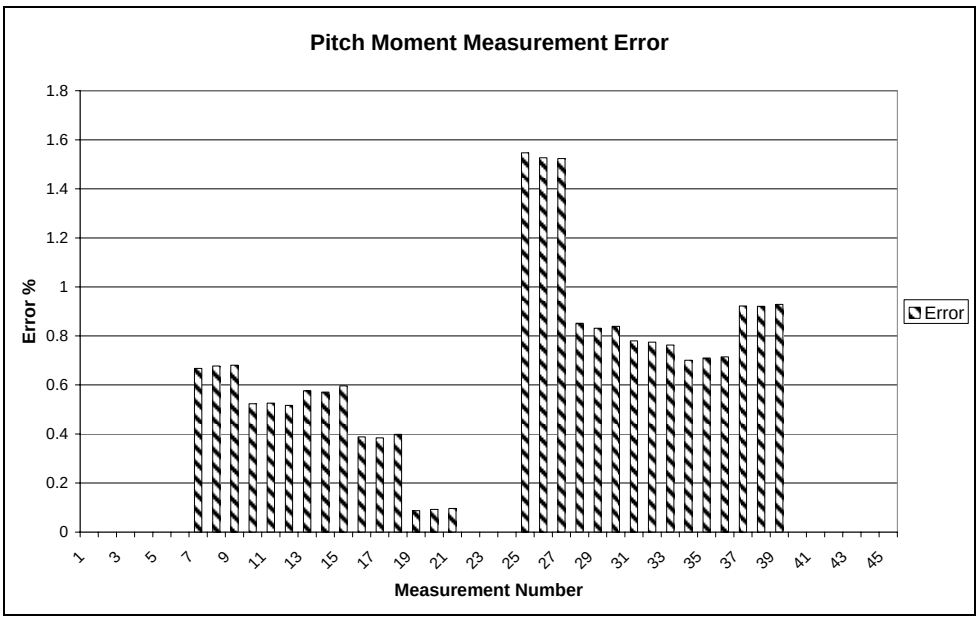

Figure 135 Pitch Moment Readings Error

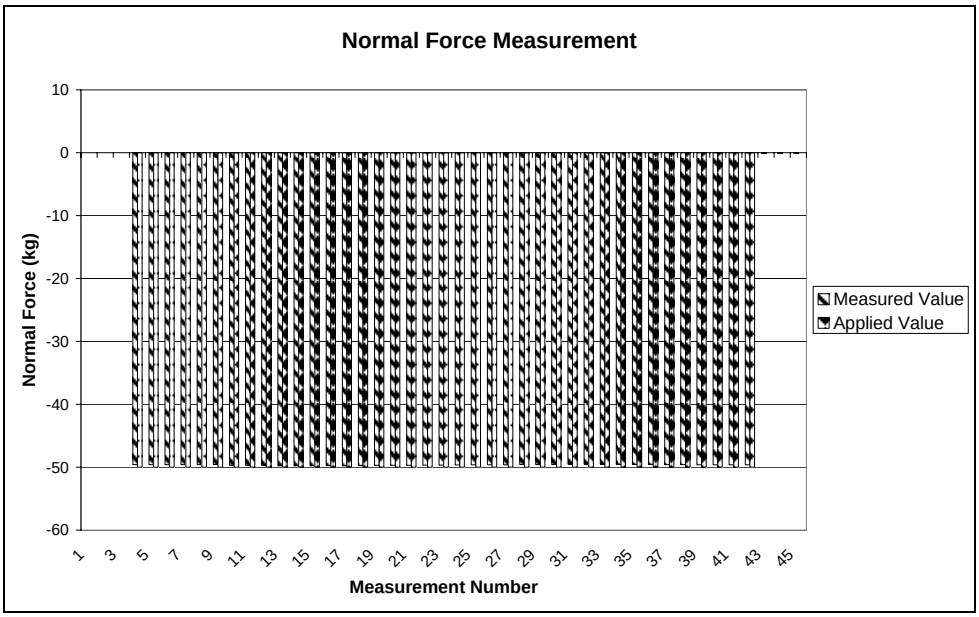

Figure 136 Normal Force Loadings and Readings

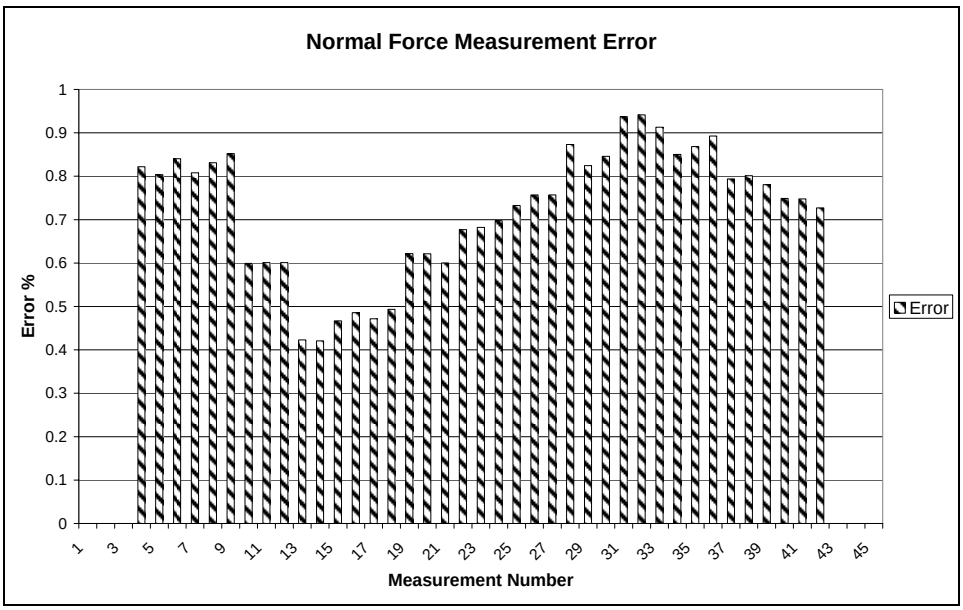

Figure 137 Normal Force Readings Error

F.7. RESULTS of NORMAL F. LOADING with DRAG F.

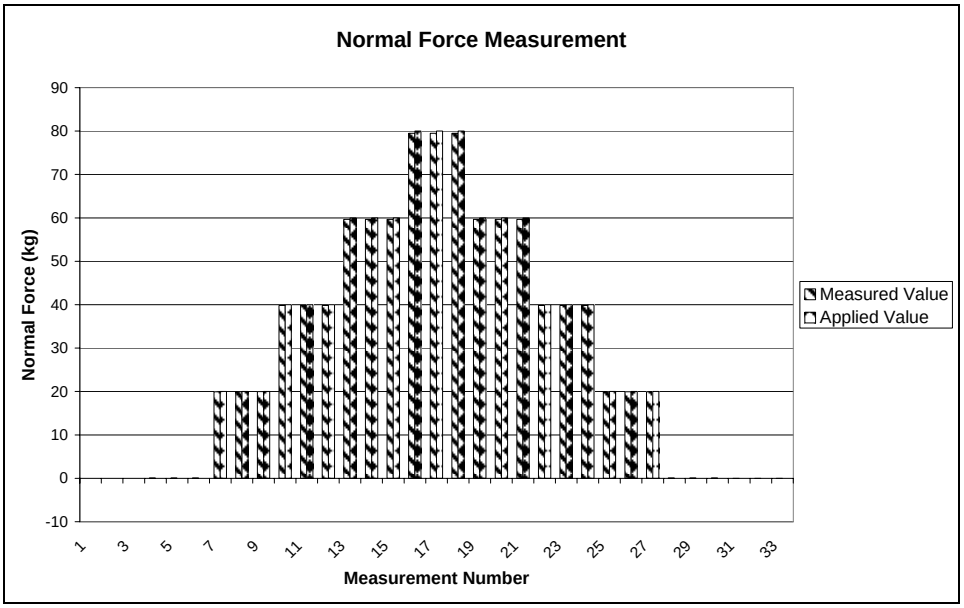

Figure 138 Normal Force Loadings and Readings

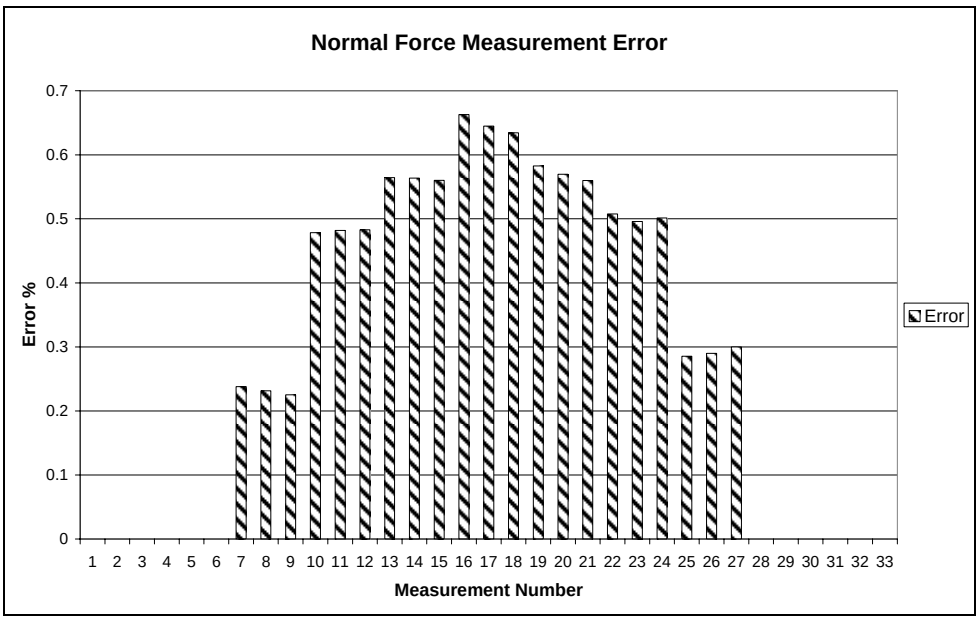

Figure 139 Normal Force Readings Error

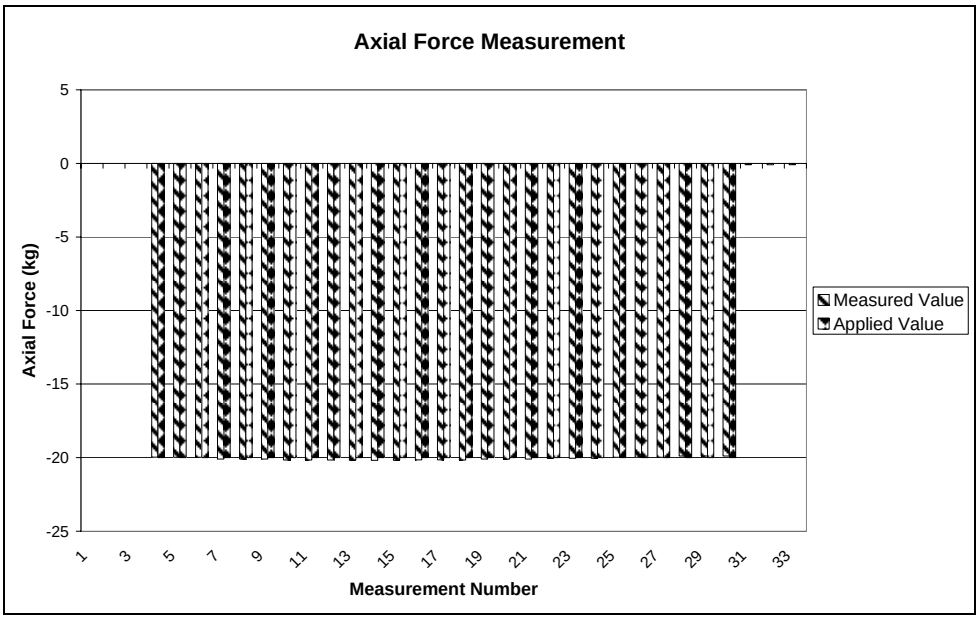

Figure 140 Axial Force Loadings and Readings

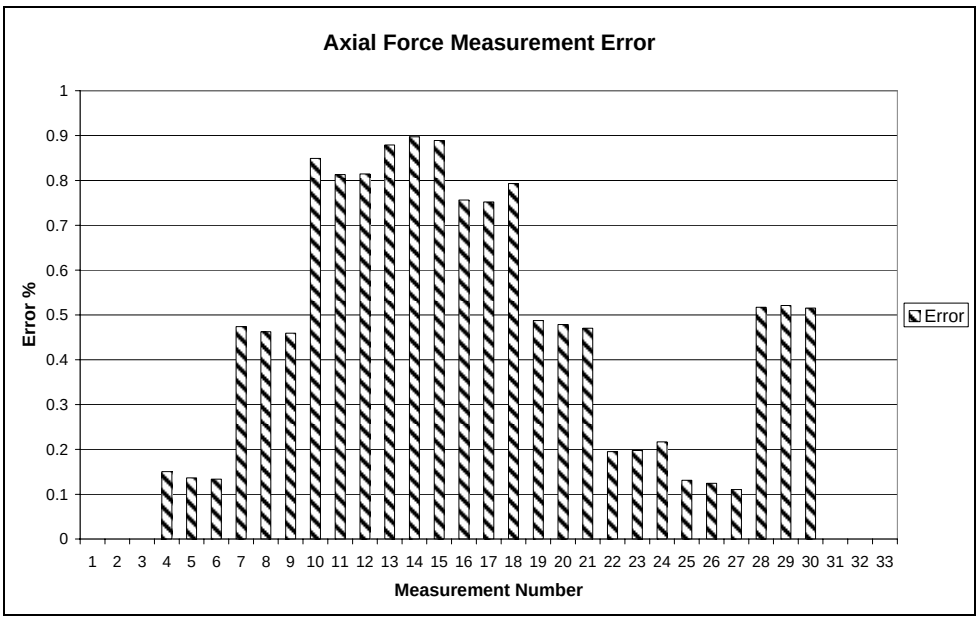

Figure 141 Axial Force Readings Error

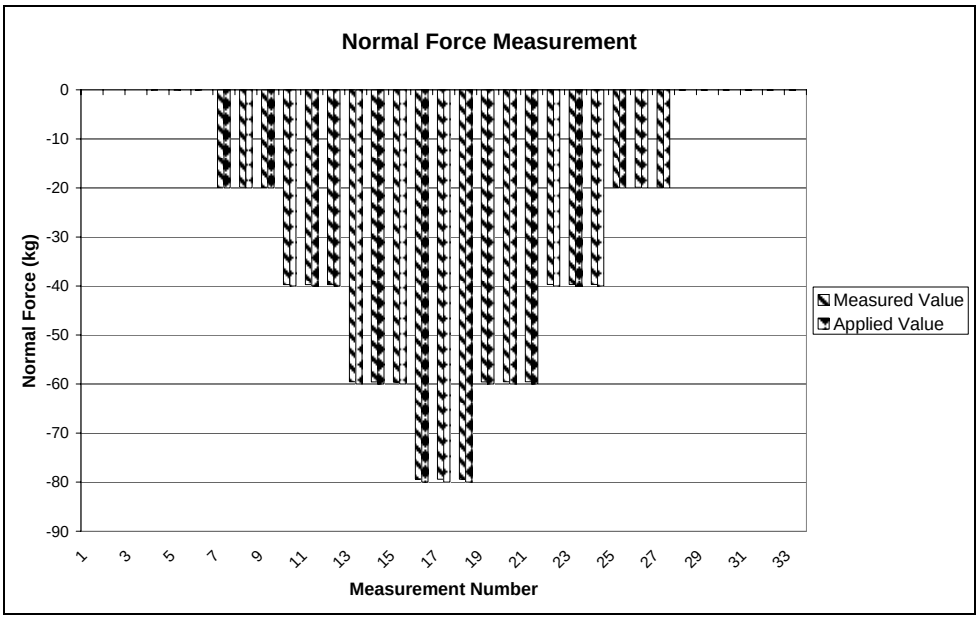

Figure 142 Normal Force Loadings and Readings

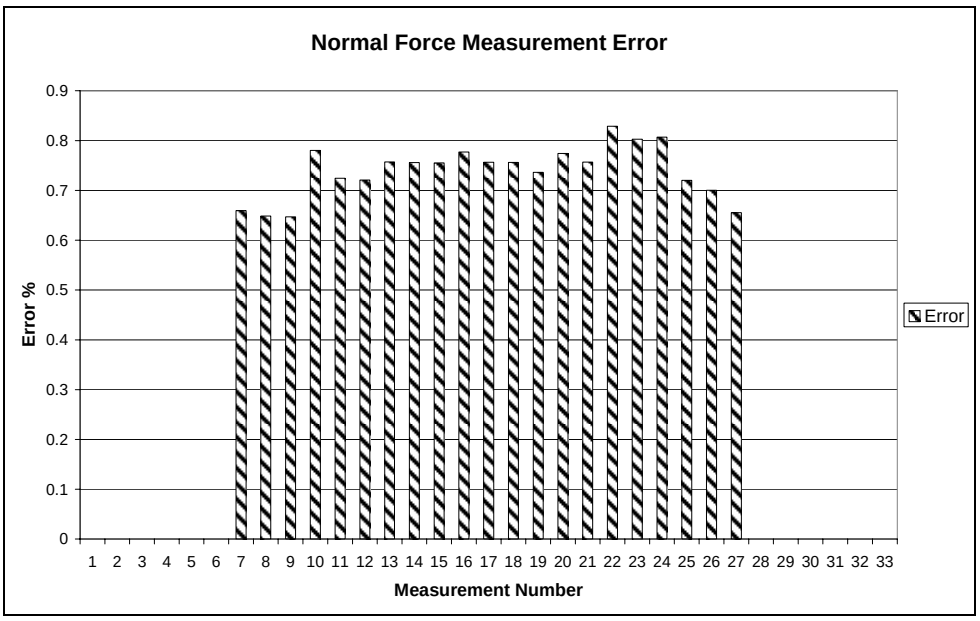

Figure 143 Normal Force Readings Error

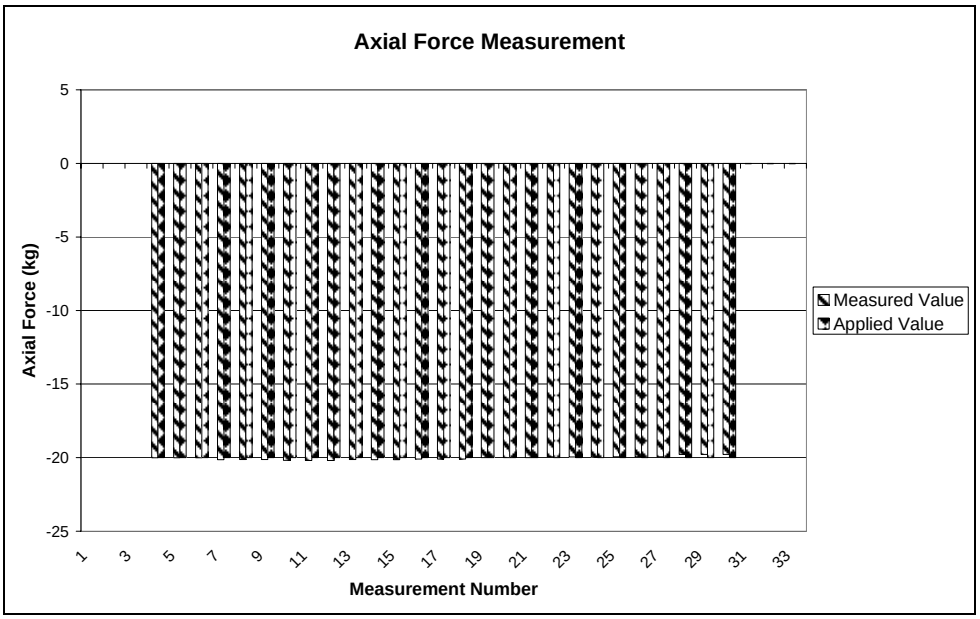

Figure 144 Axial Force Loadings and Readings

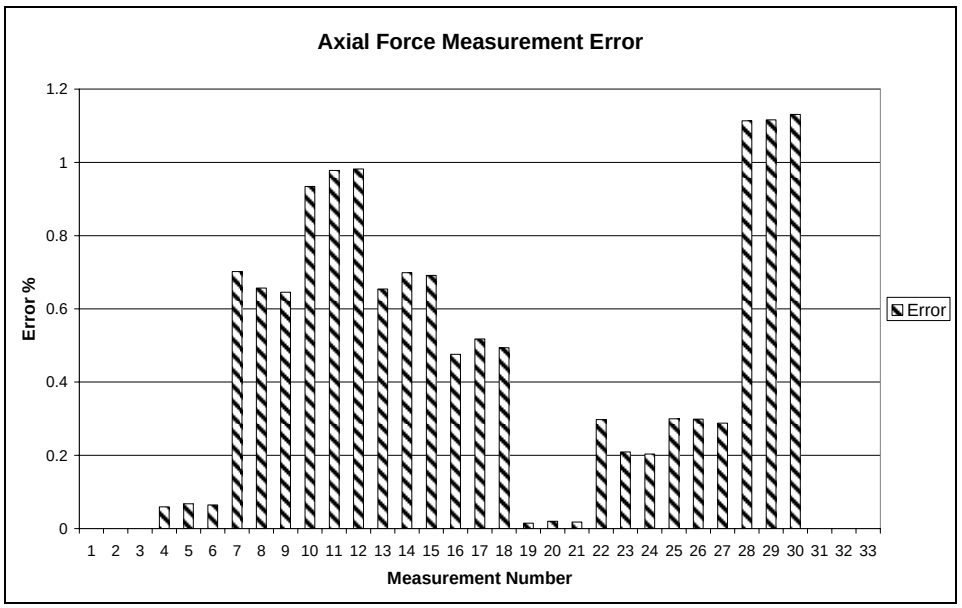

Figure 145 Axial Force Readings Error

F.8. RESULTS of SIDE FORCE LOADING with DRAG FORCE

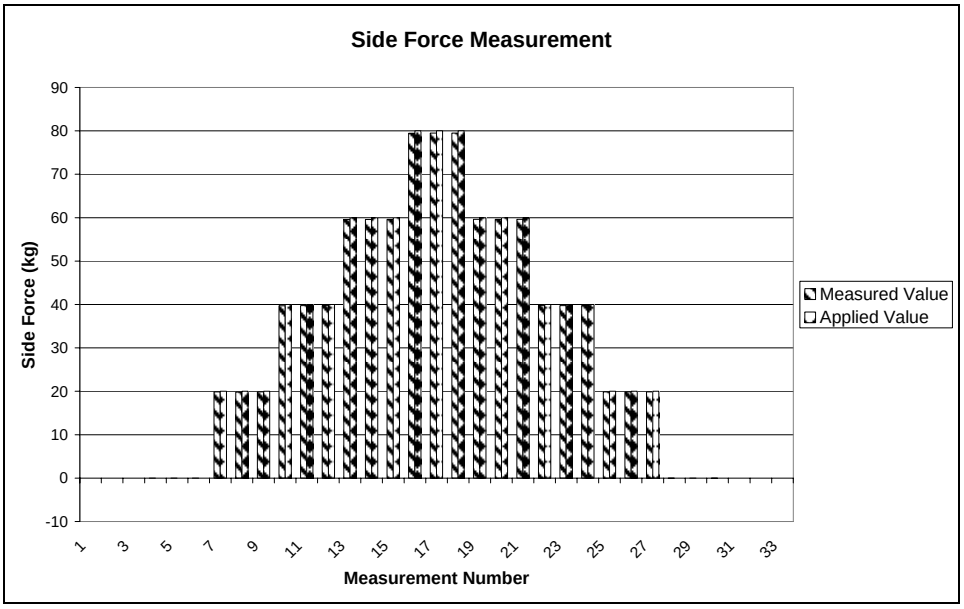

Figure 146 Side Force Loadings and Readings

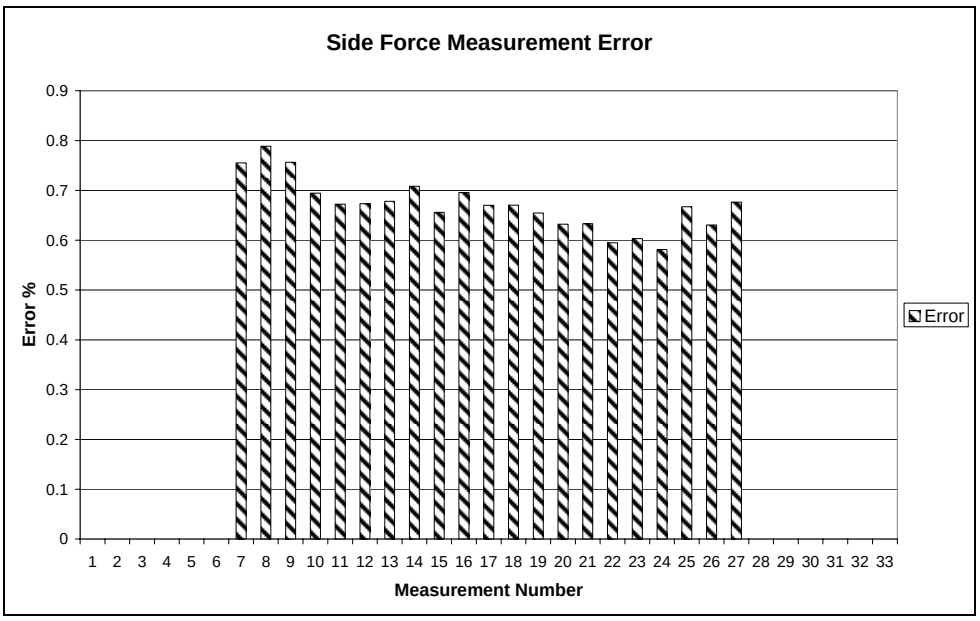

Figure 147 Side Force Readings Error

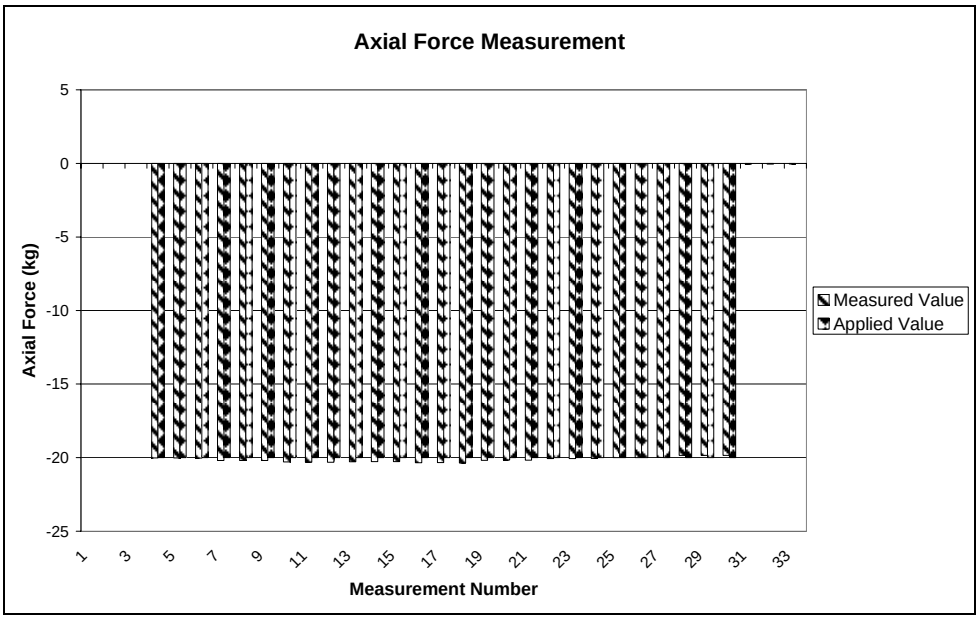

Figure 148 Axial Force Loadings and Readings

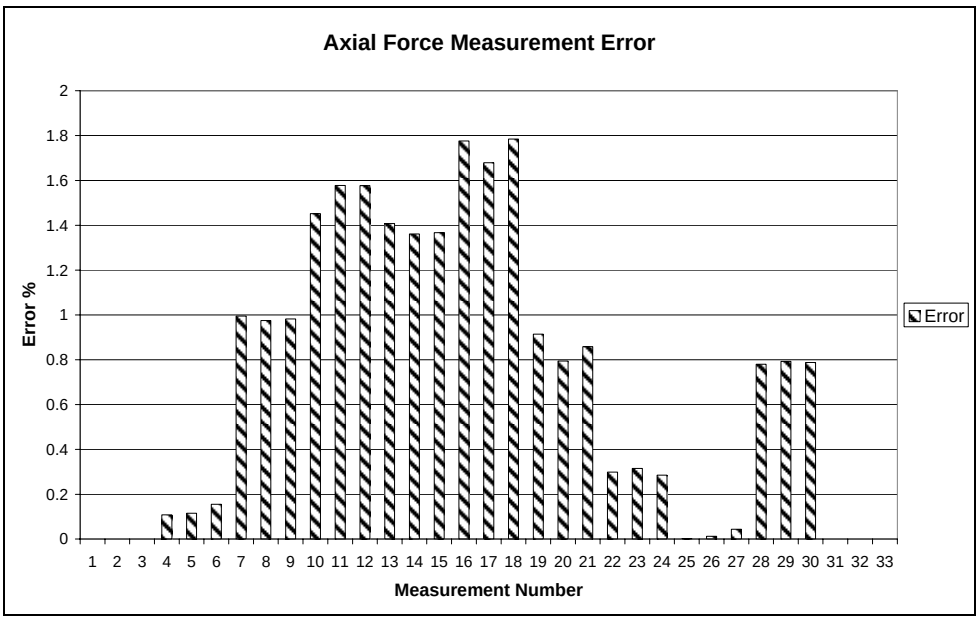

Figure 149 Axial Force Readings Error

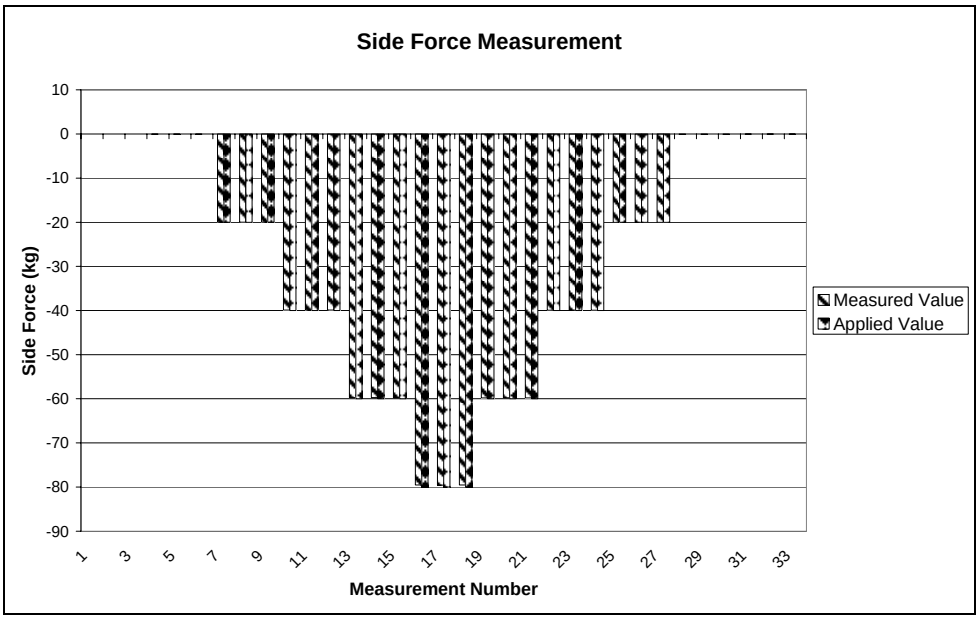

Figure 150 Side Force Loadings and Readings

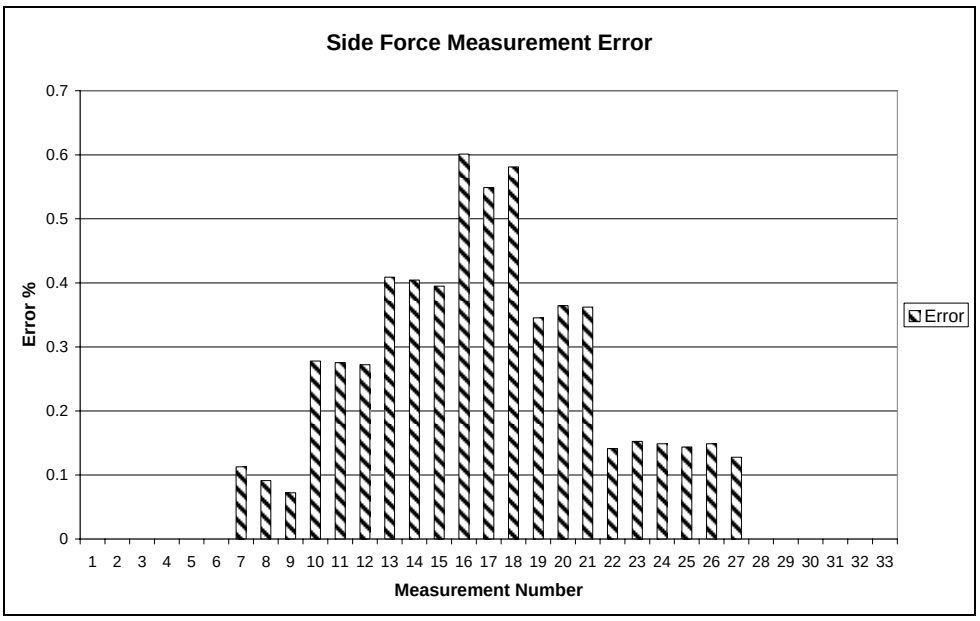

Figure 151Side Force Readings Error

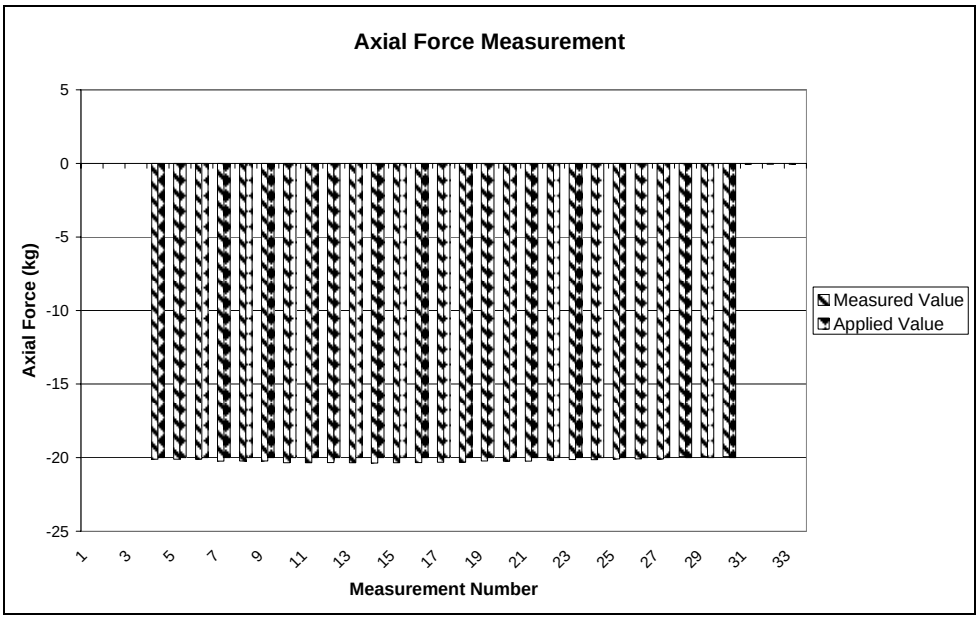

Figure 152 Axial Force Loadings and Readings

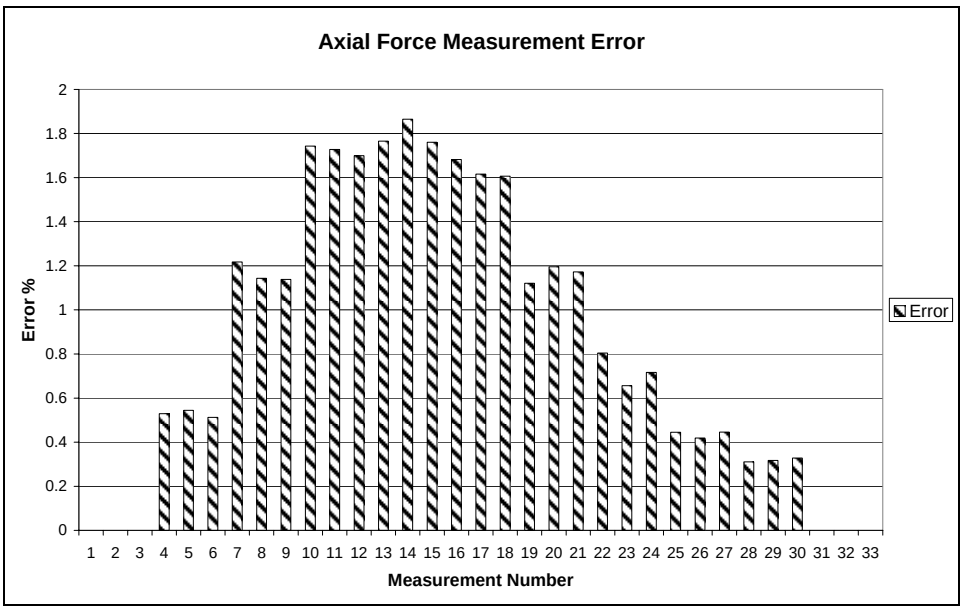

Figure 153 Axial Force Readings Error

F.9 RESULTS of 3-COMBINATION LOADING (P-N-A)

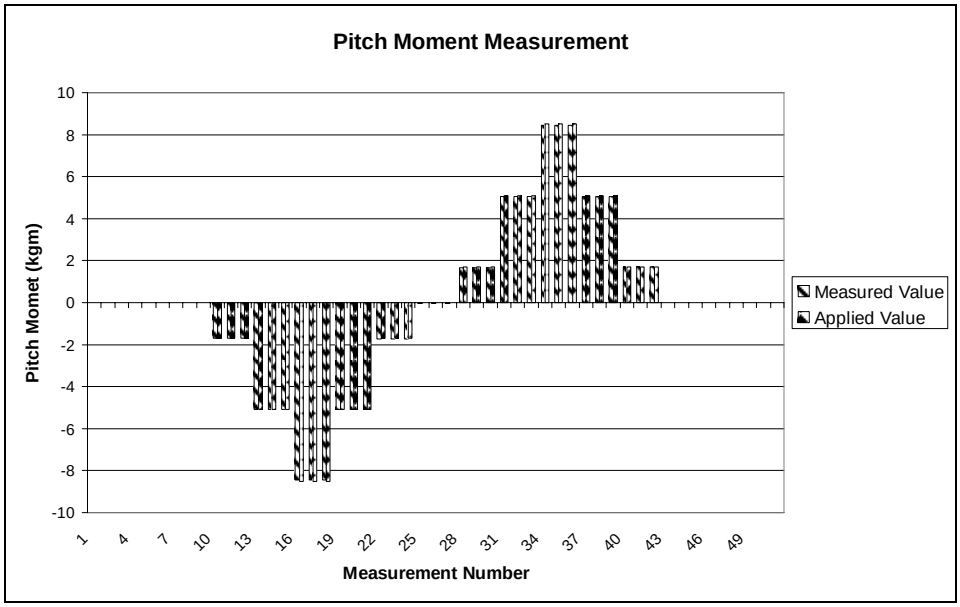

Figure 154 Pitch Moment Loadings and Readings

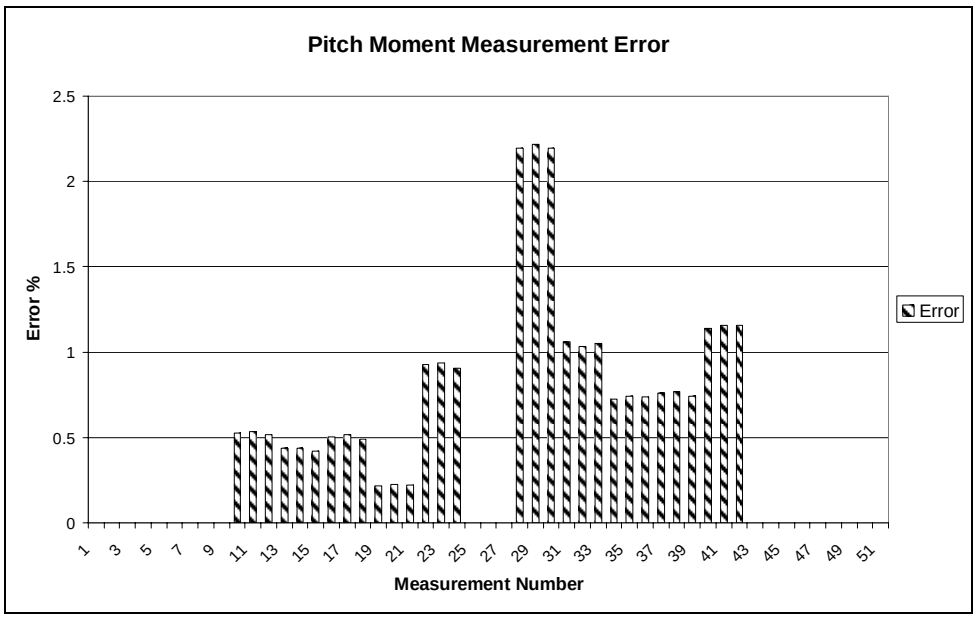

Figure 155 Pitch Moment Readings Error

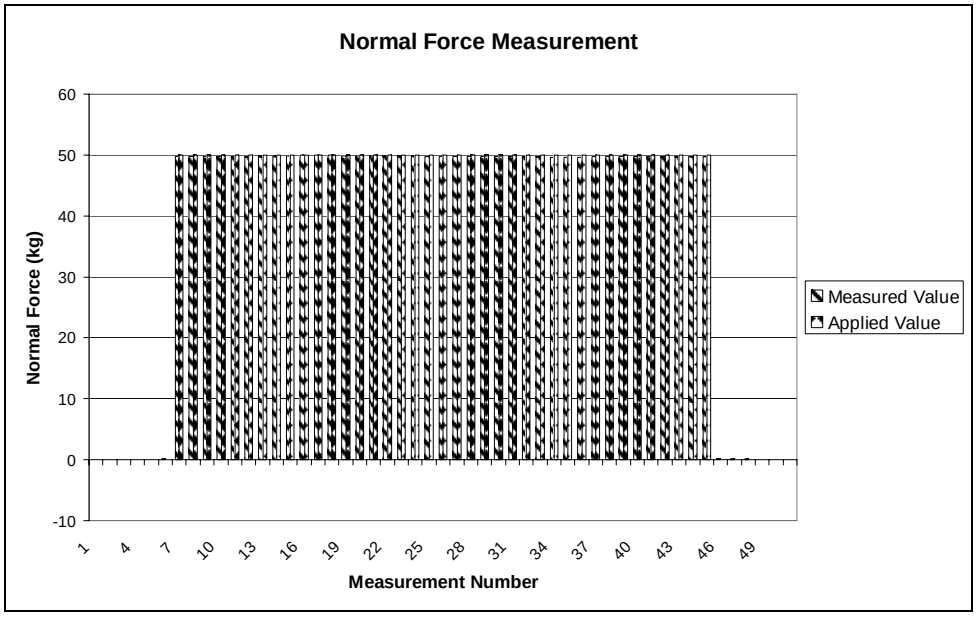

Figure 156 Normal Force Loadings and Readings

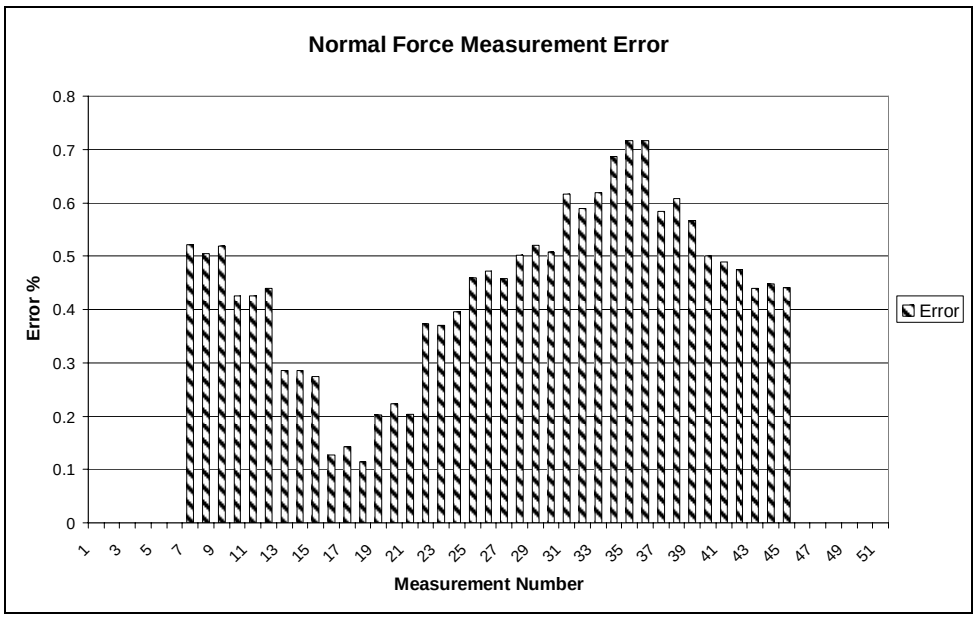

Figure 157 Normal Force Readings Error

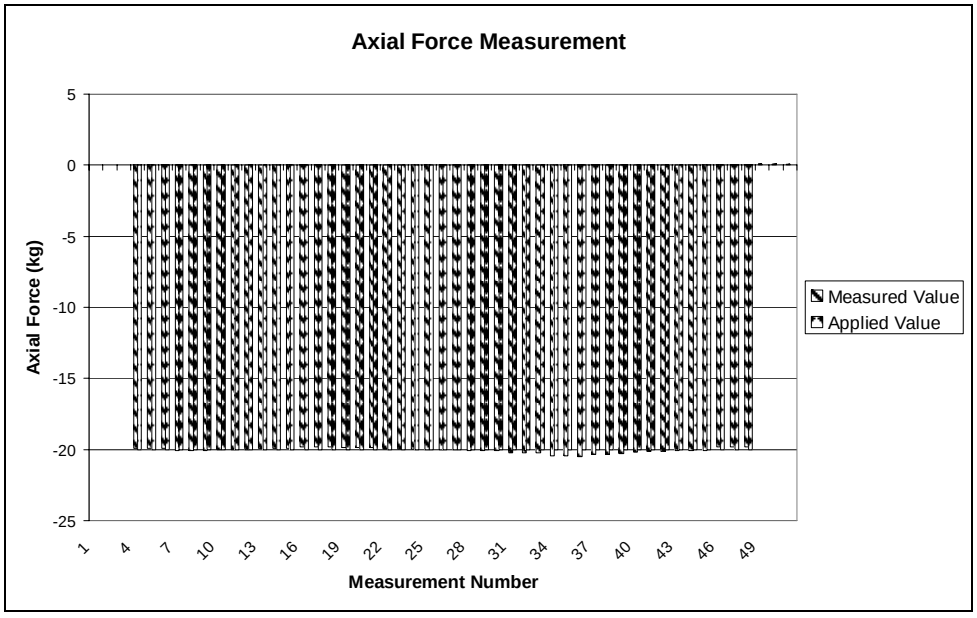

Figure 158 Axial Force Loadings and Readings

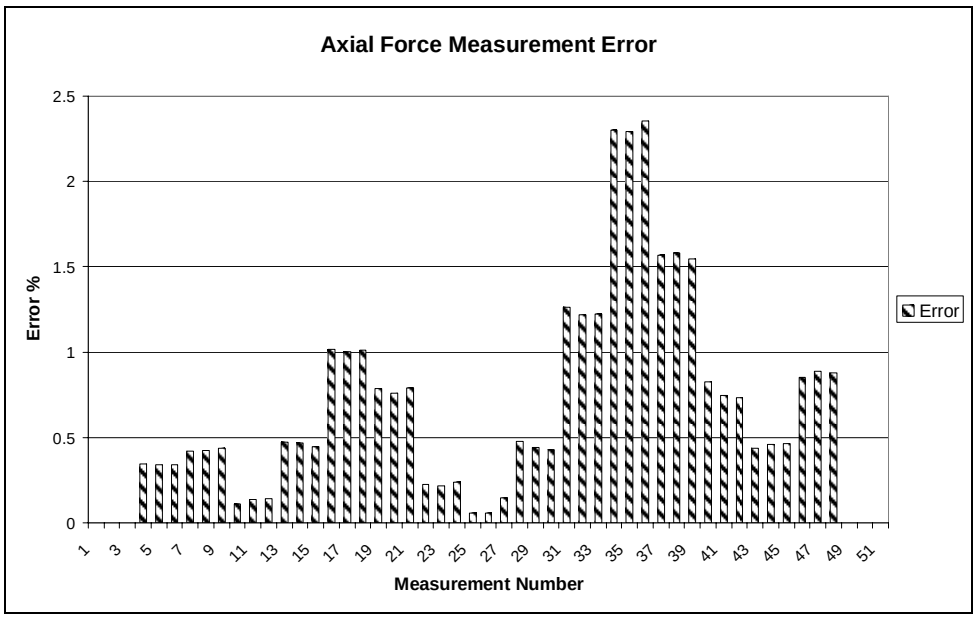

Figure 159 Axial Force Readings Error

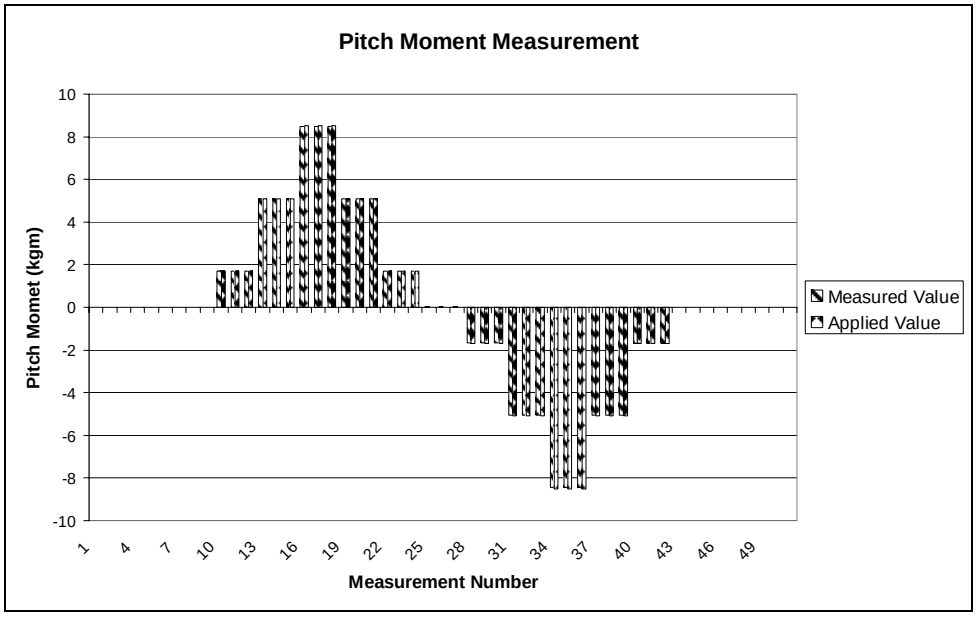

Figure Pitch Moment Loadings and Readings

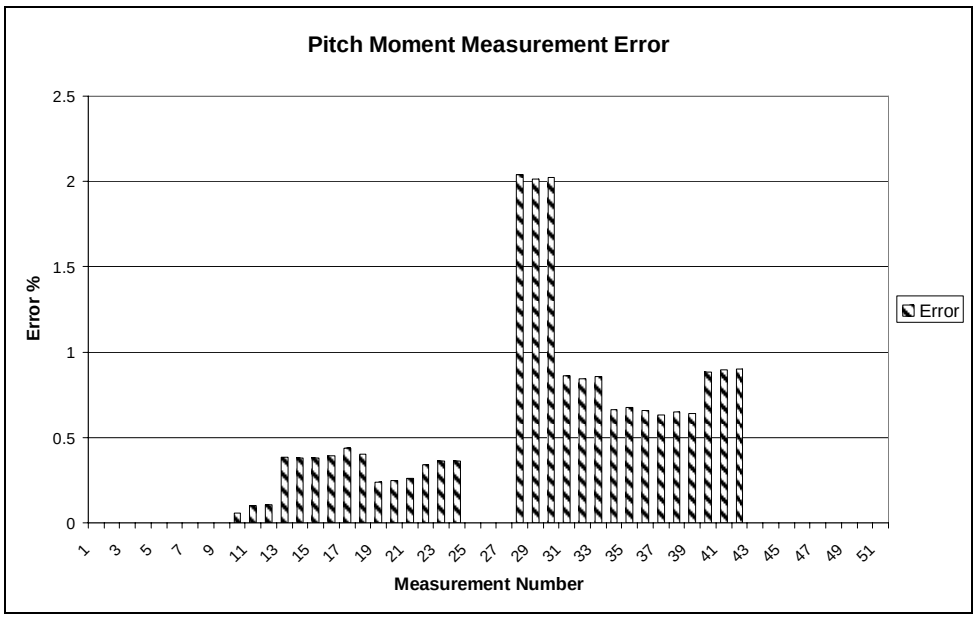

Figure 160Pitch Moment Readings Error

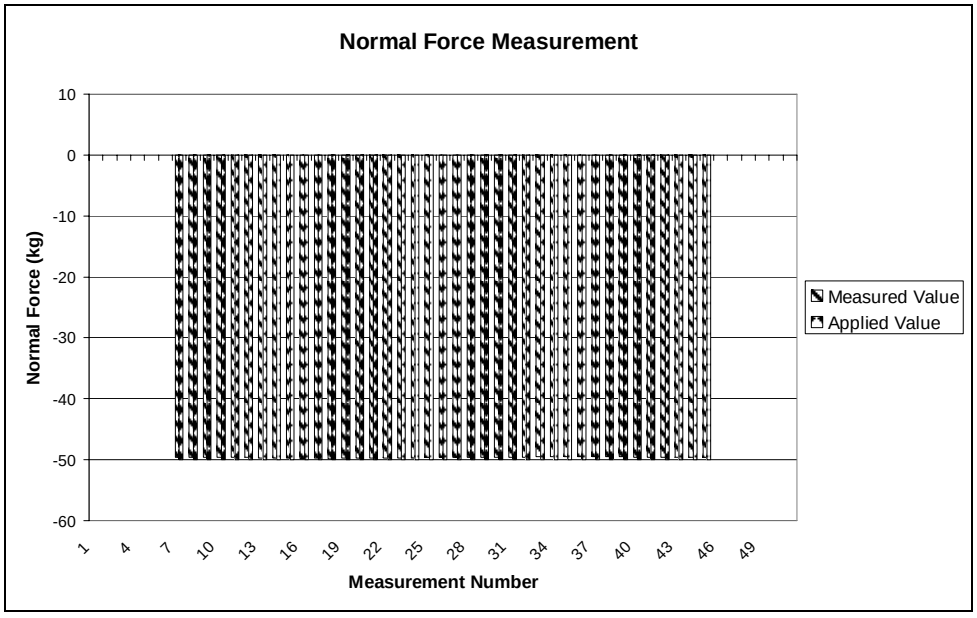

Figure 161 Normal Force Loadings and Readings

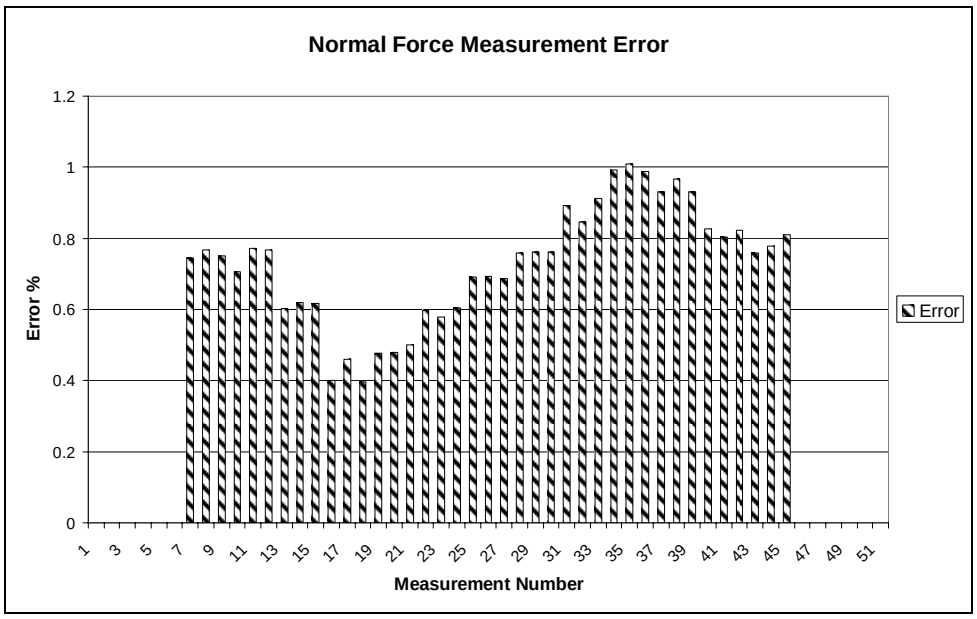

Figure 162 Normal Force Readings Error

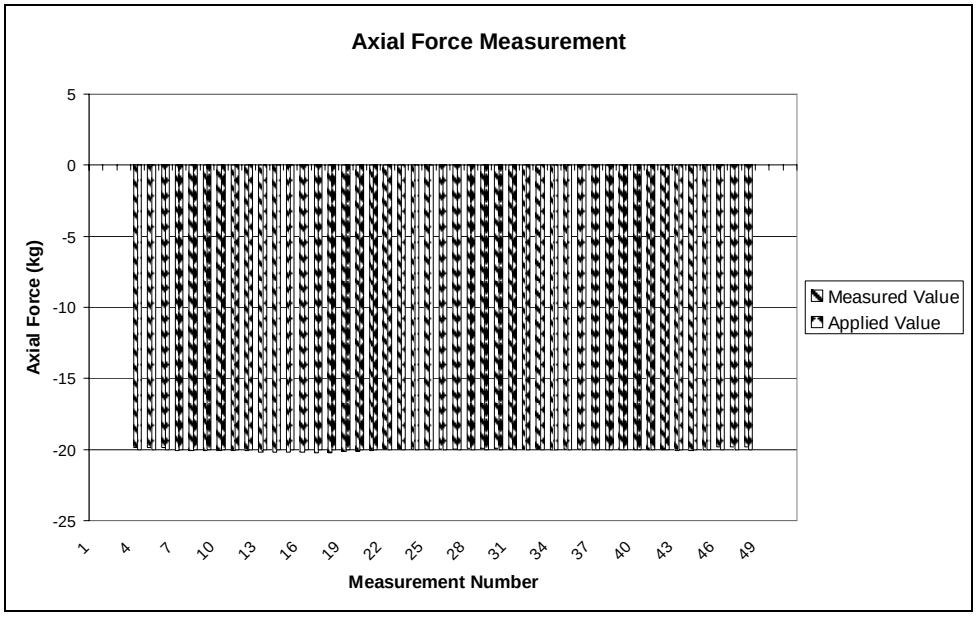

Figure 163 Axial Force Loadings and Readings

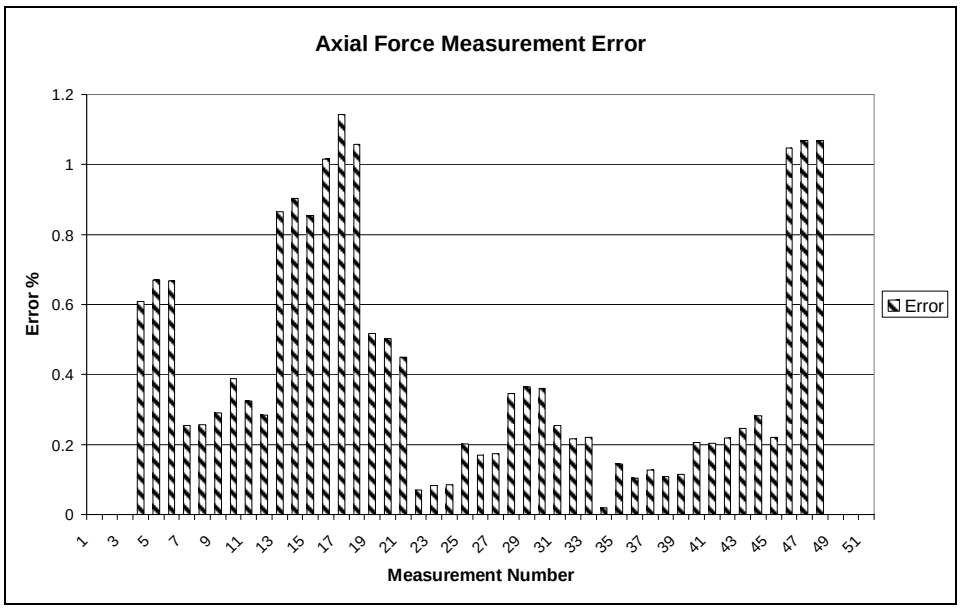

Figure 164 Axial Force Readings Error

F.10 RESULTS of 3-COMBINATION LOADING (R-N-A)

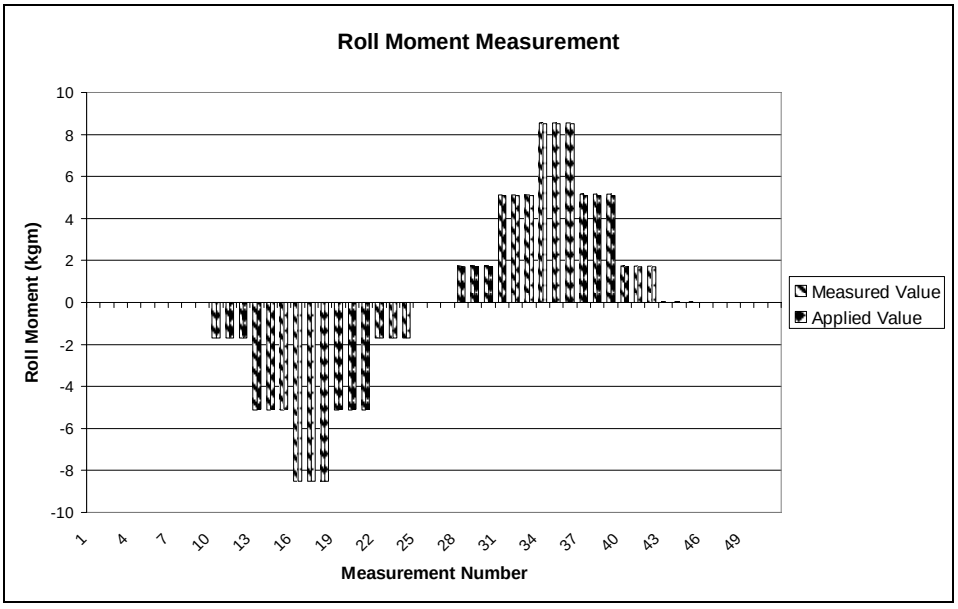

Figure 165 Roll Moment Loadings and Readings

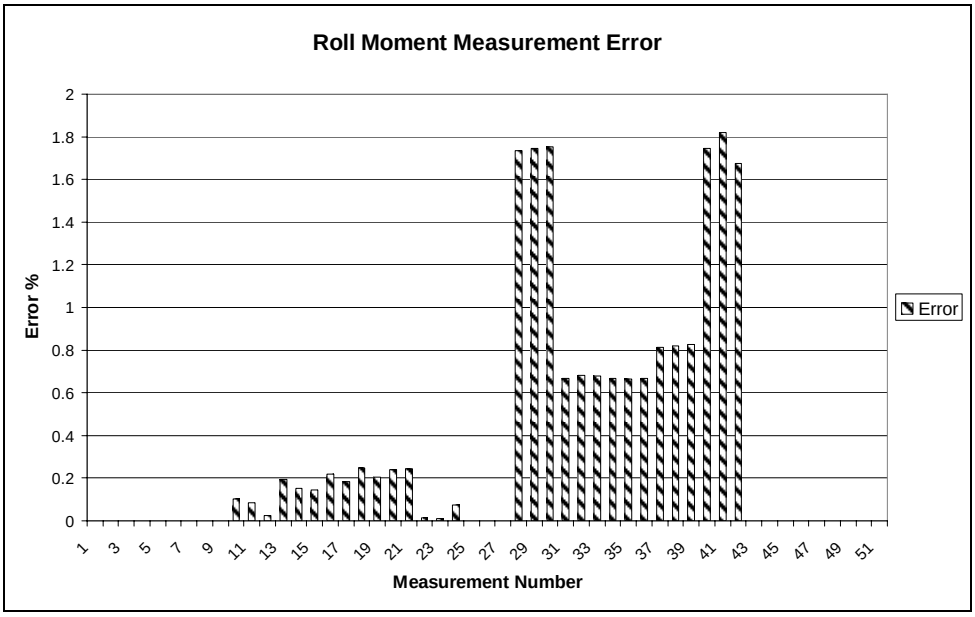

Figure 166 Roll Moment Readings Error

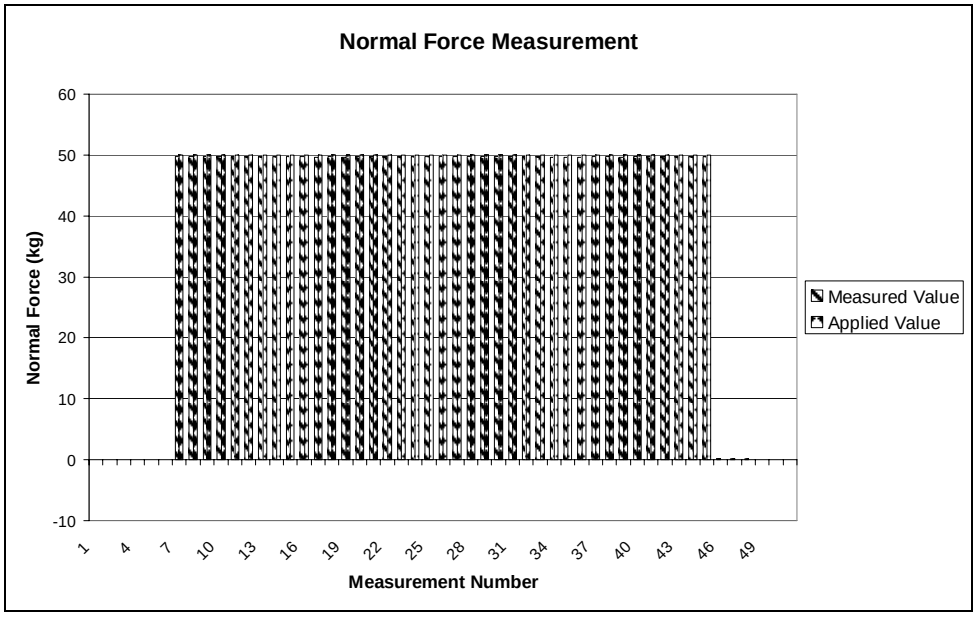

Figure 167 Normal Force Loadings and Readings

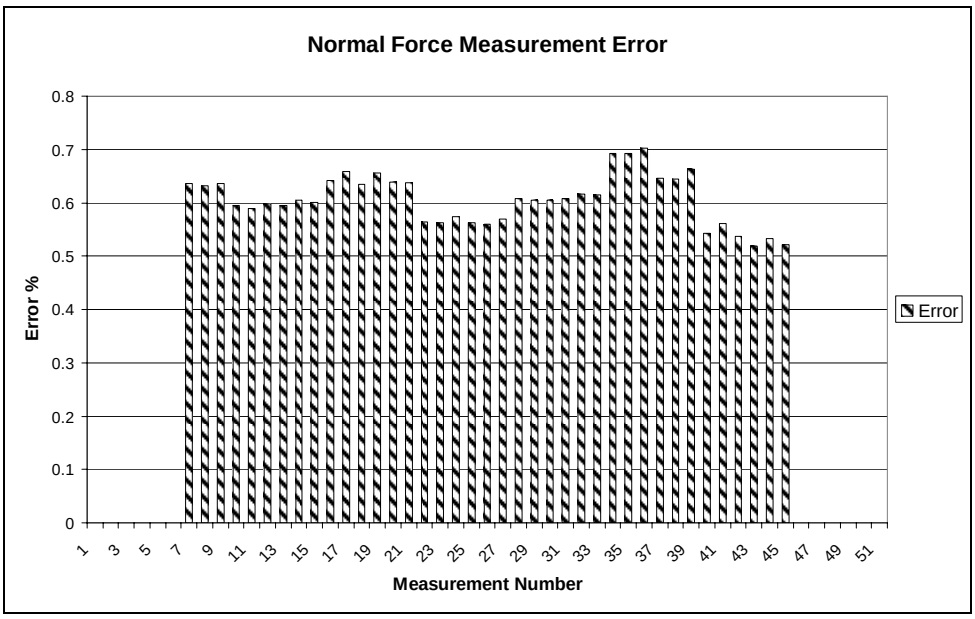

Figure 168 Normal Force Loadings and Readings

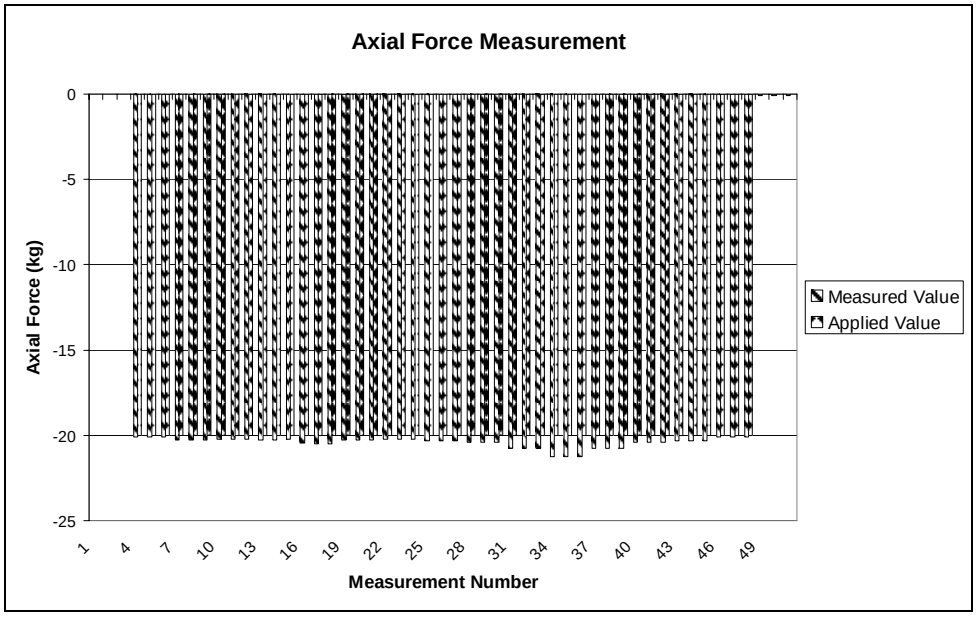

Figure 169 Axial Force Loadings and Readings

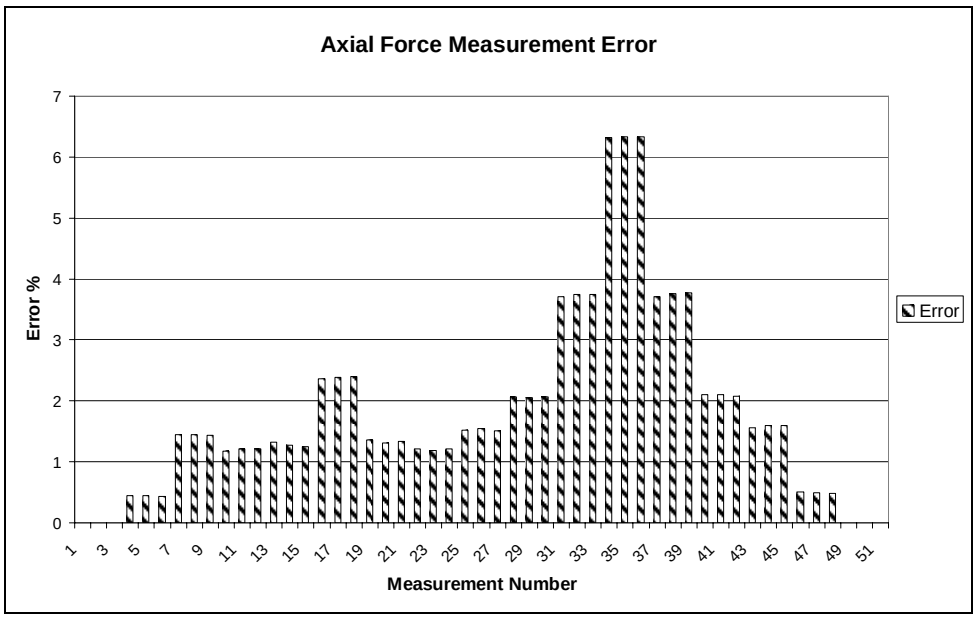

Figure 170 Axial Force Readings Error

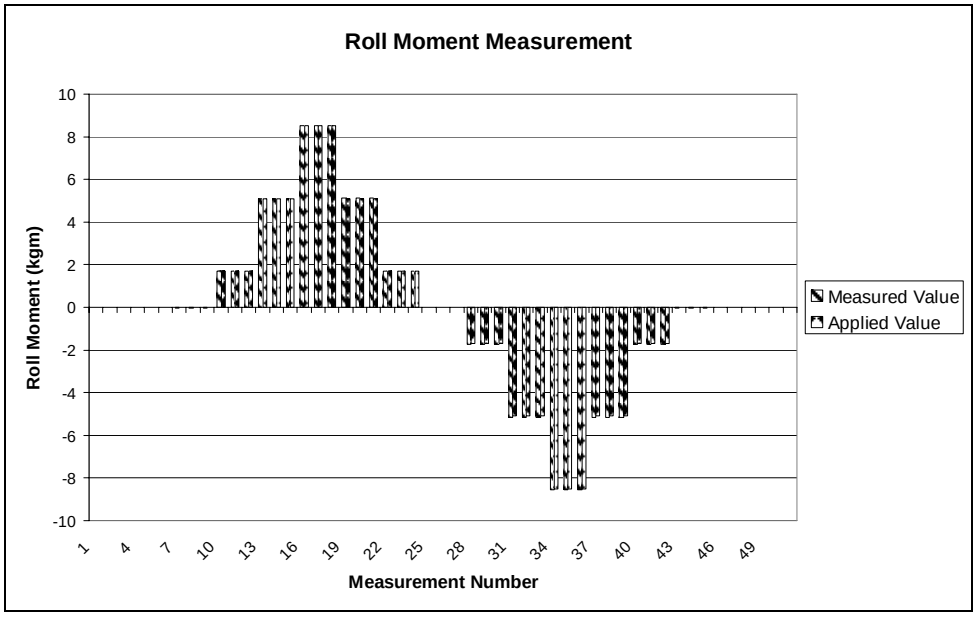

Figure 171 Roll Moment Loadings and Readings

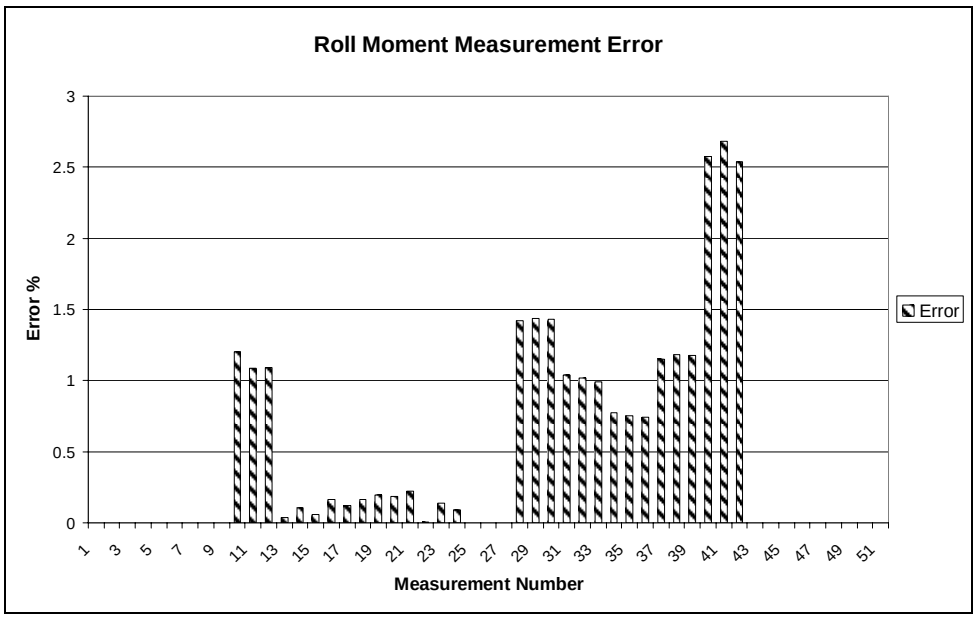

Figure 172 Roll Moment Readings Error

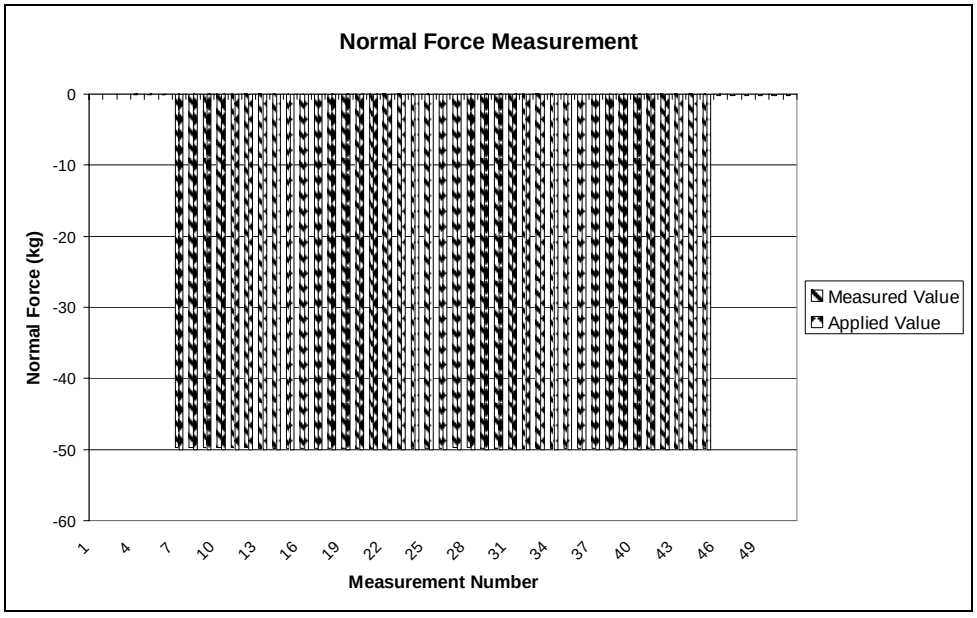

Figure 173 Normal Force Loadings and Readings

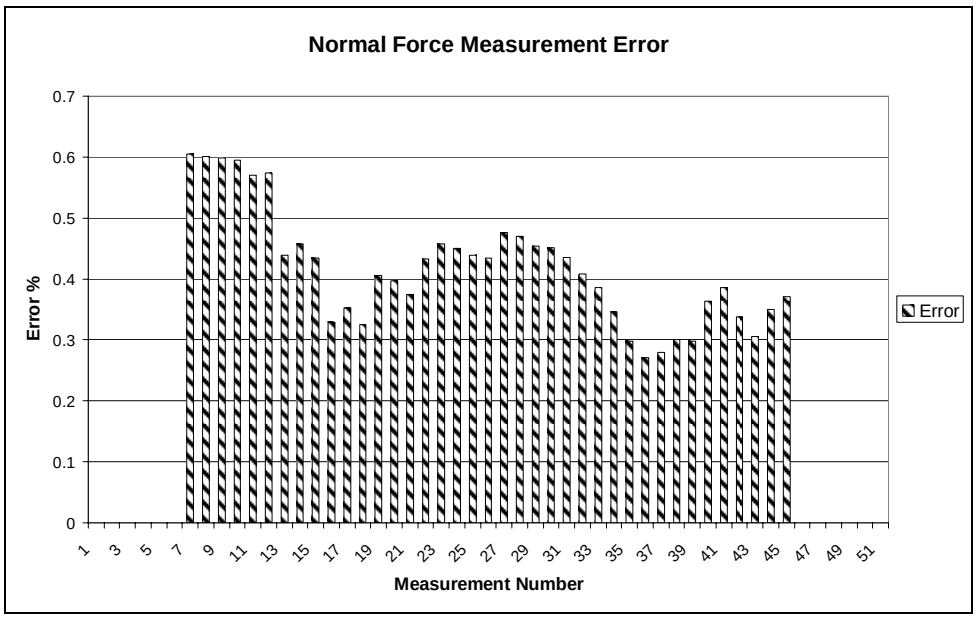

Figure 174 Normal Force Readings Error

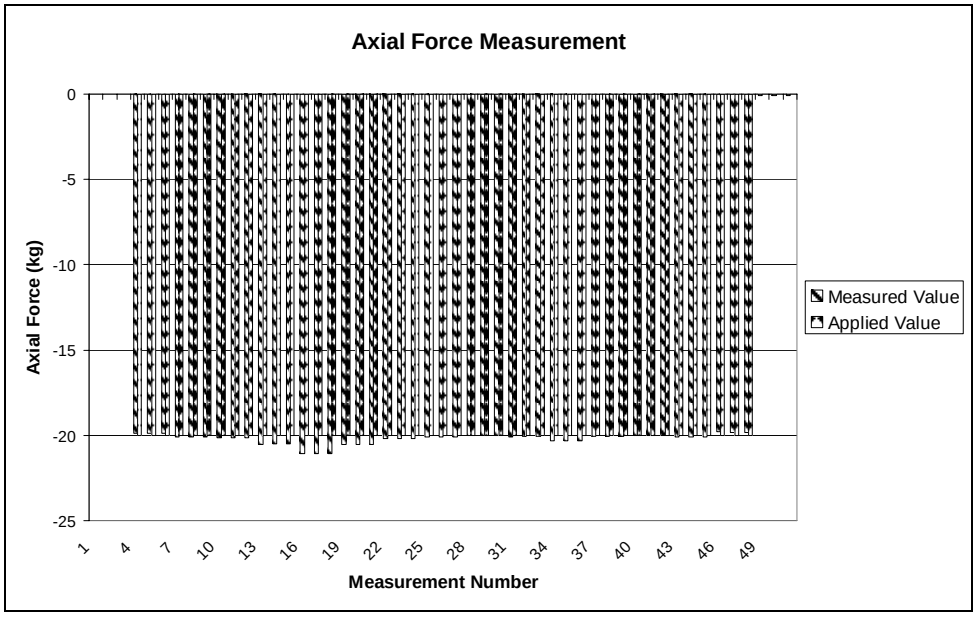

Figure 175 Axial Force Loadings and Readings

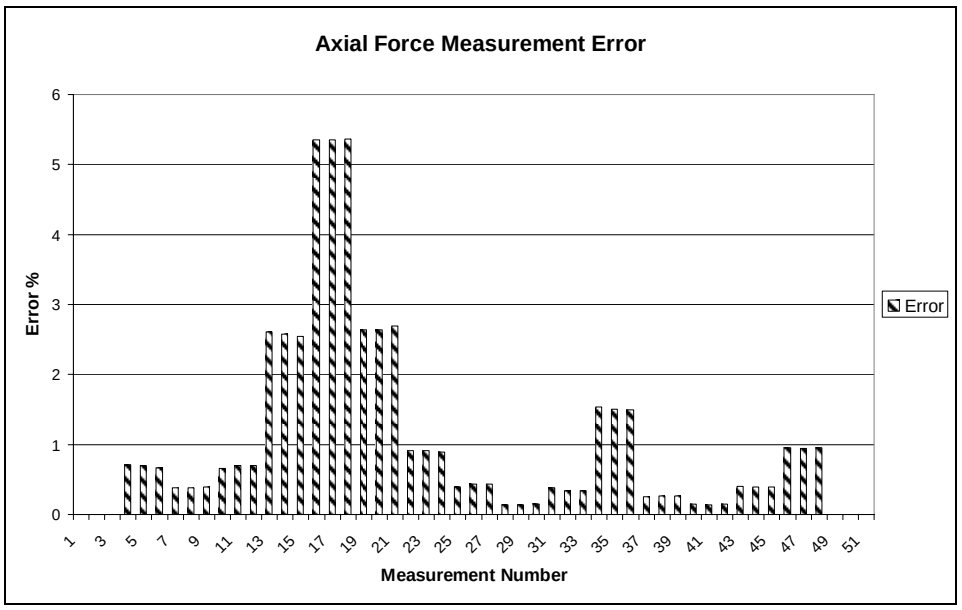

Figure 176 Axial Force Readings Error

F.11 RESULTS of 3-COMBINATION LOADING (R-S-A)

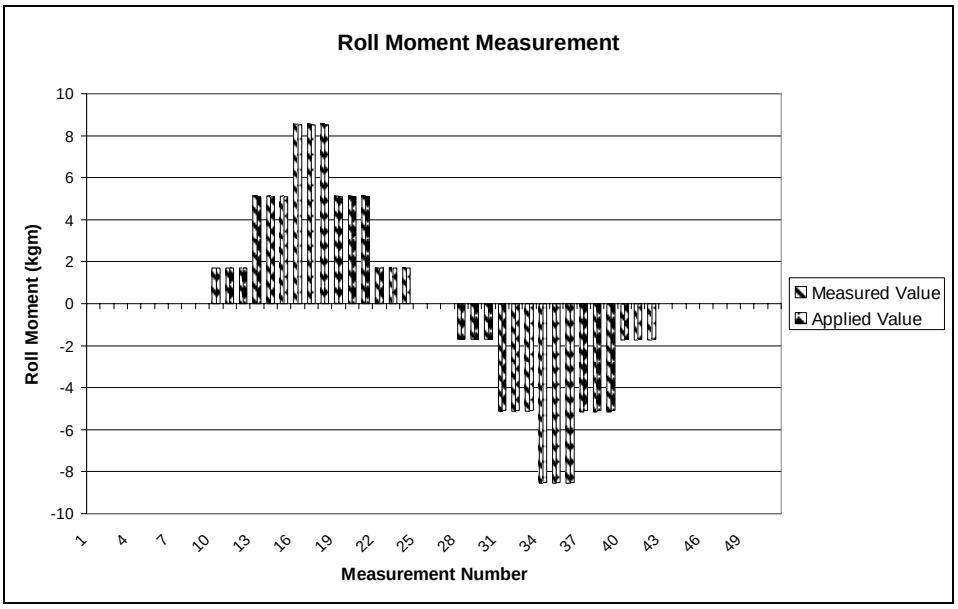

Figure 177 Roll Moment Loadings and Readings

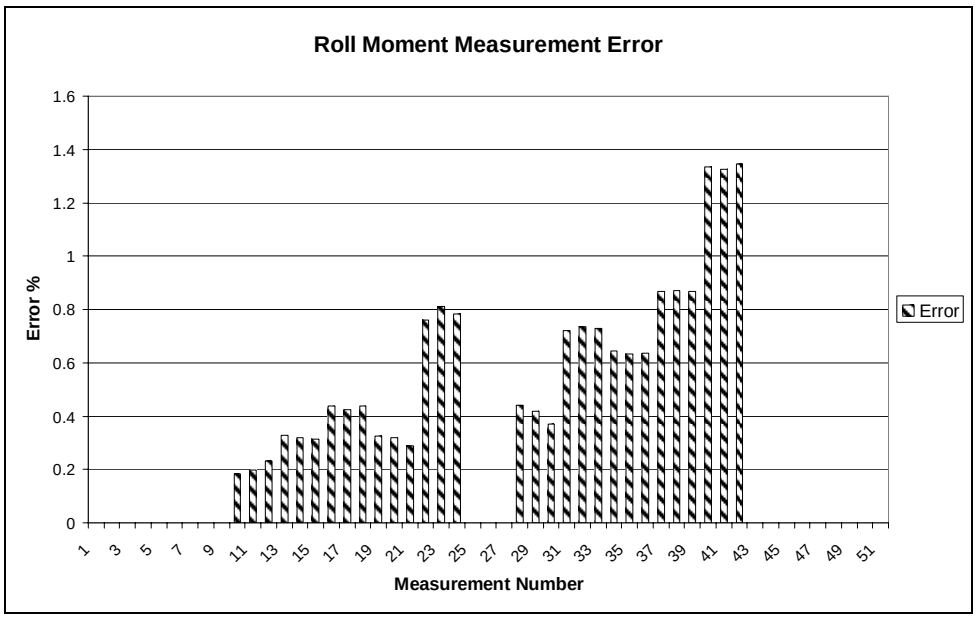

Figure 178 Roll Moment Readings Error

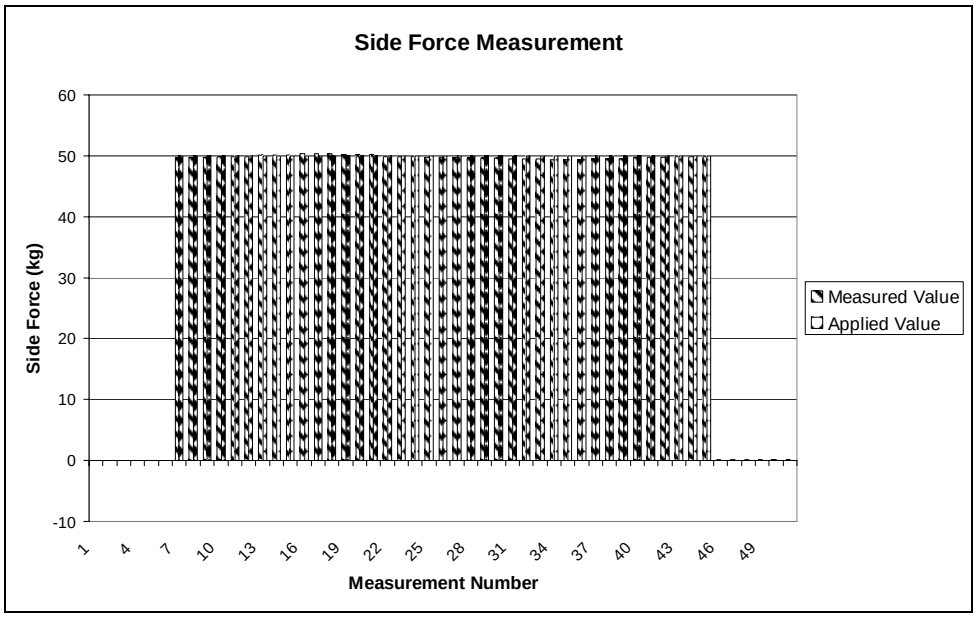

Figure 179 Side Force Loadings and Readings

Figure 180 Side Force Readings Error

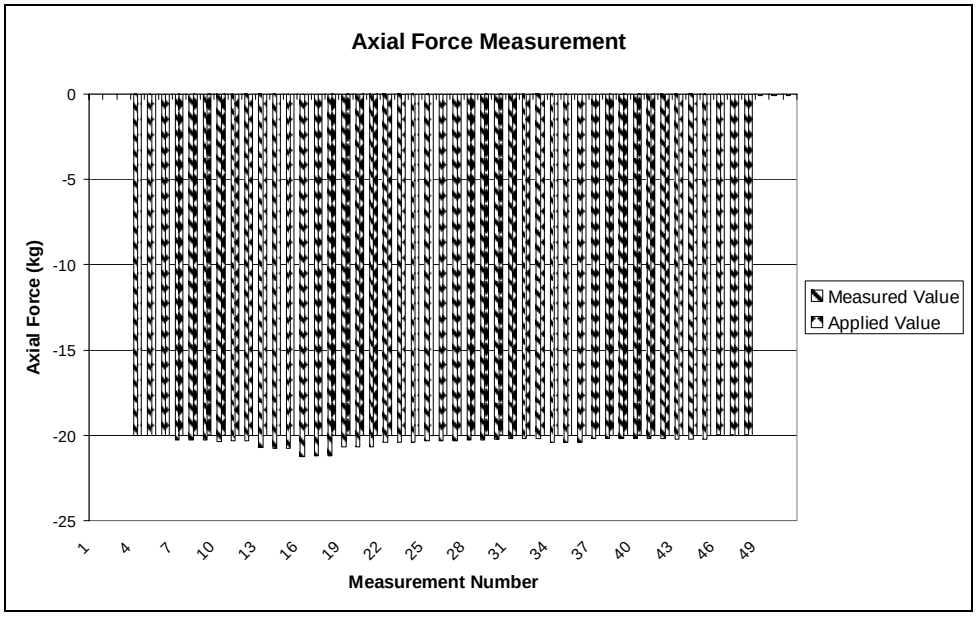

Figure 181 Axial Force Loadings and Readings

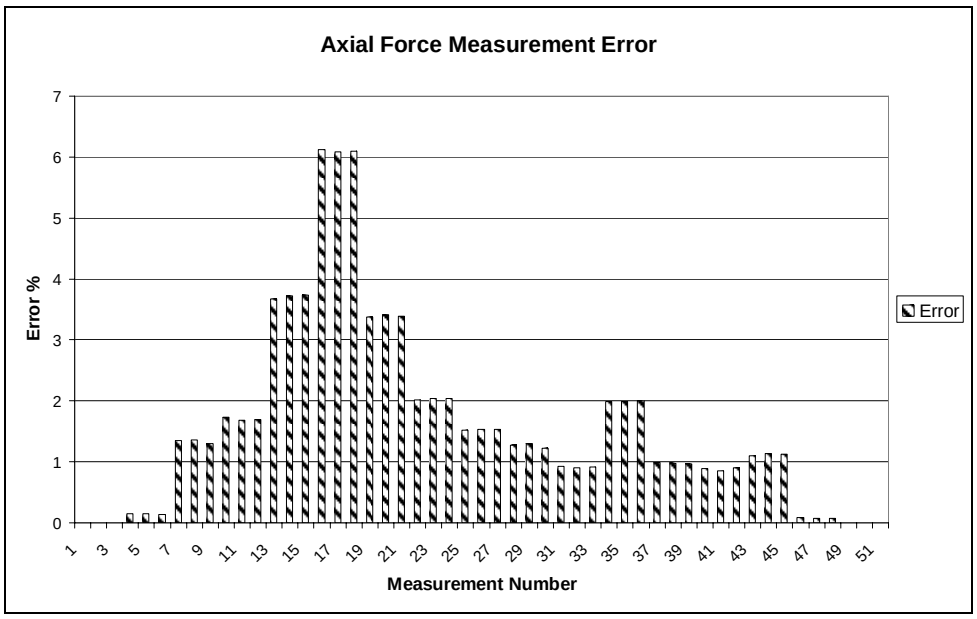

Figure 182 Axial Force Readings Error

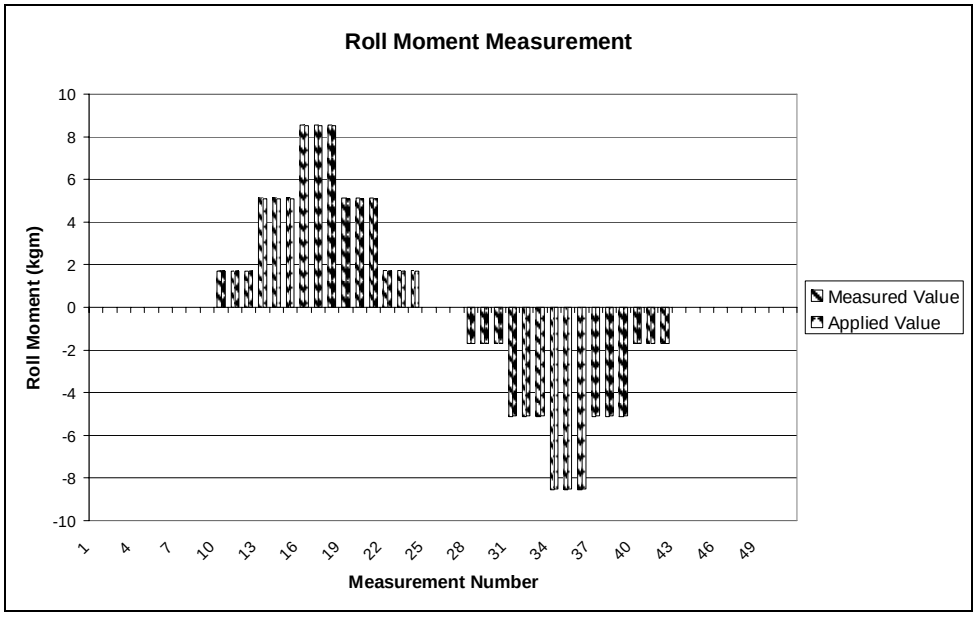

Figure 183 Roll Moment Loadings and Readings

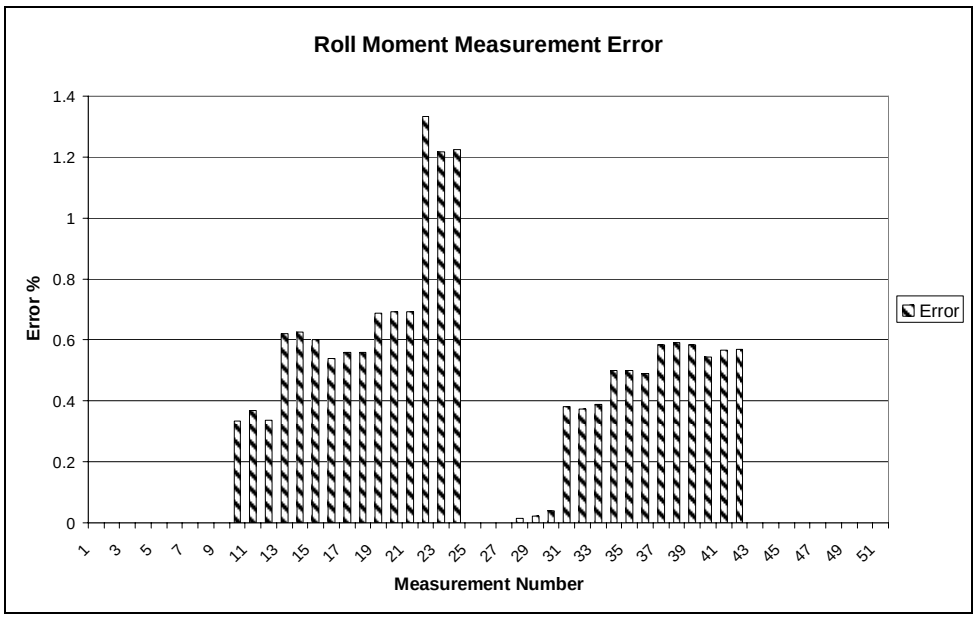

Figure 184 Roll Moment Readings Error

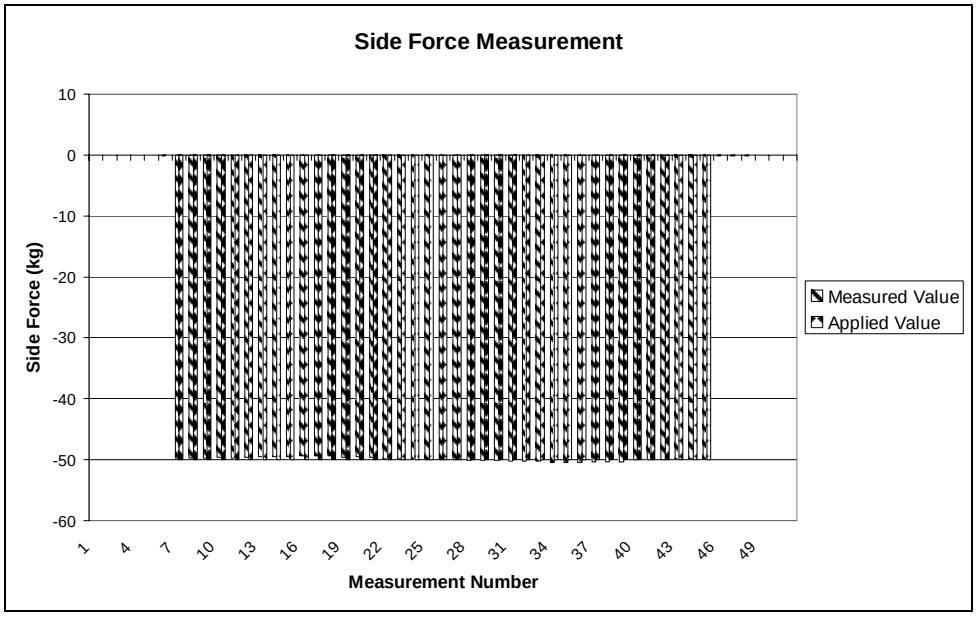

Figure 185 Side Force Loadings and Readings

Figure 186 Side Force Readings Error

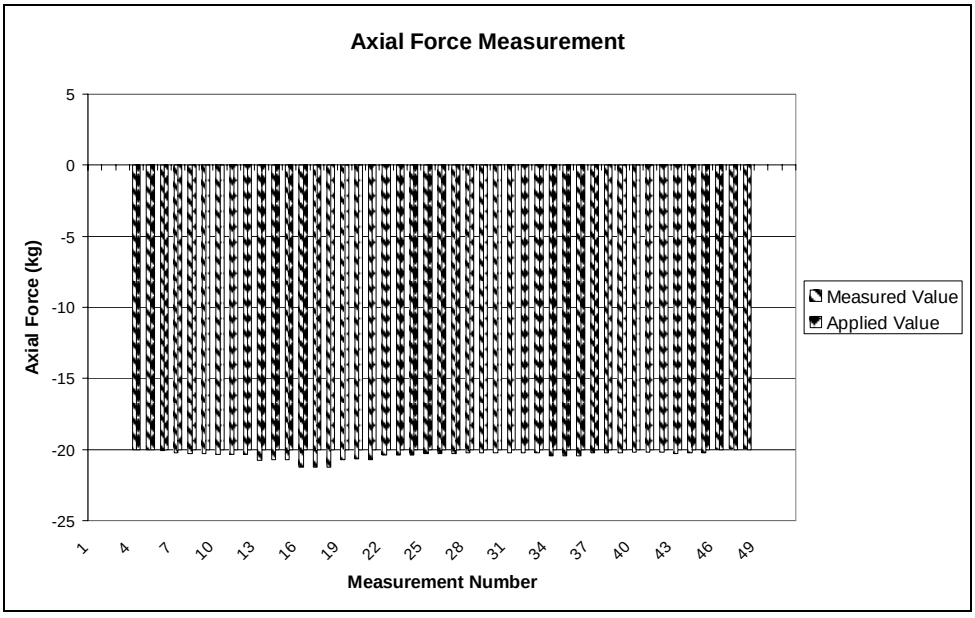

Figure 187 Axial Force Loadings and Readings

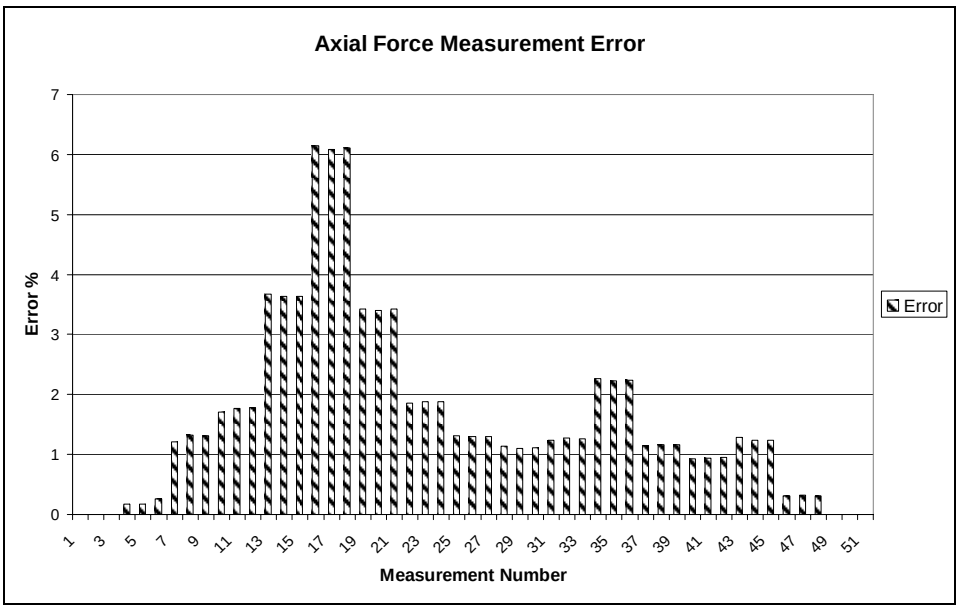

Figure 188 Axial Force Readings Error

F.12 RESULTS of 3-COMBINATION LOADING (Y-S-A)

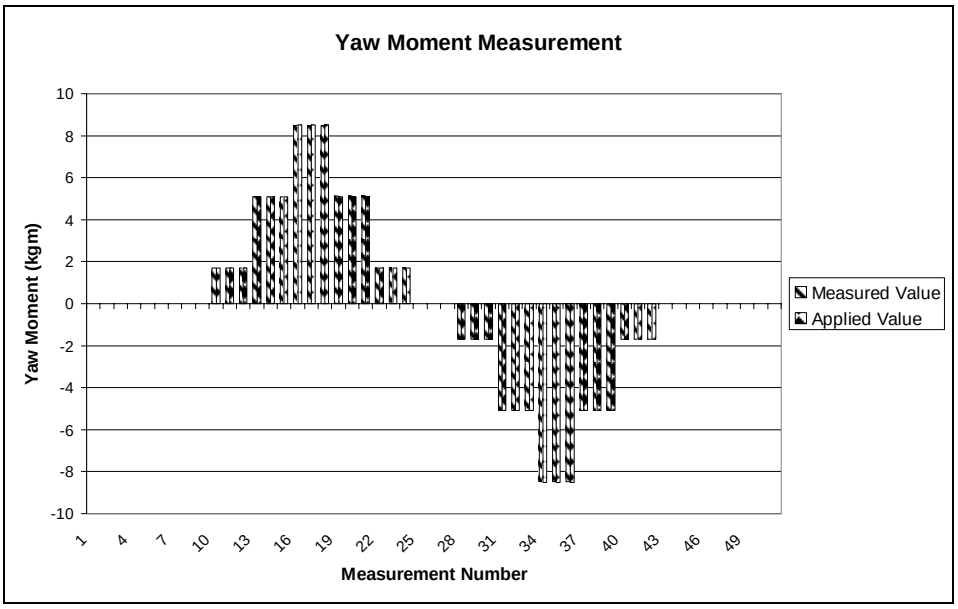

Figure 189 Yaw Moment Loadings and Readings

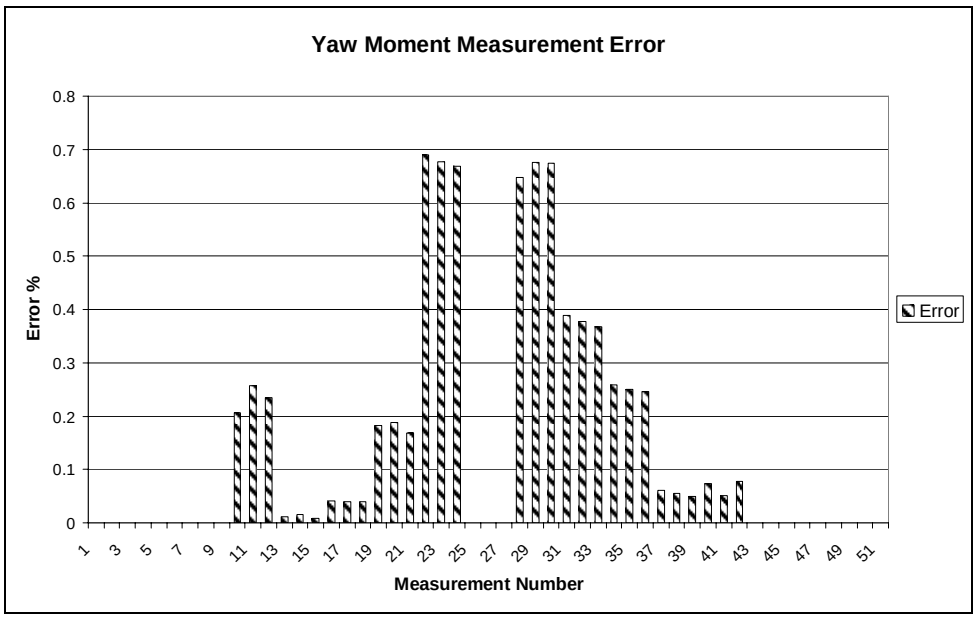

Figure 190 Yaw Moment Readings Error

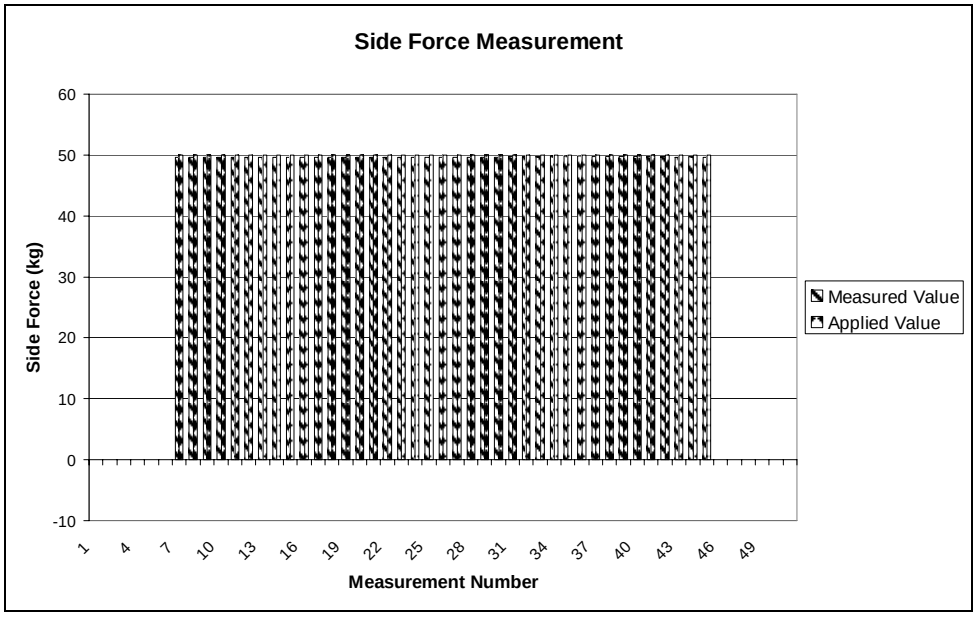

Figure 191 Side Force Loadings and Readings

Figure 192 Side Force Readings Error

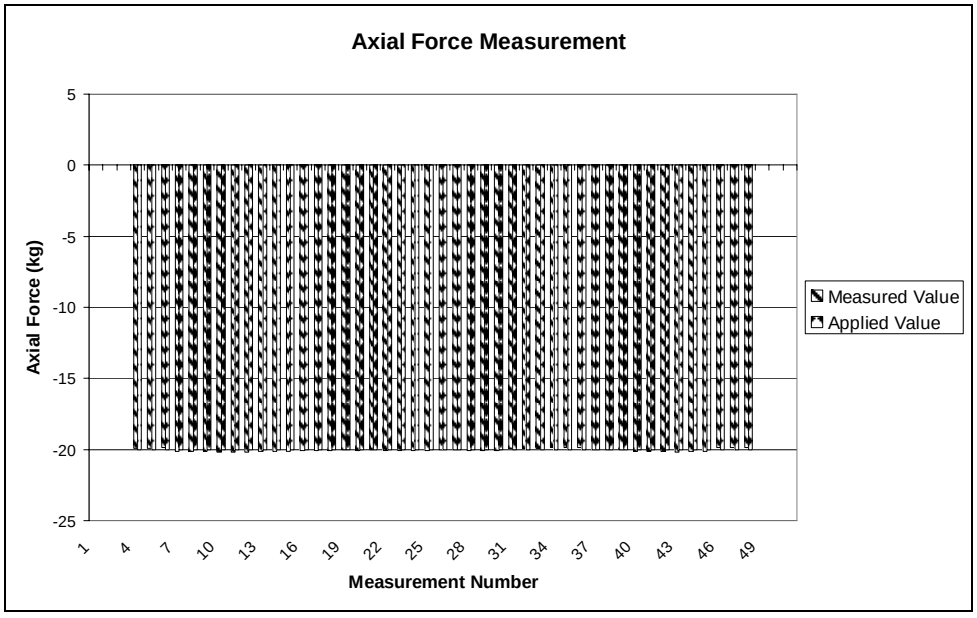

Figure 193 Axial Force Loadings and Readings

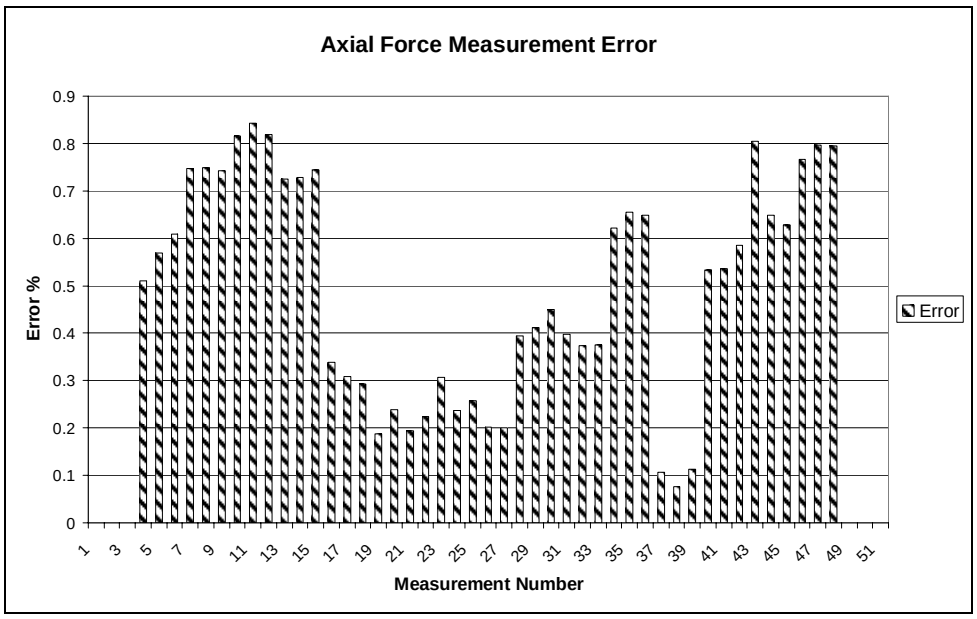

Figure 194 Axial Force Readings Error

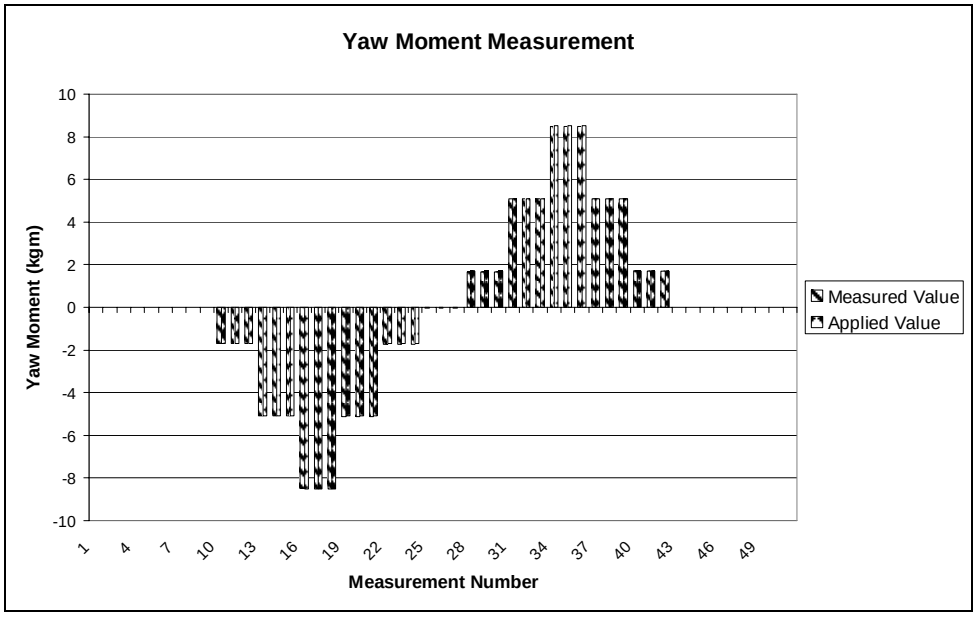

Figure 195 Yaw Moment Loadings and Readings

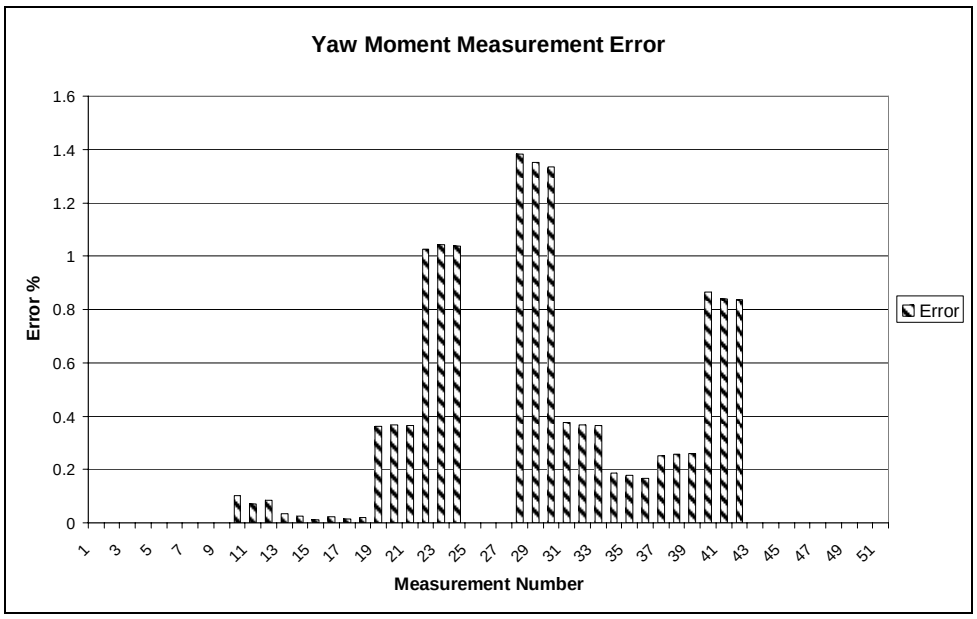

Figure 196 Yaw Moment Loadings and Readings

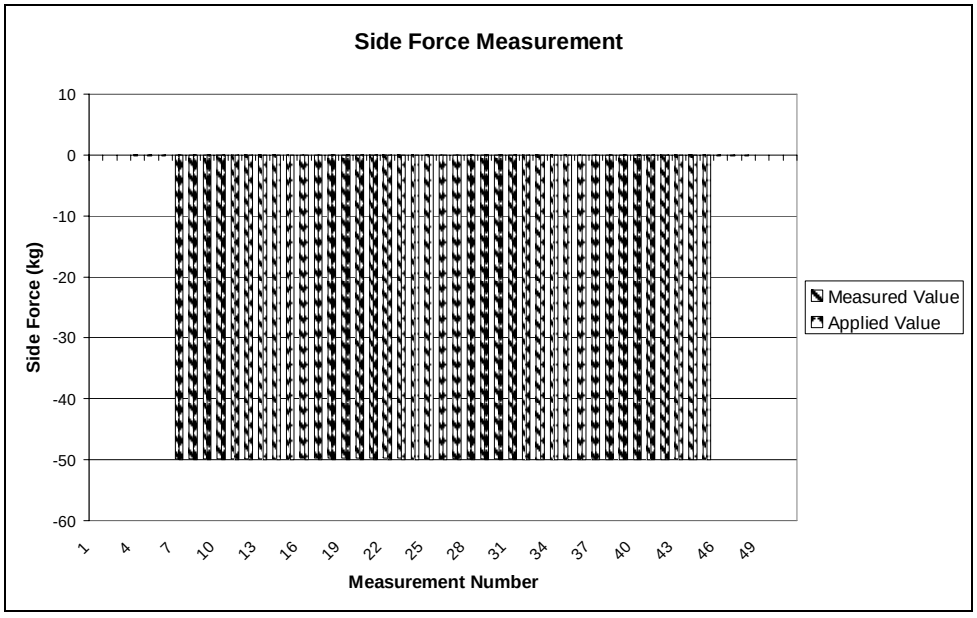

Figure 197 Side Force Loadings and Readings

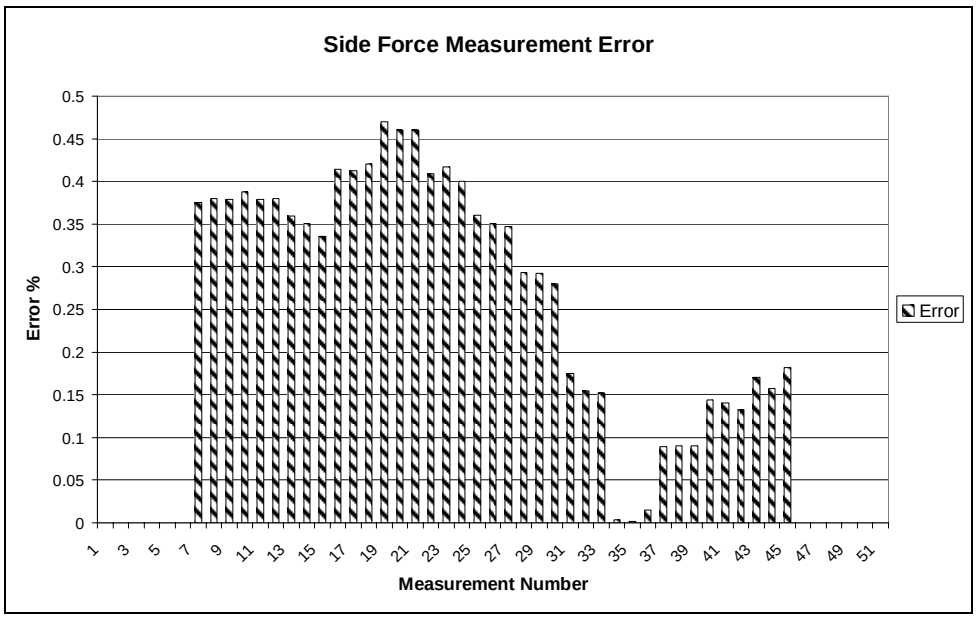

Figure 198 Side Force Readings Error

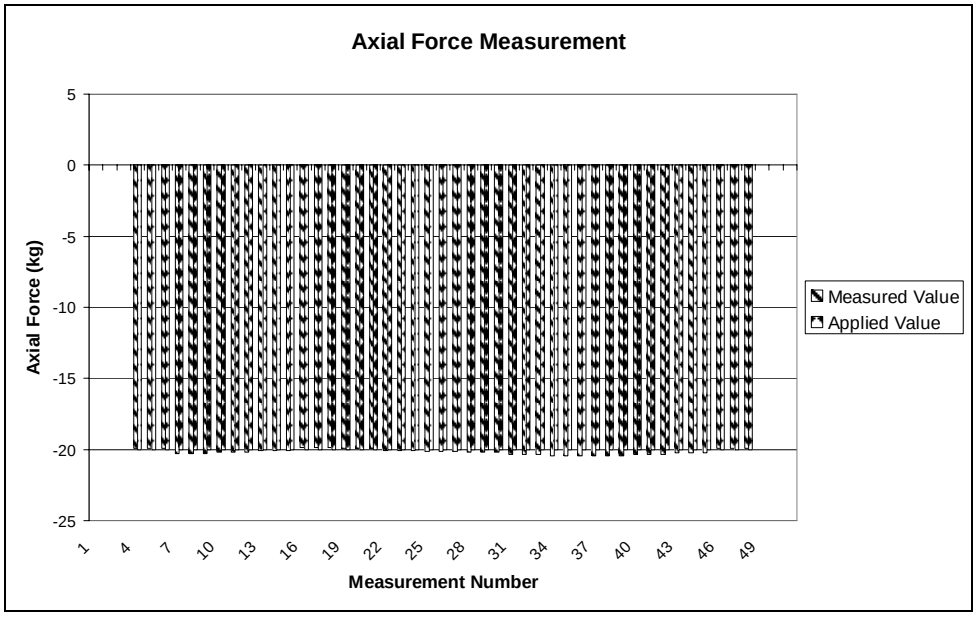

Figure 199 Axial Force Loadings and Readings

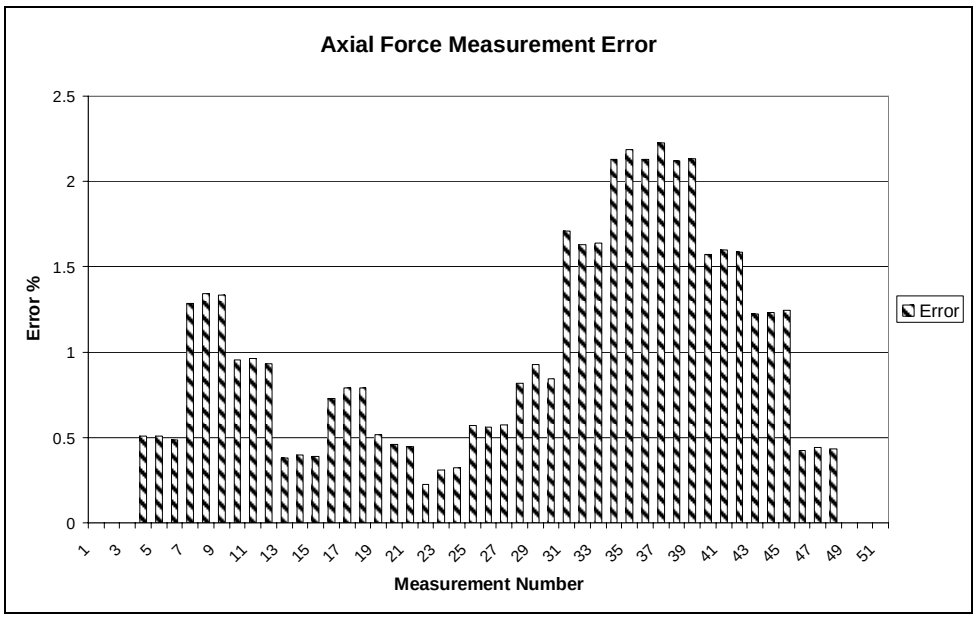

Figure 200 Axial Force Readings Error